PERFORMANCE OF STEEL PIPE PILE-TO-CONCRETE BENT CAP CONNECTIONS SUBJECT TO SEISMIC OR HIGH TRANSVERSE LOADING: PHASE II

FHWA/MT-05-001/8144

Final Report

prepared by
Jerry E. Stephens
Ladean R. McKittrick
Civil Engineering Department
Montana State University

RESEARCH PROGRAMS

Performance of
Steel Pipe Pile-to-Concrete Bent Cap Connections
Subject to Seismic or High Transverse Loading:
Phase II

by
J.E. Stephens and L.R. McKittrick
of the
Civil Engineering Dept.
Montana State University - Bozeman

TECHNICAL REPORT DOCUMENTATION PAGE

1. Report No. FHWA/MT-05-001/8144	2. Government Access No.	3. Recipient's Catalog No.	
4. Title and Subtitle Performance of Steel Pipe Pile-to-Concrete Bent Cap Connections Subject to Seismic or High Transverse Loading: Phase II		5. Report Date February 2005	
		6. Performing Organization Code	
7. Author(s) Jerry Stephens & Ladean McKittrick		8. Performing Organization Report Code	
9. Performing Organization Name and Address Civil Engineering Department Montana State University - Bozeman Bozeman, Montana 59717		10. Work Unit No. (TRAIS)	
		11. Contract or Grant No. MSU G&C Z0261 MDT Project 8144	
12. Sponsoring Agency Name and Address Montana Department of Transportation 2701 Prospect Avenue Helena, Montana 59620-1001		13. Type of Report and Period Covered Final Report July 1999 – November 2004	
		14. Sponsoring Agency Code 5401	

16. Abstract
The response of a concrete filled, steel pipe pile-to-concrete pile cap connection subjected to extreme lateral loads was experimentally and analytically investigated in this project. This connection is part of a bridge support system used by the Montana Department of Transportation that consists of a linear array of piles connected at the top by a concrete pile cap. Five ½ size models of this connection were tested to failure under monotonically increasing and/or cyclic lateral loads. The primary attribute of the connection that was varied between tests was the amount and layout of the reinforcing steel in the pile cap. The depth of embedment of the pipe pile in the cap was held constant. The first tests were done on lightly reinforced pile cap cross-sections, and failure occurred in the pile caps due to tensile cracking of the concrete and yielding of the reinforcing steel adjacent to the pile. In subsequent connections, the amount of reinforcing steel in the cap was increased, and its arrangement was modified, until a plastic hinge occurred in the pipe pile before failure of the cap occurred.

The behavior of each connection was analyzed using hand calculations, strut and tie models, and solid finite element models. The hand calculations accurately predicted the nature of the failure mechanism for each connection, but only poorly predicted the magnitude of the failure load. The strut and tie models used in this investigation were created and analyzed using conventional structural analysis software. The resulting models offered significant detail relative the response throughout the pile cap, but were unable to fully represent yielding of the reinforcing steel and the attendant redistribution of stresses within the cap. Sufficiently promising results were obtained relative to predicting the load and location at which inelastic behavior will initiate, that this analysis methodology possibly should be pursued further. Finally, though finite element models were not successfully used to model the damage cycle through cyclic loads as originally hoped, they did prove useful for extracting 3D information leading up to a state of permanent damage. They also show immediate promise for modeling responses to monotonic load conditions, particularly for analysis where concrete damage is not the controlling failure mechanism.

17. Key Words Bridge substructure, pipe piles, concrete pile caps, bridge testing		18. Distribution Statement No restrictions. This document is available to the public through NTIS, Springfield, Virginia 22161.	
19. Security Classif. (of this report) Unclassified	20. Security Classif. (of this page) Unclassified	21. No. of Pages 151	22. Price

ACKNOWLEDGEMENTS

DISCLAIMER

ALTERNATIVE FORMAT STATEMENT

Unit Conversions

	English	Metric
Length	1 inch	2.540 cm
	1 foot	0.305 m
	1 yard	0.914 m
Area	1 inch^2	6.452 cm^2
	1 foot	0.305 m
Mass	1 lbm	0.454 kg
Force	1 lbf	4.448 N
	1 kip	4.448 kN
Pressure	1 psi	6.895 kPa
(Stress)	1 ksi	6.895 MPa

Contents

List of Figures

List of Tables

Executive Summary

The objective of this project was to study the behavior of a concrete filled, steel pipe pile-to-concrete pile cap connection under extreme lateral loads. The specific connection that was investigated is part of a bridge support system that consists of a linear array of concrete filled steel pipe piles connected at the top by a concrete pile cap. The Montana Department of Transportation (MDT) has found that this support system is very cost effective for short and medium span bridges. Currently, the design of the pile-to-cap connection used in this bent system is based on a rational but approximate method of analysis. Connection performance under extreme lateral loads, however, may not be adequately understood from these approximate methods. This problem is not unique to Montana, and several research projects have been conducted around the country over the past decade to better understand the behavior of pile-to-pile cap connections under extreme lateral loads. After a review of these projects in an earlier effort, it was concluded that none of this information adequately addressed the specific configuration of the pile-to-pile cap connection used in Montana. Therefore, the decision was made to move ahead with the research program described in this report.

The behavior of the concrete filled, steel pipe pile-to-concrete pile cap connection was investigated using a combination of experimental testing and analytical modeling. The purpose of the experimental testing was twofold. The experiments were designed to provide a general indication of the manner in which these connections behaved relative to their ultimate capacity, ductility, and energy dissipation characteristics. The results of the experiments were also used to evaluate various methodologies that are available to analytically characterize the behavior of these connections. Three analysis approaches were investigated, namely, simple "hand" calculations, strut and tie modeling, and finite element analysis.

In the experimental program, five 1/2 size models of the connection were tested to failure under monotonically increasing and/or cyclic lateral loads. The basic model geometry and test set up were determined to replicate the behavior of a typical interior connection in a full size bent subjected to lateral seismic loads. Attributes of the connection that were varied between tests consisted of the wall thickness of the steel pipe pile and the amount and arrangement of the reinforcing steel in the concrete cap. Connection parameters that were kept constant between tests included the depth of embedment of the pile into the pile cap (set at 1/2 of the depth of the cap) and the materials used in constructing the pile and cap (although some inadvertent variations did occur in these properties, notably relative to the strength of the concrete in the cap).

Each model consisted of a single pile and an attendant length of pile cap. The pile cap was held in position on each end (at the theoretical points of inflection in the cap of a full bent when subjected to a lateral load), while a lateral load was applied to the tip of the pile. In addition to subjecting the connections to a lateral load, a constant axial force was applied during the tests to generate the gravity load effects that were expected to be present in the real structures during a lateral load event. Measurements were subsequently made during each test of the loads applied to the connection, and of the global displacements and internal strains that resulted from these loads.

The first connection model (PC-1) was constructed with a pile cap that was reinforced consistent with typical practice for full size structures. The reinforcing steel ratios in the longitudinal and transverse directions of the cap were 0.41 and 0.09 percent, respectively. The steel pipe pile in this test had a diameter to wall thickness ratio (D/t) of 27. The predicted ratio of the moment capacity of the pipe pile to the moment capacity of the cap in this test was 1.46, which was somewhat higher than the ratio of 1.1 calculated for the actual full size connections. Indeed, when the connection was subjected to an increasing lateral load, it failed in the cap through cracking of the concrete and subsequent generation of large strains in the reinforcing steel adjacent to the pipe pile. The pipe pile, itself, was generally undamaged during the test. Relative to the failure, it appeared that the reinforcing steel was unable to carry the tension forces transferred to it when the concrete cracked without sustaining large strains. The displacement ductility of this connection at its maximum resistance was approximately 3.3.

In the second connection test (PC-2), a thinner walled pipe was used for the pile cap (D/t = 34.5), and the resulting ratio of the calculated moment capacity of the pipe pile to the moment capacity of the cap of 1.2 was closer to that calculated for actual full size structures. Despite the decreased moment capacity of the pipe pile, failure in this test once again occurred in the cap through tensile cracking of the concrete and excessive strains in the reinforcing steel adjacent to the pipe pile, at a load similar in magnitude to that observed in test PC-1. Following the initial failure, this connection was subjected to two cycles of fully reversed load. The maximum resistance of the connection, as well as its energy dissipation capacity, were observed to decrease during each successive load cycle. The hysteresis curves exhibited the "pinched" behavior often seen in reinforced concrete elements that have inadequate confining steel to maintain their resistance across multiple cycles of damaging response.

In succeeding tests (PC-3, 3a, and 4), the amount of longitudinal and transverse steel used in the cap was further increased relative to earlier tests. The details of the reinforcing were also changed in tests PC-3a and 4, to improve the effectiveness of the longitudinal steel in the vicinity of the pile to resist local tension forces generated by the pile. As the lateral load applied to the connection increased, failure of the connection still occurred through tensile cracking of the concrete and excessive deformation of the reinforcing steel in the cap in tests PC-3 and PC-3a, although an increase in the moment capacity of the connection was seen, notably in test PC-3a. The final connection tested in this program (PC-4) failed through the formation of a plastic hinge in the steel pipe pile. The longitudinal and transverse steel ratios for this model were 2.83 and 0.70 percent, respectively (an increase by approximately a factor of 7 in the amount of steel that was used in the cap relative to that in the first two tests).

From a ductility perspective, the displacement ductilities calculated at the point of maximum resistance of the connection were 3.3, 3.3, 3.5, 2.6, and 3.9, respectively, in tests PC-1, 2, 3, 3a, and 4. The reduced displacement ductility in test PC-3a may in some manner be related to the increased reinforcement that was used in the cap in this test, and a possible shift in the characteristics of the failure mechanism relative to earlier tests on more lightly reinforced sections. In interpreting the displacement ductility reported for test PC-4, it is essential to note that this is only the maximum ductility demonstrated during the test; the ultimate ductility of this connection could well be much greater in magnitude. This test had to be terminated when the maximum allowable displacement of the test frame was reached; there was no evidence at this point that the full yield capacity (or yield displacement) of the connection had been realized. Model PC-4 was also subjected to a fully reversed cycle of lateral load. No reduction in the maximum capacity of the connection or in its energy dissipation capacity was observed during this cycle of reversed load.

The simple hand calculations used in this investigation were found to reasonably predict the nature of the failure in each test. They were further found to reasonably predict the failure capacity in moderately to heavily reinforced cross-sections. In implementing these simple analyses, the moment carrying capacities of the steel pipe pile and of the reinforced concrete cap were calculated independently. A recently developed equation recommended for use in the seismic design of bridge structures was used to calculate the plastic moment capacity of the concrete filled, steel pipe pile. In the single test in which the connection failed by formation of a full plastic hinge in the pipe pile, the actual plastic moment capacity of the pipe exceeded the calculated value by 26 percent.

The moment capacity of the pile cap was determined based on two possible modes of failure, crushing of the concrete in compression on opposite sides of the pile along the pile embedment length, and tensile yielding of the reinforcing steel adjacent to the embedded pile. For the former mode of failure, a compression couple was assumed to form in the cap concrete to resist the moment introduced by the pile. By assuming some value for the limiting compression strength of the concrete, the moment capacity of the cap for this mode of failure could be calculated. The value of this limiting strength is known to be affected by the confinement provided by the reinforcing steel. For the reinforcing situations encountered in this investigation, this calculation was found to underestimate the actual capacity of the connection (by up to a factor of two) when the limiting strength was assumed at 85 percent of the unconfined compression strength (f_c') of the concrete. However, none of the connections tested in this investigation failed through this mechanism, thus, a more thorough assessment of this approach to modeling this failure mode could not be done.

The failure mechanism of tension yielding of the reinforcement in the cap adjacent to the pile was evaluated by assuming that the compression forces in the cap discussed above were internally resisted by tension forces in the longitudinal reinforcing steel adjacent to the cap. The tensile capacity of the concrete was ignored in these calculations. This approach yielded good results for moderate to heavily reinforced cross-sections. That is, in a connection with 2.11 longitudinal and 0.65 percent transverse steel in the cap cross-section, the capacity calculated following this approach was within 10 percent of the actual capacity of the cap. This model, however, significantly under predicted (i.e., by up to 70 percent) the capacity of lightly reinforced cross sections (as was the case for PC-1 and 2 with only 0.41 percent longitudinal steel in the cross section). This under prediction of capacity in this situation was attributed to ignoring the tension capacity of the concrete, which may play a proportionately larger role in the total capacity of the section in lightly as opposed to more heavily reinforced cross-sections.

The pile-to-pile cap connections were also analyzed using a strut and tie approach. Following this analysis methodology, the solid block of reinforced concrete that comprises the cap was replaced with an equivalent truss structure. The concrete generally was assumed to carry compression only, and formed the compression struts of the truss, while the reinforcing steel formed the tension ties. These models offered significantly more information on the behavior of the various elements of the cap than was available from the simple hand models described above, without stepping up to the level of complexity of solid finite element models. While hand methods only address compression in the concrete and tension in the longitudinal reinforcing immediately adjacent to the pile, the strut and tie models provided an indication of the stresses in the transverse ties, the stresses along the length of the longitudinal steel, and the stresses throughout the concrete.

A new approach was experimented with for developing and analyzing strut and tie models in which these tasks were accomplished using commonly available structural engineering analysis software. The attraction of using such software was the ability to create and analyze strut and tie models that offer highly redundant load paths through the structure. In traditional strut and tie analysis, to

reduce calculational requirements, the analyst pre-selects compression load paths through the structure (which naturally can influence the subsequent results). The one drawback of implementing strut and tie models in conventional structural engineering software was that such software generally only performs elastic analyses, so the load redistribution that takes place during plastic behavior was not represented. In any event, similar to the hand calculations discussed above, and possibly for the same reasons, the strut and tie models used in this investigation were found to give poor results for lightly reinforced cap sections, while they generated good results for moderately reinforced sections. Relative to the hand calculations, the strut and tie models did offer considerably more information on the internal force distributions throughout the model (as opposed to just at the critical cross-sections), and they highlighted the role of the transverse steel in resisting the forces generated in the cap by the rotation of the pipe pile.

With regards to finite element models, the codes that were tested seemed to work well for evaluating the initial elastic response of the connection and hence as a tool for evaluating the initial location and onset of permanent deformation. Additionally, the finite element model was quite useful for evaluating three dimensional variations in the stress-strain responses. However, the codes evaluated did not work sufficiently well for tracking the nonlinear behavior associated with concrete damage, particularly for cases concerning cyclic loads where significant concrete damage was involved. That being said, the models do still show promise for evaluating monotonic load cases where concrete damage is minimized. As a consequence, these evaluations may prove quite useful as indicators of desirable designs, since concrete damage is typically not considered desirable as a mechanism for energy dissipation, particularly in seismic areas.

In closing, this study primarily investigated a single parameter known to influence the behavior of steel pile-to-concrete pile cap connections, that is, the reinforcement used in the pile cap. Further work needs to be done to address other parameters known to affect the performance of such connections, including a) the depth of embedment of the pile in the cap, and b) the nature of the cyclic load history. Additionally, more work could be done on the specific arrangement of the reinforcement steel used in the cap. In all cases, due to continuing concerns relative to the ability of existing analytical techniques to reliably predict the response of this connection under extreme lateral loads, further study of these issues should include both experimental and analytical components.

Chapter 1

Introduction

1.1 BACKGROUND

A common bridge support system used by the Montana Department of Transportation (MDT) consists of a linear array of concrete filled steel pipe piles connected at the top by a concrete pile cap. This bridge support system is popular because of its low initial cost, short construction time, low maintenance requirements, and long service life. To simplify construction and maintain a positive connection between the piles and the pile cap, the steel pipe piles typically are extended up into the reinforced concrete cap. Conventional structural design methodologies, however, do not explicitly address the situation of a large rigid pipe element embedded in a conventionally reinforced concrete structure. While these methodologies can confidently be extended to predict the capacity of such a connection to carry in-service gravity loads, the direction to follow in determining the capacity of such a connection under extreme lateral loads (say, of seismic and ice origin) is much less clear.

In assessing the lateral load capacity of a structure following current design philosophies, it is essential to know both the ultimate capacity of the element, as well as its ductility and energy dissipation characteristics up through and beyond failure. Determining these properties of a structure is a complex problem, that often can only be practically solved using a combination of engineering principles and empirical performance observations. It is the empirical aspect of these solutions that makes extending them to new situations (such as a steel pipe pile embedded in a reinforced concrete pile cap) an uncertain process.

In light of this situation, MDT initiated a project at Montana State University (MSU) to investigate the behavior of steel pipe pile-to-concrete pile cap connections under extreme lateral loads. The project was divided into two phases. Phase I, completed a few years ago (McKittrick et al., 1998), consisted of reviewing the available information on the analysis, design, and performance of steel pipe pile-to-concrete pile cap connections, setting up a finite element model for analyzing the behavior of these connections, and investigating a method for experimentally testing these connections. It was discovered in Phase I that:

a) only nominal research has been done to-date on the behavior of the specific pile-to-cap connection used by MDT,

b) it is possible to run simple and informative physical tests in which models of the pile-to-pile cap connection zone are subjected to lateral loads,

c) finite element methods may provide a reasonable approach for analytically studying the behavior of the pile-to-pile cap connection, and

d) demands placed on the connection by ice loads are small compared to the demands from seismic ground motions, if deck motion is restrained by the abutments.

Complete results from Phase I are presented in the final report for this part of the effort.

The decision was subsequently made to move ahead with a more thorough investigation of the steel pipe pile-to-concrete pile cap connections typically used by MDT as Phase II of the project. The proposed objective of the initial work of Phase II was to characterize the basic load-deformation response of generic steel pipe pile-to-concrete pile cap connections. The results of the work completed to-date on this task is presented in this report. Later work in Phase II was planned to focus on developing, as necessary, retrofit strategies for existing connections and design recommendations for new connections to insure that these connections provide the required level of performance under extreme lateral load events.

1.2   OBJECTIVE AND SCOPE

The objective of this investigation was to study the load-deformation response of steel pipe pile-to-concrete pile cap connections under extreme lateral loads. This investigation was accomplished using a combination of experimental and analytical work. The objective of the experimental effort was to generally characterize the behavior of the connection and to validate the performance of the analytical models. Five models of a typical connection were laterally loaded to failure, and the results were compared with those obtained using simple "hand" calculations, strut and tie analyses, and finite element analyses.

The test articles used in this study were approximately 1/2-size models of a subsection of a typical bridge bent constructed with steel pipe piles joined by a reinforced concrete pile cap. The models were designed to represent an interior section of such a bent, centerline-to-centerline between pile supports. Thus, each model consisted of a single pile and an attendant length of pile cap. The baseline configuration of the models was intended to represent a typical connection configuration used by MDT. Parameters that were varied between the models consisted of the wall thickness of the steel pipe pile, the amount of reinforcing steel used in the cap, and the configuration of the reinforcing steel used in the cap. Parameters that remained generally constant between the models included the strength of the materials, the basic geometry of the pile and the cap, and the depth of embedment of the pile within the cap. As the project advanced, the configuration of each successive model was adjusted based on the results of the preceding model test, in an effort to generate a range of results from failure of the connection through cracking the concrete or yielding of the reinforcing steel in the cap, to the formation of a plastic hinge in the pipe pile.

Each model was subjected to a slowly increasing lateral load applied to the tip of the pile, while the pile cap was held stationary. Coincident with the lateral load, a constant axial force was applied to represent gravity load effects. While some preliminary tests were conducted on the models at elastic load levels, in the primary load event for each model, the lateral load was monotonically increased until the lateral capacity of the connection was achieved. In some cases, the model was subsequently subjected to reversed load cycles, to assess the residual strength and energy dissipation characteristics of the connection. During each test, the load and displacement response of the connection was

measured and recorded. Measurements were also made of the strains in the pipe pile and in the cap concrete. In selected tests, strains in various bars in the reinforcing cage were also measured.

The performance of these test articles was analytically modeled using "hand" methods, strut and tie models, and finite element analysis. In analyzing the moment capacity of the connection by "hand" the capacity of the concrete filled steel pipe pile and that of the reinforced concrete cap were considered independently. The plastic capacity of the pipe pile was simply calculated using equations available from the seismic design guide for bridges specifications. The capacity of the concrete cap was calculated by assuming the moment from the pipe pile was carried by a compression couple in the cap. Simple compression stress fields were assumed to develop in the concrete at the interface between in pipe pile and the cap in the embedment zone. Local tension forces in the reinforcing steel in this area were calculated using basic equilibrium considerations.

The behavior of the concrete cap when lateral loads are applied to the steel pipe pile was also analyzed using a strut and tie approach. For these analyses, the steel pipe pile was assumed to be a rigid element embedded in the concrete cap. Following the strut and tie methodology, the solid cap was modeled as a collection of discrete members. These members consisted of "compression struts" in the concrete interconnected with "tension ties" formed by the reinforcing steel. In early models, professional judgment was used in selecting the locations of the compression struts. In later models, a regular grid of struts was provided in the models, with the objective of allowing the analysis, itself, to select critical compression paths through the structure. All models were created and analyzed using a structural member based finite element program. While an elastic analysis was performed, the program offered the option of specifying compression only members. Initially, all of the concrete struts were modeled as compression only members, while the steel ties were modeled as capable of carrying compression and tension. In using this approach, however, the distribution of internal forces between the concrete and reinforcing steel was believed to be poorly represented in regions of low stress (i.e., regions stressed below the tensile cracking limit of the concrete). Therefore a further refinement of these models was experimented with, in which the compression struts were allowed to carry both tension and compression in areas of low stress.

For the finite element (FE) modeling portion of the project, the goal of modeling the pile cap behavior well into the damage regime and even through cyclic loads was not attained. However, the FE models did prove very useful for the evaluation stress-strain variations in three dimensions, particularly in the elastic regime. The FE models also showed promise for modeling cases where monotonic loads are applied and where concrete damage is minimized or not a dominant player in the nonlinear behavior of the structure. For one of the last cases evaluated, the permanent deformation was dominated by plastic deformation in the steel pile jacket. As such, the finite element model yielded reasonable agreement with the experimental outcomes. Because behaviors associated with concrete damage are not typically considered desirable, these models may be useful for evaluating more desirable connection behaviors dominated by plastic deformation of steel. In particular, concrete damage is not considered a desirable mode of inelastic deformation as it has a tendency to be associated with a degradation of the structural integrity of the component. Similarly, relative to plastic deformation associated with steel, it is not as efficient at dissipating energy, as required for designs in seismic zones.

Chapter 2

Description of the Problem

2.1   GENERAL REMARKS

The Montana Department of Transportation (MDT) has made wide use of steel pipe piles connected to concrete pile caps as substructures for bridges in the state. These substructure systems are favored because of their speed of construction, low maintenance and low cost. However, there is no rational procedure for the design of the pipe pile-to-pile cap connection. The designs that are currently used rely on an approximate, empirical method. Notably, there are no well-developed and validated design procedures that account for lateral demands placed on these systems. Research has been done on a variety of pile foundation systems, simply not quite this one. Nonetheless, it is useful to see what others have done to obtain a sense of what parameters are important to the connection performance, and what behaviors have been observed.

2.2   DESCRIPTION OF THE STRUCTURAL SYSTEM

The specific connection investigated in this study is intended to generically represent MDT's practice of using steel pipe piles to support concrete pile caps in general purpose bridge construction. This substructure system is often used on small bridges, and it consists of a concrete pile cap that spans across four pipe piles which are positioned immediately below the location of the bridge stringers, as shown in Figure 2.1. The general geometry of the piles and pile caps is fairly uniform across the various applications for which this system is used. The concrete filled, steel pipe piles have diameters in the range of 16 to 20 inches, and pipe wall thickness of 1/2 inch. The concrete pile caps typically are on the order of magnitude of 3 foot square in cross-section, as shown in Figure 2.1. The reinforcing in the caps generally consists of 13 to 16 ~# 6 longitudinal bars distributed around the perimeter of the cross-section, confined by # 4 transverse rectangular hoops spaced at 1 foot on center.

One factor that can vary between bridges is the connection detail between the steel pipe piles and the concrete caps, based on the individual designer's view of what is required for a robust and constructible connection. Some typical details for this connection are shown in Figure 2.2, and range from no positive connection between the pile and the cap, to inserting reinforcing bars transverse to the longitudinal axis of the pipe (parallel to the longitudinal axis of the cap), to constructing a reinforcing cage that extends up out of the end of the pipe pile into the cap.

Relative to materials, MDT standard specifications (MDT, 1995) require concrete with a 28-day unconfined compression strength of 3,400 psi (for full payment for a Class AD mixture), the reinforcing steel must be Grade 60, and the pipe pile must be ASTM A252 Grade 2 steel, which has a minimum yield strength of 35,000 psi.

Pile Cap

Pipe Pile

2 at 60' = 120'

Stringer,
Prestressed Beam
(Type A)

Pile Cap to Pipe Pile
Connection Zone

Deck, t = 7"

Pile cap, 36" x 36"

Concrete filled,
steel pipe pile, D = 16"
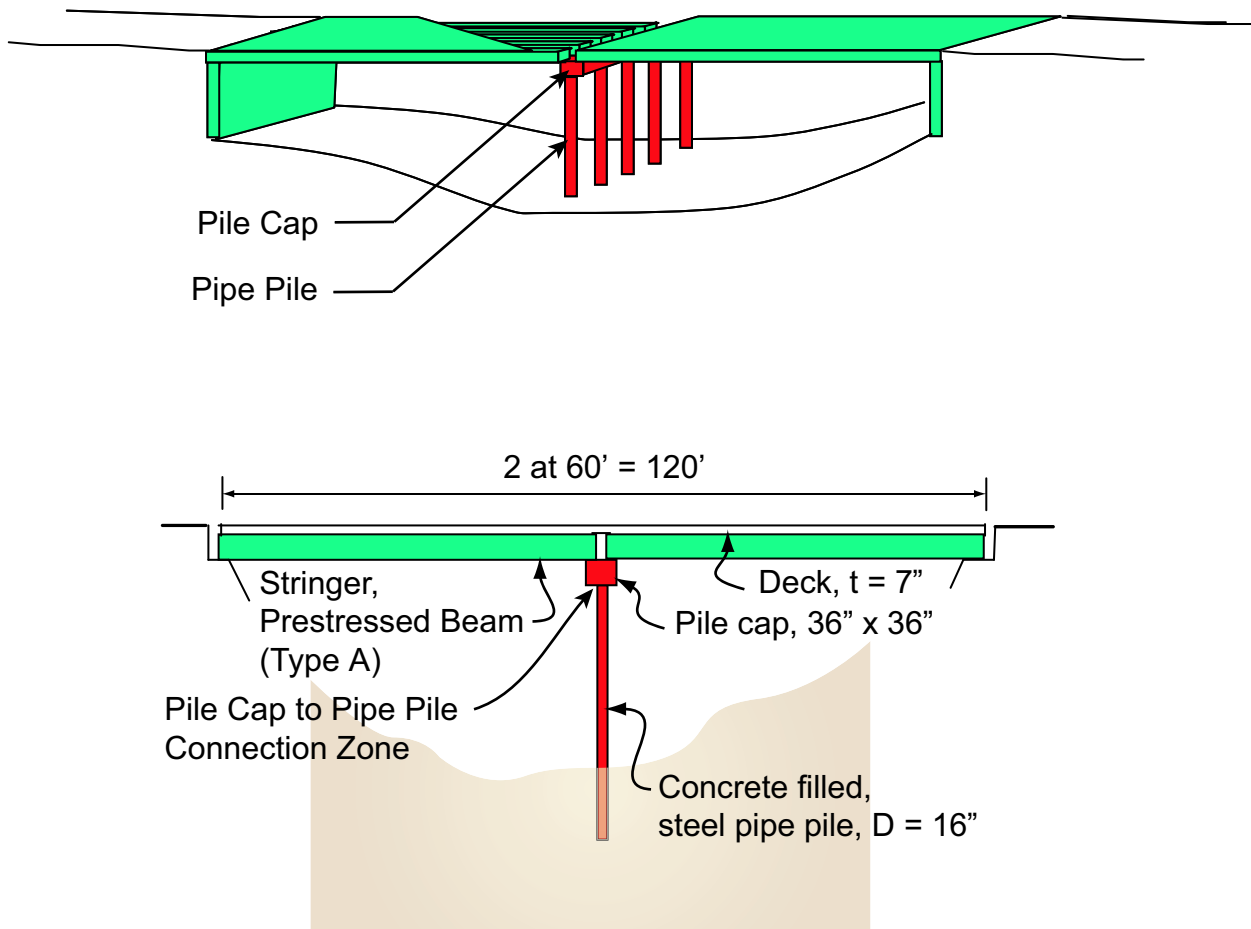
Figure 2.1: Overall Bridge Configuration

36 inches

36 inches

6 Bar, Typical, Top
and Bottom Face

4 Bar, Typical, Side
Faces

4 Tie

6 Bar, Typical,
Through Pile

4 Hoop

16 inch Diameter Pipe
1/2 inch Wall

48 inches

36 inches

6 Bar, Typical, Extends
From Pile into Cap

24 inch Diameter Pipe
1/2 inch Wall

4 Hoop
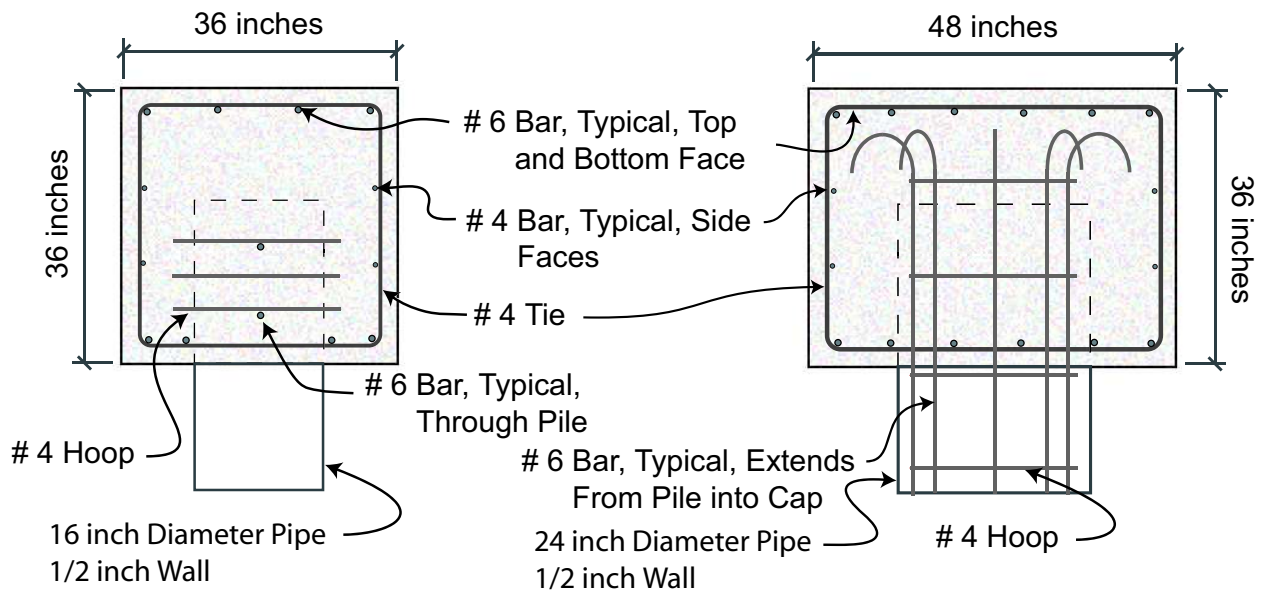
Figure 2.2: Typical Cross Sections: Pile and Pile Cap

2.3   STRUCTURAL BEHAVIOR OF INTEREST

Under a lateral load (say, during a seismic event or in the presence of an ice jam), the pile cap and pipe pile support system are expected to deflect laterally in the shape shown in Figure 2.3. This investiga-
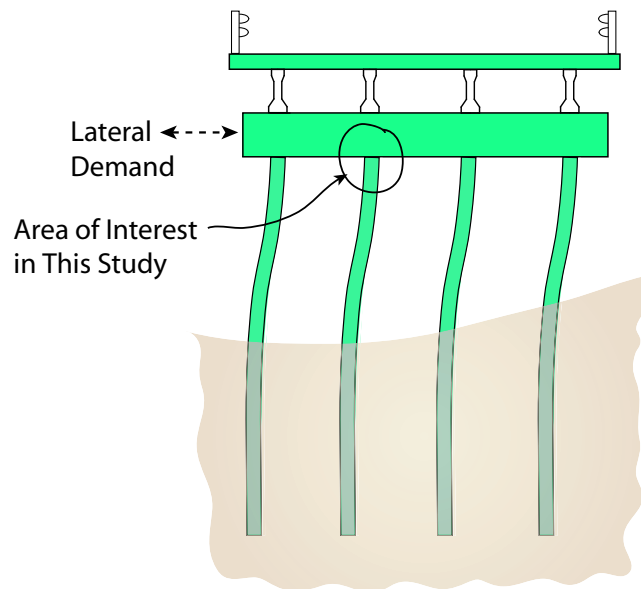
Figure 2.3: Expected Effect of Lateral Loads Acting on the Support System

tion is focused on the behavior of the structure in the connection zone as it deforms to this position. While the gross behavior of the pile and cap can be readily described using established engineering principles for reinforced concrete, the behavior of the cap in the immediate vicinity of the embedded pipe pile is more difficult to determine. The primary concern with this behavior revolved around the embedment and subsequent rotation of a relatively rigid object, the pipe pile, in the concrete pile cap. Possible failure mechanisms were believed to be crushing and/or splitting of the concrete in the cap immediately adjacent to the steel pipe pile, formation of a plastic hinge in the pipe pile, or some combination of these behaviors. For design purposes, it is important to be able to predict what failure mechanism will occur when this system experiences extreme lateral loads, the ultimate capacity of the connection at failure, and the failure behavior (ductile or brittle).

2.4   LITERATURE REVIEW

Several research projects have been conducted over the past few years on the performance of various pile and pile to pile cap connection configurations under lateral loads, which is a direct reflection of the uncertainties that exist in using current design methodologies to predict the capacity and behavior of these systems. Certainly, prior to undertaking a new study of this problem, it is important to review what may already be available on its solution. While some of these efforts focused primarily on the behavior of the pipe pile independent of the cap, most of them encompassed an assembly of the pile and the cap. These studies invariably used a reinforced concrete cap coupled with a steel or concrete pile. In the case of the steel piles, however, the specific configurations investigated only partially modeled the situation of interest in this study. That is, the steel pile was embedded in the cap, but it was an H-section rather than a pipe section, or a pipe section was used for the pile, but the pipe was

terminated immediately before the pile entered the cap. Thus, while this information is useful, it does not fully resolve all the issues related to the performance of the pile to pile cap connection that is the subject of this investigation.

Presented below are reviews of several of the research projects conducted recently on pipe pile and pile to pile cap connections. The intention of these reviews was twofold 1) to collect direct information on how various connection configurations have performed, and 2) to collect information on how investigations of these connections have been conducted. To some extent, the review is ordered from the most to least pertinent study relative to the objectives of this investigation.

Concrete Filled Pipe Pile to Concrete Encased Steel Fixed Base Connection   The most current information available on the behavior of concrete filled steel pipe piles subjected to lateral loads is from Marson and Bruneau (2004). They report on a study in which four full size models of concrete filled steel piers were tested to failure under combined lateral and vertical loads. Marson and Bruneau specifically looked at 12 and 16 inch diameter piers, with 1/2 and 3/8 inch thick steel walls, with attendant pile diameter to wall thickness (D/t) ratios ranging from 34 to 64 (note that the generic steel pile used in this analysis had a nominal diameter of 16 inches and a wall thickness of 1/2 in for a D/t ratio of approximately 32). The piles were anchored to a steel assembly consisting of transverse channels with two 1/2 and 3/8 inch bottom and top plates, respectively, which was embedded in a concrete foundation. A section of a full bent assembly consisting of a single pile and an associated length of pile cap were modeled in the investigation. The models were subjective to a constant axial load and cyclic lateral load.

In all of Marson and Bruneau's tests, failure of the pipe pile to concrete foundation connection occurred by formation of a plastic hinge in the pipe pile. Based on their test results, and the results of physical tests conducted by four other investigators over the past several years, Bruneau and Marson (2004) developed and validated new equations to predict the flexural strength of concrete filled steel pipe piles in terms of the geometry and materials used in their construction. These equations subsequently were included in the recommended guidelines for the seismic design of highway bridges (ATC/MCEER, 2001).

Behaviorally, Marson and Bruneau (2004) found that the connections they tested, in which failure occurred in the pipe pile, all offered good seismic performance relative to ductility and energy dissipation. The ductility ratios (displacement at maximum resistance divided by displacement at yield) was on the order of magnitude of 4, and favorable hysteresis behavior (good energy dissipation) was observed in all cases.

Concrete Filled Steel Pipe Piles Anchored by Reinforcing to a Concrete Cap   Silva and Seible (2001) investigated the lateral load performance of concrete filled steel pipe piles embedded 3 and 5 inches into a concrete cap. They conducted their investigation by analyzing and testing two approximately 7/12 size models of this connection configuration, each consisting of a single pile anchored to a requisite length of pile cap. The pipe piles in the models had an outside diameter of 14 inches and a wall thickness of 7/16 of an inch (D/t of = 32). Two different reinforcing schemes were used to anchor the pipe pile to the cap. In one case, the longitudinal bars in the pipe pile simply extended out into the cap and were encircled by a spiral. In the second case, two additional "V" bars were added to the connection; they were threaded through holes in the embedded end of the pipe pile with the legs of the "V" extending down into the cap.

Failure of both of the models described above occurred in the pile cap. In the model without the V bars, early damage consisted of the formation of cracks in the cap emanating at 45 degrees from the pile base toward the sides of the pile cap. "Joint shear cracking" subsequently occurred along the principal tension planes in the cap, and was believed to happen almost simultaneously with the pile reaching its elastic limit. Joint shear failure then occurred, in which the reinforcing steel in the cap yielded and the lateral force resistance of the cap diminished.

Analytical models were developed to predict the load-deformation response of the pipe pile and connection zone. Notably, models were created to calculate the internal force resultants generated at the interface between the pipe pile and the cap due to the axial and lateral loads applied to the pile. These internal force resultants included a compression "couple" acting on opposite sides of the pile in the embedment zone, as well as compression and shear resultants acting on the end of the embedded pile. The stress distribution associated with the compression resultants were determined based on equilibrium and displacement compatibility conditions.

Concrete Filled Steel Pipe Pile with Steel Shell Terminated Near Face of Concrete Pile Cap
Silva (Silva et al., 1999) was also involved in tests conducted for the Alaska Department of Transportation on the seismic performance of a steel pipe pile, concrete pile cap bent system. In this system, the steel shell on the pipe pile was terminated 2 inches from the face of the pile cap. The longitudinal steel in the pipe piles (and the attendant confining spiral) continued on up into the cap. The pipe piles in the full size bent were 36 inches in diameter; the reinforced concrete cap was 54 inches wide and 42 inches deep. The longitudinal and transverse steel ratios in the connection area of the cap (for an interior pile) were 1.18 percent and 0.09 percent, respectively.

A full size bent consisting of 3 piles was subjected to a cyclic lateral load history in the presence of a constant vertical load. The bent failed through the formation of plastic hinges in the top of the columns, without any significant damage occurring in the cap beam. The bent was exercised to a ductility ratio of 8, without any degradation in strength. A moderate loss in strength (10 percent) was observed when a ductility ratio of 10 was reached. The energy dissipation characteristics of the bent, as evaluated from the force displacement response, was excellent (i.e., robust rather then pinched hysteresis curves).

Hollow Steel Pipe Pile to Precast Concrete Cap Connection   Steunenberg and his colleagues (Steunenberg et al., 1998) investigated the connection between hollow steel pipe piles and precast concrete caps. In their case, the connection between the pile cap and pipe pile was made by welding the top of the pipe pile to a steel plate embedded flush in the face of the pile cap. The pipe pile was 12 3/4 inch in diameter with a 1/2 in wall thickness. Based on the D/t ratio for the pipe section (25.5), a plastic hinge was expected to form in the pile before local buckling occurred. The embedded plate in the pile cap was approximately 25 inches by 24 inches by 2 inches, and was anchored to the concrete using 30 deformed studs, each 0.59 inches in diameter and 23.6 inches long.

A physical model of the connection described above, consisting of a single pile and attendant length of pipe cap, was constructed and cyclic tested under cyclic lateral loads. The load carrying capacity of the connection was controlled by the formation of a plastic hinge in the pipe pile. The subsequent hysteresis behavior observed during the test was desirable from a seismic performance perspective (i.e., the hysteresis curves were full, rather than pinched), leading the researchers to conclude that the energy dissipation capacity of the connection was "impressive". While apparently there

was little evidence of distress in the cap throughout the test, the instrumentation did reveal that bond slip may have occurred on some of the anchor bars on the embedded steel plate.

Precast Concrete Piles Connected to Concrete Pile Caps   Joen and Park (1990) investigated (among other things) possible approaches to connecting cast-in-place concrete pile caps to precast concrete piles. The specific situation they investigated involved 15.7 inch octagonal piles supporting a 3 foot square pile cap. This situation is generally similar to that investigated in this study (16 inch diameter circular pile supporting a 3 foot square pile cap). The connection approaches that they studied consisted of a) embedding the piles in the cap (with an embedment length of 31.5 inches, and a light spiral encircling the pile along the embedment length), b) breaking away the concrete on the end of the pile over a 600 mm length and embedding it in the cap to this depth, and c) embedding dowel bars in the pile that extended into the cap. The reinforcement ratios used in the cap were approximately 0.55 and 0.09 percent in the longitudinal and transverse directions, respectively.

Tests were conducted on full size models of each connection configuration. The models consisted of a single pile and attendant length of pile cap. The connection was pinned at a single point in the pile cap and at the tip of the precast pile. A moment was then introduced into the connection by rotating the pile cap. The moment was applied cyclically while a constant axial load was applied to the pile.

In all tests, the connection failed by the formation of a plastic hinge in the precast pile at the face of the pile cap, only minor cracking was observed in the pile cap. In all but one test, a minimum ductility ratio of 8 was observed.

Spirally Reinforced Concrete Columns Subjected to Inelastic Loads   Six one-sixth scale models of prototype bridge columns were tested by Cheok and Stone (1990) to characterize their behavior under inelastic cyclic lateral loads. In each of their tests, a single column anchored in a block of concrete was subjected to a constant vertical load and cyclically increasing lateral loads applied at the tip of the column. This model configuration (with fixed hinged end support conditions) was believed to accurately represent the boundary conditions for a broad class of bridge columns used in seismic regions. The overall dimensions of the models were directly scaled from the full-size column dimensions. The amount of reinforcing steel in the models was determined by providing the same steel ratio in the models as was used in the full size columns, with the layout for the steel being determined by directly scaling, as possible, the layout from the full size structure. When tested, the models failed by the formation of plastic hinges at the base of the columns (which was the intended failure mechanism). The displacement ductilities of the models ranged from 6 to 10, depending on the length to diameter ratio of the column.

Seismic Performance of Steel H-Piles Embedded in Concrete Pile Caps   Two models of connections typically used in the central and eastern parts of the country for steel H-piles supporting concrete pile caps were tested to failure under axial and cyclic lateral loads by Shama and his colleagues (Shama et al., 2002). The full-size test specimen consisted of two piles embedded in an attendant length of concrete pile cap. One pile in the model was loaded laterally in the strong direction of the H-pile; the second pile, in the weak direction of the H-pile. The cap had a nominal depth of 36 inches, a width of 39 inches, and it was 94 inches long. The cap was reinforced with #9 bars nominally 1 foot on center in each direction in each face (corresponding to a steel ratio of 0.5 percent).

The specimen that Shama and his associates loaded along the strong axis of the H-pile experienced a brittle failure in the concrete in the cap. This failure consisted of two wide cracks that ran from the

tips of the flanges of the H-pile to the transverse edge and side faces of the pile cap. This failure was accompanied by a 30 percent loss in strength. The initial damage seen in the specimen loaded along the weak axis of the H-pile consisted of local buckling of the pile immediately adjacent to the cap. As the pile continued to be displaced laterally, the cap experienced a brittle failure, similar to that described above.

In analyzing the connection response, Shama and his associates developed some simple equations to determine the required depth of embedment and amount of tension reinforcement required in the cap to force the connection failure to occur in the pile. These equations are both based on a simple response model in which a pair of compression forces in the cap acting along the embedment length resist the applied moment from the pipe pile. The underlying compression stress distribution was assumed to be linear, with a maximum allowable stress of $0.85 f_c'$. The area of tension steel was calculated by assuming that the cracked concrete could carry no tension, and thus the moment from the pipe pile was equal to the tension resultant in the cap acting at a moment arm equal to two-thirds of the embedment depth. The resulting equations for the moment capacity of the connection based on the capacities of the concrete and the reinforcing steel in the cap were:

$$M_{jc} = \frac{f_c b_f l_{emb}^2}{\left(6 + \frac{l_{emb}}{L^*}\right)} \tag{2.4.1}$$

where

$\begin{aligned}
M_{jc} &= \text{moment capacity of the concrete} \\
f_c &= \text{allowable concrete compressive stress at the extreme fiber} \\
&\quad \text{in the front face of the connection} \\
b_f &= \text{flange width of the pile section} \\
l_{emb} &= \text{embedment depth of the pile} \\
L^* &= \text{distance from the point of application of the lateral load} \\
&\quad \text{to the neutral axis of the joint}
\end{aligned}$

and

$$M_{jt} = \frac{2}{3} A_s f_y l_{emb} \tag{2.4.2}$$

where

$\begin{aligned}
A_s &= \text{area of reinforcing steel} \\
M_{jt} &= \text{moment capacity of the reinforcing steel} \\
f_y &= \text{yield strength of the reinforcing steel}
\end{aligned}$

2.4.1 Summary

A significant amount of work has been done over the past several years on the performance of pile to pile-cap connections under lateral (and axial) loads. The intention of most of this work was determine the load deformation response of these connections during seismic events. A variety of configurations have been tested, from precast concrete piles anchored in reinforced concrete caps, to steel jacketed piles anchored by embedment plates, to steel H-piles embedded in reinforced concrete caps. None of this work, however, directly addresses the concrete filled steel pipe pile to reinforced concrete pile cap connection being investigated in this study. Nonetheless, a lot of the work done by these investigators is pertinent in some way to this investigation. Notably,

1. The response of a system of piles connected by a continuous pile cap often is investigated using a single pile and an attendant length of the cap.

2. Both full and reduced size models have been used in conducting connection investigations.

3. Depending on the relative strength of the pile and the cap, the behavior of the connection can be dominated by failure of one, or the other of these elements. Often, if the pile cap fails, the nature of the failure is less desirable than if the pile fails. Cap failures are not as ductile and dissipate relatively less energy than pile failures.

4. Simple calculations using some measure of allow stresses in the connection materials appear to generate useful results relative to connection capacity.

These observations helped in planning and conducting this investigation, as well as in interpreting the results.

Chapter 3

Experimental Program

3.1   GENERAL REMARKS

Ideally, to study the behavior of the steel pipe pile to pile cap connection under dynamic lateral loads, a full size bent would be constructed and subjected to the expected in-service load conditions. In the case of seismic demands, the applied "load" would consist of the base accelerations expected during the design earthquake, which would then be applied to the structure using a shake table. In the absence of the considerable resources required to conduct tests of this kind, a test program was designed to investigate the connection behavior at substantially less expense. The decision was made to reproduce in the laboratory the critical stress conditions that would actually develop in the field in a full bent at the pile to cap connections under dynamic lateral loads by using a reduced size model of part of the bent subjected to quasi-static loads.

A total of five models were formally tested as part of this investigation, as described in Table 3.1. The intended variable between the tests was the amount and placement of the reinforcement in the pile cap, although in the final program, the strength of the steel pipe pile and of the concrete also varied in some tests. In general, the amount of reinforcement in the cap was increased in each test, starting with a model depicting current practice, up to a model with 7 times this amount of reinforcing steel, which failed through formation of a plastic hinge in the pipe pile rather than in the cap. Development of the general geometry of the test article used in this investigation is presented below, followed by a more detailed description of the pipe pile, reinforcing steel, and concrete used in each model. The general manner in which the tests were conducted is then described, and finally the results obtained during each test are presented.

Table 3.1: Test Matrix

Item	Pipe Pile Wall Thickness, in	Longitudinal Steel Ratio[a], %	Transverse Steel Ratio[a], %	Yield Strength of Pile Steel[b], psi	Concrete Strength[b], psi	Comments	Reinforcing Layout
Full Size	0.5	0.40	0.09	35,000	4,000[b]	Timber Creek Bridge, Powder River County, MT	
PC-1	0.32	0.41	0.09	53,000	4,832	Relative amount of reinforcement similar to that in full size structure	
PC-2	0.25	0.41	0.09	56,000	5,326	Same reinforcement as in PC-1, reduced wall thickness for pipe pile	
PC-3	0.25	1.09	0.24	53,000	3,150	Reinforcement increased by a factor of 3 compared to PC-1, concrete strength noticeably low compared to other models	
PC-3a	0.25	2.11	0.65	53,000	3,945	Reinforcement increased by a factor of 5 compared to PC-1	
PC-4	0.25	2.83	0.70	60,000	4,682	Longitudinal reinforcement increased by a factor of 7 compared to PC-1	
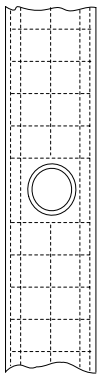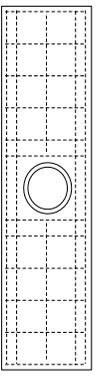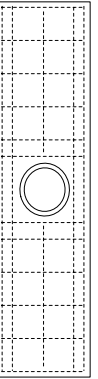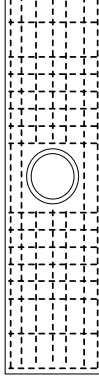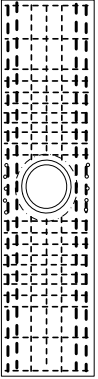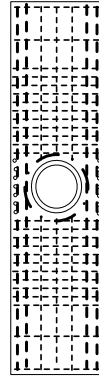
[a] see Figure 3.5 for specific manner in which these ratios were calculated
[b] actual strengths at time of test reported for models, minimum design values reported for full size bridge

3.2   MODEL CONFIGURATION

The behavior of a single interior steel pipe pile to concrete cap connection was modeled in this investigation. The deflected shape of a complete bent under lateral loads as determined by an elastic 2-D analysis is shown in Figure 3.1. As might be expected, the behavior of the interior of the bent is repetitive in nature, with fairly regularly spaced points of inflection occurring in the cap at the mid-point between the piles, and approximately at mid-height of each pile. Thus, the behavior of an interior connection can be characterized using a model bounded by these points of inflection, as shown in Figure 3.1.
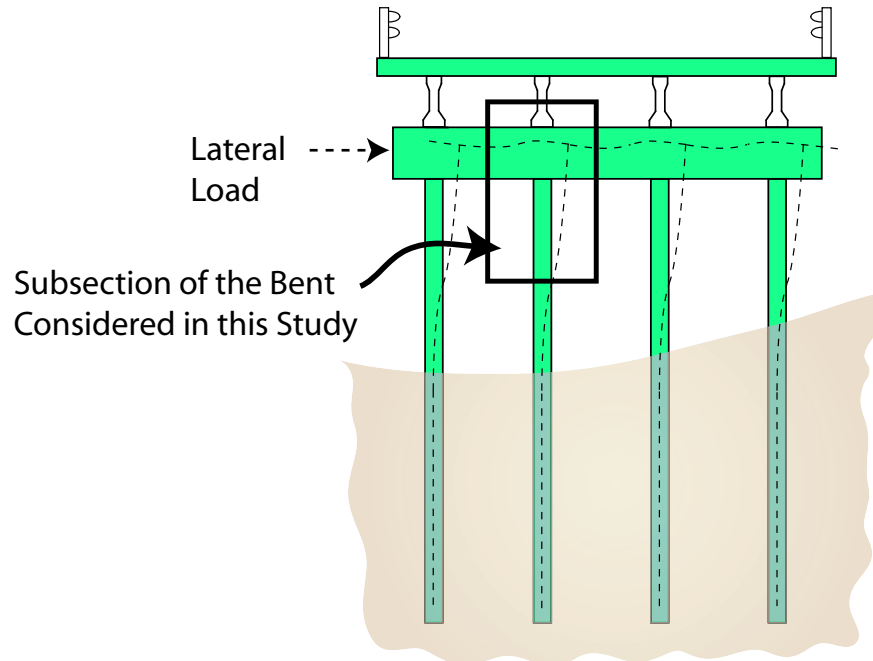
Figure 3.1: Section of the Bent Used to Study the Behavior of the Pile to Pile Cap Connection

The actual model selected for testing was a $1/2$ size representation of the section of the full bent identified above. While it would have been desirable to test a full size model to avoid the introduction of scaling uncertainties, even this subsection of the bent was large in size and capable of carrying considerable force. In light of the capacity of the structural testing facilities at MSU, and in the interest of reducing costs, the $1/2$ size model was selected. At this scale, it was judged that conventional concrete and reinforcing steel could be used in model construction.

Each $1/2$ size model consisted of a single pile embedded in the center of a section of pile cap, as shown in Figure 3.2. The over-all dimensions of each model were the same, and they were specifically patterned after the pile and cap configuration used in the bridge over Timber Creek on County Route 38218 in Powder River County, MT (Federal Aid Project BR9038(9)). The model geometry was simply determined by multiplying the dimensions of the full size structure by one-half. The pile cap in the resulting model was 18 inches square in cross-section, and had an effective length (between points of support) of 4.24 feet. Note that the length of the model did exceed one-half of the centerline to centerline spacing of the piles in the full size structure. While the piles were spaced at 6.67 ft on-center in the Timber Creek Bridge, which would translate to a model length of 3.33 feet, the actual effective length of the model was increased to 4.24 feet to a) mitigate any influence of the supports on

14
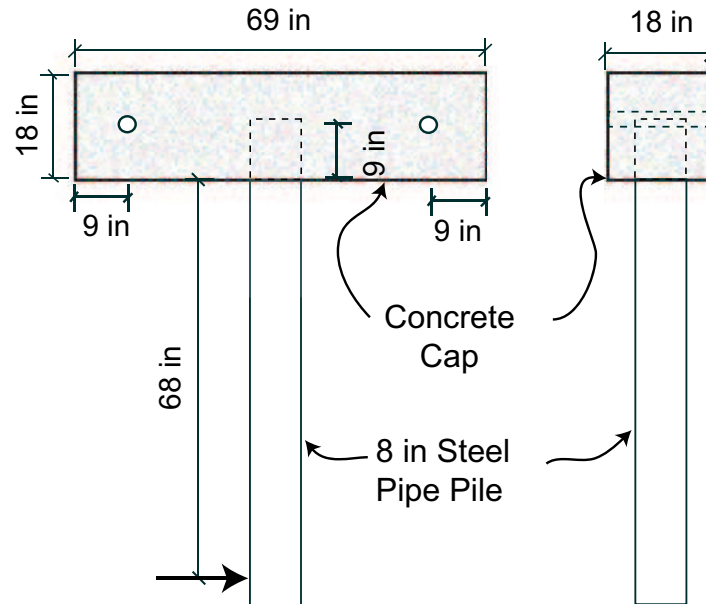
Figure 3.2: Model Geometry

the connection zone and b) accommodate the tie down points available in the test facility. The pipe pile in the model had a nominal diameter of 8 inches, and it was embedded mid-depth into the cap.

In designing the models, the concrete in the full size structure was assumed to be MDT's Class AD mixture (MDT, 1995), which has a design strength of 3400 psi (for full payment). In light of probable over-strength of the concrete due to conservatism in the mix design and long term strength gains, the target strength of the concrete used in the models was 4000 psi. The conventional reinforcing steel used in both the full size structure and the models was Grade 60. Based on MDT's standard specifications (1995), the pipe piles in the full size structure were assumed to be ASTM A252 Grade 2 steel, which has a minimum tensile yield strength of 35,000 psi. The pipe piles used in the models were made of ASTM A53 Grade B steel, which also has a minimum yield strength of 35,000 psi. The actual yield strength of this steel, as determined by coupon tests, is given in Table 3.1. These yield strengths are clustered around an average value of 55,000 psi.

3.2.1   Pile Cap Model 1 (PC-1)

The location of the reinforcing steel in the pile cap of the first model (designated model PC-1) was directly scaled from the full size structure. The layout of the reinforcing steel in this model is shown in Figure 3.3. The completed reinforcing cage is pictured in Figure 3.4. This layout for the reinforcing steel provided the same steel ratio in the longitudinal and transverse directions in the model of the cap as in the actual structure (as reported in Table 3.1). By matching the location and amount of steel in the model in this fashion, it was believed that similar stress conditions would be generated in the concrete in the model of the cap as would be generated in the full size structure.

The specific manner in which the gross steel ratios were determined in the longitudinal and transverse directions is shown in Figure 3.5. Note that the location as well as the amount of longitudinal steel in the cap may be critical to its performance. While the global moment demands in the cap may be reasonably satisfied using the same amount of longitudinal steel in its top and bottom faces, the

All dimensions in inches

2 1/4 steel sleeve

68

4 @ 6
=24

3

1 in clear cover, outside
1 1/2 in clear around pipe

18

3 @
5
= 15

18.00

3 longitudinal
bar

3 circular hoop

2 rectangular
transverse tie

8.625 inch outside diameter,
steel pipe, filled with concrete
0.32 inch wall - Model PC-1
0.25 inch wall - Model PC-2
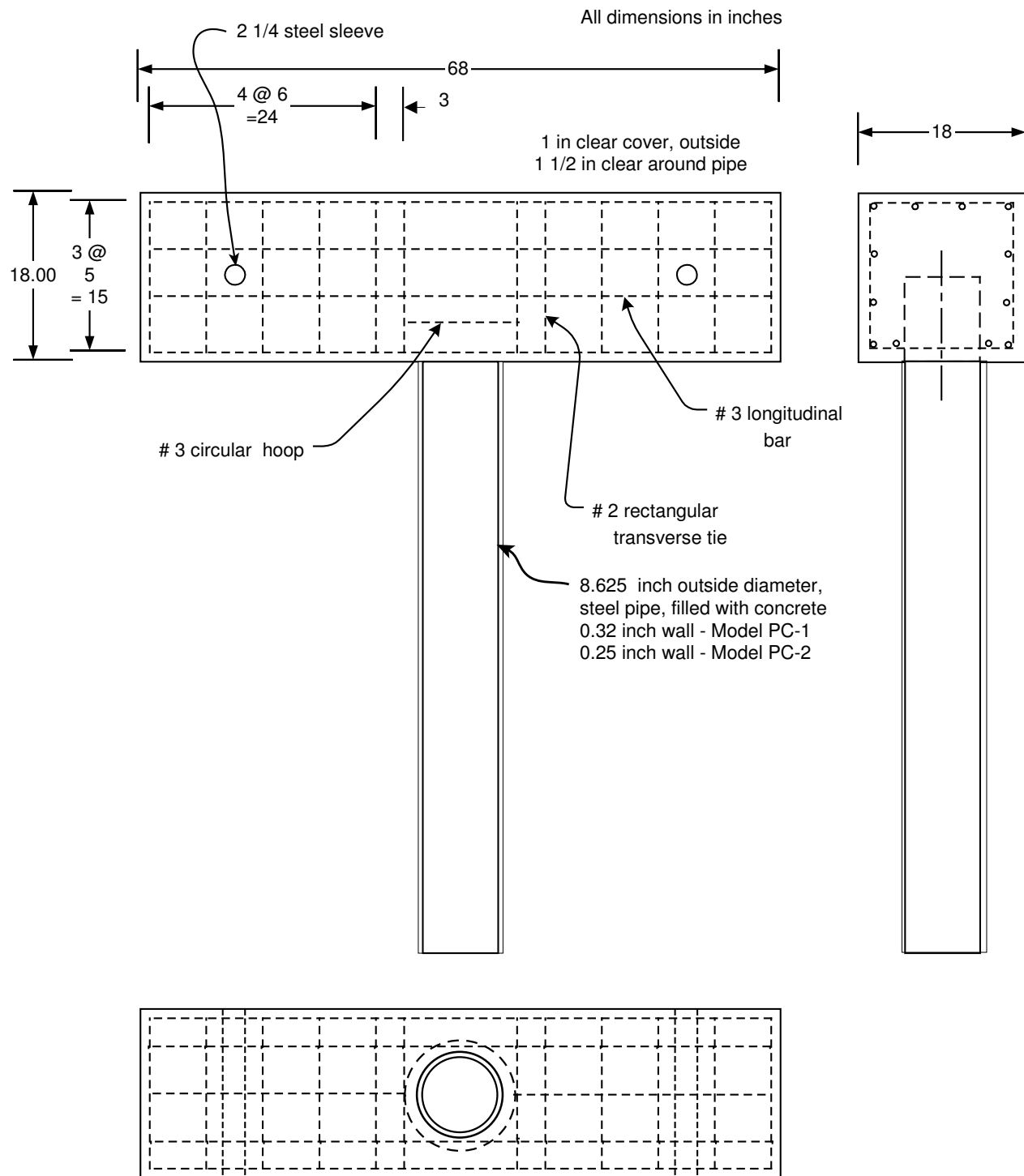
Figure 3.3: PC-1 & PC-2 Reinforcing Details

longitudinal steel required in the bottom face of the cap may also be influenced by the localized load demands immediately in the pile embedment zone. The decision was made therefore to represent the amount of longitudinal steel in the cap using a longitudinal steel ratio calculated for a cross section extending from the bottom face of the cap to the tip of the embedded pile. Note that the distribution of the longitudinal steel in the models used in this investigation (as well as in the full size caps shown in Figure 2.2) was fairly uniform between the top and bottom faces of the cap, so the steel ratios
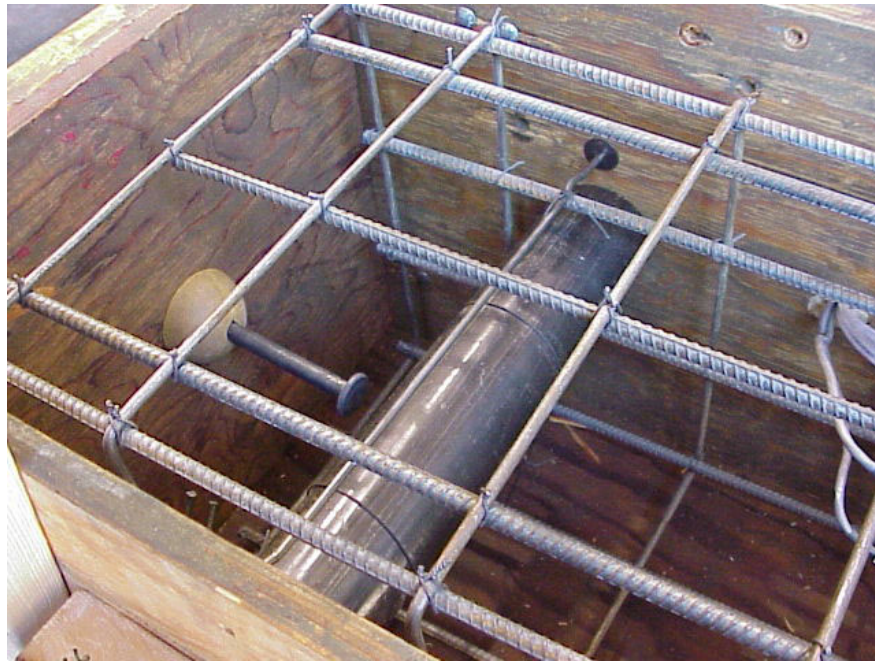
Figure 3.4: PC-1 & PC-2 Reinforcing Cage

calculated for the embedment zone and for the entire cross-section were within 10 percent in magnitude. Finally, a further decision was made to only include bars in this calculation that were anchored sufficiently to develop their yield capacity. Thus, for example, the longitudinal bar in the bottom face of Model PC-1 that intersected the pipe pile was not included in the calculation of the longitudinal steel ratio.

The resulting reinforcement in model PC-1 consisted of #3 longitudinal bars spaced at approximately five inches on center around the perimeter of the cap, #2 transverse ties spaced at approximately six inches along the length of the cap, and a single #3 hoop that encircled the pile in the embedment region. The steel ratios in the longitudinal and transverse directions were 0.41 and 0.09 percent, respectively. Problems were encountered in purchasing #2 reinforcing bar for the transverse ties. While a local steel supplier indicated this bar was available, it was discovered that only plain bars (no deformations) were available in the #2 size. Concerns were raised about the ability of these bars to develop adequate anchorage in the concrete, so a general search was conducted for a substitute bar that would offer approximately the same steel material properties and surface texture as conventional reinforcing steel. No reasonable substitute bar was found. The closest substitute was determined to be all-thread rod, in which deformations were created by intermittently removing the threads, leaving single threads (deformations) at regularly spaced intervals along the length of the bar. The all-thread also had to undergo a simple heat treatment to create the stress-strain properties of Grade 60 reinforcing steel. Thus, turning all thread-rod into #2 reinforcing became a relatively expensive endeavor.

The decision eventually was made to use plain bars fabricated with mild steel (yield strength of 53,000 psi) for the ties in the pile cap in the first model. The predicted stress level in the ties was low, and the geometry of the bars (closed hoops with hooked ends) was expected to provide adequately for their anchorage. The reinforcing cage in the actual Timber Creek Bridge also included three #4 hoops that encircled the pipe pile in the embedment zone. Initially, the decision was made to use two #2 hoops to represent these bars in the model. Stresses in this area were predicted to be relatively high,

17
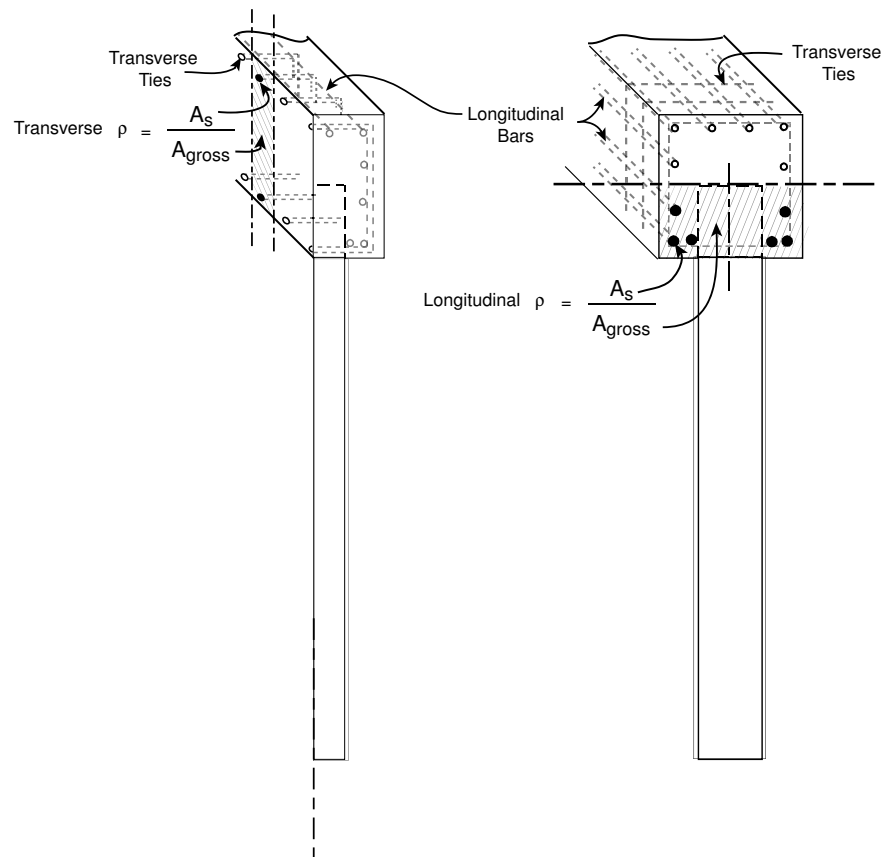
Figure 3.5: Longitudinal and Transverse Steel Ratios in the Pile Cap

and in light of concerns about anchorage, the decision was made to use a single #3 deformed bar to replace the two smooth #2 hoops.

In sizing the pipe pile in the test specimen, the intention was to keep the relative bending strength of the pile compared to the cap on the same order of magnitude as in the full size structure. The failure behavior of the connection was expected to be directly related to the relative strength of these two components. In this case, whether the connection failed through formation of a plastic hinge in the pipe pile or local failure of the cap in the connection zone would be controlled by the relative strengths of the two components.

The bending strength of the concrete filled pipe pile was calculated using the approach given in the Recommended LRFD Guidelines for the Seismic Design of Highway Bridges (ATC/MCEER, 2001). This capacity equation, based on theoretical mechanics and experimental testing, takes into account the composite behavior of the steel shell and the concrete, as appropriate:

$$M_{rc} = \phi_f \left[C_r e + C_r' e' \right] \tag{3.2.1}$$

where ϕ_f is a capacity reduction factor and

$$C_r = F_y\beta\frac{Dt}{2} \tag{3.2.2}$$

$$C_r' = f_c'\left[\frac{\beta D^2}{8} - \frac{b_c}{2}\left(\frac{D}{2} - a\right)\right] \tag{3.2.3}$$

$$e = b_c\left[\frac{1}{(2\pi - \beta)} + \frac{1}{\beta}\right] \tag{3.2.4}$$

$$e' = b_c\left[\frac{1}{(2\pi - \beta)} + \frac{b_c^2}{1.5\beta D^2 - 6b_c(0.5D - a)}\right] \tag{3.2.5}$$

$$a = \frac{b_c}{2}\tan\left(\frac{\beta}{4}\right) \tag{3.2.6}$$

$$b_c = D\sin\left(\frac{\beta}{2}\right) \tag{3.2.7}$$

Then β is in radians and can be found via the following recursive equation:

$$\beta = \frac{A_sF_y + 0.25D^2f_c'\left[\sin(\beta/2) - \sin^2(\beta/2)\tan(\beta/4)\right]}{(0.125D^2f_c' + DtF_y)} \tag{3.2.8}$$

Relative to the specific values for these various parameters used in this calculation, the full size steel pipe piles were assumed to have an outside diameter of 16 inches and a 1/2 inch wall thickness (Timber Creek Bridge). The yield strength of the pipe pile steel was assumed to be 35,000 psi, and 4,000 psi was used for the unconfined compression strength of the concrete. Based on these values, the plastic moment capacity of a full size pile was calculated to be 397 ft-k. Note that the 15 k load applied axially to the pipe pile was ignored in this calculation, as it represented less than 3 percent of the axial load carrying capacity of the pipe pile.

The capacity of the concrete cap was calculated using a simple model of the internal force resultants that develop in the concrete as the steel pipe pile tries to rotate along the embedment length. This model is shown in Figure 3.6. Two moment capacity equations were considered: 1) an equation based on a simple rectangular Whitney stress block (which is similar to the approach used by MDT in modeling the behavior of this zone), and 2) an equation suggested by Marcakis and Mitchell (1980) that takes into account to a limited extent the parabolic shape of the stress block that develops in the concrete. Both approaches yielded similar results; only the results from the Marcakis and Mitchell equation are presented herein. The equation, which calculates the lateral load that can be applied to the embedded part, states:

$$V_c = \frac{0.85f_c'bl_e}{1 + 3.6(e/l_e)}, \tag{3.2.9}$$

where the variables in the equation are defined in Figure 3.7. The cap moment capacity was calculated by multiplying the lateral load determined from this equation by its moment arm. In completing this calculation, the steel pipe pile was assumed to be embedded 18 inches into the cap (equivalent to one-half the depth of the pile cap), and the lateral load was assumed to be applied at a moment arm of 144 inches. Note that confined concrete can develop significantly greater compression strength than unconfined concrete. For reinforced concrete, this strength enhancement is a function of the effectiveness of the reinforcing steel in providing confinement to the concrete. For the purposes of
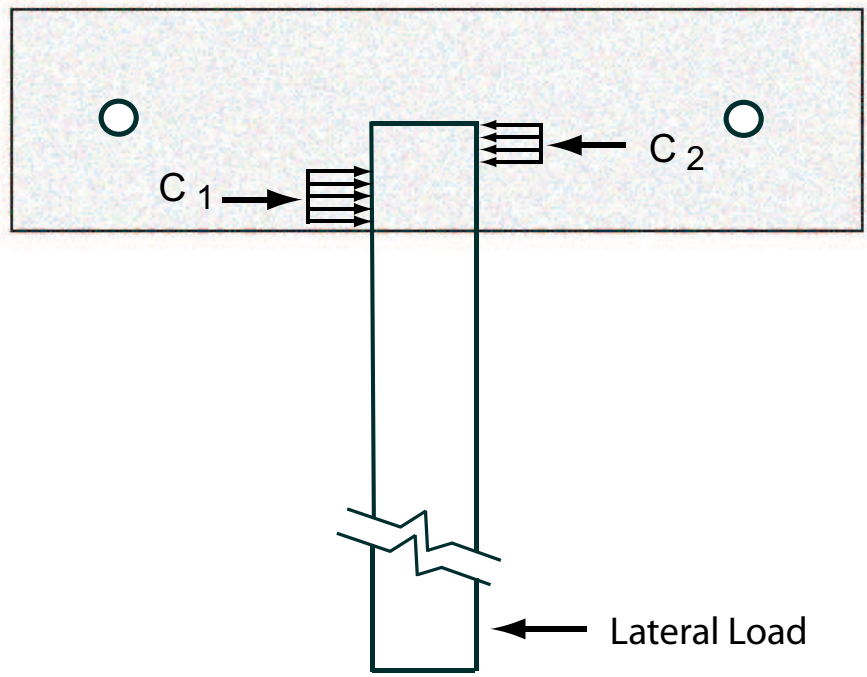
Figure 3.6: Simple "Hand" Model of Stresses in the Connection Zone from the Lateral Load
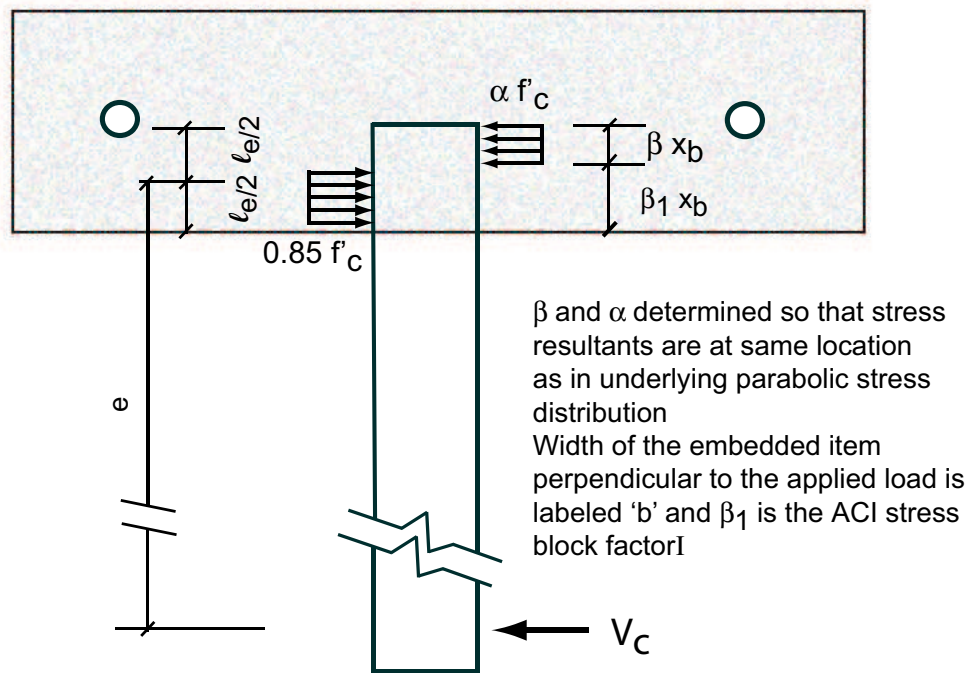
Figure 3.7: PCI Analysis Model

this calculation, it was assumed that any such effect would be similar in the full structure and the 1/2 size model. The capacity of both systems was simply calculated using the unconfined compression strength of the concrete (assumed to be 4,000 psi). The local moment capacity of the cap in the connection zone was calculated to be 370 ft-k.

Thus, in the full size model, the ratio of the bending strength of the concrete filled steel pipe pile to the pile cap was found to be 1.07 (equal to 397 ft-k/370 ft-k). The intent in sizing the steel pipe pile for the test specimen was to generate this same strength ratio between the components of the 1/2 size model. Dimensionally, it was deemed reasonable in the model to target an embedment depth equal to one-half of the depth of the cap (as is commonly done in the full size structure). Therefore, a target embedment depth of 9 in was used. Similarly, it was deemed reasonable to use a pipe pile nominally one-half the diameter of the pipe pile in the full size structure, which in this case would be 8 inches. Eight inch steel pipe, with an actual outside diameter of 8.625 inches, was selected for the steel pipe pile in the model. With these dimensions established, the wall thickness of the pile was varied to obtain the desired ratio of pipe pile to pile cap bending strengths.

Assuming concrete with an unconfined compression strength of 4000 psi and a moment arm of 72.5 inches, the moment capacity of the pile cap in the model was found to be 50 ft-k . The moment capacity of an 8 inch concrete filled steel pipe, calculated using the equation presented above, was found to be 45, 58, and 73 ft-k, respectively, for wall thicknesses of 0.19, 0.25, and 0.32 inches. These moment capacities result in pipe pile to pile cap strength ratios of 0.90, 1.16, and 1.46 for the 0.19, 0.25, and 0.32 inch wall thicknesses, respectively. While either the 0.19 or 0.25 inch wall thickness pipe piles appear to be reasonable choices for test specimens, model PC-1 was constructed with a 0.32 inch wall thickness pipe pile as a result of an error in the original sizing calculation. Thus, the pipe pile in model PC-1 was substantially stronger in bending compared to the pile cap relative to the relative strength ratio of these elements in the full size structure.

Model PC-1 was cast an inverted position, with pipe pile straight up and down. The pile cap was cast first. As the concrete in the cap began to set, the pipe pile was filled. All the models were cast following this same procedure, using concrete purchased from local readi-mix suppliers. Typical photographs of a model prior to casting are presented in Figure 3.8. On test day, the unconfined compression strength of the concrete in model PC-1 was 4,832 psi (compared to a target value of 4,000 psi).

a) Overall View of Casting Operation

b) Close-up of Pipe Pile and Reinforcing Cage

Figure 3.8: Concrete Being Placed in a Typical Model (Model PC-4 Shown)

3.2.2   Pile Cap Model 2 (PC-2)

The primary difference between the first and second pile cap models was the strength of the steel pipe pile. The second model was constructed with an 8 inch steel pipe with a wall thickness of 0.25 inches, compared to the 0.32 wall thickness used in model PC-1. Thus, the relative ratio of the moment capacity of the pipe pile to the local moment capacity of the pile cap in the embedment region was believed to better match that of the full size structure relative to the pile used in model PC-1. The reinforcing cage was identical to that used in model PC-1. On test day, the concrete test cylinders cured with the model had an unconfined compression strength of 5,326 psi (10 percent higher than in model PC-1).

3.2.3   Pile Cap Model 3 (PC-3)

In light of the connection performance observed in the first two tests (as reported in more detail below, the steel pipe pile was relatively undamaged, while the concrete in the cap experienced extensive cracking), and in concert with MDT, the decision was made to increase the percentage of reinforcing steel used in the pile cap in model PC-3. In determining how much more reinforcing steel should be placed in the model, consideration was given to the minimum and maximum steel areas traditionally suggested in flexural members, and to the specific demands placed on the cap by the pipe pile. The longitudinal reinforcing steel in the second model (PC-2) comprised 0.41 percent of the gross cross-sectional area. According to bridge and building codes (AASHTO, 2000; ACI, 2002), the minimum steel ratio required for flexural members in the absence of a detailed calculation is approximately 0.40 and 0.58 percent, respectively (calculated on the gross cross-section, for fully reversed loads, assuming Grade 60 reinforcing steel). These limits were established based on the amount of steel necessary to carry the load transferred to the steel when/if the concrete cracks in flexural tension. In this case, the concrete clearly was cracking at failure of the connection, and it seemed necessary to more than satisfy these minimum steel ratios, if the post-cracking deformations in the reinforcing steel and the cap were to be reduced.

There is a limit on the maximum amount of steel that can be put in a member and still allow for placing and consolidating the concrete in the member. Experience has shown that constructibility problems may arise if the steel ratio exceeds around 2.5 percent (even though bridge and building codes allow up to 8 percent steel in column cross-sections).

Thus, for the pile cap, suggested steel limits ranged from a value greater than 0.4 to 0.6 percent to a value of less than approximately 2.5 percent of the cross-section. Within this range, the exact amount of steel required was further evaluated based on the specific structural demands placed on the cap. In this case, the design demand on the cap was calculated for the situation when the lateral load applied at the tip of the pipe pile produced a moment in the pile at the face of the cap equal to its plastic moment capacity (i.e., the cap was to be designed so that failure (loss of load carrying capacity) would occur first in the pipe pile rather than in the cap). Earlier predictions of the capacity of the cap focused on a failure mechanism in which the concrete crushed along the embedded length of the pile. Calculations were now done that focused on a failure mechanism in which the reinforcing steel in the cap yielded in tension. Similar to the approach followed by Shama et al. (2002), these calculations were performed by extending the simple models introduced in Figure 3.6 and Figure 3.7 above to address the internal tension resultants that develop in the cap in the immediate vicinity of the pipe pile. The compression resultants identified above were assumed to react against the reinforcing steel, thus generating tension forces of this same magnitude in these bars (this approach inherently

neglects the tensile capacity of the concrete, and further ignores any complexities introduced into the load paths by the support pins and the specific geometry of the reinforcing cage). The area of longitudinal reinforcing steel required in the face layer of the cage was then simply calculated as the compression resultant divided by the allowable stress in the steel:

$$C = T = A_s f_y \tag{3.2.10}$$
$$A_s = C/f_y \tag{3.2.11}$$

This equation was solved for the area of reinforcing steel required to carry the resultant compression force in the cap when the demand from the pipe pile was equal to its plastic moment capacity. For this calculation, the moment capacity of the steel pipe pile was calculated using the as-measured strength of the pipe pile steel, which was found to be 53,000 psi, and an assumed concrete strength of 4,000 psi. The resulting moment capacity of the steel pipe pile was calculated to be 84 ft-k. This moment was then assumed to be carried by a pair of resultant compression forces in the concrete, spaced at a distance equal to 2/3 of the depth of embedment of the pipe pile (in this case, 6 inches). The magnitude of the resultant compression forces was found to be 168 kips, and the corresponding area of steel required to carry this resultant (at yield) was found to be 2.8 square inches. This amount of longitudinal steel was required across the embedment zone, alone, to balance the resultant compression force in this region of the cap. The corresponding longitudinal steel ratio (calculated across the depth of embedment) was 1.73 percent.

Ultimately, the decision was made to use 1.09 percent longitudinal reinforcing steel in the PC-3 model. This amount of steel fell comfortably in between the 0.41 percent steel used in both the PC-1 and PC-2 models and the 1.73 percent steel suggested by the simple analysis discussed above. Note that a more sophisticated strut and tie based model of the problem (described in more detail in the analysis section of this report) did produce similar results to the simple analysis; it indicated that a longitudinal steel ratio of 1.57 percent was required for a balanced failure in the pipe pile and the cap. The transverse steel was increased in proportion to the longitudinal steel, from 0.09 percent in models PC-1 and PC-2 to 0.24 percent in model PC-3. Note again, that the more sophisticated strut and tie model referenced above also indicated that the transverse steel area had to be increased for the cap to provide additional moment resistance.

Details of the reinforcing cage in model PC-3 are shown in Figure 3.9. The completed cage is pictured in Figure 3.10. The longitudinal steel consisted of #4 bars nominally spaced at 2 1/2 inches on-center around the perimeter of the cap. The transverse steel consisted of #3 ties spaced at 3 inches on-center in the region adjacent to the pipe pile. The single #3 hoop that encircled the pipe pile in models PC-1 and PC-2 was replaced by a #3 spiral consisting of a single twist over a length of approximately 9 inches and terminated with a full hoop at each end.

While the concrete in model PC-3 was purchased from the same supplier as was used for models PC-1 and PC-2, early strengths were considerably below expected values. The entire model was subsequently submerged in a lime solution in an effort to promote thorough curing and optimum strength gain. Some improvement in strength was realized in this process, although on test day, the unconfined compression strength of the concrete was only 3,150 psi approximately 65 percent of the strength of the concrete in model PC-2).

All dimensions in inches

2 1/4 steel sleeve

68

5 @ 3
= 15

3@
6
=18

1 in clear cover, outside
1 1/2 in clear around pipe

18

6@
2.5
=15

18.00

4 longitudinal
bars

3 rectangular
transverse ties

3 spiral

8.625 inch outside diameter,
steel pipe, filled with concrete
0.25 inch wall
(same as in Model PC-2)
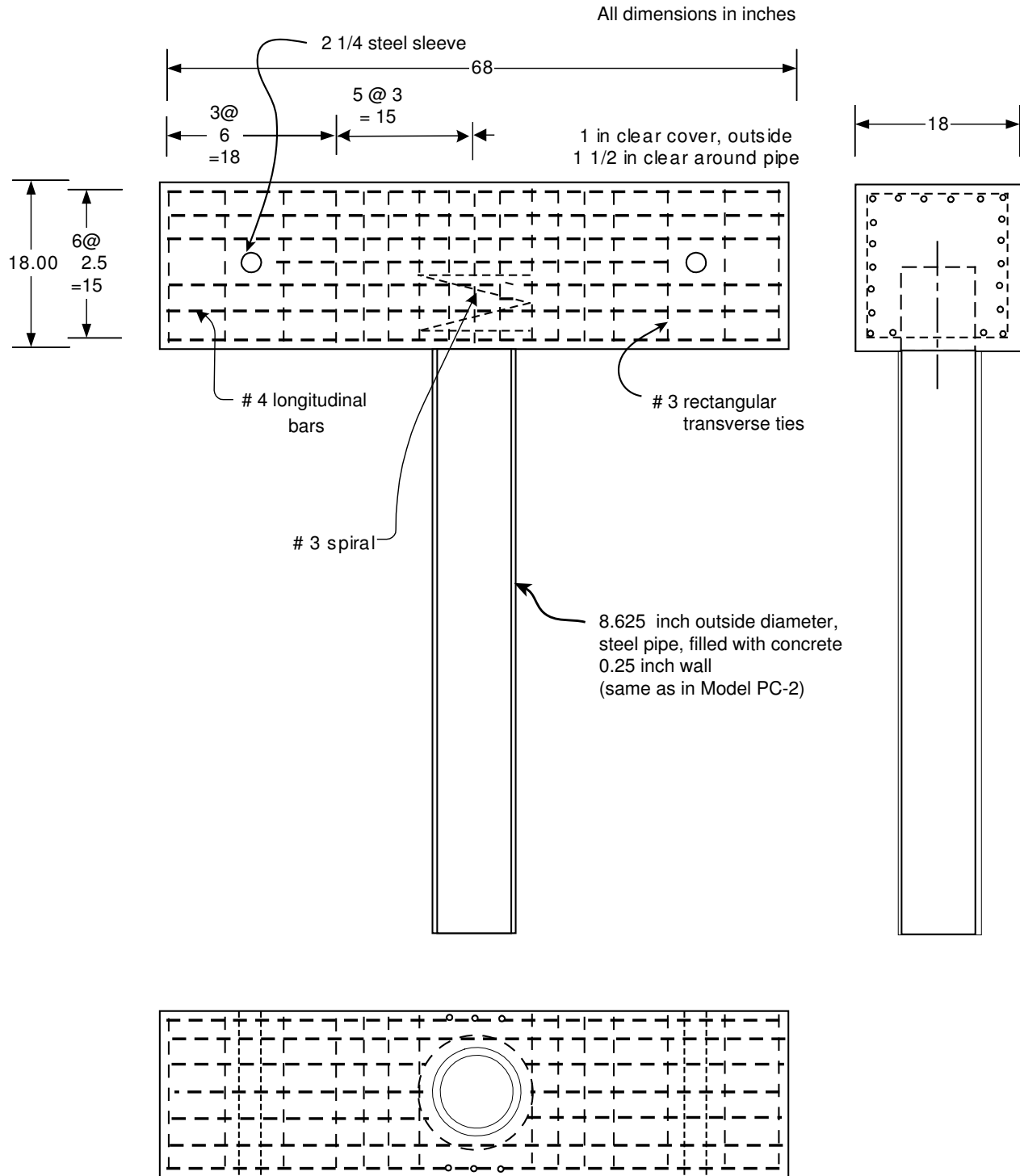
Figure 3.9: PC-3 Reinforcing Details
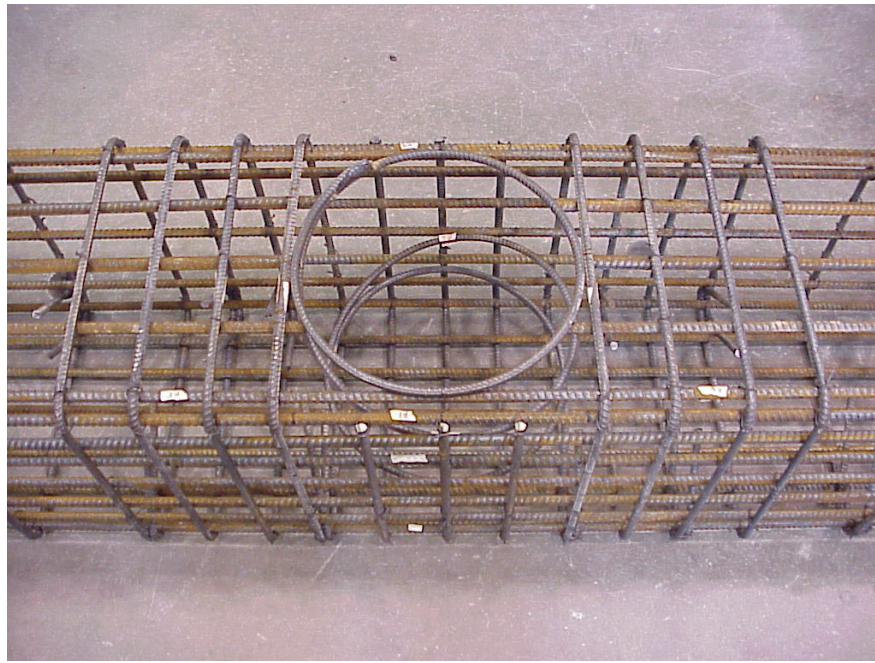
Figure 3.10: PC-3 Reinforcing Cage

3.2.4   Pile Cap Model 3a (PC-3a)

The decision was made following the third pile cap test to further increase the area of longitudinal steel in the pile cap, approximately to the level suggested by the simple calculation described above. This calculation does not address the area of transverse steel required in the cap. Therefore, similar to model PC-3, the decision was made to increase the area of this steel at least in proportion to the increase in the longitudinal steel. Specifically, the decision was made to place the transverse ties at a spacing approaching the minimum value at which concrete could still be placed in the model. The resulting longitudinal and transverse steel ratios in model PC-3a were 2.11 and 0.65 percent, respectively. The details of the reinforcing cage in the pile cap for Model PC-3a is shown in Figure 3.11. The actual reinforcing cage is pictured in Figure 3.12. The longitudinal steel consisted of #6 bars at approximately 3 inches on center along the sides of the pile cap. The longitudinal bars that intersected the pipe pile (a total of 3 bars) were #4 bars. Unlike earlier models, these bars were hooked through the depth of the cap, rather than simply being stubbed off at the face of the pile (see Figure 3.13). These bars were hooked through a new full depth spiral (#3 bar, with a pitch of approximately 1.75 inches) that encircled the steel pipe pile. The transverse steel consisted of #3 ties spaced at approximately 2 inches on center. The unconfined compression strength of the concrete in model PC-3a was 3945 psi on test day.

All dimensions in inches

8 @ 2
= 16

1 in clear cover, outside
1 1/2 in clear around pipe

68

12

18.00   15

18

6 longitudinal
bars

3 rectangular
transverse ties

3 longitudinal bars
hooked through
spiral

3 spiral

8.625 inch outside diameter,
steel pipe, filled with concrete
0.25 inch wall
(same as in Model PC-2,3)
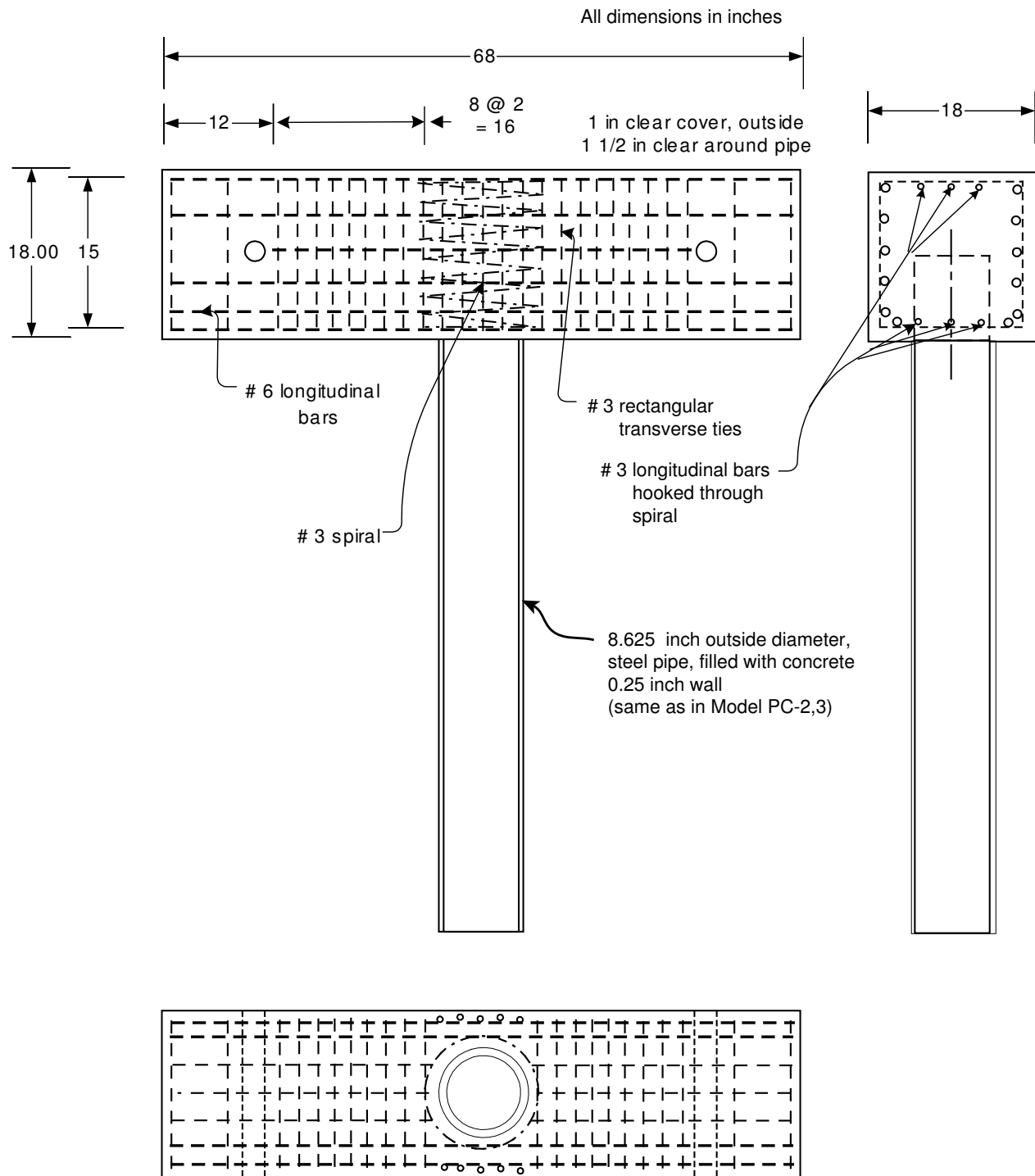
Figure 3.11: PC-3a Reinforcing Details
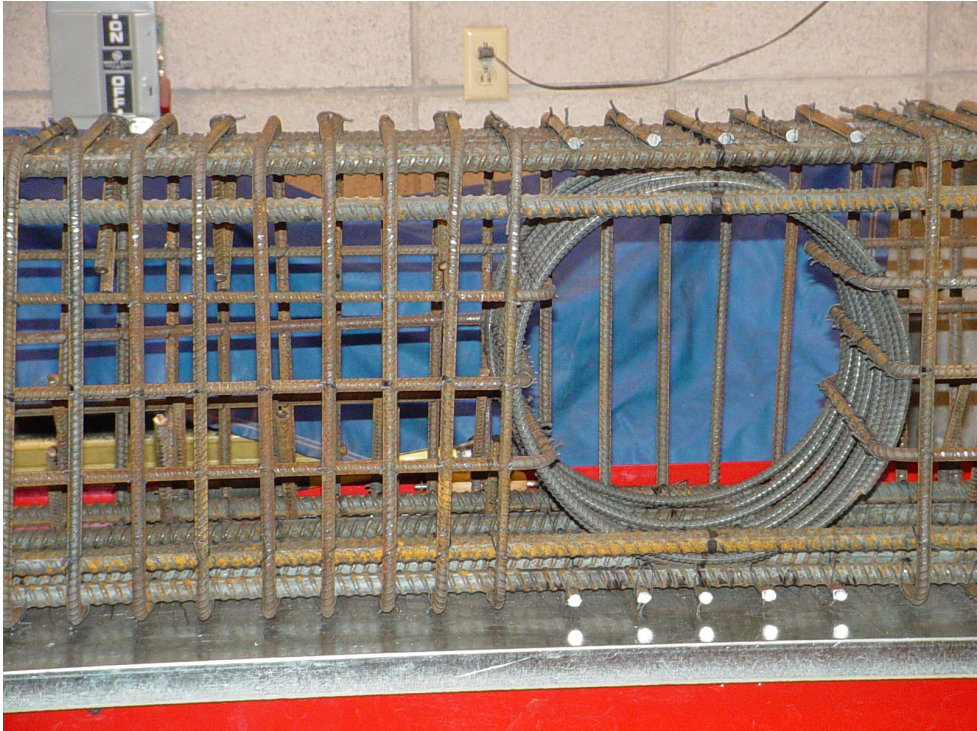
a) Side View

b) End View

Figure 3.12: PC-3a: Reinforcing Cage

Figure 3.13: PC-3a View of Longitudinal Bars That Were Hooked Through the Embedded Spiral

3.2.5   Pile Cap Model 4 (PC-4)

In selecting the reinforcing steel in the final pile cap test, the decision was made to closely approach the limit on the maximum amount of steel that can be placed in the cap based on constructibility concerns. As previously mentioned, the maximum amount of reinforcing steel that can be placed around the perimeter of a cross section without encountering congestion problems is on the order of magnitude of 2.5 percent of the gross cross-sectional area. In the final pile cap model, the longitudinal steel ratio across the embedment depth was 2.83 percent. The reinforcing cage, detailed in Figure 3.14, consisted of #7 bars at approximately 3 inches on center on the sides of the cap, with #4 bars, also spaced at approximately 3 inches on center, hooked through a full depth spiral on the top and bottom faces of the cap. In a major departure from earlier cap models, the bottommost #7 "longitudinal" bars were actually "U" shaped. These bars looped around the steel pipe pile just under the surface of the cap concrete where the pipe pile exited the cap. These bars were expected to be optimally positioned to help resist rotation of the pipe pile within the pile cap. The transverse reinforcing ratio in model PC-4 was 0.70 percent. This steel consisted of #3 hoops spaced at approximately 1.77 inches on center. This amount of steel once again was close to the maximum amount of confining steel that could be used around the perimeter of the cap and still be able to place the concrete in the cap. The completed reinforcing cage for model PC-4 is shown in Figure 3.15.   The unconfined compression strength of the cap concrete was 4,682 psi on test day.

All dimensions in inches

68

11

26 @ 1.77

18

18   15

7 lontitudinal bars

3 rectagular transverse ties

#3 spiral starts below longitudinal U bars

4 longitudinal bars hooked through spiral

8 inch pipe
78 inches long
including 9 in embedded
wall t = 0.25 in
(same as Test 2, 3, 3a)

1 in clear cover outside
1 1/2 in clear around pipe

7 U bar circles pipe pile 1 1/2 in clear
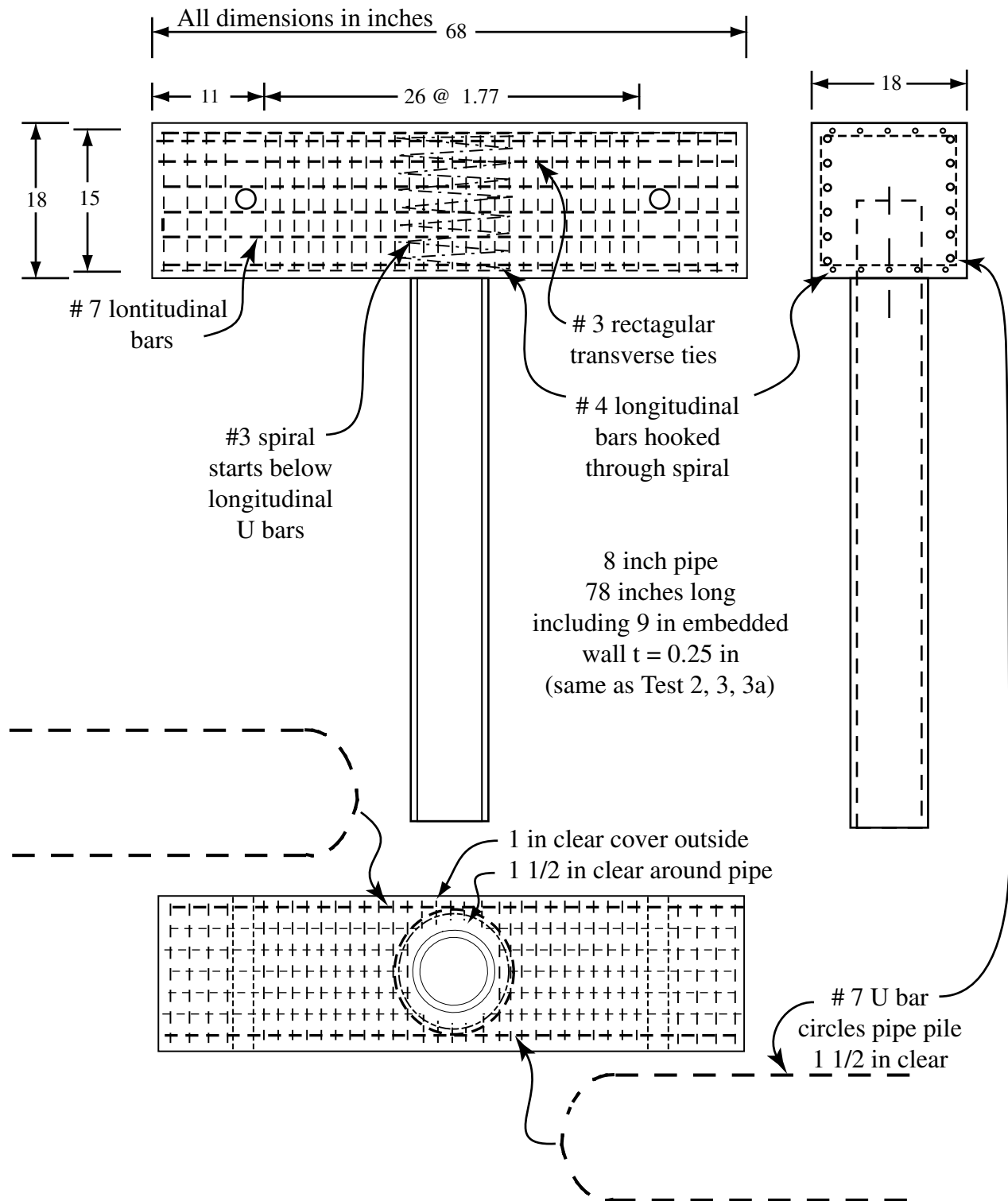
Figure 3.14: PC-4 Reinforcing Details
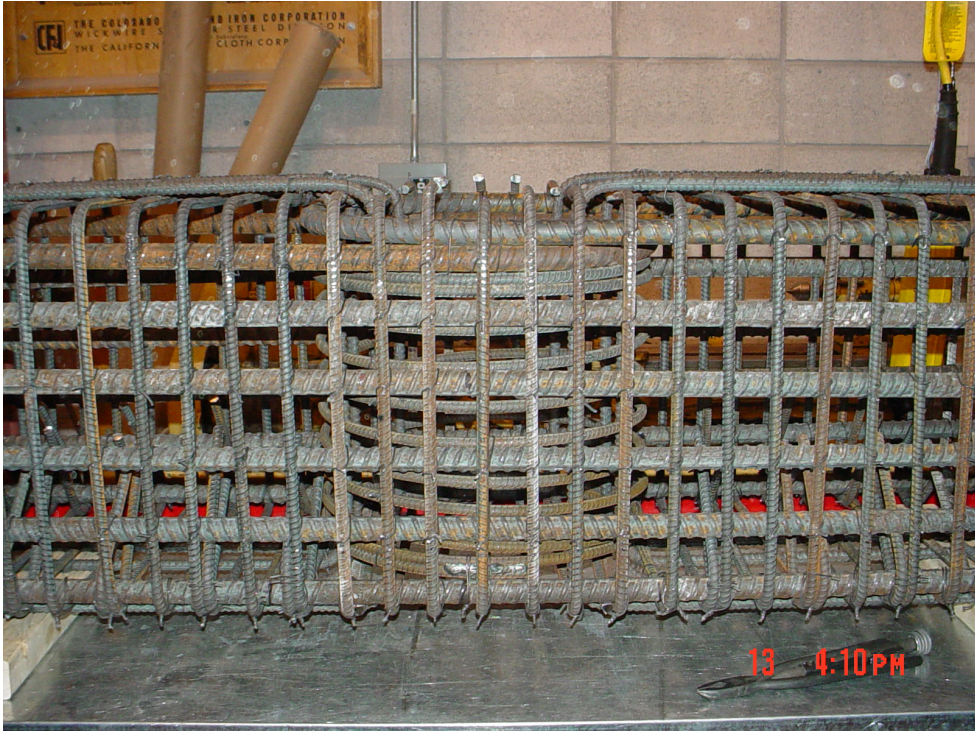
a) Side View

b) End View

Figure 3.15: PC-4 Reinforcing Cage

3.3   TEST SETUP: MODEL SUPPORT CONDITIONS AND APPLIED LOADS

The pipe pile-to-pile cap connection models were tested so as to generate the deflected shape expected in this subsection of a full size bent when it is subjected to a lateral load (see Figure 2.3). While in the actual structure the pile cap displaces laterally while the base of the pipe piles remains relatively stationary, the same deflected shape was generated in these tests by holding the pile cap and displacing the pipe pile. In this regard, the points of inflection in the actual pile cap were considered to be pinned supports in the model, while a lateral point load was applied at the tip of the pipe pile, as shown in Figure 3.16. The frame used to test the models is shown in Figure 3.17. Note that for convenience, the model was tested in the horizontal plane, rather than in the vertical plane of the real structure.
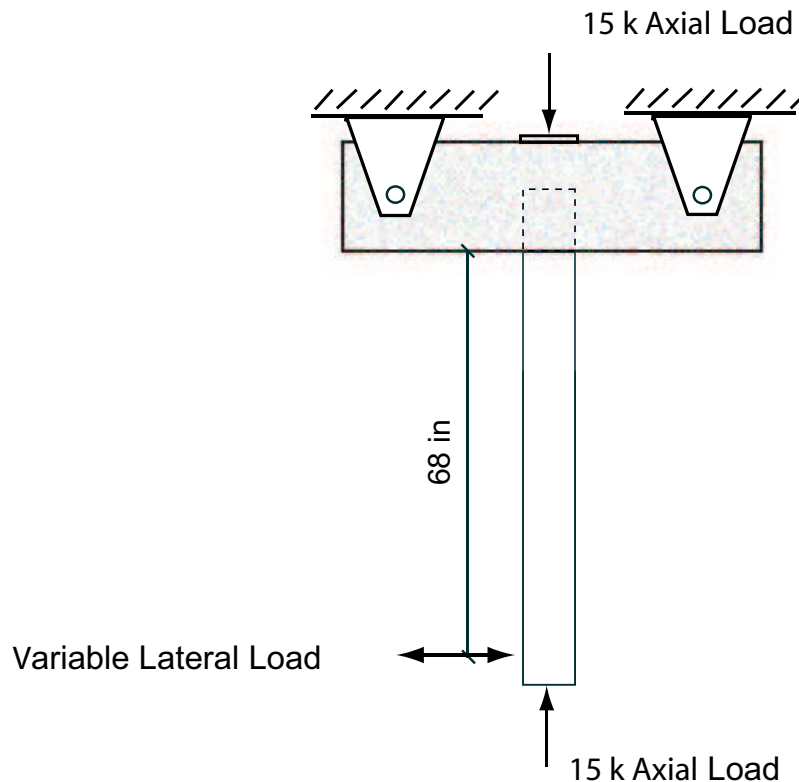
Figure 3.16: Support Scheme Used in the Physical Tests on the Pile to Pile Cap Connection

The models were subjected to an axial load along the longitudinal axis of the pipe pile, in addition to the lateral load applied at the tip of the pile. This axial load modeled the gravity dead load of the bridge superstructure that is carried by the bents. In most cases, these bents are used to support lon-gitudinal stringers, which subsequently support the bridge deck. The stringers are positioned directly over the pipe piles. Therefore, the gravity loads from the stringers are passed to the pipe piles without generating shear or bending moment demands on the pile cap. This situation was created in these tests by simultaneously applying equal magnitude axial loads at the free end of the pipe pile and on the opposing side of the pile cap (where the stringer typically would rest), as shown in Figure 3.17. The actuators used for this purpose were plumbed to a common hydraulic source to ensure that the applied "gravity" load and pipe pile reaction had the same magnitude. At the tip of the pipe pile, the axial load was applied simultaneously to both the steel pipe pile and its concrete core using a load
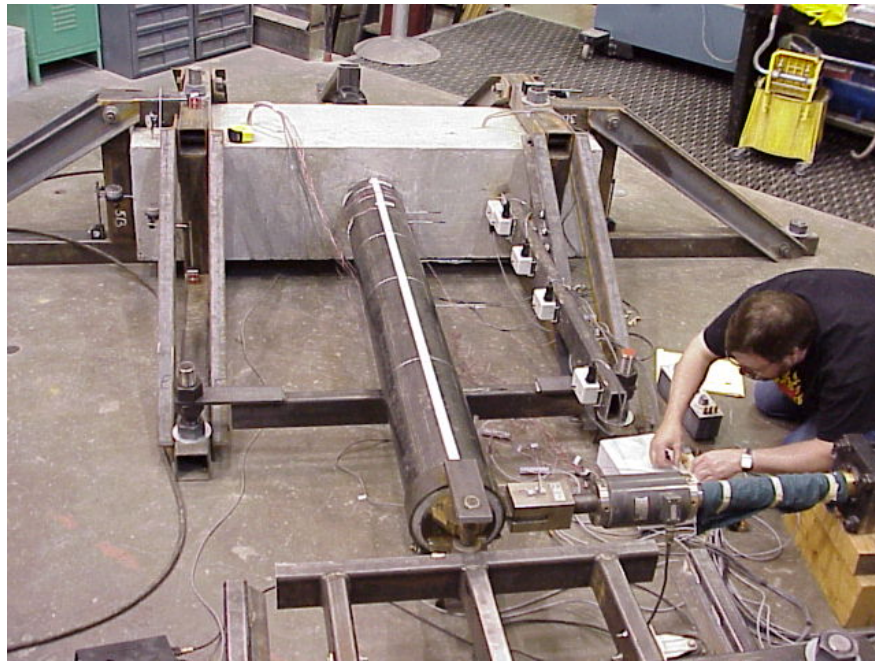
Figure 3.17: Typical Model Mounted in the Test Frame

head and collar designed so that this load could be applied coincident with the lateral load, as shown in Figure 3.18.

The magnitude of the axial load applied in all these tests was 15,000 lbs. The gravity dead load acting on each pipe pile in a real bent is dependent on several factors, including the number, size, and span of the stringers, and the thickness of the deck. Calculations were done for the gravity dead load force produced in an interior pipe pile for a typical bent supporting 4 stringers on two adjacent 50 foot spans. The axial compression stress which this force generated in a 16 inch diameter pipe pile was then calculated. The axial load of 15,000 pounds used in these tests was determined so as to generate this same level of axial compression stress in the concrete in the 8 inch pipe piles used in these models.

All loads were applied quasi-statically. At the beginning of each test, the axial load of 15,000 pounds was applied first, followed by the lateral load. The subsequent lateral load history applied to each model varied between tests, as summarized in Table 3.2. In general, the pipe piles were pushed laterally in one direction until the connection "failed", either in a single load cycle or in a few cycles of increasing load. Failure typically was defined as the loss of approximately 15 percent of the connection's maximum load carrying capacity. In two tests (PC-2 and PC-4), the model was subjected to a few cycles of fully reversed load, after initial failure was observed. Not all models were subjected to fully reversed cycles of load following initial failure, in that it was found to be difficult to discern during and following such tests precisely how much damage was sustained at initial failure.
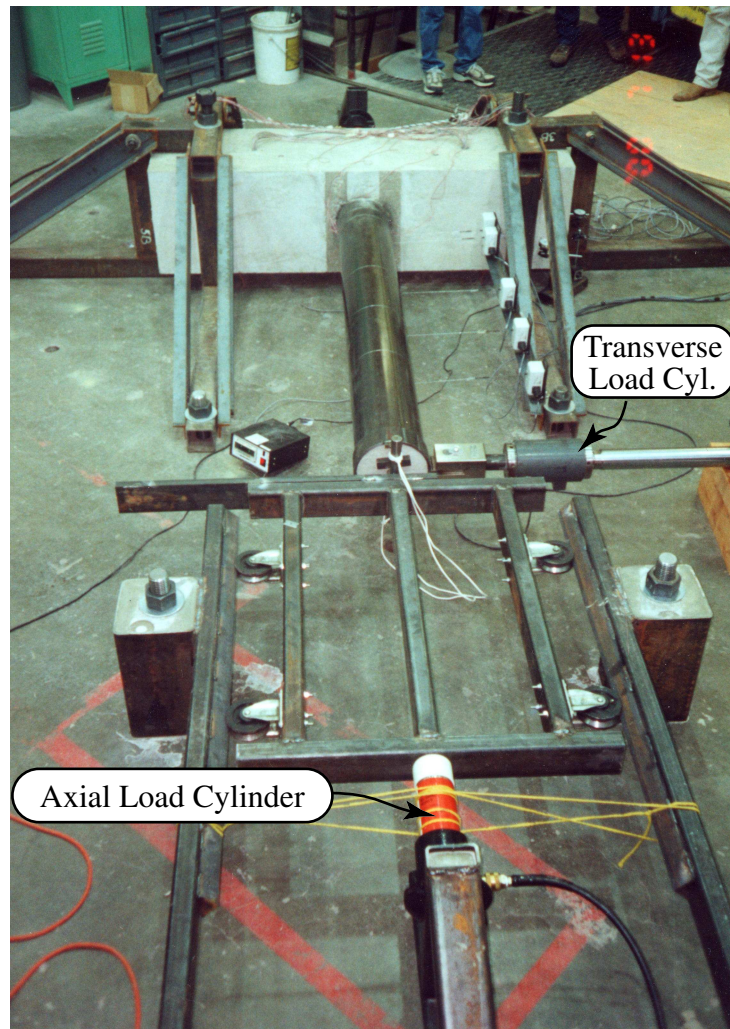
Figure 3.18: Load Collar Attached to the Free End of the Pipe Pile

Table 3.2: Load Histories

Test	Objective of Test	No. of Events	Description of Load Event[a]
PC-1	Monotonic push to failure	5	Axial load only Axial load and one monotonic push to 6,000 lbs of lateral force Axial load and one monotonic push to 7,000 lbs of lateral force Axial load and one fully reversed cycle of lateral load: - push cycle to 6,000 lbs - pull cycle to 6,000 lbs Axial load and one monotonic push to 11.4 in of tip displacement (model significantly damaged during this event)
PC-2	Monotonic push to failure followed by two cycles of reversed displacement	1	Axial load and two fully reversed displacement cycles: - push cycle to 9.3 in of tip displacement (model significantly damaged during this event) - pull cycle to –9.2 in of tip displacement - push cycle to 11.1 in of tip displacement - pull cycle to –10.5 in of tip displacement
PC-3	Monotonic push to failure	3	Axial load and monotonic push to 4200 lbs Axial load and monotonic push to 9200 lbs Axial load and one monotonic push to 7.5 in of tip displacement (model significantly damaged during this event)
PC-3a	Monotonic push to failure	1	Axial load and monotonic push to 10.9 in of tip displacement (model significantly damaged during this event)
PC-4	Monotonic push to failure followed by one cycle of reversed displacement	1	Axial load and one fully reversed displacement cycles: - push cycle to 11.1 in of tip displacement (model significantly damaged during this event) - pull cycle to 8.9 in of tip displacement

[a] events listed chronologically

3.4 INSTRUMENTATION

The instrumentation used in this program consisted of bonded strain gages on the reinforcing steel and pipe pile, embedded strain gages in the concrete, displacement gages, and load cells. The instrumentation varied between tests in response to behaviors observed in earlier tests as well changes in test objectives.

In all tests, the axial and lateral loads applied to the model, the lateral displacement of the pile, and the longitudinal strains in the steel pipe in the vicinity of the pile cap were measured and recorded, as shown in Figure 3.19. In the first 3 tests, additional strain gages were placed in the pile cap, both bonded on the reinforcing steel and embedded in the concrete. This instrumentation was placed to characterize the demands placed a) on the longitudinal reinforcing steel and on the transverse hoops in the vicinity of the embedded pipe pile and b) on the concrete in the expected compression and tension zones immediately adjacent to the pipe pile in the direction of the applied moment. Locations for these gages are shown in Figure 3.20. Model PC-3 particularly included a large number of strain measurements on the longitudinal reinforcing bars and transverse ties in the cap to more completely characterize the behavior of these elements of the connection. The amount of instrumentation used in tests PC-3a and PC-4 was reduced relative to earlier tests, to allow more connection configurations to be experimentally evaluated within the resources available to the project.
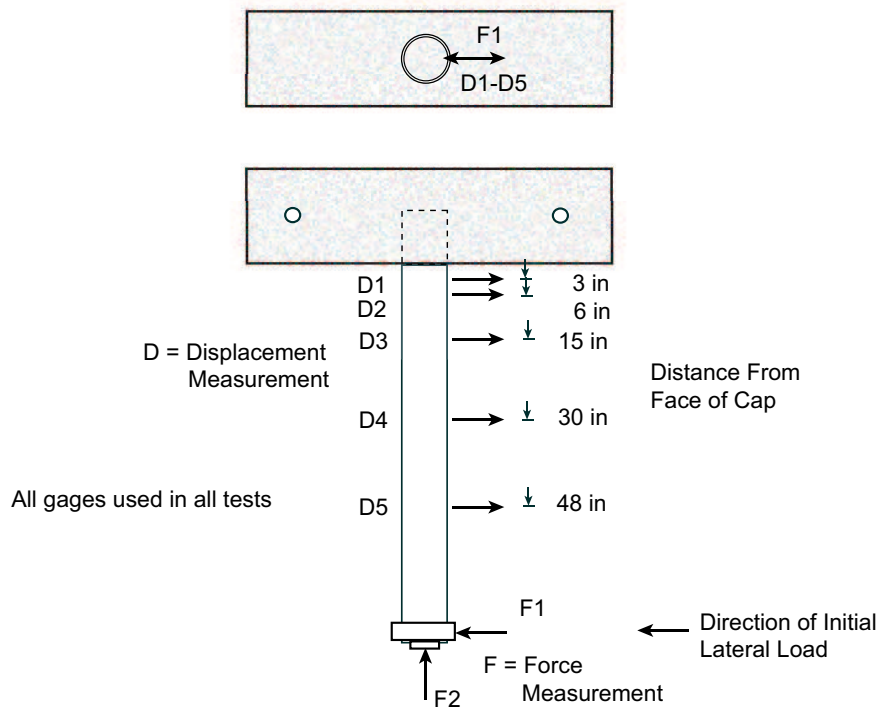
a) Applied Load and Pile Displacements
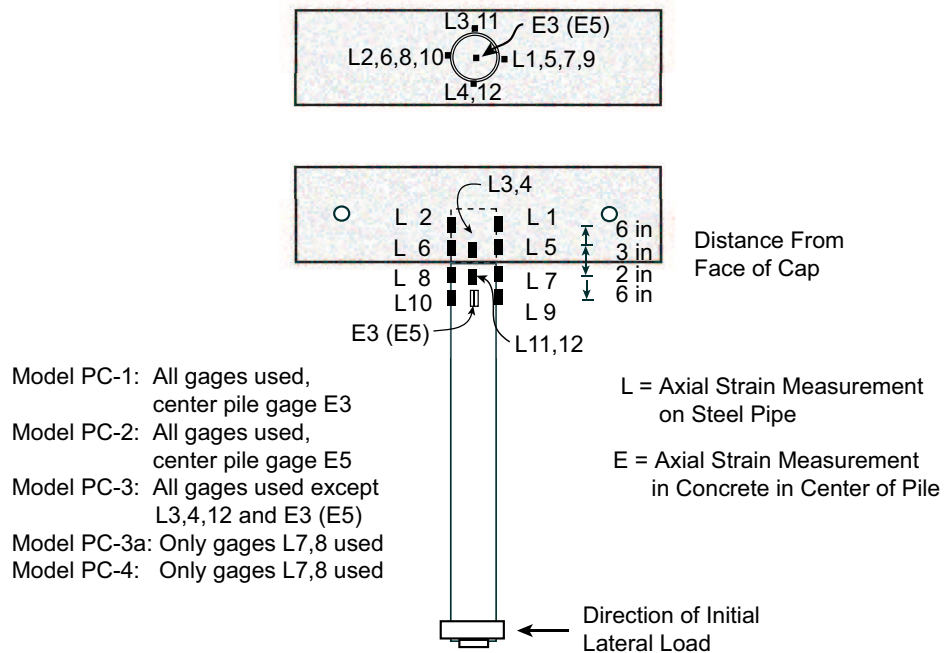
b) Pile Strains

Figure 3.19: Typical Measurement Locations: Applied Load, Displacements, and Strains (Axial)
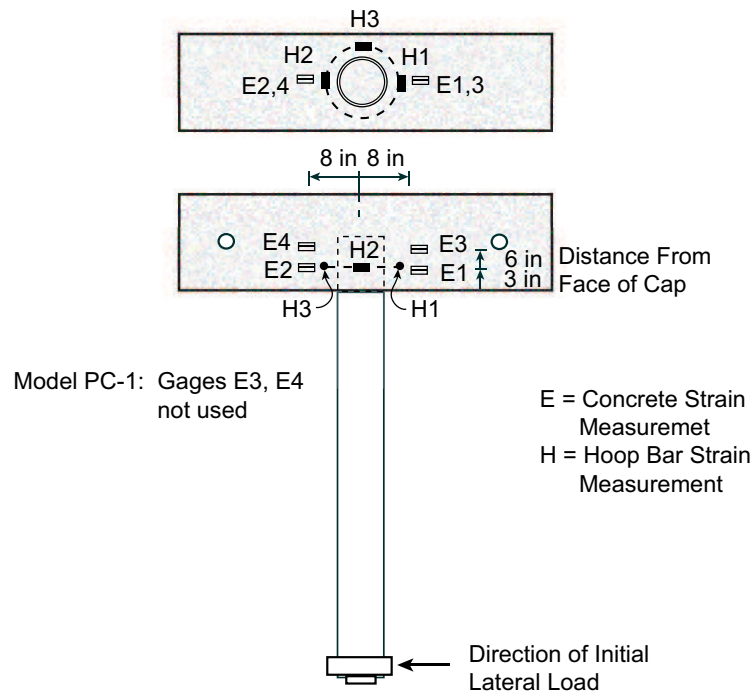
a) Pile Cap Instrumentation, Tests PC-1 and PC-2
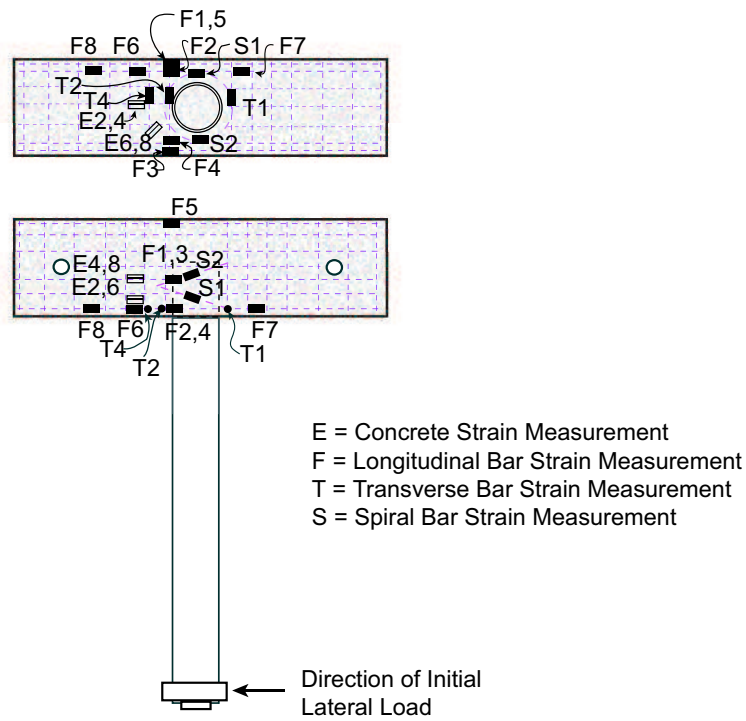
b) Pile Cap Instrumentation, Test PC-3

Figure 3.20: Typical Measurement Locations: Strains in the Pile Cap

3.5   TEST RESULTS

The results of the five steel pipe pile to pile cap connection tests conducted in this study are summarized in Table 3.3. Photographs of each model at initial failure are included in Table 3.3. In all these photographs, the lateral load in the first load cycle was applied in the direction left to right across the field of view. In each successive test, changes were made in the model configuration (as previously described) based on the results of the previous test. These changes were made in an effort to gain information on the behavior of the pile-to-cap connection across the possible range of failure mechanisms from failure of the concrete cap to plastic hinging of the steel pipe pile.

The connections in the first four tests (PC-1, 2, 3, 3a) all failed in the cap with little obvious distress to the pipe pile, while in the final test, a plastic hinge formed in the steel pipe pile before the capacity of the cap was reached. This change in failure mechanism was realized by substantially increasing the amount of reinforcing steel in the cap as well as altering its layout. The reinforcing steel in the first models was patterned after that used in actual full size bents, and it amounted to 0.41 and 0.09 percent of the cross section in the longitudinal and transverse directions, respectively. In the final model, the reinforcing steel amounted to 2.83 and 0.70 percent of the cross-section in the longitudinal and transverse directions, respectively. Presented in the following subsections (3.5.1 thru 3.5.5) is a more detailed description and discussion of the results of each test.

Table 3.3: Summary of Test Results

Test	Distinguishing Feature of the Test	Long Steel[a] (%)	Trans Steel[a] (%)	Pile Configuration	Failure Mechanism	Maximum Moment at Failure(ft-k)	Displacement Ductility	Condition at Failure
Full Size	generic full size cap and pile	0.40	0.09	0.50 inch wall, D/t = 32	unknown	unknown	unknown	unknown
1	believed to be scale model of full size structure, pipe pile judged to be relatively stiffer than it should have been	0.41	0.09	0.32 inch wall, D/t = 27	cracking of concrete cap	82	3.3	
2	same cap configuration as in PC-2, decreased wall thickness of pipe	0.41	0.09	0.25 inch wall, D/t = 34.5	cracking of concrete cap	74	3.3	
3	same pipe configuration, increased reinforcing steel in the cap	1.09	0.24	0.25 inch wall, D/t = 34.5	cracking of concrete cap	76	3.5	
3a	same pipe configuration, further increased reinforcing steel in the cap	2.11	0.65	0.25 inch wall, D/t = 34.5	cracking of concrete cap	102	2.6	
4	same pipe pile configuration, further increased reinforcing steel in the cap	2.83	0.70	0.25 inch wall, D/t = 34.5	plastic hinge in steel pipe pile	121	>3.9*	

[a] see Figure 3.5 for specific manner in which these ratios were calculated
* minimum value, connection was still carrying full failure load at point at which test was terminated

3.5.1   Test PC-1

In the first test, a connection model believed to be representative of existing pile and cap configurations was used. This model was subjected to a total of 5 load events. The first four of these events were used to evaluate the performance of the load frame and instrumentation. In the first event, the axial load was run up to 15 k and then removed (no lateral load was applied). Selected strains measured longitudinally on the pipe pile and in the concrete in the pile are presented in Figure 3.21. All strains linearly increased with load, as might be expected at load levels well below the elastic capacity of the pipe pile. The strains in the pile steel at maximum load were approximately 0.004 percent compression, while the corresponding strain in the concrete in the center of the pipe was only 0.0025 percent compression. The difference in these strains implies either imperfect composite action between the steel shell and the concrete infill, or possible shear lag in distributing the applied load between the steel shell and the concrete infill. Assuming linear elastic behavior in both materials, the load carried in each part of the pile was calculated as the measured strain multiplied by Young's modulus for the material and its cross-sectional area. The results of this calculation were within 5 percent of the measured 15 k axial load applied to the pile.

In the second test event using model PC-1, the 15 k axial load was applied, and the lateral load was then gradually increased to approximately 6 kips. The bearing in the axial load apparatus failed at this applied load, and the test was terminated. The bearing was subsequently replaced with a bushing system, and the model was successfully loaded to 7 kips of lateral force (third shakedown event). Before proceeding to monotonically load the model to failure, the decision was made to run one more shakedown event to verify the ability of the test frame to apply reversed cycles of lateral load in the presence of a 15 k axial load. The model was laterally loaded to 6 kips of force in one direction,
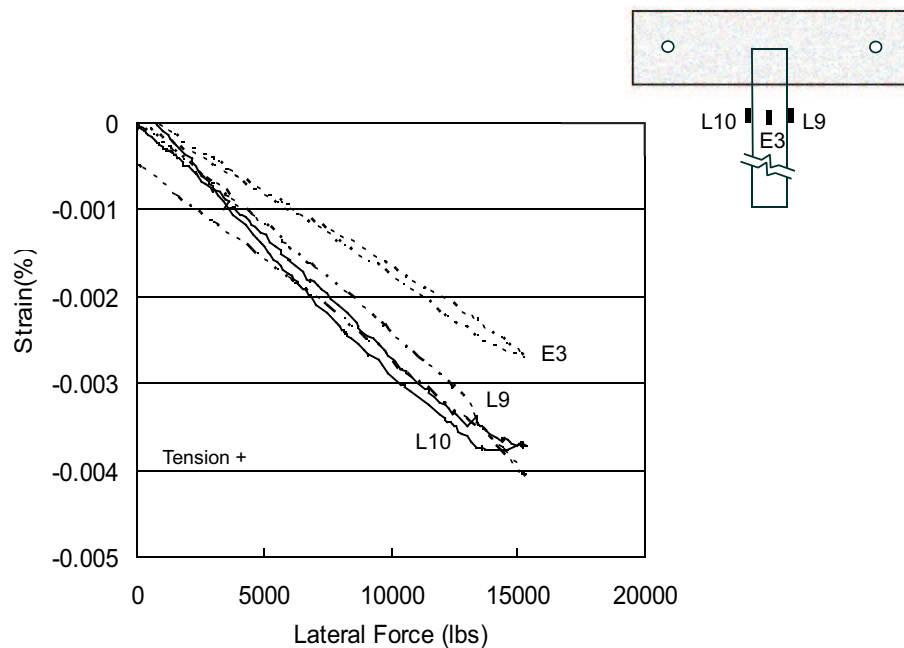
Figure 3.21: PC-1 Pipe Pile Strain Response (Axial Load Only)

followed by a load cycle to approximately 5 kips of lateral force in the other direction. A typical load deflection curve from this fourth and final shakedown event is shown in Figure 3.22.

Referring to Figure 3.22, it was suspected that some rigid body motion of the model occurred during each cycle of this load event. At the completion of the first push cycle and a return to a zero load condition, the tip of the pile remained displaced approximately 3/8 in. The model was expected to remain well within its elastic limit during this event, so the majority of this displacement was believed to result from rigid body movement of the model within its pinned supports (rather than from deformation and damage related effects). This conclusion was supported in part by dial gage measurements made of the horizontal movements of the cap during the load event. In subsequent tests, special care was taken to reduce these rigid body motions by thoroughly grouting the annular space between the support pins and their embedded receptacles in the model. The reference frame for measuring the lateral displacements of the pipe pile was also shifted to the body of the cap, so that this reference frame would automatically shift with any rigid body movement of the model. Finally, detailed measurements were made of the horizontal movements of the cap during each test, with the intent of analytically removing rigid body effects from the results after the fact. None of these measures proved to be satisfactory in eliminating the perceived rigid body motion of the model, which led to the conclusion that part of this displacement (which had a maximum magnitude of 3/8 in) was attributable to real changes in the model that prevented it from returning to its original position, even under "elastic" load levels.

Typical longitudinal strains measured on the pipe pile during the third shakedown event are presented in Figure 3.23. Gages L8 and L10 registered compression strains consistent with the bending normal stresses generated by the lateral load on the pile tip. Correspondingly, gages L7 and L9, located on the opposite side of the pile, registered bending tensile strains. The strains measured on
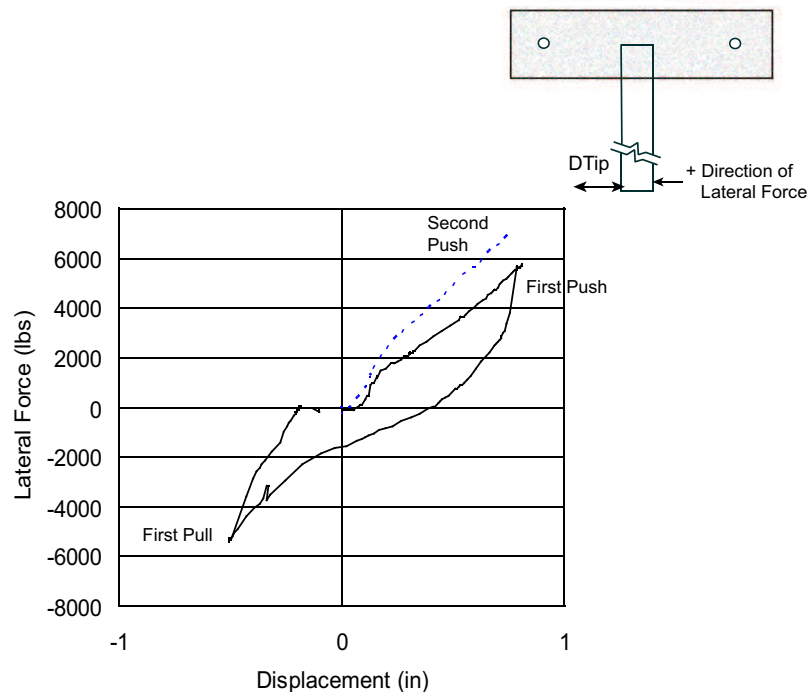
Figure 3.22: PC-1 Pipe Pile Lateral Load vs. Lateral Displacement (Prelim. Load Event)

opposite sides of the pile are similar in magnitude, with a slight compressive shift generated by the compression strain from the 15 kip axial load.

Following these four shakedown tests, model PC-1 was tested under a monotonically increasing lateral load (in the presence of the 15 k axial load) until its maximum lateral load resistance was reached. Model PC-1 failed at a lateral load of 13,400 predominantly through splitting of the cap concrete, as shown in Figure 3.24. Subsequent to the test, it was discovered that the pipe pile used in the model was stronger relative to the pile cap than in a typical full size structure. Thus, while this test provided an indication of the capacity of the pile cap under lateral loads, it may not have provided a good representation of how the full-size connection would behave.

None-the-less, this test on model PC-1 did characterize the behavior of the connection for the case of a cap controlled failure, and it did establish the order of magnitude of the moment capacity of this configuration of the concrete pile cap. As the lateral load was applied in this test, the cap generally remained undamaged until the load reached approximately 11,300 pounds (approximately 85 percent of its ultimate resistance), at a tip displacement of 1.5 inches. Beginning at this load level, existing transverse tensile cracks adjacent to the pipe pile widened significantly, and new tension cracks opened up at the compression face of the pile running at an acute angle from the face of the pile to edge the cap (see Figure 3.24). Up until this point, the gross behavior of the connection was fairly linear in nature, as can be seen in the graph of tip displacement as a function of applied load presented in Figure 3.25. Cracks continued to form and widen in the cap in the connection zone, as the lateral load slowly climbed to a peak value of 13,400 pounds at a tip deflection of 5.4 inches. The test was terminated at a tip displacement of 11.4 inches and an applied lateral load of 9,700 lbs. Throughout the large lateral displacements experienced during the test, the axial load was uniformly maintained at a constant value of 15 kips, as shown in Figure 3.25. At the end of the test, when the
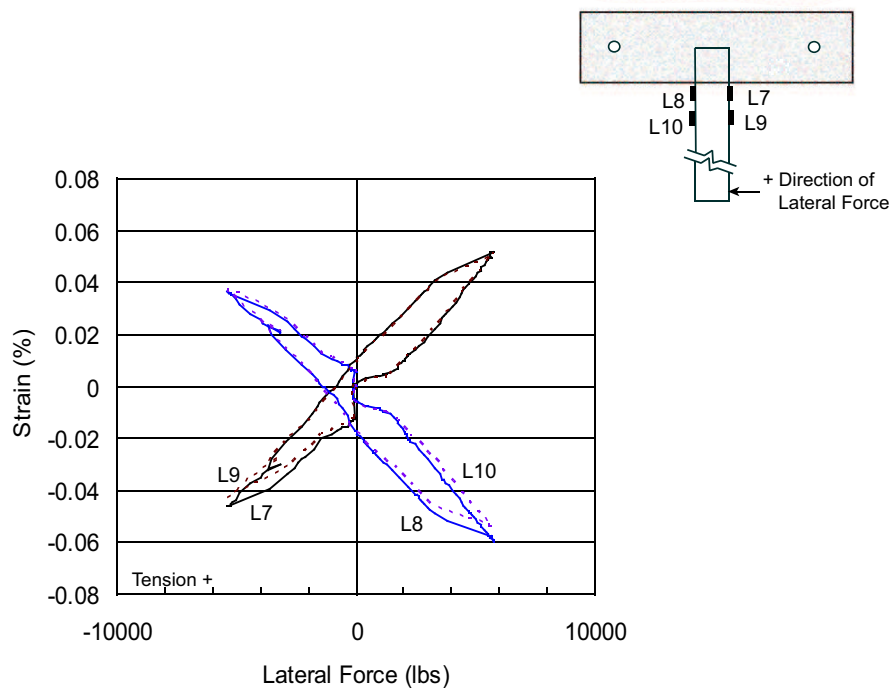
Figure 3.23: PC-1 Pipe Pile Longitudinal Strain vs. Lateral Displacement (Prelim. Load Event)

a) Prior to Failure, at a Lateral Load of 12,500 lbs
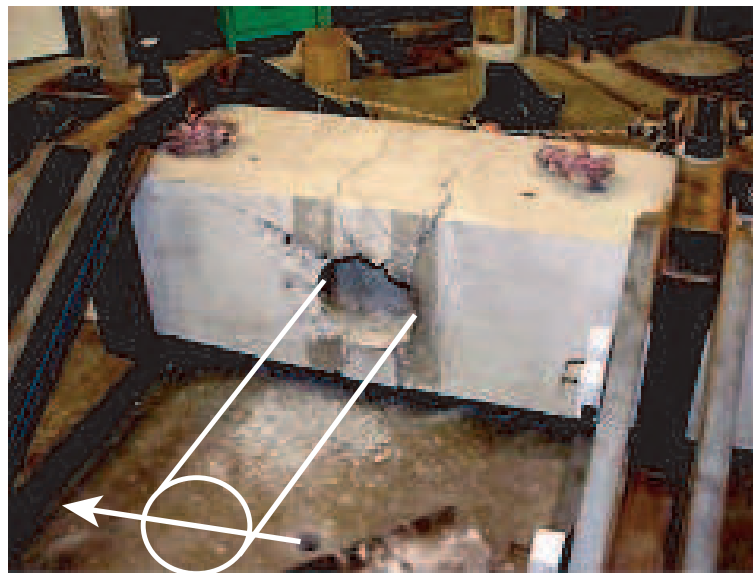
b) At Failure, Immediately Following Maximum Lateral Resistance of 13,400 lbs

Figure 3.24: PC-1 Model Condition Immediately Before and After Failure

axial force was removed, it was discovered that no positive mechanical connection remained between the cap and the pile. The pile was easily removed from its socket in the cap.

The pipe pile-to-pile cap connection did exhibit some level of ductility during the test, as shown in the load/deformation plot presented in Figure 3.25. The displacement ductility, defined as the ratio of the tip displacement at maximum (ultimate) capacity divided by the displacement at yield, was ~3.3. The yield point was analytically defined as the intersection of the extension of the initial linear portion of the response with the final plateau at failure, as shown in Figure 3.26. At the termination of the test, the connection was still carrying 75 percent of the peak applied load at a ductility ratio of ~8. It is important to note, however, that this ductility was realized through permanent cracking (and some local crushing) of the concrete in the cap.
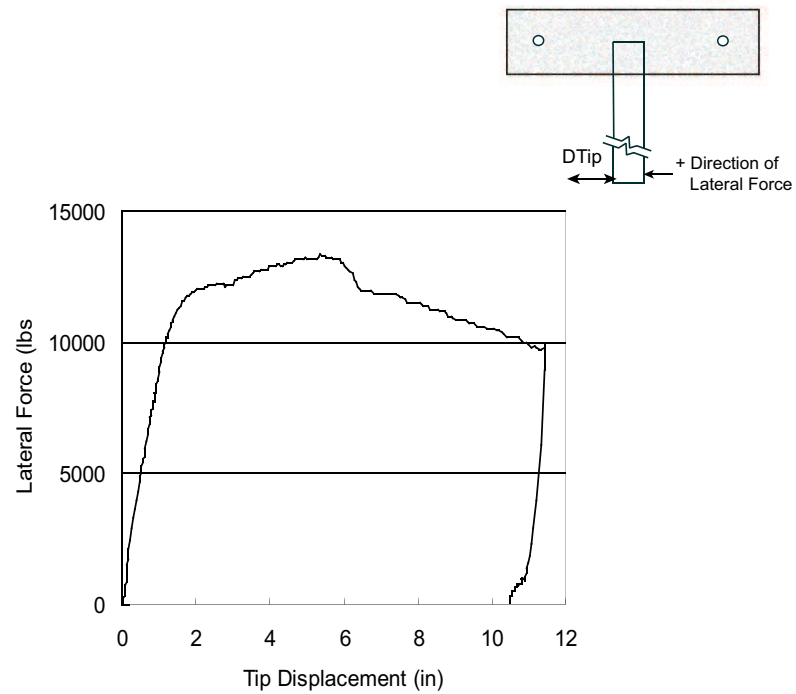
Figure 3.25: PC-1 Pipe Pile Lateral Load vs. Lateral Displacement (Main Load Event)
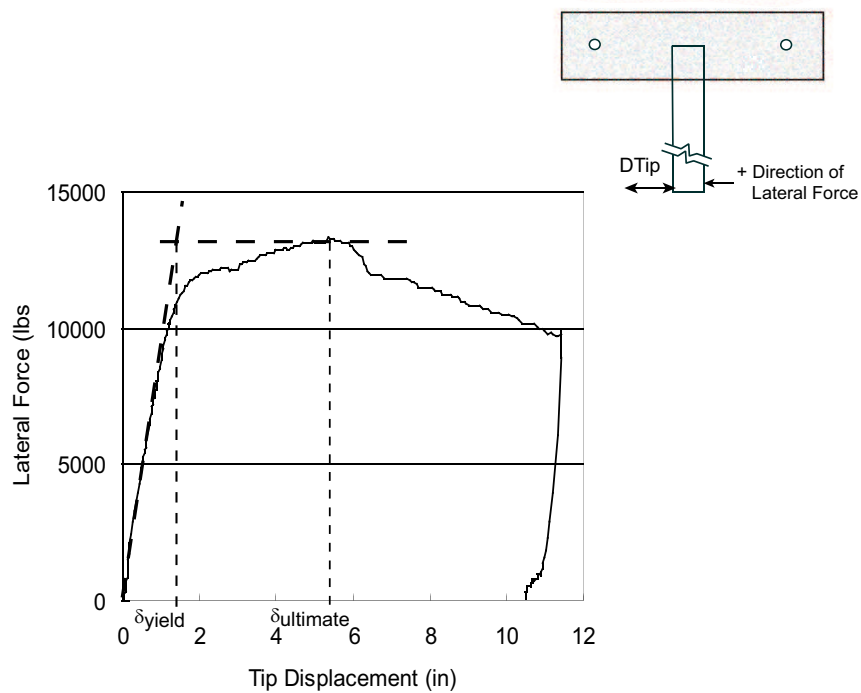
Figure 3.26: Technique Used to Evaluate Displacement Ductility

   Within the cap, the hoop bar around the embedded pile appeared to be active in restraining rotation of the pile within the cap. Significant bending strains occurred at location H3 on the hoop as it attempted to straighten, as indicated by the strain traces from the inner and outer surfaces of the bar at this location (see Figure 3.27). These bending strains were superimposed on axial tensile strains generated as the rotating pipe pile also stretched the hoop. The net axial tension strain in the bar at the maximum applied load was 0.10 percent (estimated to be approximately 50 percent of the yield strain of the bar). At the extreme tension fiber of the bar, the tensile strain had reached 0.24 percent by the end of the test. Note, however, that at both the onset of significant cracking (load of 11,300 pounds) and at the ultimate load carried by the connection (load of 13,400 pounds), the strains across the hoop bar at location H3 were below the yield strain of the hoop steel. The strains in the bar did begin to increase dramatically when significant cracks opened up in the cap concrete at a lateral load of 11,300 pounds.

   The gages embedded in the cap in the compression zones adjacent to the pipe pile only recorded moderate strains in the concrete throughout the test. As shown in Figure 3.28, a maximum strain of 0.03 percent was recorded by the gage near the surface of the cap, which is only 10 percent of the estimated crushing strain of the cap concrete. These strains increased sharply as the tension cracks in the cap opened up as the applied load increased above 12,000 lbs. At these loads and at this condition of physical damage, the cap was transitioning to a strut and tie condition, in which internal tension forces are carried predominantly by the reinforcing steel and internal compression forces are focused along concrete "struts".

   The relatively low magnitude of the compression strains in the concrete at gage E1 may indicate that this area of concrete is not a primary compression load path in the strut and tie condition. That is, the compression forces that develop in the cap from the rotation of the pipe pile need to be reacted
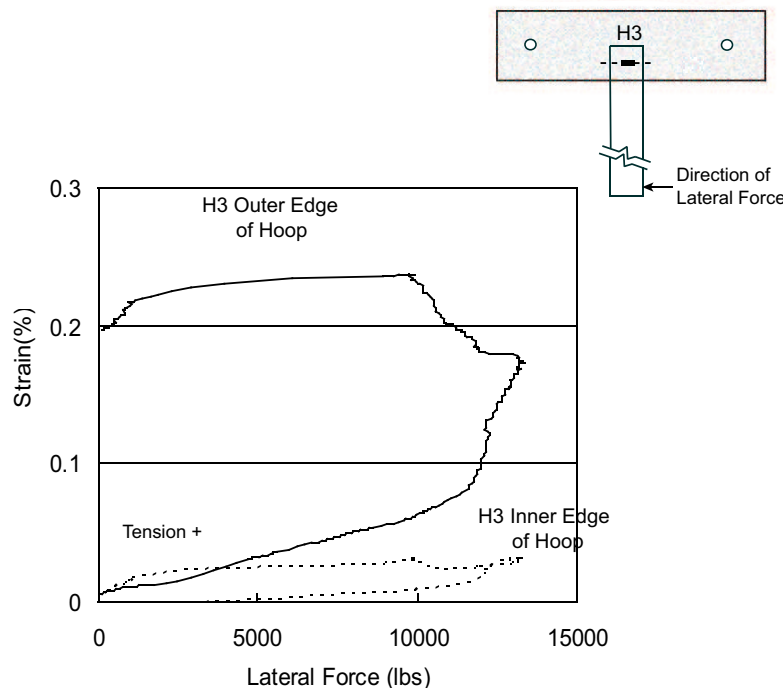
Figure 3.27: PC-1 Hoop Bar Strains (Main Load Event)
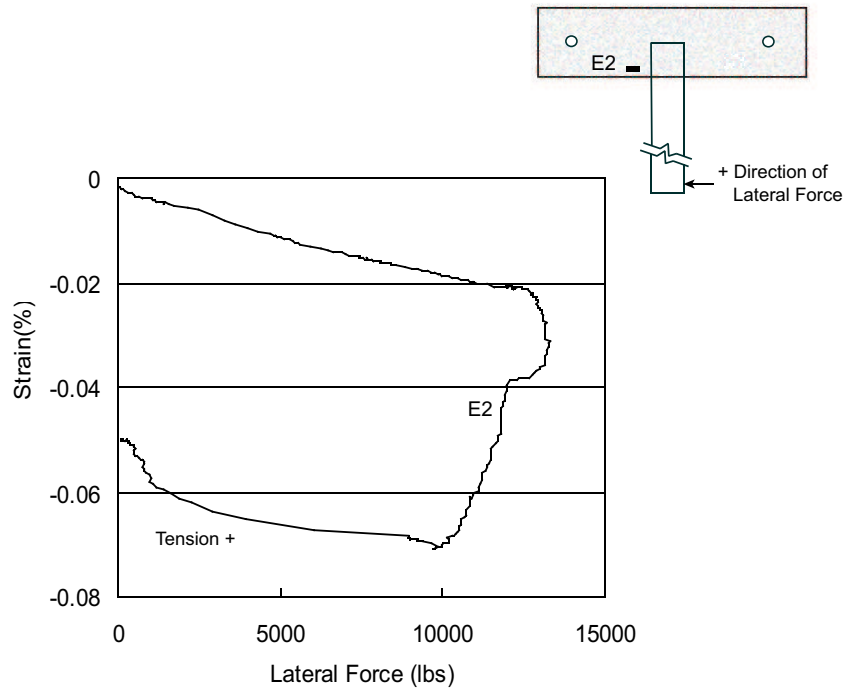
Figure 3.28: PC-1 Cap Concrete Strains (Main Load Event)

by the steel reinforcing cage. The cage is stiffest in this regard along its faces. Thus, compression struts would be expected to form running diagonally from the steel pipe pile to the faces of the cap, as shown in Figure 3.29. The actual existence of such struts can be inferred from the diagonal tension cracks that opened up in the cap at failure at this location. If these struts carry the majority of the compression forces generated in the cap by the rotation of the pile, low compression forces and strains would be expected in the interior of the cap, consistent with the low strains measured by the embedded strain gages in this location. The crushed concrete immediately opposite the crown of the pile was certainly indicative of an area of high stress. Nonetheless, the compressive damage at this location was limited in extent. The distress appeared to have occurred primarily in the cover concrete outside the reinforcing cage and only extended 3 to 4 inches along the longitudinal axis of the cap.

The pipe pile, itself, sustained only nominal damage during the test (check on any permanent deflection along entire length). Maximum longitudinal strains of 0.15 percent (estimated to be approximately 80 percent of the yield strain of the pile steel) were experienced in the steel pile at the extreme fibers in bending near the face of the cap. The strain histories from opposing sides of the pile near the face of the cap (see Figure 3.30) indicate the presence of a dominant bending effect from the lateral load (the nearly equal and opposite strains on the opposing sides of the cap), superimposed on a relatively small axial effect generated by the axial load (the strains are nominally offset in the compression direction). The longitudinal strains experienced in the steel pipe close to the embedded tip had a maximum magnitude of only 0.03 percent (see Figure 3.30).

The longitudinal strains recorded on the pipe pile inside the pile cap decreased with depth below the surface of the concrete, as shown in Figure 3.31. This behavior is consistent with a "gradual" transfer of the pile forces into the cap along the length of embedment. The strains 3 and 6 inches below the surface of the cap were approximately 80 and 30 percent of the strains recorded 3 inches
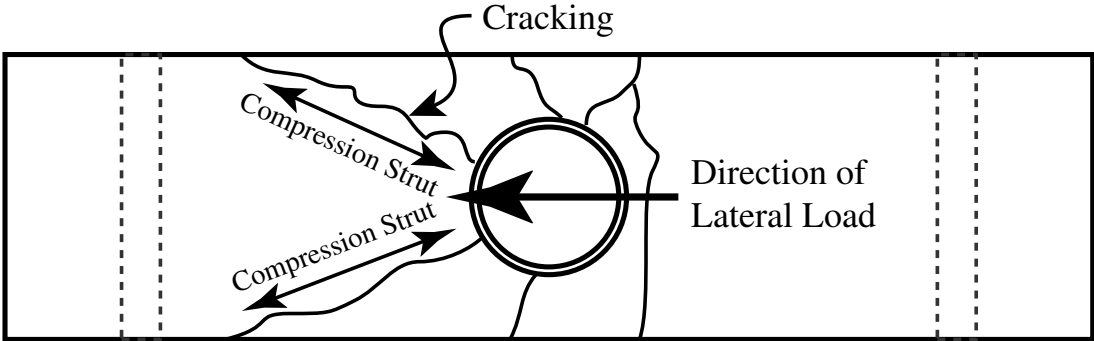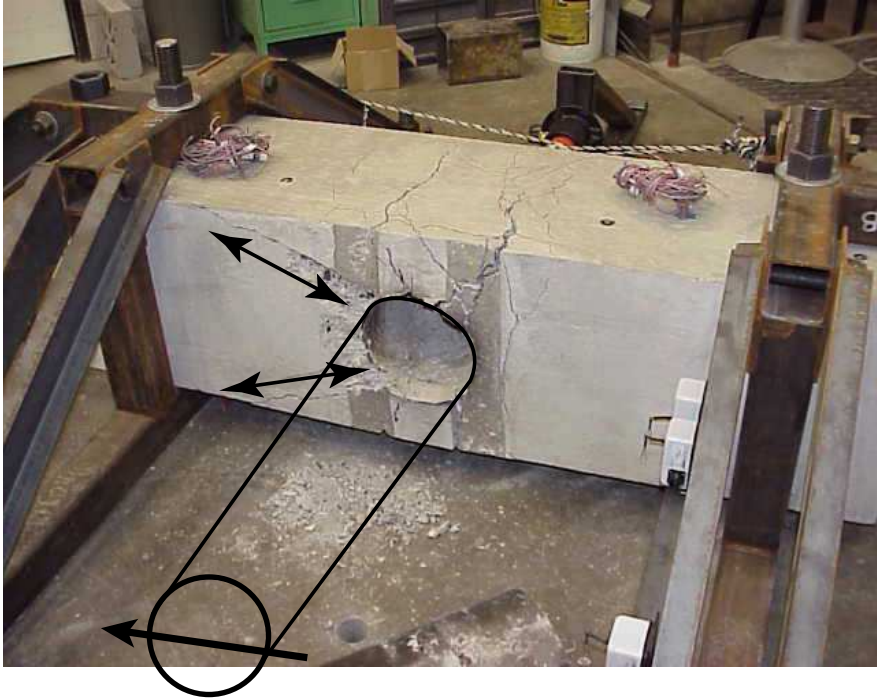
Figure 3.29: PC-1 Hypothesized Strut Behavior in the Cap
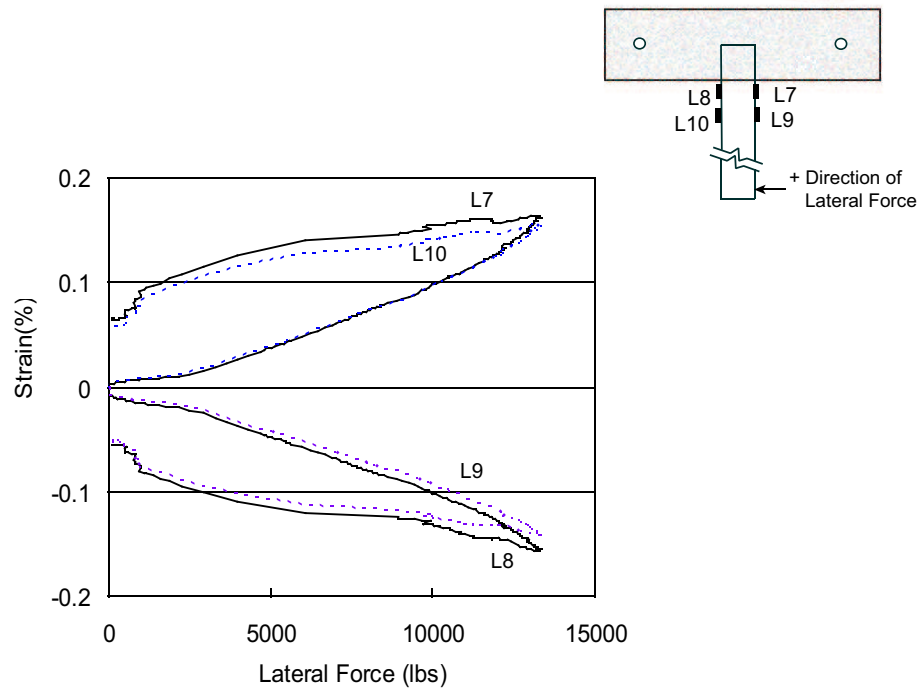
Figure 3.30: PC-1 Pipe Pile Longitudinal Strains Outside the Cap (Main Load Event)
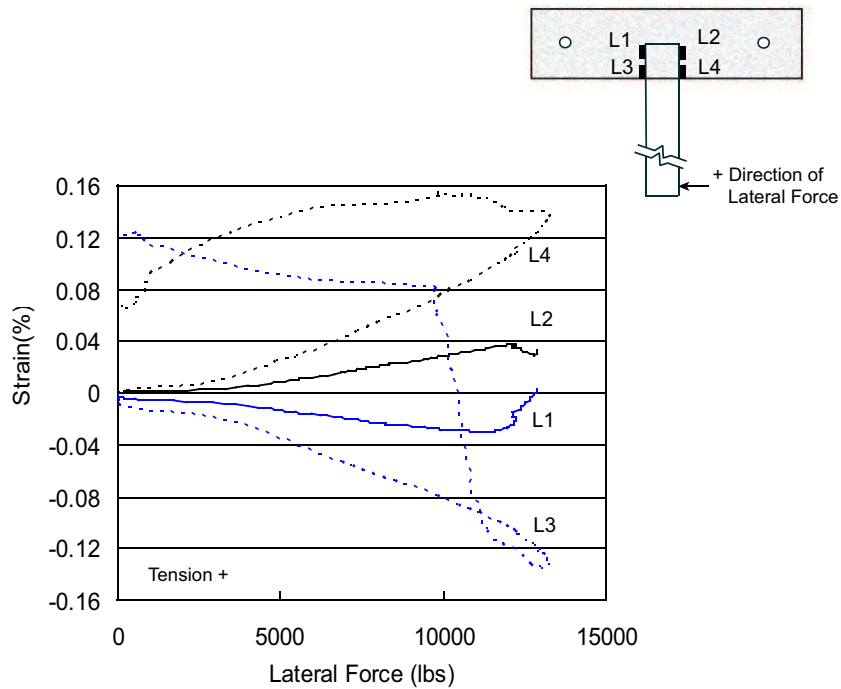
Figure 3.31: PC-1 Pipe Pile Longitudinal Strains Inside the Cap (Main Load Event)

outside of the surface of the cap concrete. The relative magnitudes of these strains remained the same even as and after the peak capacity of the connection was reached and significant damage occurred to the cap.

Following the test, the pipe pile was loose in the cap, so it was removed and examined for damage in the embedment zone. In the compression region near the tip of the pile, some plastic deformation of the steel pile is evident. This deformation is shown in Figure 3.32.

Figure 3.32: PC-1 Pipe Pile Embedded End Following the Test

Overall, the results from test PC-1 obviously indicate that the capacity of the steel pipe pile to concrete pile cap connection was controlled by the strength of the pile cap. The maximum moment carried by the pile cap as it failed was estimated to be 82 ft-kips (including P-delta effects). The cap failure primarily consisted of tension cracking of the concrete; only limited crushing of the concrete was observed in the compression areas adjacent to the pipe pile. These results suggest that as the tension capacity of the concrete was reached, and tensile demands were transferred to the reinforcing steel, this steel was quickly overwhelmed and subsequently yielded, resulting in large deformations and large crack widths in the cap concrete.

3.5.2   Test PC-2

In test PC-2, in which the wall thickness of the pipe pile was decreased to 0.25 inches compared to 0.32 inches used in the first test, failure of the connection once again occurred in the pile cap. The sequence of crack formation as a function of applied load is indicated in Figure 3.33. The steel pipe pile only experienced nominal damage during the test. This result was not unexpected, as the predicted moment capacity of the pipe pile used in the second test was approximately 100 ft-kips, while the moment resisting capacity of the pile cap was known from the first test to be approximately 82 ft-kips. The nature of the failure of the second model was similar to that of the first test. Failure occurred through cracking and limited crushing of the concrete in the cap, with the ultimate lateral resistance of the cap being 11,650 pounds (88 percent of the maximum lateral load carried in test PC-1) observed at a displacement of 6.5 inches.
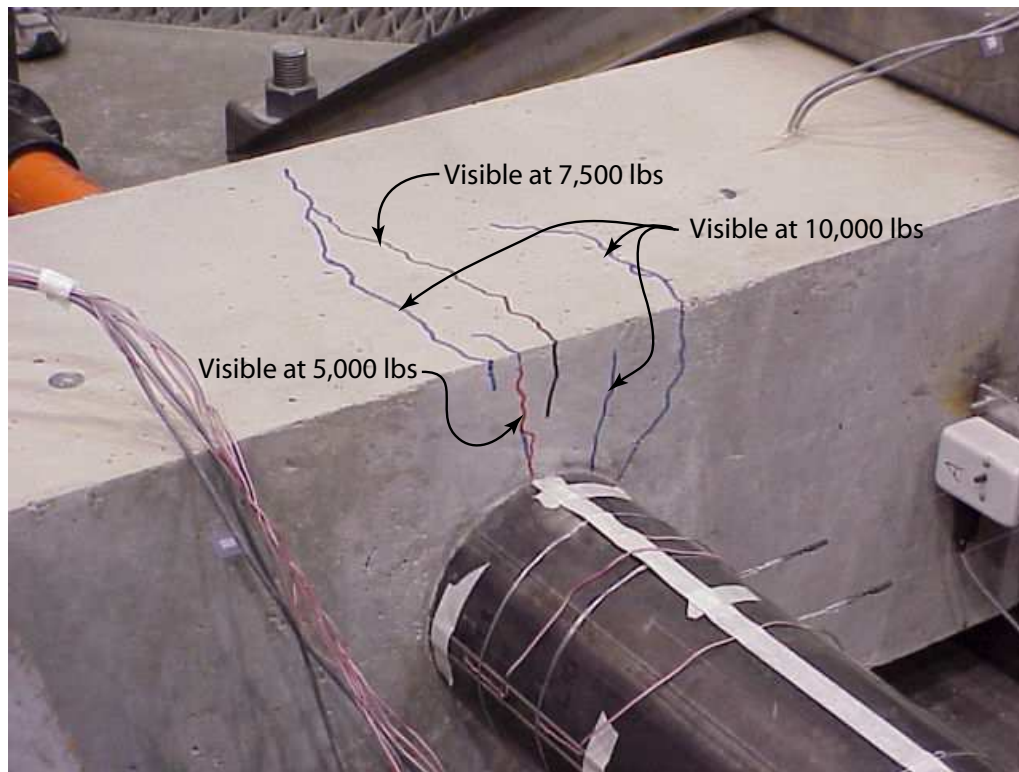
a) Prior to Failure, at a Lateral Load of 10,000 lbs
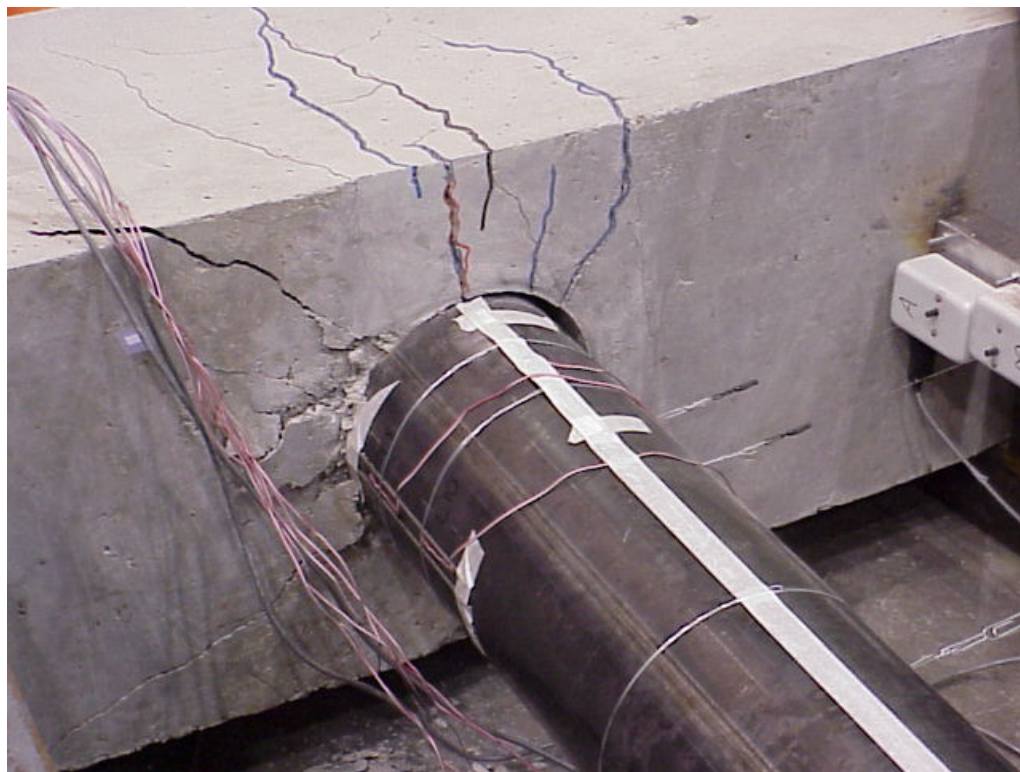
b) At Failure, Immediately Following Maximum Lateral Resistance of 11,650 lbs

Figure 3.33: PC-2 Model Condition Immediately Before and After Failure

Once again, minimal distress was observed in the cap until the load exceeded approximately 85 percent of the ultimate capacity of the cap. Up until this point, the global force displacement response was fairly linear in nature, as shown in Figure 3.34. As the load increased above this point (10,000 lbs of lateral force), the cracks in the cap abruptly widened (see Figure 3.33b), while the resistance only slowly increased.

While the intention in this test was to load the connection monotonically to failure, the load and reaction frames performed well during the initial load excursion, and the decision was made to expose the model to a few cycles of fully reversed displacements. The model was subjected to four cycles of reversed load, two in each direction, with the tip of the pile being deflected a maximum of 10 inches (approximately) in each cycle. The complete force displacement history for this test is shown in Figure 3.35. The condition of the model at its maximum displacement after the first full load reversal and after all load cycles is shown in Figure 3.36. During the first reversed cycle of load, as might be expected, the distress pattern that developed initially on one side of the cap also developed on the other side of the cap. Few new cracks were observed in subsequent load cycles.

The force-displacement response of the connection followed the customary hysteresis behavior observed for reinforced concrete elements subjected to reversed cycles of damaging load (Figure 3.34). In this case, a substantial decrease (33 percent) occurred in the load carrying capacity of the connection between the first and second cycles of response, followed by a more gradual decline in capacity during each of the following cycles of response (on the order of magnitude of 12 to 20 percent per cycle). Also following the first cycle of response, the hysteresis loops became "pinched" in shape, as the connection softened during the earlier stages of each load reversal.

From a seismic performance perspective, the behavior of the connection as described above is both good and bad. Despite the failure mechanism (cracking of the concrete in the cap as opposed to hinging in the steel pipe pile), the connection displayed reasonable displacement ductility during the first load excursion (recall that displacement ductility is defined as the ratio of the displacement at maximum (ultimate) capacity divided by the displacement at yield). The displacement ductility of this connection was 3 to 4, depending on the specific values used for the yield and ultimate displacements (as estimated from the force-deformation response reported in Figure 3.34). In buildings, it is essential to have substantial displacement ductility (on the order of magnitude of 6) to insure adequate seismic performance, in that buildings are not generally designed to resist the forces that would develop if they responded elastically during a seismic event. Following AASHTO design requirements, however, bridge pile-to-cap connections must either be designed to elastically resist seismic forces, or so that a plastic hinge will form in the pile before the cap fails. In the former case, while ductility is still desirable, it is not essential to successful performance of the connection. The latter case implies some requirements on displacement ductility, but these requirements are focused on the behavior of the pipe pile, rather than the cap. Certainly, the behavior of model PC-2, while ductile in nature, does not meet the criteria of plastic hinging in the column before failure of the cap.

While the second pile-to-pile cap connection exhibited some level of displacement ductility, the strength degraded significantly on each subsequent cycle of fully reversed displacement. A more desirable behavior (and the required behavior in many building elements) would be for the connection to withstand at least a few cycles of displacement at this level of ductility without degradation in strength. Due to the nature of the materials involved, if the failure were forced to occur in the pipe pile before the cap, this type of behavior might be realized. The degradation in strength was accompanied by a reduction in the amount of energy dissipated in each cycle of response. In concrete building design, energy dissipation of at least 70 to 80 percent of that which would be realized using an elastic-perfectly plastic model is considered desirable, with little degradation in energy dissipation capacity
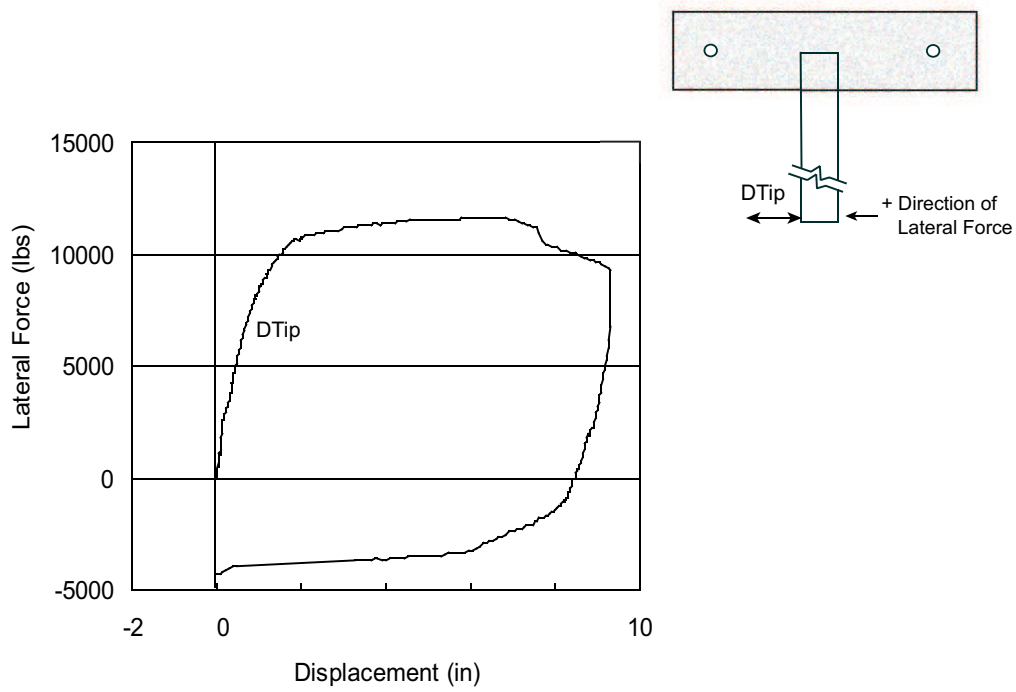
Figure 3.34: PC-2 Pipe Pile Lateral Load vs. Displacement (First Load Cycle to Failure)
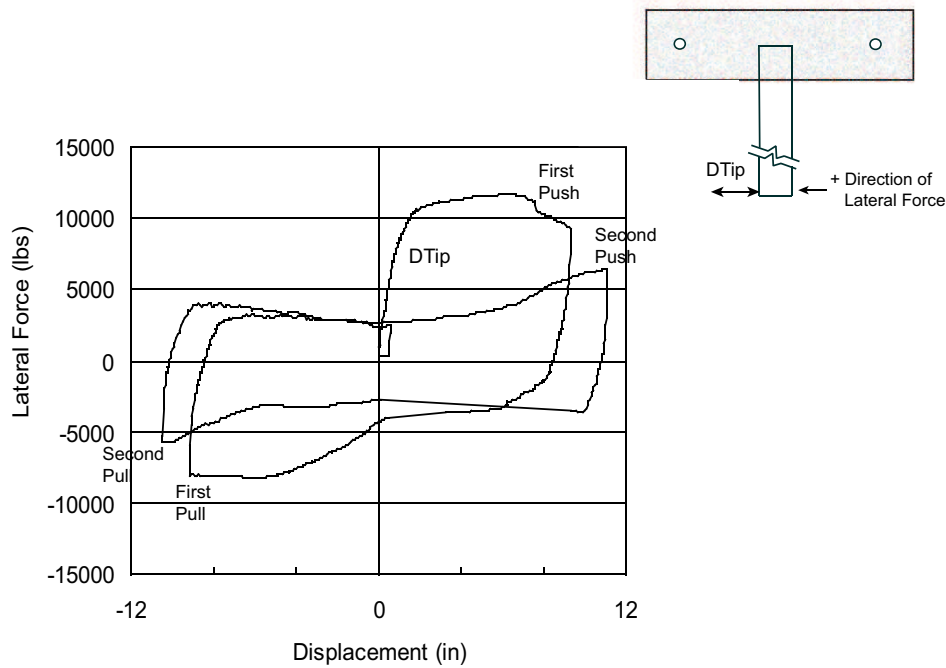
Figure 3.35: PC-2 Pipe Pile Lateral Load vs. Lateral Displacement (All Load Cycles)
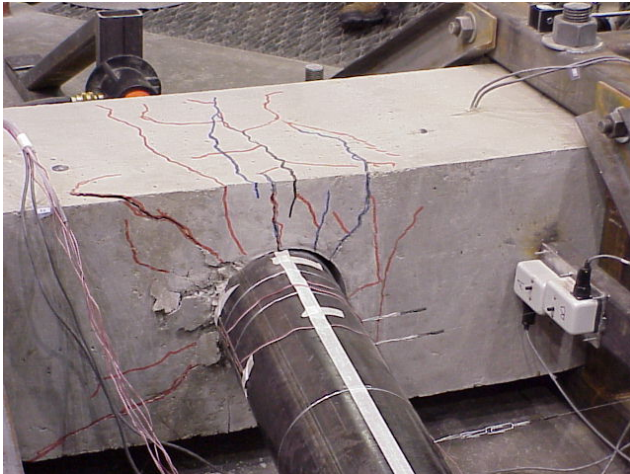
a) Maximum Displacement, 1st Push Cycle   b) Return to Zero Displ., Following 1st Push Cycle
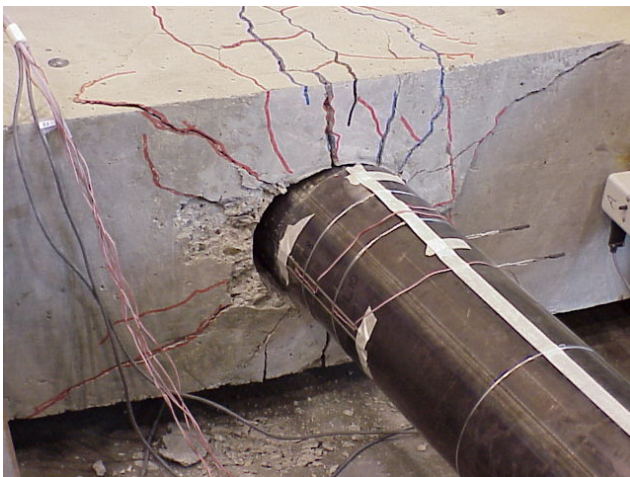
c) Maximum Displacement, 1st Pull Cycle   d) After All Load Cycles
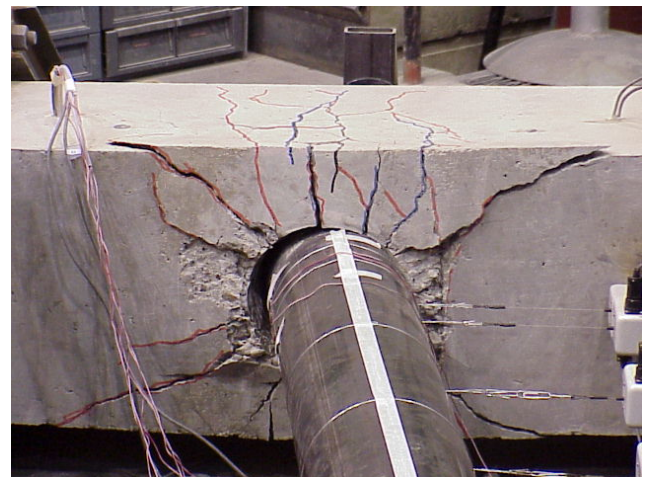
Figure 3.36: PC-2 Progressive Condition (First Full Cycle of Reversed Load and Displacement)

with each successive cycle of displacement. While the actual energy dissipated in the first cycle of response in this test was approximately 85 percent of the energy that would have been dissipated if the response had been elastic perfectly plastic (see Figure 3.37), only 60 percent of this energy was dissipated in the second cycle of response.

As observed in Test PC-1, the strains measured in the concrete in the pile cap during the test were low in magnitude. The low strains measured in the concrete directly in line with the direction of rotation of the pipe pile may once again reflect the presence of load paths in the cap concrete that were directed at an oblique angle from the pile to the face of the cap (as previously illustrated in Figure 3.29). Strain histories collected in the cap concrete during the first load cycle of test PC-2 are presented in Figure 3.38.

The largest strain observed at location E2, for example, which is directly in front of the pipe pile in the expected compression zone during the first load cycle, approached 0.025 percent, which once again is an order of magnitude below the generally assumed crushing strain for concrete of 0.3 percent. At low load levels, compression strains were observed at locations E2 and E3, while tension strains were seen at location E1 (note that gage E4 malfunctioned). This strain pattern is consistent with the development of a compression couple in the cap on opposing sides of the pipe pile to resist the rotation of the pile, as illustrated in Figure 3.39. As damage in the cap increased at load levels above 10,000 to 11,000 lbs, the load carrying mechanisms in the cap abruptly began to shift, and the compression strains at locations E2 and E3 increased sharply, while the response at location E1 shifted from tension to compression.

A typical strain record from the cap concrete for the entire cyclic load history applied to model PC-2 is presented in Figure 3.40. This strain history is for location E3 (see Figure 3.39). Referring to Figure 3.40, the effects of the four load cycles on the concrete at this location are clearly evident.

During the first and third load cycles, the concrete at this location goes into compression, consistent with the pile attempting to rotate and push on the concrete in the vicinity of the gage. Indeed, the largest compression strains at this location were observed for these load cycles. During the two alternate load cycles (the second and fourth cycles), the concrete in the area of this gage was expected to be unstrained, as the pile physically pulled away from the concrete. During these cycles of load, however, the concrete at this location still experienced nominal compression strains. In the second response cycle, as the reversed load was applied, the compression strain in the concrete at this location did drop to zero, but rather than continue on into tension, the strain gradient abruptly reversed, and increasing compression strains were observed in the concrete. This strain behavior is consistent with the presence of tensile cracks in the concrete in the vicinity of this gage, which prevented the concrete from carrying tensile stresses and strains. An alternate load path instead developed, that placed this concrete in compression. A similar behavior was seen relative to the strains experienced during the fourth load cycle, where once again the compression strains dropped at this location as the load was reversed, only to resurge at increasing displacements.

The manner in which the single hoop of reinforcing steel that encircles the embedded steel pile assisted in resisting the applied load during the test is uncertain. This hoop crossed many of the tensile cracks described above. The maximum axial strains observed in the hoop were only 1/3 to 1/2 the magnitude of the yield strain for the reinforcing steel. The gages on the hoop, however, only survived through the point at which the maximum load was applied during the first cycle of load. During subsequent cycles of displacement, the hoop noticeably pulled apart/opened up at the lap splice, decreasing its load carrying ability.
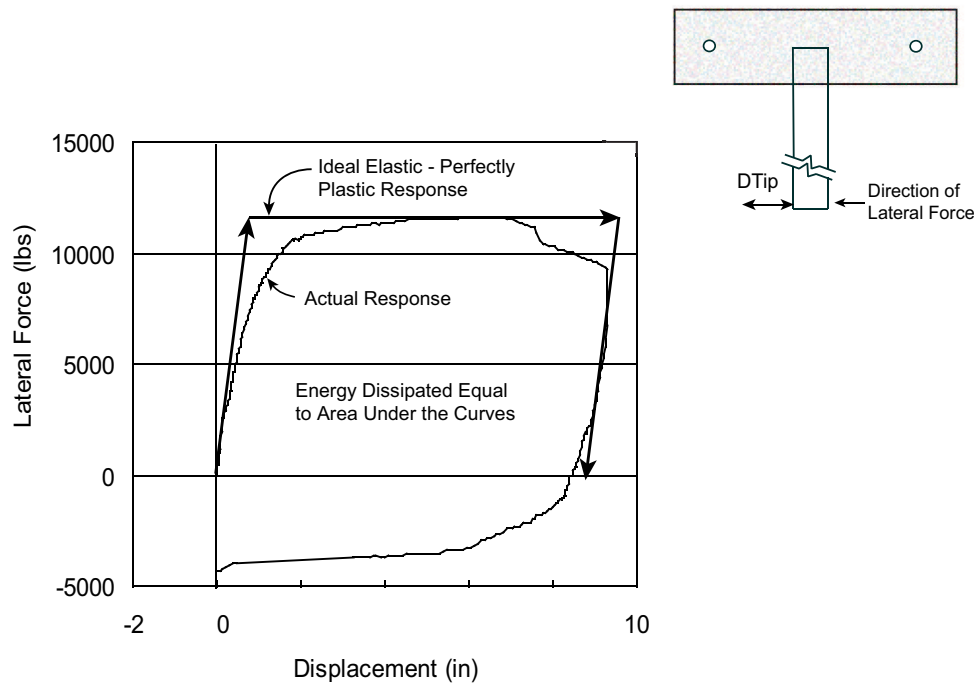
Figure 3.37: Ideal Elastic–Perfectly Plastic Load Displacement Behavior vs. Actual
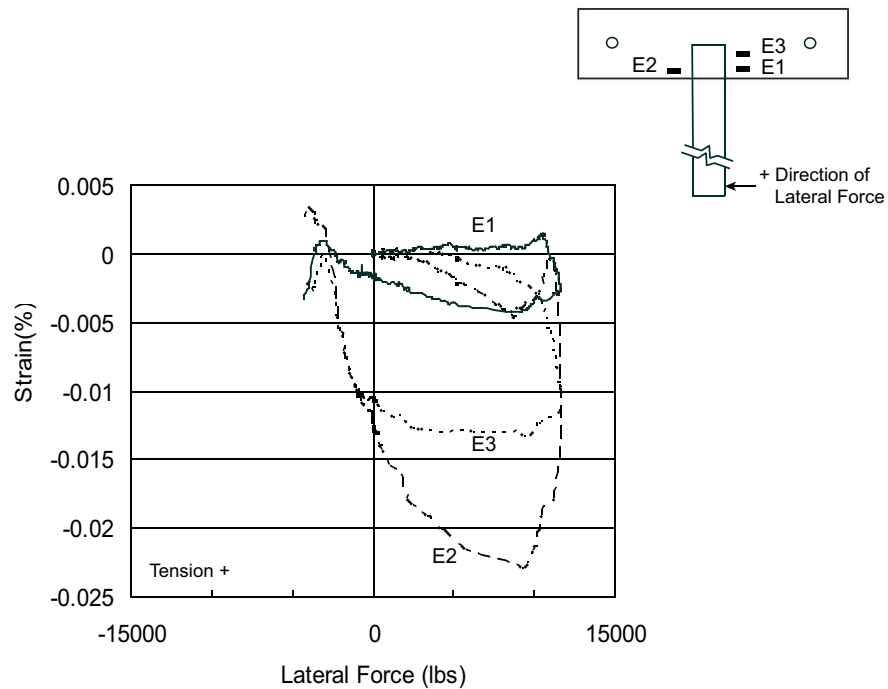
Figure 3.38: PC-2 Cap Concrete Strains (First Pull Cycle)
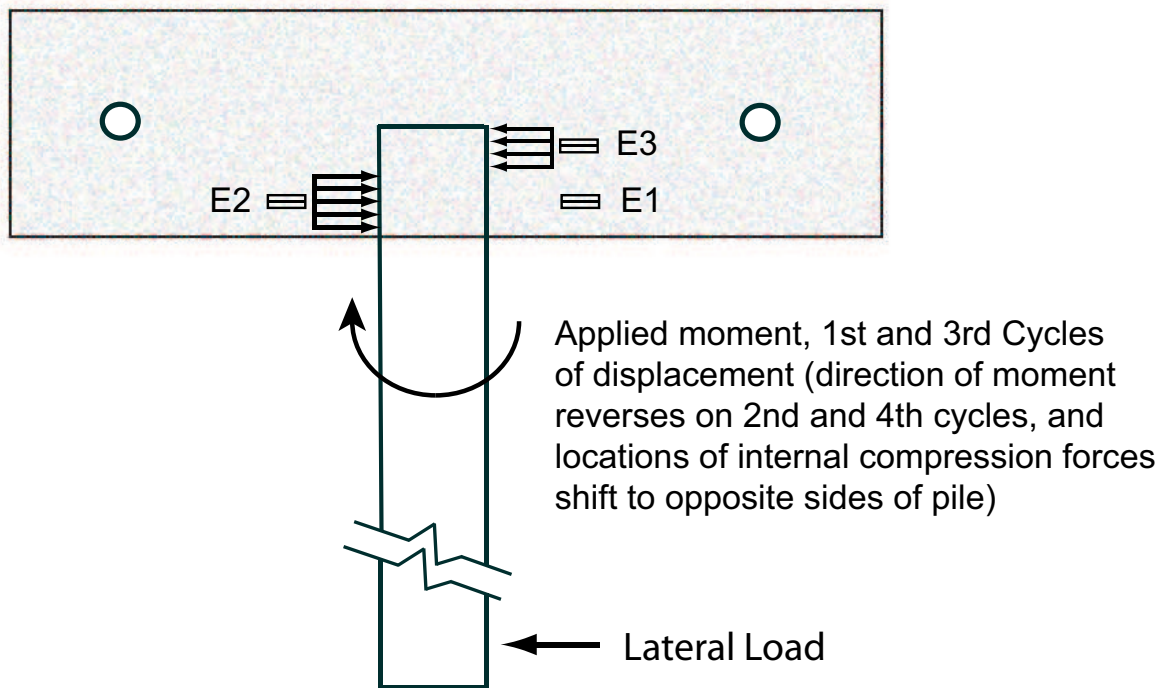
Figure 3.39: Embedded Strain Gage Locations in the Cap Relative to Expected Compression Areas
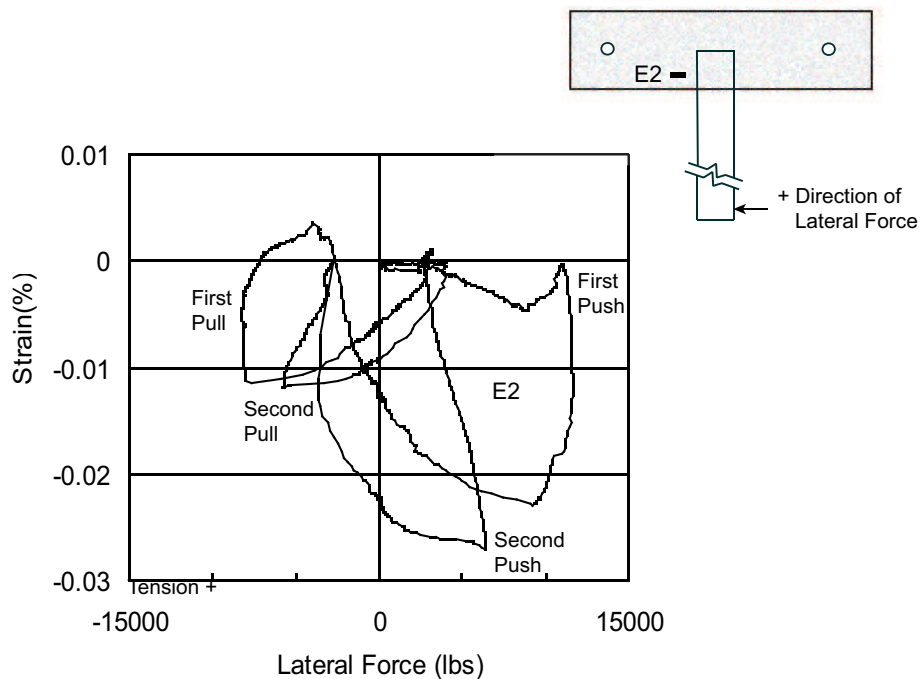
Figure 3.40: PC-2 Cap Concrete Strain (All Load Cycles)

With respect to the controlling failure mechanism for the connection, i.e., hinging in the pile or the pile cap, the strains in the extreme tension fibers of the steel pile clearly exceeded the yield strain of the steel near the face of the pile cap when the maximum capacity of the pile was reached. The longitudinal strains on the face of the pile, 2 inches outside the face of the cap (in the plane of bending), are shown in Figure 3.41. The maximum-recorded strain at this location was 0.28 percent, which was experienced when the maximum resistance of the connection was mobilized. The yield strain of the pipe steel was 0.19 percent (as determined from stress-strain tests on coupons cut from the unused portion of the pipe).

Referring to Figure 3.41, the strains measured on opposite sides of the pipe in the plane of bending were similar in magnitude, which implies that the neutral axis in the pipe pile was close to the geometric center of the pipe. A nominal shift was expected in the position of the neutral axis, due to the 15 k axial compression load applied to the pipe pile and concrete infill. Such a shift, however, is not evident in the data, although the strains generated by the axial load were expected to be an order of magnitude smaller than the bending strains generated by the transverse load. Based on the magnitude of the maximum strains at the extreme fibers of the pipe pile, the middle 2/3 of the cross-section remained elastic. A full and obvious plastic hinge did not form in the pipe during the test, and only nominal residual deformation was observed in the pipe pile at the conclusion of the test.

The magnitude of the longitudinal strains in the pipe pile decreased on each successive load cycle, as can be seen in Figure 3.41. Following initial failure of the cap, its resistance to rotation of the pipe pile deteriorated with each subsequent load cycle, resulting in an attendant reduction in the bending demands placed on the pipe pile.
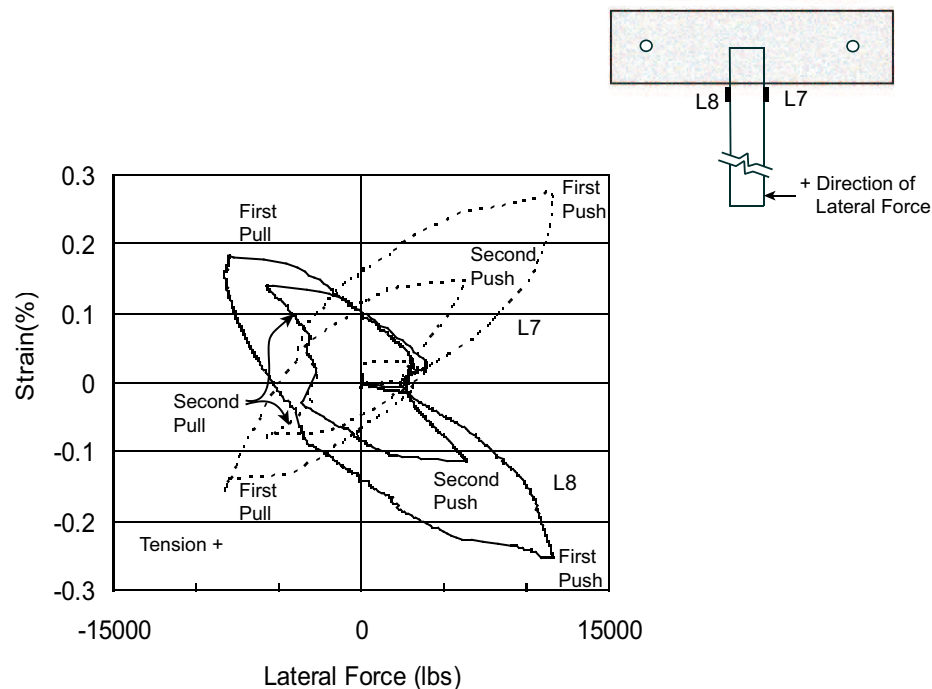
Figure 3.41: PC-2 Longitudinal Strains Measured on the Pipe Pile (Outside the Cap)

The bending strains measured on the pipe pile, 3 inches inside the cap, were approximately 50 to 75 percent of the magnitude of the strains measured just outside the cap, as shown in Figure 3.42. Thus, as seen in model PC-1, the transfer of the applied moment from the pile into the cap began close to the surface of the cap concrete. These strains remained significantly below the strains outside the cap, even after the model sustained damage. These results indicate that even in the presence of such damage, which included spalling of surficial concrete in the compression zones adjacent to the pile and visible separation of the pile from the cap in the tension zones adjacent to the pile, moment transfer from the pile to the cap began close to the surface of the cap concrete.

The behavior portrayed by the longitudinal strains measured 6 inches below the surface of the cap is difficult to interpret. By this point along the embedded length, the moment demand carried in the pipe pile was being transferred into the pile cap. While the specific mechanism of this transfer is not well characterized using longitudinal strain data, the longitudinal strains measured on opposite sides of the pile (shown in Figure 3.43) are no longer consistently of the same behavior (as seen in Figure 3.42). One particularly unusual aspect of the response of the pipe pile at this point is the direction of the initial longitudinal strains in the plane of bending. The longitudinal strains at the extreme fiber opposite the applied load initially go into tension (even though this location would be considered a compression zone based on the gross moment in the pile), while the longitudinal strains on the same side of the pile go into compression (even though this location would be considered a tension zone based on the gross moment in the pile).

Overall, the results from test PC-2 once again indicated that the capacity of the steel pipe pile to concrete pile cap connection was controlled by the strength of the pile cap. The maximum moment carried by the pile cap as it failed in test PC-2 was estimated to be 74 ft-kips (including P-delta effects), within 10 percent of the 82 ft-kip moment capacity of the similar cap used in the first test. As in the first test, the cap failure in test PC-2 primarily consisted of tension cracking of the concrete; only limited crushing of the concrete was observed in the compression areas adjacent to the pipe pile. These results suggest that as the tension capacity of the concrete was reached, and tensile demands were transferred to the reinforcing steel; this steel was quickly overwhelmed and subsequently yielded, resulting in large deformations and large crack widths in the cap concrete. Unlike the first test, the bending normal strains in the extreme fibers of the steel pipe pile at the face of the cap did exceed the yield strain of the pipe material at the time the cap failed, although a full plastic hinge did not form.
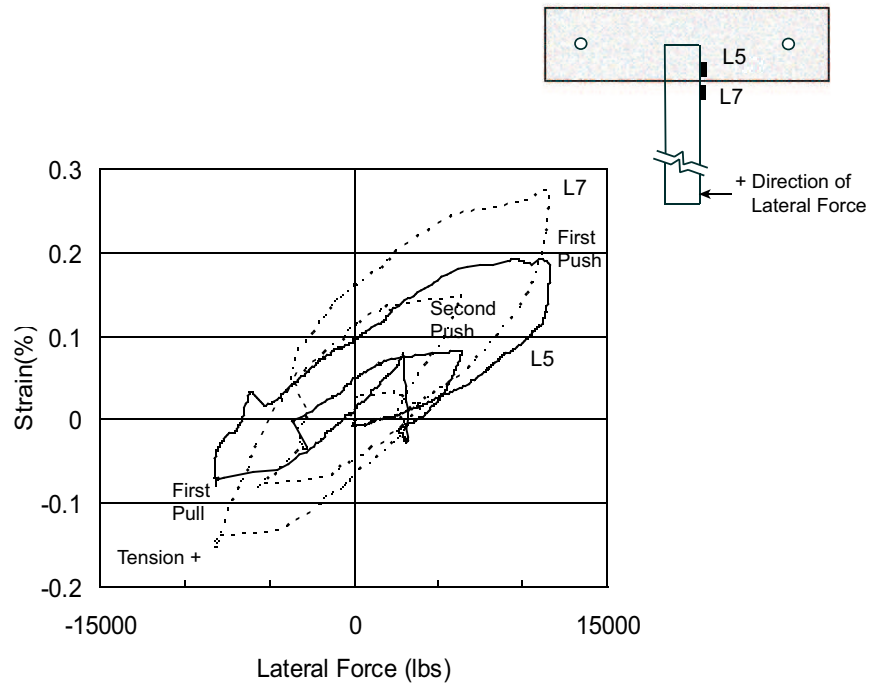
Figure 3.42: PC-2 Longitudinal Strains Measured on the Pipe Pile (Outside and Inside the Cap)
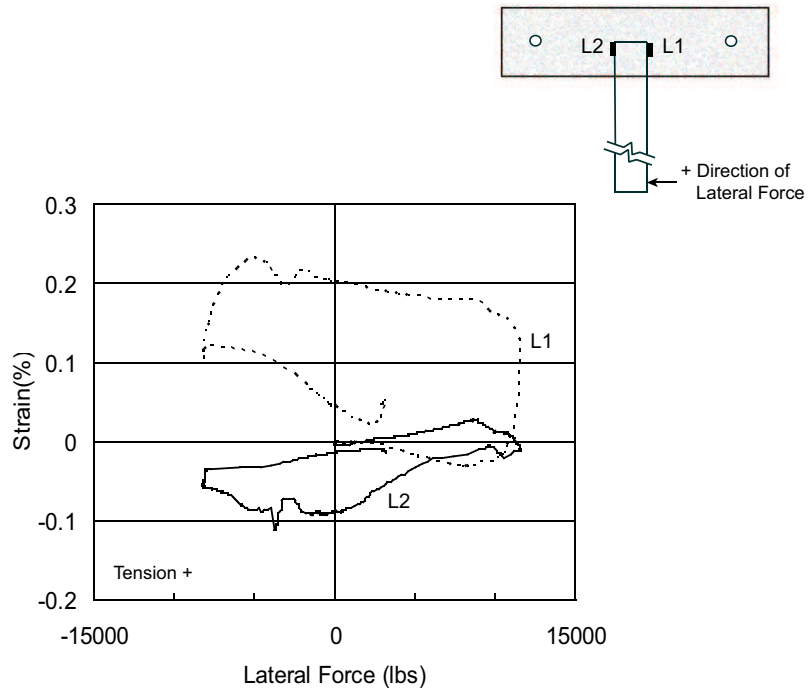
Figure 3.43: PC-2 Longitudinal Strains Measured on the Pipe Pile (Inside the Cap)

3.5.3 Test PC-3

In the third test, despite substantially increasing both the longitudinal and transverse reinforcing steel in the pile cap (by a factor of approximately 2.5), the connection again failed in the pile cap before a full plastic hinge formed in the pipe pile. Model PC-3 was subjected to three load events in which increasingly large lateral loads were applied. In the first event, the lateral load was run up to 4,200 lbs in each direction. At this load level, only hairline cracks were observed in the cap immediately adjacent to the pile, as shown in Figure 3.44. In the second event, the lateral load was run up to 9,200 lbs in just one direction. At this load, the hairline cracks in the cap from the previous test noticeably opened and began to propagate down the side of the cap, as shown in Figure 3.45. While the global load-deformation response during this test was generally linear in nature (see Figure 3.46), the cracks in the cap appeared to be growing and propagating at an accelerated rate at 9,200 lbs of load. The measured compression strains in the concrete during this load event never exceeded 0.07 percent (around 20 percent of the generally assumed crushing strain of 0.3 percent in concrete). The maximum measured strains in the pipe pile steel were on the order of 0.12 percent (approximately 67 percent of the yield strain of this material). The reinforcing steel strains peaked at approximately 0.04 percent (only 15 percent of the yield strain of this material). In the third and final load event, the lateral load was re-applied monotonically until the capacity of the connection was reached, at a load of 12,800 lbs. In light of the elastic nature of the response in the earlier load events, the remainder of this discussion is focused on the results of this third and final load event.

In the third load event, Model PC-3 failed predominantly through cracking of the concrete in the pile (see Figure 3.47), with the damage and distress generally following the same pattern observed in tests PC-1 and PC-2. The maximum load carried by model PC-3 of 12,800 lbs nominally exceeded the maximum load of 11,651 lbs observed in test PC-2. Normally, this magnitude of increase in load carrying capacity would not necessarily be viewed as significant, in light of the inherent variations in the strength of cast-in-place concrete members. In this case, however, due to problems at the concrete batch plant, the concrete in model PC-3 had a tension strength that was only 75 percent of that of the
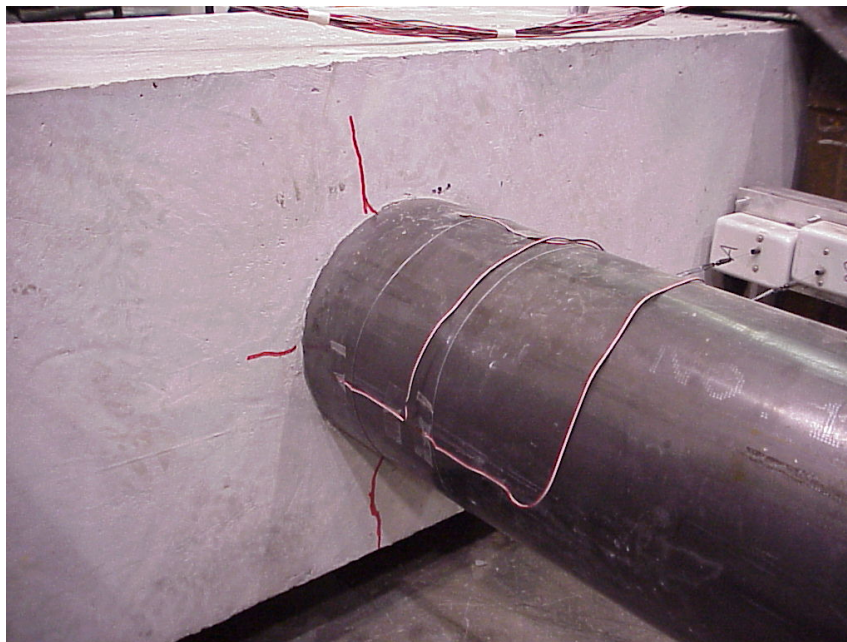
Figure 3.44: PC-3 Condition Following the First Load Event (4,200 lb Lateral Force)

Figure 3.45: PC-3 Condition Following the Second Load Event (9,200 lb Lateral Force)
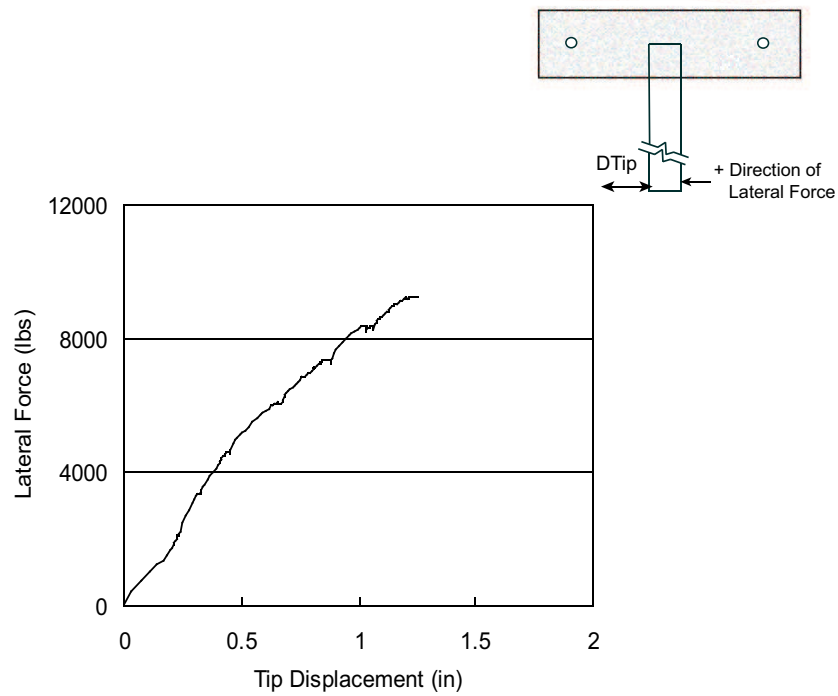
Figure 3.46: PC-3 Lateral Load vs. Lateral Displacement of the Pile (Second Load Event)
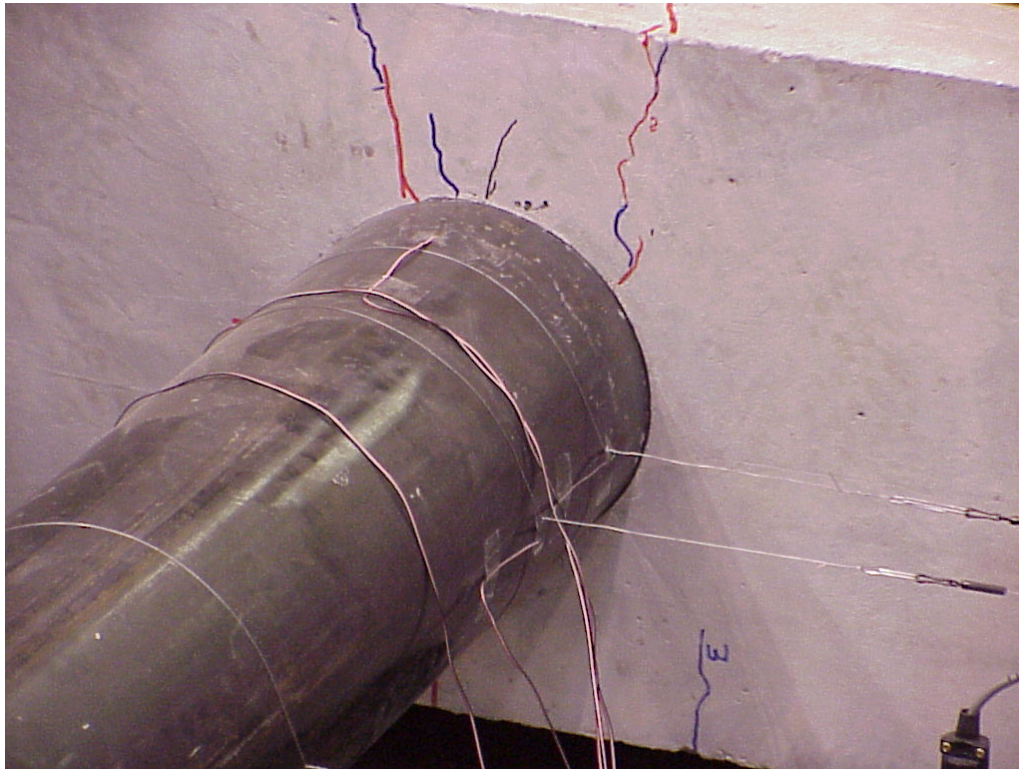
a) Prior to Failure, at a Lateral Load of 11,200 lbs

b) At Failure, Immediately Following Maximum Lateral Resistance of 12,800 lbs

Figure 3.47: PC-3 Model Condition Immediately Before and After Failure

concrete in model PC-2. While in simple models the capacity of concrete in tension is completely ignored, more sophisticated analysis approaches are beginning to recognize the importance of modeling the load carrying capacity of cracked concrete. Thus, the reduced tension capacity of the concrete in model PC-3 may have had a role in compromising its capacity relative to model PC-2. The displacement ductility of the connection, estimated from the load-displacement response to be 3.5, was similar to that observed in tests PC-1 and PC-2.

The basic load displacement response during test PC-3 is presented in Figure 3.48. The response is linear in nature up to an applied load of approximately 9,000 lbs. At loads in excess of 9,000 lbs, the response is increasingly non-linear, implying that some change occurred in the load carrying mechanism within the connection above this load. Much of the non-linearity in the response coincides with the initiation and/or growth of substantial tensile cracks in the cap. The strains in the longitudinal (Gage F2) and transverse (Gage T2) reinforcing steel inside the pile cap immediately adjacent to the pipe pile were 0.05 and 0.03 percent, respectively (see Figure 3.49), at a load of 9,000 lbs. These strains somewhat reflect conditions in the concrete immediately adjacent to the bars. Note that based on published work by others (Collins and Mitchell, 1991), the concrete in the cap was expected to begin cracking at a strain of approximately 0.01 percent, with an eventual loss of all tensile load carrying capacity at a strain of approximately 0.12 percent. Thus, at the 9,000 lb load level, the strains in the concrete in the vicinity of Gages F2 and T2 exceeded the expected tensile cracking strain of the concrete, and indeed, cracks were observed in the cap concrete immediately adjacent to the pipe pile, perpendicular to the longitudinal bars (near Gage F2).

Strains in the reinforcing steel began to climb rapidly when the applied load reached approximately 10,400 lbs, as internal forces in the cap were transferred from the damaged concrete to the reinforcing steel. The concrete in the cap subsequently appeared to lose its ability to carry all local tensile stresses when the strain reached approximately 0.15 percent at a lateral load of 12,800 lbs (the maximum lateral load that the connection was able to carry). At this strain level, the cracks widened, resulting in the formation of new load paths that fully engaged the reinforcing steel. The strains in the reinforcing steel climbed from 0.15 percent (below the yield strain of the bar material) to approximately 0.21 percent (approximately at the yield strain of the bar material), without any increase in the externally applied load. This strain event corresponded to the appearance and rapid growth of the large diagonal cracks seen in the cap (Figure 3.47), running from the bearing area of the pipe pile to the side faces of the pile cap. During this strain event, the cap made the transition from a relatively uncracked solid elastic block, at loads below 9,000 lbs, to a fully cracked strut-and-tie structure at a load of 12,800 lbs.

Stress and strain conditions in the cap can be studied in more detail using the strains measured at various locations throughout the cap. The strains measured at four locations along the length of the longitudinal bar in the face of the cap adjacent to the pipe pile are reported in Figure 3.50. As the test began, the most rapid rise in strain was seen at location F2, immediately adjacent to the pipe pile. As mentioned above, this strain increased in direct proportion to the applied lateral load up to 9,000 lbs, at which point the gross behavior of the model became non-linear. At location F7 (approximately one foot further along the bar from location F2), the strain initially increased more slowly than at location F2. The strain at this location, however, rapidly increased as the applied load passed 10,000 lbs, and beginning at a load of 11,000 lbs and a strain of 0.10 percent, the strain at location F7 closely mimicked that at location F2. Similar to the behavior at F7, the strain at location F6 began to increase rapidly at a load of approximately 10,000 lbs. At a load of 12,000 lbs, the strain began to climb even more sharply at F6. This event corresponded with the appearance and growth of the large diagonal cracks in the concrete running from the pile to the side face of the cap (note that
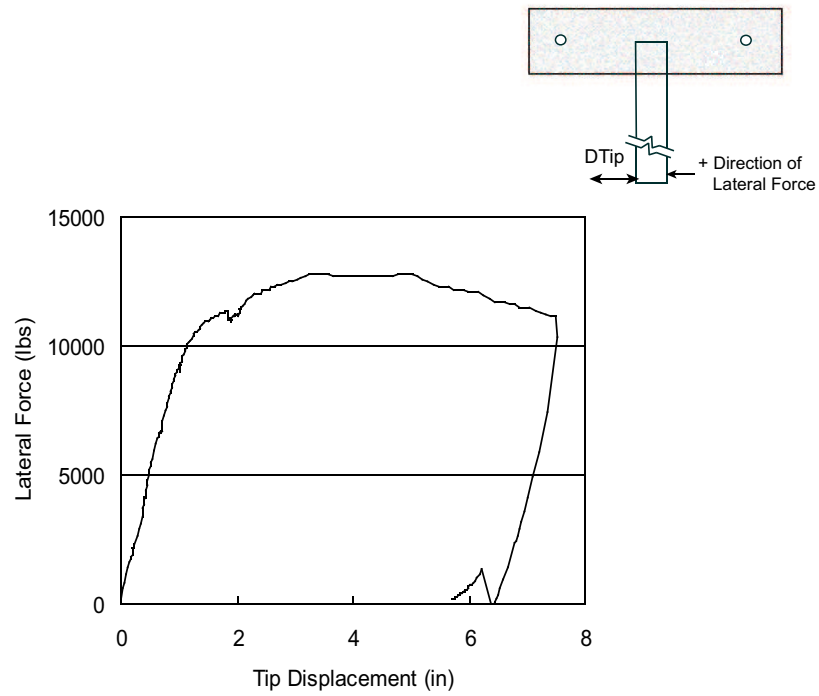
Figure 3.48: PC-3 Pipe Pile Lateral Load vs. Lateral Displacement (Main Load Event)
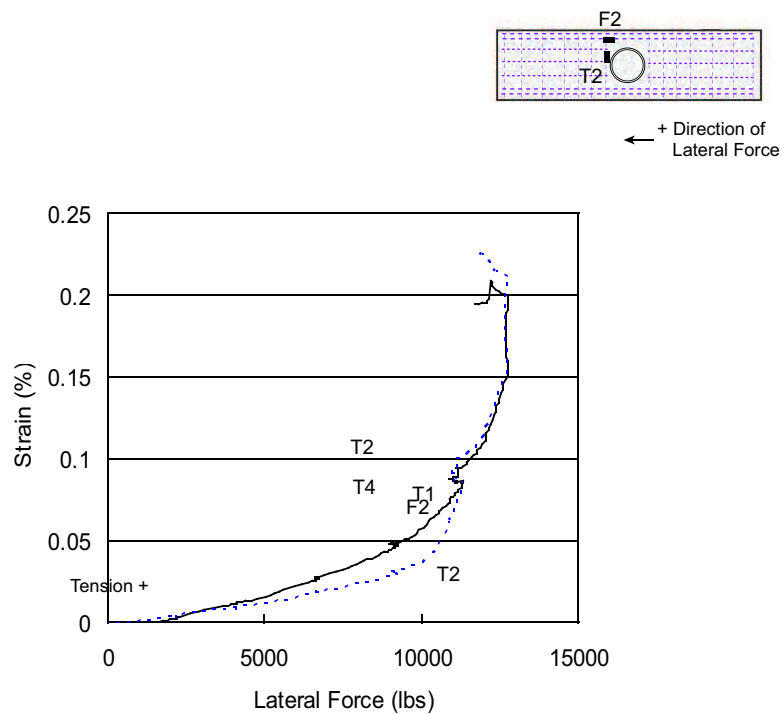
Figure 3.49: PC-3 Longitudinal and Transverse Reinforcing Steel Strains (Main Load Event)
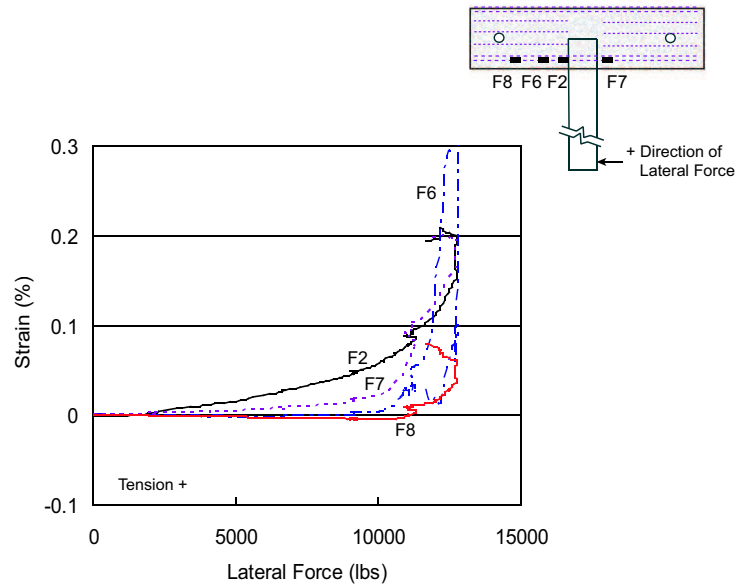
Figure 3.50: PC-3 Longitudinal Reinforcing Steel Strains (Main Load Event)

location F6 is very close to where this crack crossed the longitudinal reinforcement). The strain at F6 subsequently peaked at 0.32 percent (which is approaching 150 percent of the yield strain of the bar) at the peak resistance of the connection of 12,800 lbs. The gage ceased to function at this time, possibly due to a lead wire failure associated with the large displacement occurring in the vicinity of the diagonal crack. These results generally indicate that as the concrete cracked in tension, this region of the bar increasingly behaved as a tension tie, spanning at least between locations F6 and F7.

The strains measured on three different transverse ties in the pile cap are presented in Figure 3.51. In all cases, strain was measured on the leg of the tie in the bottom face of the cap, as shown in Figure 3.51. Tensile strains were observed in all three ties, with a maximum value of 0.23 percent occurring in tie T2, the tie closest to the pipe pile in the direction of applied lateral load. This strain occurred at the maximum load of 12,800 lbs, and is approximately equal to the yield strain of the bar. Strains in the corresponding tie on the opposite side of the pile, tie T1, initially were approximately one-half of the magnitude of the strains in tie T2. Smaller strains were expected at T1 than at T2, in that the pipe pile was expected to pull away from the concrete in this area. After the peak load of 12,752 lbs was applied to the model, the strain in tie T1 rapidly increased, reaching a peak value of 0.214 percent at the termination of the test. The strains in the second tie away from the pile, tie T4, only reached a maximum value of 0.125 percent. Thus, most of the tendency of the rotating pile to split the cap apart was resisted by the ties immediately adjacent to the cap.

The strains measured in the concrete at two locations near the bottom face of the cap are shown in Figure 3.52. The gage at location E6 was purposefully oriented at approximately 45 degrees to the longitudinal axis of the cap to be approximately parallel to the diagonal cracks observed in tests PC-1 and PC-2. Significant compression "struts" were expected to act in the concrete parallel to these cracks, running diagonally from the pile to the side face of the cap. While in an obvious compression zone, the concrete at location E2 was not expected to act as a primary compression strut.

Referring to Figure 3.52, the compression strains measured at E6 and E2 are relatively low in magnitude relative to the nominal crushing strain of concrete, which is typically assumed to be 0.3 percent.
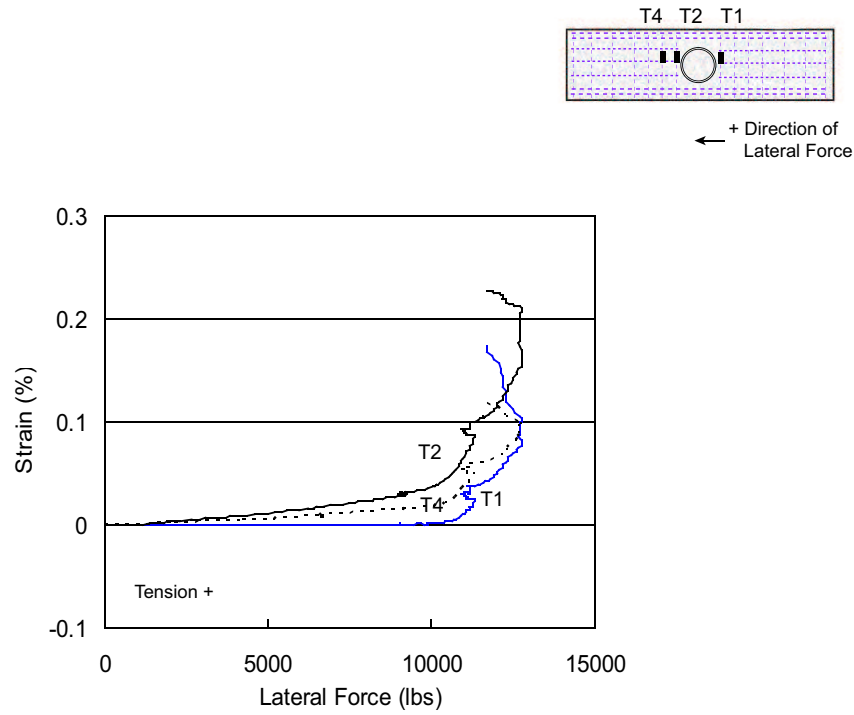
Figure 3.51: PC-3 Transverse Reinforcing Steel Strains (Main Load Event)
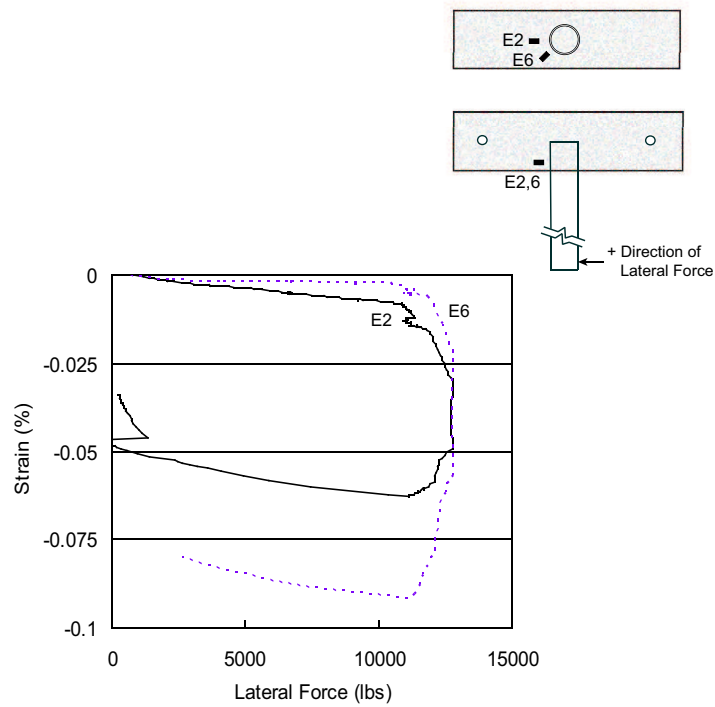
Figure 3.52: PC-3 Cap Concrete Strains (Main Load Event)

Concrete often is assumed to behave linear elastic in compression up to a stress of $0.45 f_c'$, which corresponds to a strain of approximately 0.05 percent for concrete with an unconfined compression strength of 4,000 psi. The maximum measured strains in the concrete at E6 and E2 at the maximum lateral load of 12,800 lbs were of this order of magnitude. As the connection shifted toward strut and tie behavior as the 12,800 lb capacity of the connection was reached, larger strains were measured at location E6 relative to location E2, as a primary strut formed at this location.

While the obvious damage sustained by the connection in test PC-3 occurred in the cap, the steel pipe pile also experienced significant plastic deformation during the test. As shown in Figure 3.53, the extreme fibers of the pile in bending reached their yield strain of 0.18 percent at a lateral load of 11,000 lbs. The strain at this location subsequently increased to 0.40 percent at the maximum load of 12,800 lbs carried by the connection at failure. Assuming a linear strain diagram across the depth of the cross-section, approximately the middle 1/2 of the cross-section remained elastic at this load. While this level of strain exceeded the maximum strains observed in previous tests, no obvious plastic hinge was observed in the pipe pile at the face of the pile cap. The pipe pile did exhibit obvious permanent deformation at the conclusion of testing.

Connection model PC-3 carried a total moment of 76 ft-kips, including P-delta effects; note that the theoretical capacity if the pipe pile in test PC-3 was 101 ft-kips. Relative to ductility, the yield point in the global load-displacement response was less well defined in test PC-3 relative to tests PC-1 and PC-2. Nonetheless, following the same procedure as was used in tests PC-1 and PC-2 to analytically establish a yield displacement, the ductility was calculated to be 3.5.
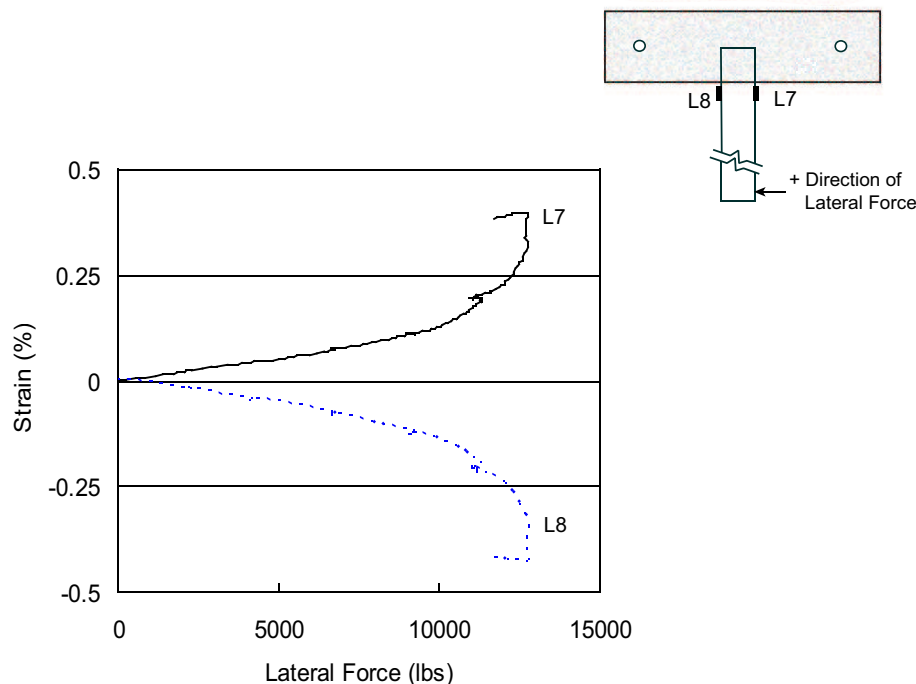
Figure 3.53: PC-3 Longitudinal Strains Measured on the Pipe Pile (Outside the Cap)

3.5.4   Test PC-3a

Once again, despite increasing the reinforcing steel used in both the longitudinal and transverse directions in model PC-3a (by a factor of approximately 5, relative to PC-1 and PC-2), and making some changes in the detailing of this steel as noted in the model description provided previously, the ultimate capacity of model PC-3a was still controlled by failure of the pile cap. The distress at failure once again resembled that observed in all the earlier tests (see Figure 3.54). In this case, however, the lateral load at failure of 17,572 lbs represented an obvious and substantial increase in the capacity of the cap over that observed in earlier tests. Recall that three changes were made to the model between test PC-3 and PC-3a, namely, a) the amount of longitudinal and transverse reinforcing steel was increased, b) the longitudinal bars interrupted by the pipe pile were hooked through the spiral that encircled the pipe pile, and c) the pitch of the spiral around the pipe pile was decreased to 1.75 in, and the spiral was extended across the full depth of the cap. It is difficult to definitively know which of these three changes was responsible for the increase in the capacity of the cap. Intuitively, the magnitude of the influence these changes were expected to have on the response paralleled the order in which they are listed above (that is, most influence - increasing the longitudinal and transverse areas of steel, least influence - running the spiral full depth of the cap).

The global load deformation response observed during test PC-3a is presented in Figure 3.55. Non-linear response began at a load of approximately 10,000 pounds. At this point, no distress was apparent in the cap. The first distress in the cap was seen at a load of 11,500 lbs, and consisted of a single hairline crack in the cap adjacent to the pile. Little additional cracking was observed in the cap up until its failure at a load of 17,600 lbs. Failure was precipitated by the opening of the cracks in the side of the cap, immediately adjacent to the pipe pile, and the formation of large diagonal cracks running from the pipe pile to the side faces of the cap, as seen in each of the previous tests. The

a) Prior to Failure, at a Lateral Load of 16,000 lbs

b) At Failure, Immediately Following Maximum Lateral Resistance of 17,600 lbs

Figure 3.54: PC-3a Model Condition Immediately Before and After Failure
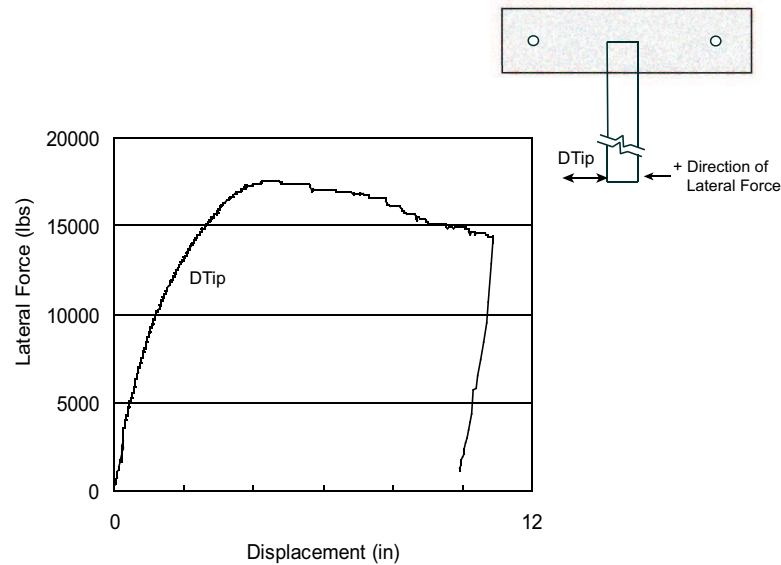
Figure 3.55: PC-3a Pipe Pile Lateral Load vs. Lateral Displacement (Main Load Event)

condition of the model after the test is shown in Figure 3.54. There was little evidence of crushing in the concrete, even in the direct bearing area adjacent to the downstream side of the pipe pile. Referring to the global load displacement response in Figure 3.55, the yield point of connection PC-3a was poorly defined, similar to the situation with model PC-3. Nonetheless, following the same procedure as used throughout this investigation, the ductility at failure was estimated to be 2.6. The decrease in ductility in test PC-3a may be related to the increase in the amount of reinforcing steel in the model. As the percentage of reinforcing steel increases, the post-failure behavior of the connection may be more dominated by the material characteristics of the concrete, as opposed to the reinforcing steel (i.e., moving from an under reinforced to more of an over reinforced situation).

The moment carried by the connection at failure was calculated to be 102 ft-kips (including P-delta effects). Strain conditions inside the cap at its failure point are unknown, as the instrumentation in model PC-3a only consisted of longitudinal strain gages on the steel pipe pile. Strain histories from these gages are reported in Figure 3.56. The yield strain of the pipe steel (approximately 0.21 percent) was exceeded at the extreme fibers of the pile in bending at a lateral load of approximately 12,200 lbs. These strains climbed to over three times the yield strain when the ultimate load carrying capacity of the connection of 17,600 lbs was realized. Based on the magnitude of these extreme fiber strains, only the middle of the cross-section remained elastic when the ultimate capacity of the cross-section was reached. Despite the magnitude of these extreme fiber strains, a full plastic hinge had not formed in the pipe pile when the capacity of the cap was reached. Recall that the theoretical moment capacity of the pipe pile in this model was only estimated to be 84 ft-kips, versus the 102 ft-kip demand that it actually carried when the cap failed.
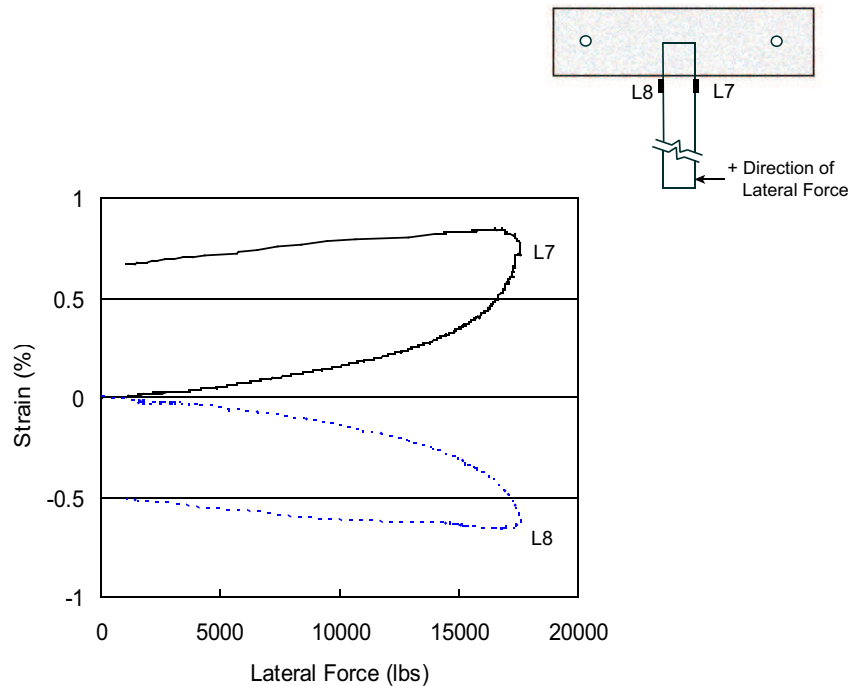
Figure 3.56: PC-3a Pipe Pile Longitudinal Strains Measured (Outside the Cap)

3.5.5   Test PC-4

Unlike the previous models, Model PC-4 failed through the formation of a plastic hinge in the steel pipe pile immediately outside the pile cap. This failure occurred at a moment of 121 ft-k (including P-delta effects). Recall that the percentage of longitudinal and transverse steel in model PC-4 was increased relative to that in model PC-3a, and the detailing of this steel once again was changed, in this case so that the primary longitudinal steel encircled the pipe pile (see Figure 3.15). The condition of model PC-4 at failure is shown in Figure 3.57. As the plastic hinge formed, the steel pipe locally buckled on the compression side in bending. Note that following AISC provisions (AISC, 2001), local buckling of an unfilled pipe section in bending is a concern at a diameter to thickness ratio (D/t) of approximately 39. The D/t ratio for the pipe used in this test of 34.5 was close to this threshold value. Only a few cracks (less than one millimeter wide) were observed in the cap when the plastic hinge formed, although the pile did pull away from the cap on the tension side.

The load-displacement response of the connection during the initial load cycle is presented in Figure 3.58. Non-linear behavior was first seen at an applied lateral load of approximately 12,500 lbs. The plastic hinge in the pipe pile was fully formed when the lateral load reached approximately 19,600 lbs at a tip displacement of 4.75 inches. The lateral load carrying capacity leveled off at this point, further increasing to only 20,400 lbs at a displacement of 11 inches. The displacement ductility at this position was estimated to be 3.9, and there was no evidence at the termination of this load cycle that the end of the yield plateau had been reached (the tip of the pile could not be pushed over any further due to load frame related constraints). The tip of the pipe pile was pulled back through its initial position and displaced 1.88 inches in the opposite direction, as indicated in Figure 3.58.
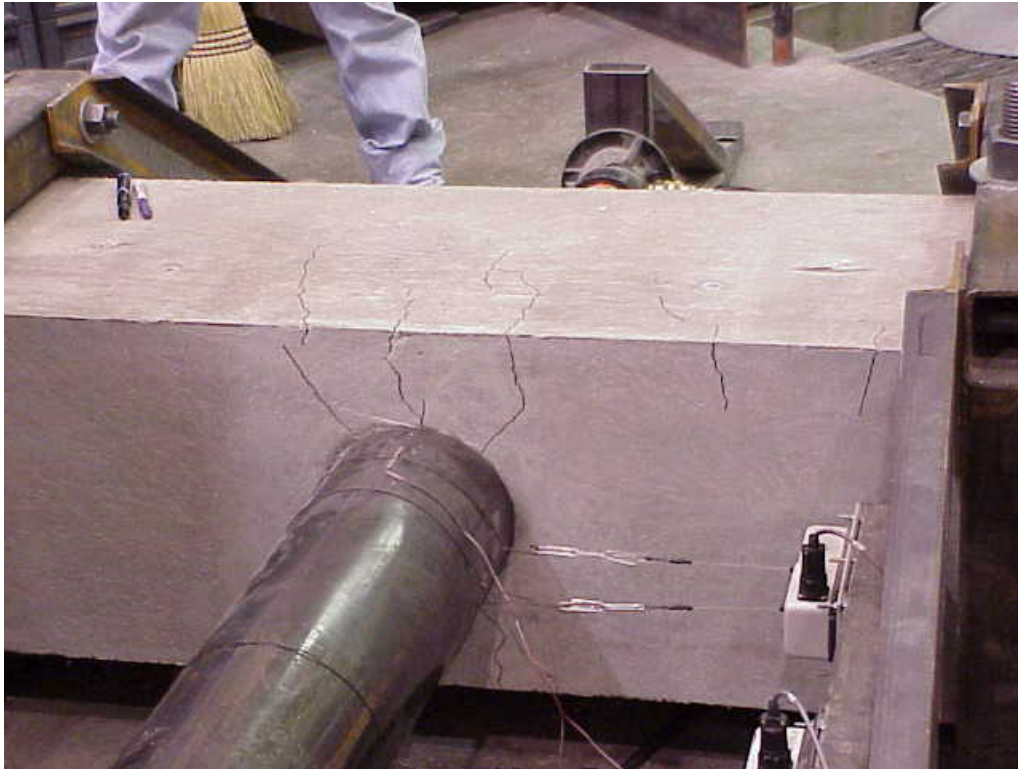
a) At 20,400 lbs, after Formation of a Plastic Hinge in the Pipe Pile in the First Push Cycle
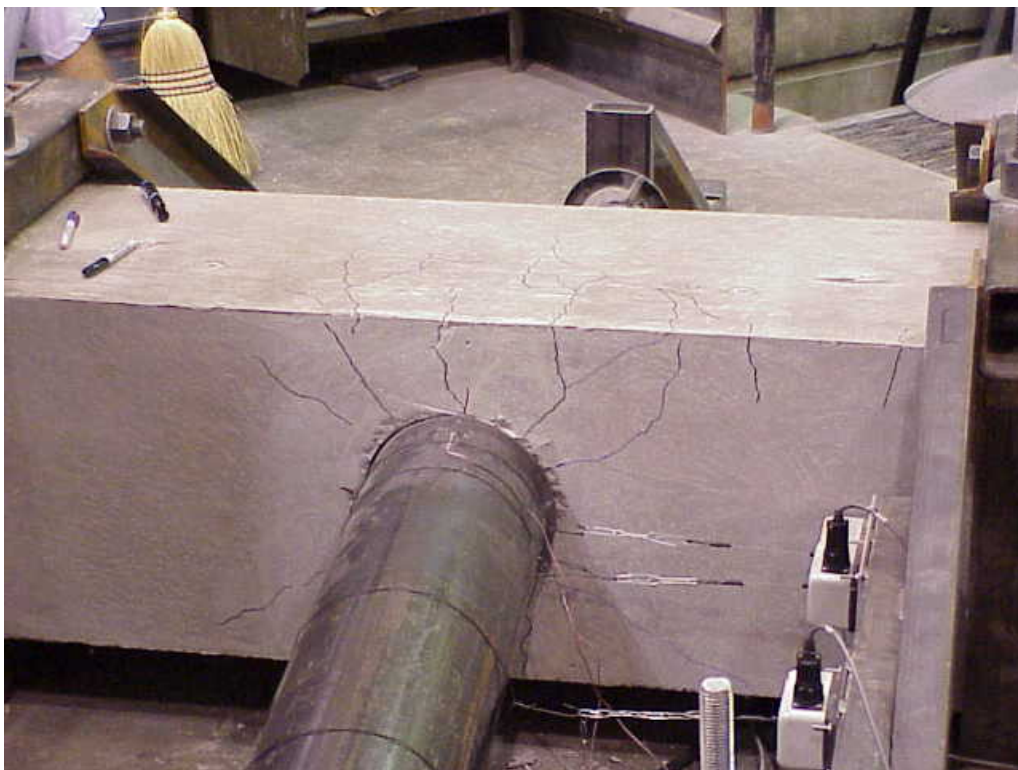
b) At 20,600 lbs, after Formation of a Plastic Hinge in the Pipe Pile in the First Pull Cycle

Figure 3.57: PC-4 Model Condition Immediately Before and After Failure
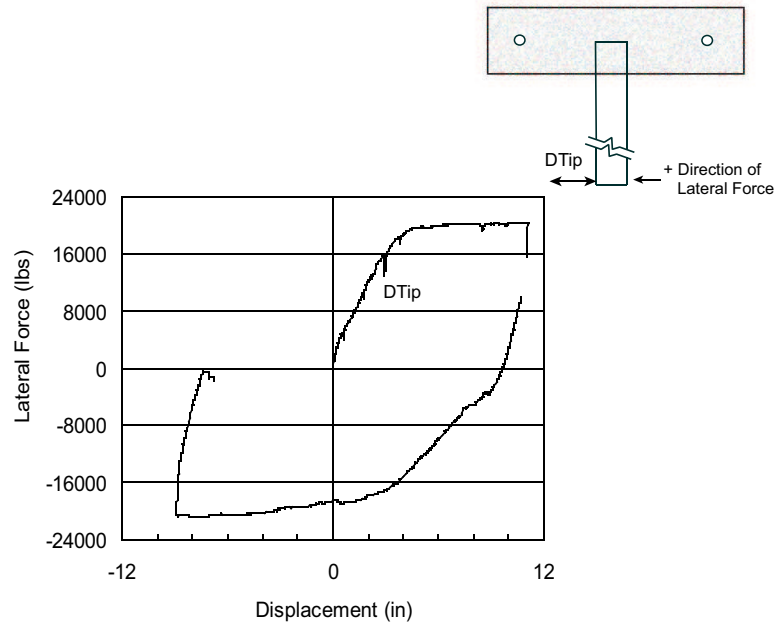
Figure 3.58: PC-4 Lateral Load vs. Lateral Displacement of the Pipe Pile (Main Load Event)

Once again, during this reversed cycle of load, a clear yield plateau is evident at a load of approximately 20,000 lbs. Furthermore, and as might be expected for a situation dominated by the yielding of a steel material, the hysteresis behavior as portrayed in Figure 3.58 is more robust than the "pinched" curves observed in test PC-2, when the failure of the connection occurred in the cap.

As in test PC-3a, only limited instrumentation was included in test PC-4. The longitudinal strains measured on the pipe pile adjacent to the pile cap are presented in Figure 3.59. The extreme fiber strains pass through the yield point of the pipe steel at a load of approximately 12,500 lbs, similar to previous tests. Gross hinging at the base of the pipe pile (as evidenced by the plateau in the global load deformation response), however, does not occur until the applied transverse load reaches almost 20,000 lbs, and the extreme fiber strains are on the order of magnitude of 2 percent (ten times the initial yield strain of the pipe steel).
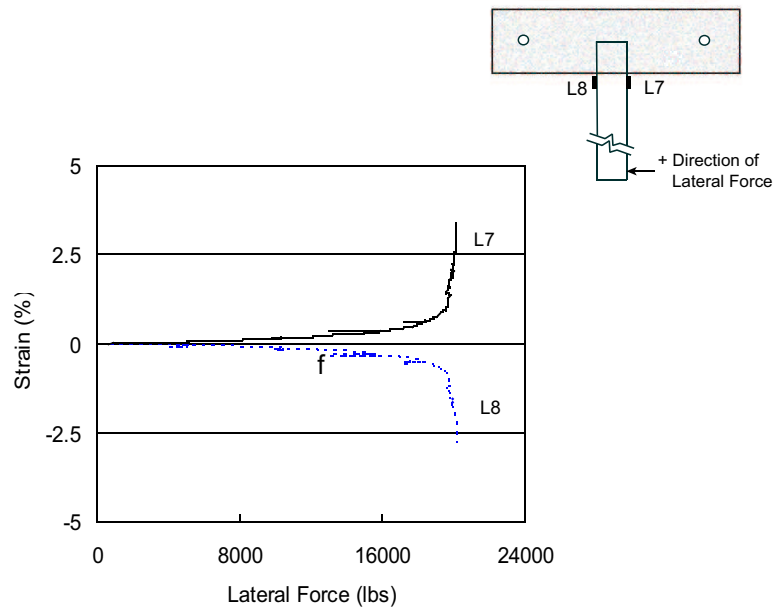
Figure 3.59: PC-4 Pipe Pile Longitudinal Strains (Outside the Cap)

3.6 SUMMARY OF TEST RESULTS

The tests described above characterize the failure behaviors under lateral loads of a steel pipe pile to concrete pile cap connection commonly used by MDT in bridge support structures. The test matrix and results were previously summarized in Table 3.3. Testing began with 1/2 size models designed to represent a specific geometry and reinforcing steel layout used by the state for this connection (models PC-1 and PC-2). As increasing transverse load was applied to these models, failure of the connection occurred in the reinforced concrete pile cap. While concern initially was focused on failure in the cap due to crushing of the concrete at the face of the embedded pile, these failures were the result of tensile cracking of the concrete adjacent to the pile, followed by yielding of the reinforcing steel. The amount of reinforcing steel was increased in subsequent models, and some of the detailing of this steel was also changed, until in the final test (PC-4), failure of the connection occurred through the formation of a plastic hinge in the steel pipe pile, outside of the cap.

The percentage of reinforcing steel used in the cap in each test is plotted as a function of moment carried at failure in Figure 3.60. The longitudinal and transverse steel ratios were varied from 0.41 and 0.09 percent, respectively, in tests PC-1 and PC-2 to 2.83 and 0.70 percent, respectively in test PC-4. As might be expected in light of the failure mechanism in early tests (failure in the cap from tension related effects, rather than through the formation of the pipe pile), the moment capacity of the connection increased as the amount of reinforcing steel in the cap increased (although these parameters may not be linearly related). The reinforcing steel in the cap in the final test was sufficient in amount and placed so as to produce a full plastic hinge in the pipe pile, before failure occurred in the cap.

Relative to the ductility and energy dissipation characteristics of this connection configuration, and again as might be expected, through the formation of a full plastic hinge in the pipe pile (model PC-4) was more ductile and had more promising energy dissipation characteristics than failure in the cap (models PC-1, 2, 3, and 3a). Post failure behavior in this failure mode (formation of a plastic
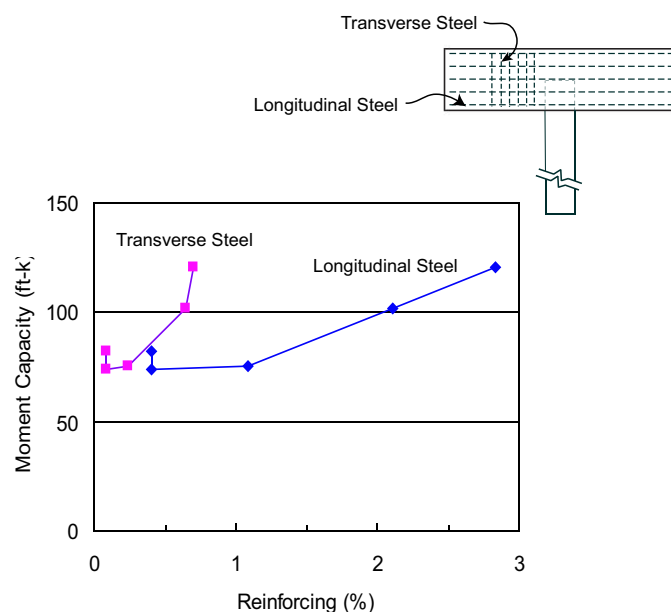
Figure 3.60: Actual Pile Cap Moment Capacity as a Function of Reinforcement Ratio of the Cap

hinge in the cap) can not be fully commented on, however, in that at the full displacement capacity of the test frame, the end of the yield plateau for this connection had not been reached. Model PC-4 was subjected to one cycle of reversed loading, and the resulting hysteresis curves were robust in nature, exhibiting little loss of load carrying or energy dissipation capacity during the reversed load cycle. Conversely, model PC-2, which experienced a failure in the cap, exhibited an immediate loss of load carrying and energy dissipation capacity in the first cycle of reversed load.

Lateral displacement as a function of lateral load during the first load cycle to failure in each test are presented in Figure 3.61. In all cases in which failure occurred in the pile cap (PC-1, 2, 3, and 3a), the load carrying capacity of the connection was seen to noticeably drop off after the peak resistance was realized and as the pile continued to be laterally displaced. The ductility ratio for models PC-1, 2, and 3 were all approximately 3.3. The ductility ratio for model PC-3a noticeably decreased to 2.0. While in all four of these models failure occurred in the concrete cap, the amount of reinforcing steel was steadily increased from model PC-2 to model PC-3a. Arguably, this increase in the amount of reinforcing steel in the models began to shift the nature of the cap failure from a ductile tension controlled situation to a more brittle compression controlled situation. Model PC-4 failed through the formation of a plastic hinge in the pipe pile. At the termination of the first load cycle (at a ductility ratio of 3.9), there was no indication that the end of the "perfectly" plastic load plateau in the force-deformation response had been reached.
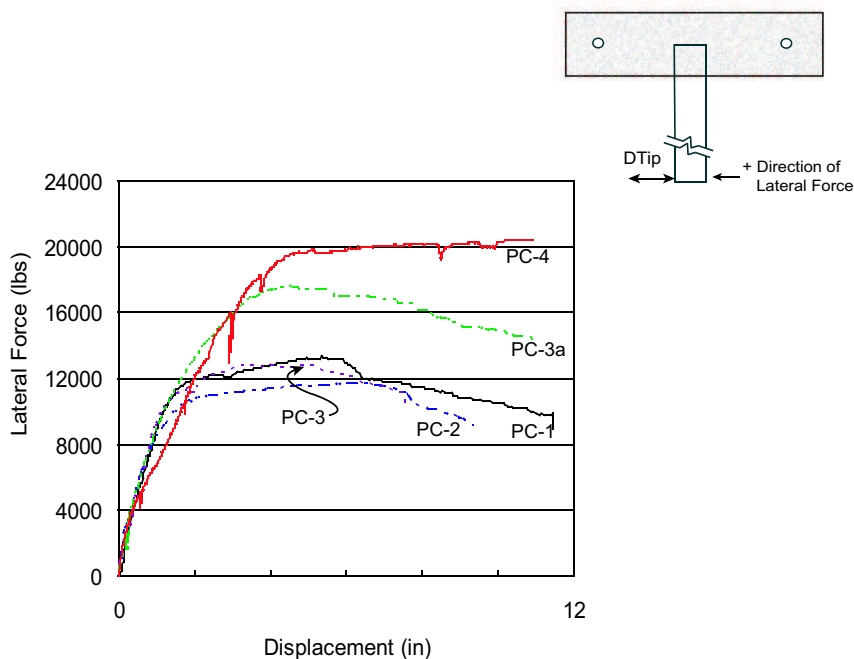
Figure 3.61: Pipe Pile Lateral Load vs. Lateral Displacement (First Load Cycle of Each Test)

Chapter 4

Analytical Effort

4.1 GENERAL REMARKS

Three approaches were used in this investigation to analytically study the behavior of the pipe pile to steel pile cap connection, namely, "hand" calculations, strut and tie calculations, and solid finite element modeling. As used in this investigation, these methods involved increasing levels of sophistication, in the order in which they are listed above. For the hand calculations, the pipe pile capacity was calculated by an equation used in the seismic design of bridges (ATC/MCEER, 2001), while the capacity of the cap was evaluated using a simple model of the compression force couple that develops in the cap as it resists rotation of the pipe pile. The hand calculations, while easy to use and understand, offered little detail relative to stress conditions throughout the cap or any quantitative information on the load-displacement behavior of the overall connection. Nonetheless, with some adjustments based on the test data, these hand calculation methods may provide useful results to the designer.

Strut and tie modeling consisted of representing the response of the reinforced concrete in the cap as a series of compression struts and tension ties (the steel pipe was modeled as an infinitely stiff and strong element). The steel reinforcement was modeled as tension ties, while the compression zones of the concrete were modeled using the compressive struts. This use of the struts and ties, which has been an emerging analysis technique over at least the past 20 years, is believed to give the designer a clearer understanding of the dominant force paths within the cap. The strut and tie approach could offer an intermediate analysis option between the "overly" simply hand calculations and the "overly" sophisticated finite element calculations. Obviously, the strut and tie approach takes into account the placement of the reinforcement in cap (as well as the amount). Additionally, this method offers information on the behavior at discrete points throughout the cap. In this investigation, the strut and tie method was implemented using a member based (rather than a solid material based) finite element program. Two limitations were encountered with this analysis, namely, 1) the strut and tie method assumes that the concrete has no tension capacity, which is only valid once the concrete has severely cracked, and 2) an elastic finite element program was used, so plastic yielding of the reinforcing steel could only be approximately modeled. While conceptually a promising analysis technique, notably as implemented by finite element, this approach will require further development before it is directly useful as a design tool.

The response of the pile-to-pile cap connection was also investigated using finite element models. Such models can incorporate non-linear behavior such as crushing, cracking, and large deformation of the material, as well as discrete reinforcement in the pile cap. These models often have difficulty converging on solutions. FEM's that include nonlinear behavior are by nature somewhat difficult to use, require a lot of computing power and user experience to accurately represent the desired behavior.

4.2 HAND CALCULATIONS

Simple (hand calculation) procedures are available to estimate the capacity of the steel pipe pile to concrete pile cap connection considered in this investigation. As used in this study, these calculations treated the capacity of the steel pipe pile and of the concrete pile cap independently, with the idea that failure will occur in that element with the lower calculated capacity. The specific capacity equations used in this investigation were already introduced in the section of this report that describes the model geometry, and therefore only a brief summary of these equations is presented below. The results obtained by these equations are subsequently compared with the actually connection capacities determined during the physical tests.

4.2.1 Steel Pipe Pile Capacity

As previously mentioned, the capacity of the concrete filled, steel pipe pile was calculated using an equation developed by Bruneau and Marson (2004) which now has been adopted into the LRFD guide for the seismic design of bridges (ATC/MCEER, 2001). This equation, reproduced as Eq. 3.2.1 in this report, was developed to provide more consistent and less conservative predictions of the strength of concrete filled pipe piles than was available from existing capacity equations (Bruneau and Marson, 2004).

The theoretical capacity of the steel pipe pile calculated using this equation with actual material properties and geometry of each pipe pile is given in Table 4.1. Note that the axial compression load in the pipe pile of 15 k was ignored in these calculations. As previously mentioned, this load was less than 3 percent of the axial capacity of the pile, and thus it was expected to have little impact on the flexural capacity of the pile section. Also presented in Table 4.1 is the plastic moment capacity of the pile neglecting any effect of the concrete infill. Traditionally, the bending capacity of concrete filled pipe sections was calculated neglecting the infill concrete, under the assumption that the presence of composite action between the infill and the steel tube was uncertain. The presence of the infill concrete was also generally assumed to only nominally increase the capacity of the net section in bending. In this case, the calculated flexural capacity of the composite infill concrete and steel pipe was 17 to 18 percent greater than the capacity calculated for the steel pipe alone.

The actual moment carried by the steel pipe pile in each test is also reported in Table 4.1. Recall that the tabled values of the theoretical capacity are for the case of a plastic hinge forming in the pipe pile. A full plastic hinge formed in the pipe pile in only one test, test PC-4. In this test, the actual plastic moment capacity of the pipe pile exceeded the theoretical capacity by 26 percent. Note that for model PC-3a, the maximum moment carried by the pipe pile during the test also exceeded the calculated plastic moment capacity (by 20 percent). In test PC-3a, however, a full plastic hinge did not actually form in the pipe pile, although significant plastic strains were seen at the extreme fiber of the pile (the tensile strains in the extreme fibers of the pipe pile were four times the yield strain of the material). In all earlier tests, (tests PC-1 through PC-3), the maximum moment demand placed on the pipe piles did not exceed their calculated plastic moment capacities. Nonetheless, plastic bending strains were measured at the extreme fiber of the pipe pile in each test. As might be expected, and as is shown in Table 4.1, the magnitudes of these strains increased as the moment demand experienced by the piles increased relative to their respective calculated plastic moment capacities. The pipe piles in these tests, however, did not experience any obvious visible damage over their exposed length.

The under prediction of the plastic moment capacity of the concrete filled pipe piles in tests PC-3a and PC-4 may in part be explained by an acknowledged deficiency in the combined axial load and

Table 4.1: Steel Pipe Pile Moment Capacities Calculated by Hand

Model	Calculated Moment Capacity of the Pipe Pile			Failure by Plastic Hinge in Pipe Pile	Actual Moment Carried by the Pipe Pile (ft-k)	Ratio, Actual to Calculated Moment Capacity	Maximum Strain Measured on the Pipe Pile, %
	Steel Pipe, Alone (ft-k) (1)	Steel Pipe and Concrete Infill (ft-k) (2)	Ratio, Moment Capacity of Steel Pipe Alone to Pipe and Infill				
PC-1	92	108	1.17	No	82	0.76	0.2
PC-2	77	91	1.18	No	74	0.81	0.3
PC-3	72	84	1.17	No	76	0.90	0.4
PC-3a	72	85	1.18	No	102	1.21	0.8
PC-4	82	96	1.17	Yes	121	1.26	4.0

bending capacity equation developed by Bruneau and Marson (2004). The commentary to the LRFD guide for the seismic design of bridges (ATC/MCEER, 2001) indicates that the equation underestimates flexural plastic moment capacity by an average of 25 percent for pipe piles with D/t ratios below $28000/F_y$. The D/t ratio of the piles used in tests PC-3a and PC-4 was 34.5, compared to values of $28000/F_y$ of 77 and 67, respectively, for each test. Thus, the calculated capacities should understate the actual strength of the piles. In more closely reviewing the performance of the equation developed by Bruneau and Marson, it appears that it gives increasingly conservative results as the axial force on the pipe pile increases. For the relatively small axial load acting on the pipe piles in this investigation, it would appear that the over estimation of the flexural capacities of the pipe piles would be substantially below the average value of 25 percent.

4.2.2   Concrete Pile Cap Capacity

The moment capacity of the concrete pile cap was calculated for each test using simple models amenable to hand calculations. The hand models considered in this investigation all involved calculating a pair of resultant compression forces in the concrete in the cap to resist the moment introduced by the pipe pile, as previously shown in Figure 3.6. The capacity of the cap was then calculated either based on crushing the concrete under these internal compression forces, or yielding the reinforcing steel under the equilibrating tension forces that develop in the reinforcing steel. This approach begins with the calculation of the compression couple in the concrete, which requires several assumptions regarding the geometry of the compression stress block. Typical assumptions include using a simple rectangular approximation of its shape, coupled with setting the magnitude of the allowable stress in the concrete at some multiplier of its unconfined compression strength. Values suggested for this multiplier range from 0.85 (the value used with the Whitney stress block) to values as large as 2 to 3 (in recognition of the ability of confining steel to increase the compression load carrying capacity of concrete).

In this investigation, the decision was made to use an equation developed by Marcakis and Mitchell (1980) to model the cap capacity. As previously mentioned, this equation is based on the model shown in Figure 3.7, with some consideration for the actual parabolic shape of the stress block (as opposed to using a simple rectangular shape). This approach neglects the effect of any axial force carried by the pile. The moment capacity of the pile cap in each model, as calculated using this equation (3.2.9), is reported in Table 4.2. The results of this calculation are presented for two cases, namely, for concrete strengths equal to 0.85 (the default value presented by Marcakis and Mitchell), and 1.8 times the unconfined compression capacity of the cap concrete (as given in Table 3.1). The actual maximum moments carried by the cap concrete in each test are also reported in Table 4.2. In all cases, when the crushing strength of the concrete was assumed at $0.85 f'_c$, the moment actually carried by the cap exceeded the calculated capacity (by a range of 20 to 110 percent). One explanation for this situation, as commented above, is that the reinforcing steel provided sufficient confinement to increase the compression strength of the concrete relative to its unconfined value. Back calibrating the prediction equation based on the experimental results suggests that the compressive strength of the concrete adjacent to the pipe pile was at least 1.8 times the value of f'_c (from test PC-3), which falls within the range observed by other investigators. Note that general crushing of the cap concrete in the bearing area of the steel pipe pile was not observed in any of the tests.

A limited investigation was done of the equation proposed by Shama et al. (2002) to predict the capacity of a pile cap based on failure of the concrete in the embedment zone. This equation, reproduced as Eq. 2.4.1 in this report, assumes a triangular (rather than rectangular) distribution of

compression stress in the concrete along the embedment length. As might be expected, the resultant calculated moment capacities for this failure mechanism are lower than the values obtained from the rectangular distribution (by approximately 35 percent). Shama and his colleagues assume a limiting compression stress value of $0.85 f_c'$ in their analyses, to insure premature crushing of the concrete will not occur. Thus, the capacities predicted following this approach also significantly underestimate the actual moments carried by the models used in this investigation.

In light of the extensive cracking that characterized the failure of the cap in tests PC-1 and PC-2, the model used by Marcakis and Mitchell (1980) was further extended to investigate the internal tension forces that developed in the cap in resisting the rotation of the steel pipe pile. Consistent with the simplicity of the model, the internal tension forces were simply estimated to be equal in magnitude and directed opposite to the internal compression resultants calculated above. The assumption was made that once the concrete cracked, these tension forces had to be carried by the reinforcing steel. Based on these assumptions, a tension controlled moment capacity was calculated for each cap based on the longitudinal steel across the embedment zone, excluding any longitudinal bars right at the full embedment depth. These capacities are also reported in Table 4.2, along with the actual maximum moment carried by the pile to pile cap connection in each test. The calculated capacities generally are consistent with the results observed during the tests. As previously discussed, the light reinforcement used in the first two tests (PC-1 and PC-2) appeared to be below the minimum reinforcement necessary to carry the internal tension forces in the structure when the concrete cracked without experiencing extensive deformation. These caps were able to carry moments significantly in excess of the 20 ft-k values predicted based simply on the tension capacity of the reinforcing steel, due to the tension capacity of the uncracked and lightly cracked concrete. As the moment demands on the caps increased and the tension capacity of the concrete was significantly exceeded, the internal tension forces were transferred from the concrete to the reinforcing steel. The steel almost immediately yielded and large deformations were experienced in the cap. At this point of force transfer, however, the models did not experience an immediate drop in moment carrying capacity to a level of 20 ft-k, as would have been expected from the results of the simple hand calculations. Secondary load paths apparently became available in the models, possibly as a result of the large deformations being experienced at this time, which allowed them to continue to carry substantial moments.

Successively increasing the amount of reinforcing steel in tests PC-3, -3a, and -4 increased the moment capacity of the cap, with model PC-4 actually failing through yielding of the pipe pile rather than the cap, as would be expected based on the calculated capacity values for plastic hinging in the pipe pile, crushing of the concrete in the cap, and tensile failure in the cap.

4.2 Concrete Pile Cap Capacity

Table 4.2: Concrete Pile Cap Moment Capacities Calculated by Hand

Model	Actual Moment Capacity	Predicted Cap Moment Capacity, ft-k					
		Compression Failure of the Concrete				Yielding of Steel Reinforcing After Cracking	
		Assumed Failure Stress of 0.85 f'c		Assumed Failure Stress of 1.8 f'c			
		Calculated Moment Capacity (ft-k)	Ratio, Calculated to Actual Moment Capacity	Calculated Moment Capacity (ft-k)	Ratio, Calculated to Actual Moment Capacity	Calculated Moment Capacity, (ft-k)	Ratio, Calculated to Actual Moment Capacity
PC-1	82	60	0.73	125	1.52	20	0.24
PC-2	74	66	0.89	137	1.85	20	0.27
PC-3	76	39	0.51	81	1.07	47	0.62
PC-3a	102	49	0.49	102	1.00	90	0.88
PC-4	121	58	0.48	122	1.01	139	1.15

4.2.3   Summary: Hand Analyses

The results of the simple hand calculations used to predict the capacity of the pile-to-pile cap connections considered in this study are summarized in Table 4.3. The actual connection capacity determined by experimental test of each configuration is also included in the table. Referring to Table 4.3, the simple hand calculations accurately predicted the actual failure mechanism in four out of five tests. In the one test in which the simple calculation predicted the wrong failure mechanism (test PC-3a), the three calculated failure capacities were closely grouped and were within 15 percent of the actual capacity at failure. The apparent degree of accuracy with which these hand calculations predict the actual failure mechanism may be serendipitous. Quantitatively, the actual moment capacities of the various models differed significantly from their predicted values. In the case of Model PC-4, for example, the results of the calculations predicted that plastic hinging of the pipe pile at a moment of 96 ft-k would control the failure mechanism by a wide margin. In reality, the actual failure (admittedly through plastic hinging of the pipe pile) occurred at 122 ft-k (26 percent above the calculated value), which is very close to the predicted failure capacity of 121 ft-k for crushing of the concrete in the cap.

Some of the differences in the calculated and predicted capacities evident in Table 4.3 can be possibly explained by the assumptions used in the modeling approach. At low levels of tensile reinforcement in the cap (e.g., in models PC-1 and PC-2), for example, it has been postulated that ignoring the tensile capacity of the concrete under estimates the moment capacity of the cap in the tension based failure mechanism. In situations where tension related behaviors in the cap controlled the connection failure, the results of the hand analyses became quantitatively more accurate as the amount of steel used in the model increased. Again, it has been postulated that the capacity of the reinforcing steel became more critical to the cap as it increased in amount (which is the case in moving from PC-2 to PC-3 and PC-3a), while the tensile capacity of the cap concrete became correspondingly less critical. The predicted failure moment in test PC-3a based on the tensile capacity of the cap was within 12 percent of the actual moment capacity of the connection. Thus, if the capacity of the steel pipe pile is sufficiently large to put the demands of the cap into this response regime, this hand analysis approach may be useful in generally estimating the amount of reinforcing steel required to fully develop the capacity of the pipe pile.

If a particular failure mechanism is to be counted upon to occur as part of a design, it is important to consider the quantitative level of uncertainty of the analytical results. As previously mentioned for test PC-4, while the hand calculations clearly indicated that a plastic hinge would form in the pipe pile, the actual point at which this occurred was very close to the predicted failure load for crushing of the concrete. This situation can be addressed by designing for some predetermined level of over-strength relative to the other failure mechanisms that the connection could experience.

In reviewing the adequacy of these hand analyses to predict the performance of this connection, it is important to recognize that the work performed in this study did not fully exercise possible failure of the connection through crushing of the concrete in the cap. Thus, whether or not the approach used to address this failure mechanism is effective remains largely unknown. The only thing that can be concluded in this regard is that the concrete in the bearing area between the embedded pipe pile and the pile cap carried an estimated compression stress of at least $1.8f_c'$ without failing.

Finally, the hand calculations used in this analysis only indirectly indicate the ductility and energy absorption characteristics that would be expected of a specific connection configuration. That is, based on the controlling failure mechanism predicted for the connection, some indication of its generic level of ductility and energy dissipation capacity could be inferred (e.g., failure of the steel pipe pile would be expected to be more ductile than failure of the concrete cap).

Table 4.3: Summary of Connection Moment Capacities Calculated by Hand

Test	Predicted Capacity by Hand Calculation, ft-k					Test Results	
	Possible Failure Mechanisms		Controlling Failure Mechanism				
	Plastic Hinge in Pile	Failure in Pile Cap		Failure Mechanism	Moment Capacity	Failure Mechanism	Moment Capacity
		Compression in the Concrete	Yielding of Reinforcing Steel after Cracking				
PC – 1	108	124	20	Yielding of reinforcing after cracking	20	Yielding of reinforcing after cracking	82
PC – 2	91	137	20	Yielding of reinforcing after cracking	20	Yielding of reinforcing after cracking	76
PC – 3	84	81	47	Yielding of reinforcing after cracking	47	Yielding of reinforcing after cracking	78
PC – 3a	85	101	90	Plastic hinge in pipe pile	85	Yielding of reinforcing after cracking	102
PC - 4	96	121	139	Plastic hinge in pipe pile	96	Plastic hinge in pipe pile	122

4.3 STRUT AND TIE MODELS

Strut and tie modeling of reinforced concrete elements is being increasingly used for situations involving stress concentration conditions and discrete applied loads. The concrete pile cap considered in this investigation fits these conditions, in that it is subjected to a concentrated moment from the steel pipe pile, which is reacted to by discrete pinned supports at either end of the cap model. Thus, the cap should be reasonably modeled using a strut and tie approach.

In general, the strut and tie approach involves modeling a reinforced concrete element as a truss consisting of compression struts and tension ties. The concrete forms the struts, which generally are modeled as compression only members, due to the basic characteristic of most concretes whereby their compression strength significantly exceeds their tension strength. The analysis process is greatly simplified by ignoring the tensile capacity of the concrete, generally without substantially compromising the accuracy and usefulness of the results. The reinforcing steel acts as tension ties in the truss model. Once again, the analysis is greatly simplified by ignoring the compression capacity of the reinforcing steel. In this case, steel as a material is obviously able to carry compression. The area of steel, however, is only a small fraction of the cross-section, and as large deformations occur, the slender bars may not be sufficiently supported in the lateral direction so as to carry substantial compression force without buckling.

While strut and tie analyses can be done by hand, an effort was made in this investigation to implement strut and tie modeling using the finite element method using a multi-purpose structural member based finite element program (as opposed to a solid element based finite element program). The program Visual Analysis (marketed by Integrated Engineering Software, Bozeman, MT) was used for this purpose. By applying the strut and tie method using a finite element program, it was not necessary to make as many assumptions on the behavior of the struts and ties as are made in conventional strut and tie modeling. In all models, for example, the steel ties were allowed to carry tension and compression. In later models, the concrete struts were allowed to carry tension in low stress regions (i.e., regions in which the tension stresses were found to be below the estimated splitting tensile strength of the concrete). In all cases, the concrete filled, steel pipe pile was modeled essentially as a rigid body embedded in the pile cap. Thus, this analysis only addressed the response of the concrete cap.

Relative to the configuration of the elements in the analytical model, the ties were placed to closely match the position of the bars in the reinforcing cage in the cap. Defining discrete struts within the continuous mass of concrete in the cap was a more difficult task. In early models, professional judgment was used in selecting strut locations believed to be representative of stress paths within the actual structure. Guidelines used in selecting struts included that a) struts originating at the pile had to act normal to the surface of the pile and b) all struts had to terminate at nodes offering resistance in three principal directions. Thus, the struts ran from the surface of the steel pipe pile to the corners of the reinforcing cage, as shown in Figure 4.1.

Based on the geometry of the cap and professional judgment, these struts were visualized as having a 2 inch square cross-section. In evaluating the results, consideration was given to circumstances where struts intersect at a common node. As may be obvious, an infinite number of strut configurations could be used to carry the compression forces from the surface of the pipe pile into the cap, and there was some concern that the nature of the results was significantly impacted by whatever choices were made in this regard. Thus, in later models, an effort was made to move away from dictating the strut locations in the model. Rather, a regular grid-work of strut members was provided, with the model, itself, subsequently exercising those struts and load paths it found useful in carrying the applied load. Such a model is shown in Figure 4.2.
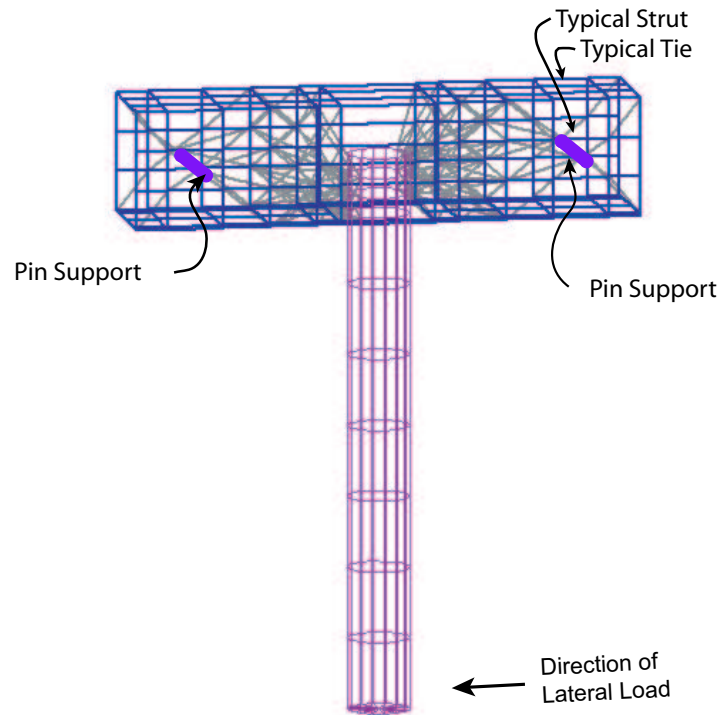
Figure 4.1: Early Configuration of a Strut and Tie Model
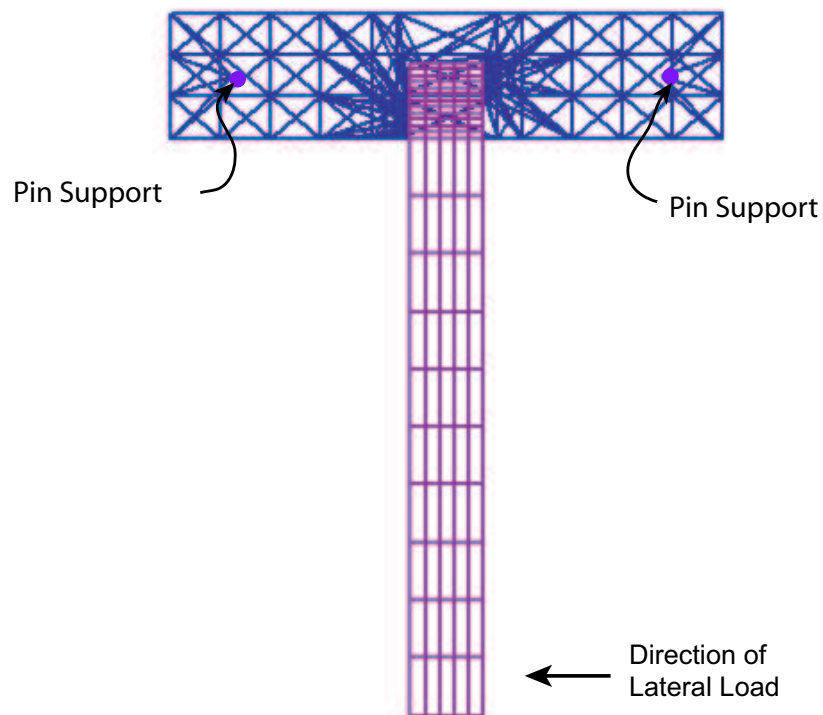
Figure 4.2: Later Configuration of a Strut and Tie Model

Both two and three dimensional strut and tie models of the pile to pile cap connection were generated. The two dimensional models were generated by collapsing the connection into a single plane parallel to the direction of the applied transverse load (which is also parallel to the longitudinal axis of the pile cap). While the 3-D models were believed to offer a more thorough view of the connection performance, the 2-D models generally offered a simpler and thus more easily understood view of this behavior.

One of the early uses of the strut and tie method was in evaluating whether or not the model configuration used in this investigation (consisting of single pipe pile and an associated section of cap, with the previously described load and support conditions) reasonably duplicated the stress conditions in a full bent subjected to a lateral displacement. The strut and tie models used for this analysis are shown in Figure 4.3. The axial forces analytically generated in the members in the full cap and in the model are presented in Figure 4.4. The general pattern of the axial forces in the members is similar in both the full cap and the model, particularly in the vicinity of the first interior column of the full cap. The maximum internal tension forces calculated in the two systems in the bars in the face of the cap adjacent to the pipe pile (see Figure 4.4) were very similar in magnitude (approximately 13,000 pounds of force were calculated to be carried by these bars in tension in both analyses). The maximum compression force of 16,000 lbs calculated in the concrete compression struts in the vicinity of the pipe pile in the full cap were approximately 70 percent of the magnitude of the corresponding stresses in the model.
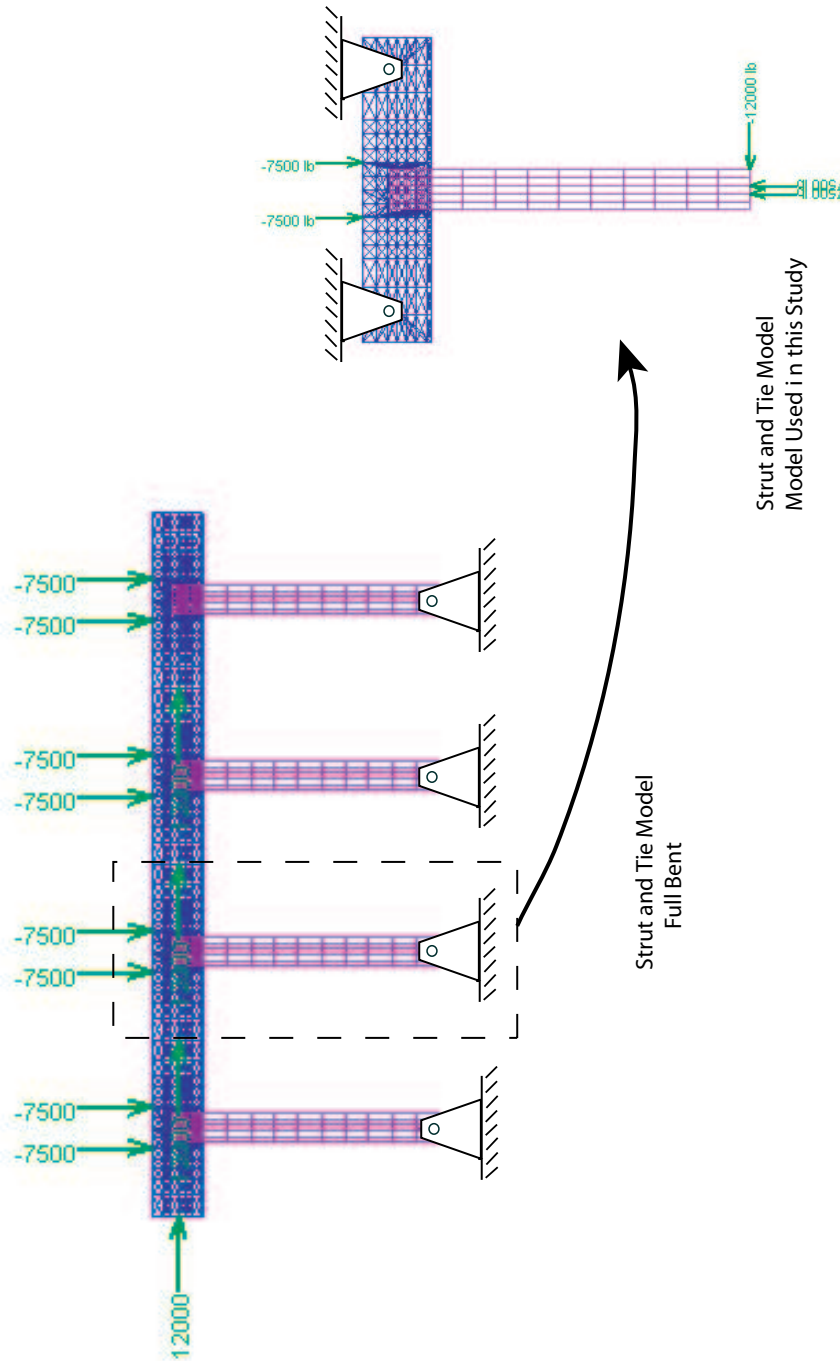
Figure 4.3: Strut & Tie Models of the Modeled Subsection and a Full Bent

Member Axial Force Diagrams for Model Used in this Study

Member Axial Force Diagrams for Full Bent
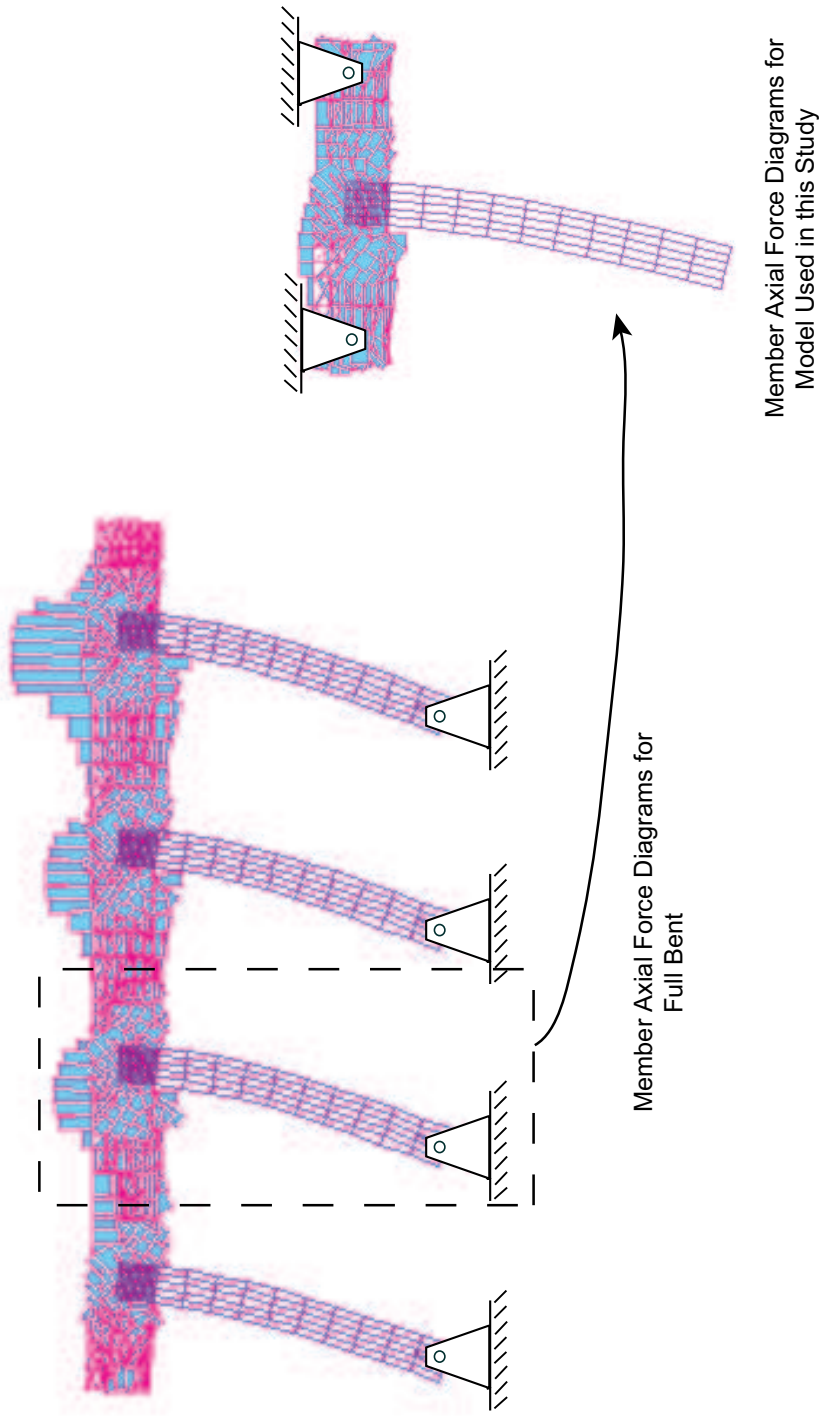
Figure 4.4: Strut & Tie Subsection Response compared with a Full Bent Response

4.3.1   Tests PC-1 and PC-2

Strut and tie modeling subsequently was used to specifically investigate the capacity of the various pile cap connections considered in this investigation. Early strut and tie models for tests PC-1 and PC-2 (specifically, using the model previously shown in Figure 4.1) found that as the lateral load on the pipe pile increased, yielding of the reinforcing steel initiated in the second transverse tie adjacent to the pile in the direction of the applied transverse load, with yielding of the first transverse tie predicted to occur shortly thereafter (see Figure 4.5). Yielding occurred at a transverse load of approximately 5,000 lbs. Note that the corresponding physical models began to exhibit severe distress when the lateral load reached 11,300 lbs and 10,000 lbs, respectively in tests PC-1 and PC-2. At this same load (5,000 lbs), the most highly stressed longitudinal bars in the strut and tie model were those longitudinal bars in the corners of the cap in the face with the pipe pile (see Figure 4.6). These bars were stressed at approximately 75 percent of their yield capacity. The stresses in the transverse ties and the longitudinal bars decreased rapidly moving away from the embedment zone in the direction of the applied load. The stress in the third tie from the face of the pile was 33 percent of that in the second tie. The tension forces in the longitudinal bars diminished in a proportional fashion.

The maximum stresses in the concrete in the strut and tie models of tests PC-1 and PC-2 occurred in the struts running from face of the pipe pile to the reinforcing steel in the face of the cap, as shown in Figure 4.7. Under the 5,000 lb lateral load at which the reinforcing steel began to yield, a maximum compressive stress equal to 2.0 times the unconfined compression strength of the concrete (assumed to be 4,000 psi) was observed at this location. Note that the concrete in the physical models was relatively undamaged in compression, leading to the tentative conclusion that its compression capacity was increased by a factor of at least 2.0 by the presence of confining steel.

Yield First Observed
in Second Tie
Away from Pile

Member Axial Force Diagrams,
Transverse Ties

Direction of
Lateral Load
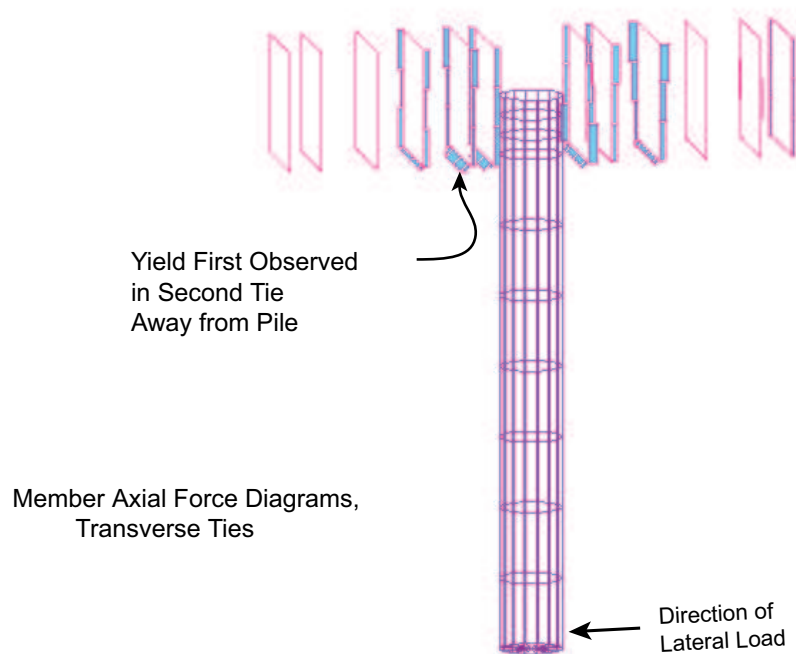
Figure 4.5: Strut & Tie Model of PC-1 and PC-2 – Axial Forces in Cap Transverse Ties

Highest Longitudinal
Bar Force (bar at 75 %
of yield stress when
transverse ties first
yielded)

Member Axial Force Diagrams,
Longitudinal Bars

Direction of
Lateral Load
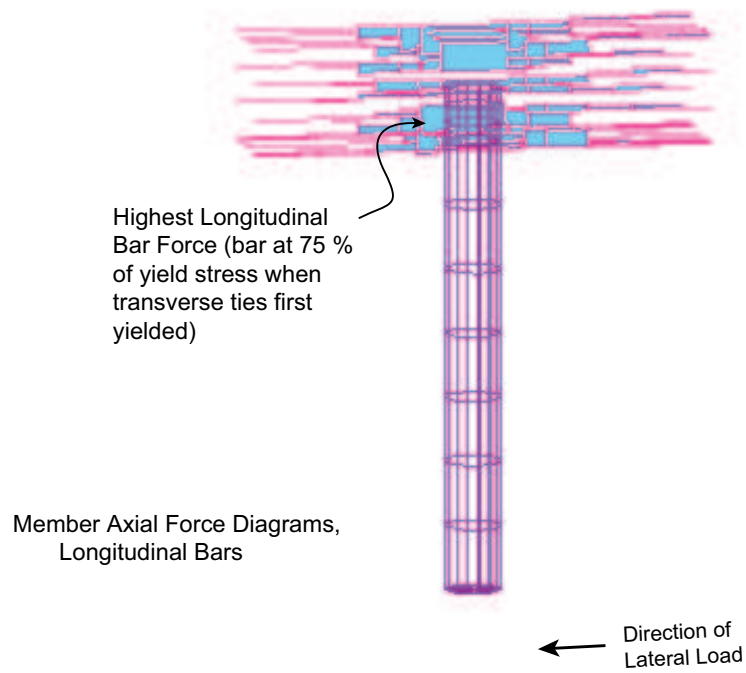
Figure 4.6: Strut & Tie Model of PC-1 and PC-2 – Axial Forces in Cap Longitudinal Bars

Highest Compression Force
in Strut Running From Pile
Face to Pin Support

Direction of
Lateral Load

Figure 4.7: Strut & Tie Model of PC-1 and PC-2 – Axial Forces in Compression Struts

The strut and tie models for tests PC-1 and PC-2 indicate that connection failure should have begun in the cap at a lateral load of 5,000 lbs, while the actual physical models did not begin to fail until the lateral load reached twice this value. This discrepancy results from disregarding the tension capacity of the concrete prior to cracking in the strut and tie models, and the inability of the reinforcing steel alone, to carry the internal tension forces in the cap.

4.3.2 Test PC-3

Prior to constructing model PC-3, a strut and tie model was created for a cap configuration in which the amount of reinforcing steel was substantially increased relative to that used in models PC-1 and PC-2. This configuration became the basis for physical model PC-3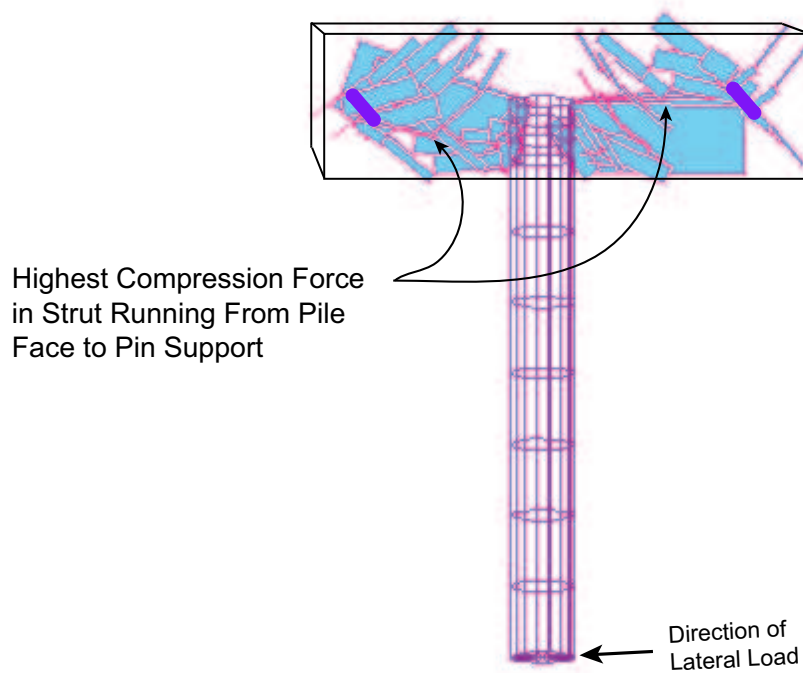. The size of the transverse steel was increased (from #2 to #3 bars) and their spacing was decreased (from 6 in to 3 in). The size of the longitudinal bars was increased from #3 to #4 bars. The strut and tie model for this cap configuration (see Figure 4.8) found that yielding of the reinforcing steel would once again initiate in the second transverse tie near the pipe pile, at a lateral load of 10,000 lbs. At this load, the corner longitudinal reinforcing steel along side the pipe pile was stressed at 85 percent of its yield strength. In the physical test of model PC-3, while non-linear behavior began at a load of approximately 10,000 lbs, the measured strains in the reinforcing steel did not exceed the yield strain until the lateral load reached approximately 12,000 lbs. Once again, this discrepancy in the results may be explained by the assumption in the strut and tie model that concrete has no tension capacity. In the physical model, the concrete began to crack at a load of 10,000 lbs, and it is suspected that its tension capacity was fully compromised at a lateral load of approximately 12,000 lbs, at which point the reinforcing steel yielded under the internal tension forces that it had to carry.

A refined strut and tie model was created for the connection configuration in test PC-3 in which a denser and more regular grid of compression struts was used. In general, the internal forces and stresses calculated using the refined model were very similar to those determined by the simpler strut and tie model of test PC-3 described above. In the refined strut and tie model, yield of the reinforcing steel now first occurred in the longitudinal reinforcing bars immediately adjacent to the pipe pile, at a lateral load of 10,000 lbs. In the data available from the test on this model, yield was first observed in the longitudinal bar immediately adjacent to the pipe pile, at a lateral load, however, of approximately 12,000 lbs. This difference was attributed, once again, to ignoring the tension capacity of the concrete in the strut and tie model. In test PC-3, strains were measured at several locations along the longitudinal bar adjacent to the pile, and the strains at first yield predicted by the strut and tie model in this bar are compared with these experimental results in Table 4.4. The distribution of the strains along the length of the bar is similar for the strut and tie and the experimental results. That is, at locations close to the pipe pile (locations F2, F6, and F7), the strains are significantly higher than at more distant locations (in this case, represented by location F8). In the strut and tie model, the longitudinal bar first yielded on both sides of the pile at locations F2 and F7, while in the physical model, this bar yielded immediately down stream of the pile at location F6, which is a mirror image of location F7, on the opposite side of the pile. The transverse strains predicted by the strut and tie model for the transverse ties immediately adjacent to the pile are also similar to the experimental results (see Table 4.4). As in the case of the longitudinal strains, the strut and tie model indicated that the maximum strain in the transverse ties (at location T1) occurred on the opposite side of the pile from where the maximum transverse strain was actually measured (at location T2).
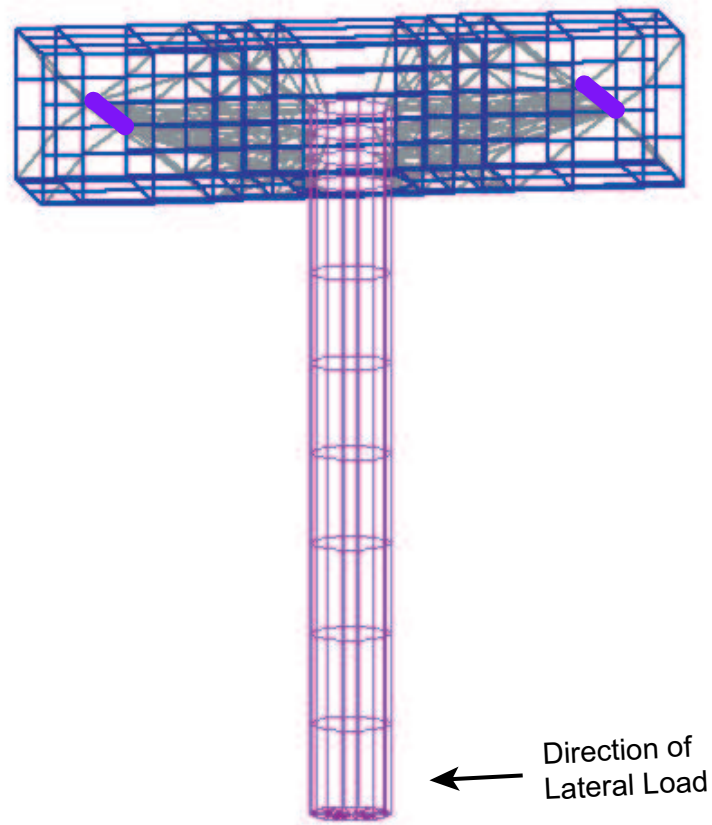
Figure 4.8: Basic Strut and Tie Model for Test PC-3

Table 4.4: Comparison of Calculated (Strut and Tie) and Measured Strains in Test PC-3

Gage Location*	Strain from Strut and Tie Model at First Yield)	Strain from PC-3 Data at First Yield
F2	0.22	0.12
F6	0.10	0.21
F7	0.23	0.14
F8	0.04	0.02
T1	0.19	0.06
T2	0.05	0.13
T4	0.10	0.07

* See Figure 3.20 for gage locations

4.3.3 Test PC-3a

A final strut and tie model was created for the connection configuration used in test PC-3a. In this 2-D analytical model, further efforts were made to replace the user selected concrete struts relied on in previous models with a regular grid of generic strut members. This model is shown in Figure 4.9. This model indicated that yield in the reinforcing steel would initiate in the longitudinal bars adjacent to the pipe pile at a lateral load of approximately 17,000 lbs. In the physical test of this connection configuration, failure occurred in the cap at a load of approximately 17,000 lbs. Care should be exercised, however, in interpreting the significance of the close match in this case between the analytical and experimental results. Notably, the ability of the 2-D model to accurately represent the 3-D reality of the connection and its failure is uncertain. In this case, it may simply be coincidence that the assumptions made in developing the 2-D model happened to generate results in such close agreement with the outcome of the physical test. Nonetheless, such results are encouraging and support further investigation of this analysis approach.
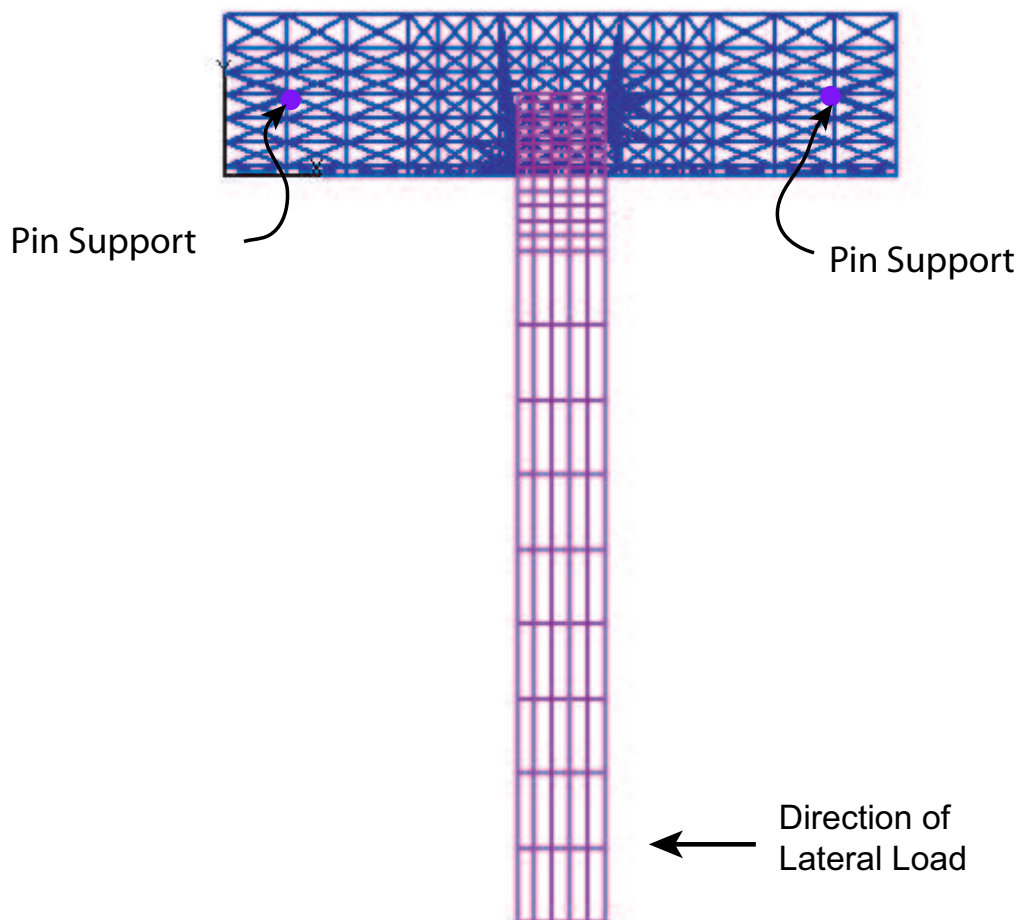
Figure 4.9: 2-D Strut and Tie Model for Test PC-3a

4.3.4   Summary: Strut and Tie Analysis

Strut and tie modeling potentially offers some valuable insights into the behavior of the steel pipe pile-to-concrete pile cap connection considered in this investigation, and such models could conceivably be developed for use in design in the future. Problems were encountered in using a conventional strut and tie approach to represent the behavior of lightly reinforced pile cap sections. The traditional strut and tie approach predicts the ultimate capacity of a cross-section after it has cracked based on the assumption that the participation of the concrete in the tension zone can be ignored. Obviously, the behavior of the cap prior to cracking will be poorly represented in such a model. Somewhat surprisingly, it was also found that the strut and tie approach poorly represented the post cracking behavior of the cap if it was lightly reinforced (in this case, specifically at 0.4 and 0.09 percent steel in the longitudinal and transverse directions, respectively). The cracked concrete in lightly reinforced sections apparently plays a relatively greater role in carrying internal stresses in the structure than it does in more heavily reinforced sections. Thus, in such situations, the strut and tie models significantly underestimated the moment capacity of the cap (in this case, by approximately 50 percent).

As the amount of reinforcing steel in the cap increased, the role of the cracked concrete in carrying tensile stresses diminished relative to that of the steel, and the strut and tie models yielded more reasonable results. When 2.11 and 0.65 percent steel was used in the longitudinal and transverse directions in the cap, for example, the strut and tie method was very accurate in predicting the location and lateral load at which the longitudinal reinforcing steel would begin to yield. If this approach is to be further considered, the specific reinforcement thresholds which strut and tie modeling can reliably be used need to be better established.

The strut and tie models used in this investigation were created and analyzed using a commercially available structural engineering analysis program. With the relatively common implementation of compression only members in such programs, they have become a possibly powerful tool for performing strut and tie analyses. Attractive features of these programs include their familiarity to structural engineers, and their obvious ability to effortlessly analyze highly redundant strut and tie models. In this regard, the models used in this project gravitated toward the use of a generic grid of compression struts, rather than a selected set of struts determined by the analyst based on professional experience. This approach was believed to represent an improvement relative to traditional strut and tie modeling, in which the analyst's choice of strut locations can influence the outcome of the analysis. A second perceived improvement was to allow concrete struts in low tension zones to carry both tension and compression forces. This concept, however, could only be imperfectly implemented, as it was impossible to predict prior to performing the analysis exactly which elements would only experience "low" tension stresses, and the stress patterns produced by the analysis were themselves influenced by the choice of concrete element type (i.e., compression only, or compression and tension).

The one major (and occasionally fatal) limitation of using common structural engineering analysis software for strut and tie modeling (including the one used in this project), is that they only employ linear elastic material models. In a linear elastic analysis, it is difficult to replicate the load sharing that occurs across a structure as individual elements reach their yield capacity. Thus, while a strut and tie model implemented using such a program should accurately predict the initiation of plastic behavior, it can only be used to approximately determine the ultimate plastic capacity of a structure. Further investigation is necessary to see if the advantages offered by implementing strut and tie modeling using such software outweighs its limitations. In this case, for example, the strut and tie model for

PC-1 and PC-2 indicated that the transverse ties were as highly stressed as the longitudinal steel; this type of observation was not available from the hand analyses.

The above limitations of using common structural analysis software for strut and tie modeling can possibly be over come by using more sophisticated solid element finite element programs. Such programs typically include non-linear material models capable of representing cracking behaviors coupled with an iterative solution procedure in which at each load increment the program checks whether or not yielding or cracking stress levels are exceeded at any point in the model, and the load carrying capacity of that part of the model is adjusted accordingly. This analysis approach is discussed in the next section of this report. The current difficulty with solid finite element modeling is that most structural engineers are unfamiliar with the sophisticated programs that it requires, and numerical instabilities can be encountered in the solution process.

4.4   FINITE ELEMENT ANALYSIS

As part of Phase II, one of the goals was to model the nonlinear response of the pile-to-pile cap response with finite element (FE) models as it was loaded to it's maximum capacity. One reason for pursuing this goal relates to the use of the $1/2$ scale models in the experimental study. If these tests could be represented accurately with FE models, then presumably the full scale bents could be modeled as well with very little concern over scaling issues. In the end, models of the complete damage cycle were not attainable. However, much was learned in the process, and the FE models were still useful for understanding some of the observed behaviors. Also, these same aspects can be modeled just as easily for the full scale bent as for a single $1/2$ scale test model.

4.4.1   Model Development Insights

The nonlinear behavior of the pile-to-pile cap connection is surprisingly complex. Not only is it necessary to model the plastic deformation of the pile jacket and the steel reinforcement in the pile cap, but also the permanent deformation of the concrete cap and the concrete interior to the pile. In particular, the modes of permanent deformation in concrete are numerous and the interactions between these modes are convoluted. To accurately model the non-linear response, factors that must be considered are: cracking, shear retention, tension stiffening, re-closing of cracks, microcracking, macrocracking, crushing, containment effects, dilation, hysteresis under cyclic loads, softening due to damage, and energy absorption due to each of these factors. Explanations of each of these factors are presented in the following paragraphs.

Cracking: As stress exceeds the tensile capacity of concrete, tensile cracks open forcing the load paths to relocate, often in a rather dynamic fashion. Chen (1982, Eq.2.4) indicates that in direct uniaxial tension this occurs at tensile stresses f_t' near

$$f_t' \approx 4\sqrt{f_c'} \text{ psi,} \qquad\qquad (4.4.1)$$

where the uniaxial compressive strength (f_c') is in psi.

For multiaxial load cases such as in the pile cap connection, a more preferred indicator of tensile strength (f_{st}') is based on empirical split-cylinder tensile failures. Data from such measurements has been similarly related to uniaxial compressive strength with the relation

$$f_{st}' = a\sqrt{f_c'} \text{ psi,} \qquad\qquad (4.4.2)$$

where *a* often varies between 7.5 and 13 (Park and Paulay, 1975, Eq.2.2).

Once cracking occurs in a finite element model, the strength in tension is assumed to reduce to zero. However, without including dynamic effects, this strength reduction must be carried out in a gradual fashion, allowing a state of "static" equilibrium to be maintained from step to step. Inherent in this process is the implication that the material in the neighborhood of the crack becomes orthotropic or at least transversely isotropic. Consequently, while strength is reduced to zero in the direction normal to the crack, a similar issue becomes, what happens to the shear capacity parallel to the plane of the crack.

Shear Retention: As a crack opens, particularly in concrete, the interface is still quite rough with aggregate extending from one side to the other. As a consequence, the crack is often capable of supporting a sizable shear stress across the crack, at least until the crack opens a distance on the order of the size of the aggregate.

In finite element (FE) codes, this effect is typically treated as a reduction in the shear modulus in the plane of the crack. This reduction is then also a function of the opening strain or displacement normal to the plane of the crack. An issue similar to shear retention is the load response of steel reinforcement that passes though a section of cracked concrete.

Tension Stiffening: When steel reinforcement passes through a section of cracking concrete, as the concrete cracks a substantial fraction of the load is then transfered to the steel reinforcement. However, because the steel re-bar is embedded in concrete except in the crack opening, the steel is not allowed to expand under load as it would independent of the encapsulating concrete.

In finite element analysis (FEA), models of this interaction depend on re-bar density, re-bar/concrete bond quality, aggregate/re-bar diameter ratio, and FE mesh density.

Crack Closure: Once a crack opens to a significant degree, the concrete loses all tensile capacity in the direction normal to the crack. However, if the crack re-closes under compression, the capacity in compression is only slightly affected.

In FEA, the opening and closing of cracks is often treated in a manner similar to contact surfaces. Unfortunately, this directionality also implies that status of each "crack" must be tracked along with the orientation. As the status changes, the material parameters must reflect the change while allowing a state of either "static" or dynamic equilibrium to be maintained from step to step.

The previous factors have been associated primarily with responses under tension. Not too surprisingly, there is a similar, though significantly different set of factors associated with compression.

Microcracking: For concrete, the term microcracking is used to refer to a separation between the cement and aggregate. This separation can occur to a certain extent during the construction phase. To say the least, the development of these microcracks progresses under increasing load. As load increases, these microcracks join and become macrocracks (Lee and Fenves, 1998; Mehta and Monteiro, 1993). Chung et al. (1989, p.260) indicate that the formation of macrocracks typically occurs at compressive stresses near $0.5 f_c'$.

Currently, most FEA codes do not address the development of microcracks or macrocracks directly but instead represent the associated nonlinearity in the stress strain response through plasticity models or more directly through damage models.

Crushing: Once the macrocracking progresses to a critical level, the cohesiveness of the material degrades significantly and the material is considered to be crushed. As the crushing progresses, the aggregate and other "debris" is pushed from it's original position, into a less form fitting position. In the process, from a macroscopic perspective, the material dilates. In certain situations, this dilation can alter the load paths and incur additional stresses. As a consequence, dilation must be accounted for to some degree as well.

With regard to finite element (FE) models, crushing and the associated loss of material cohesiveness can lead to a reduction in elastic stiffness, or more directly to a reduction in the elastic moduli. As a consequence, plasticity models can not be used to accurately represent the softening of the concrete, particularly if cyclic loads are to be considered.

Confinement: If confinement is provided, even uniaxial loads can induce a state of triaxial stress that is close to hydrostatic. In such situations the development of macrocracks is inhibited and the overall load carrying capacity of the concrete can be greatly increased. Such confinement can either be provided through embedded steel reinforcement cages (Mander et al., 1984, 1988b,a) or through external jacketing (using steel or composite materials). Priestly and Park (1987) indicate that steel reinforcing cages can effectively increase the strength of the confined concrete by as much as a factor of 2. If confinement is provided through steel jacketing, as in the case of the pile, the ultimate capacities can increase significantly more (Chai et al., 1994; Chai, 1996). For a more detailed discussion of these effects, see McKittrick et al. (1998).

To account for these affects in finite element analysis (FEA), the strength of the concrete is based on the state of stress. Concrete loaded in biaxial compression is considered "stronger" than that loaded in uniaxial compression. Similarly, concrete under a triaxial compressive stress is considered even stronger. Particularly as the stress state approaches a hydrostatic state of stress.

Hysteresis: Reinforced concrete structures often display hysteresis effects under cyclic loads. The hysteresis implies that when the structure is unloaded, it displays a "memory" indicative of permanent deformation. In a large part, in these reinforced structures, this hysteresis is a result of plastic deformation in the steel reinforcement. However, concrete does also display responses characteristic of plastic deformation.

For FEA models of concrete, it is difficult to separate permanent strains that are due to plastic deformation and those that are due to damage. Those that are due to damage, indicate a reduction in elastic moduli and an overall loss in structural capability and consequently a reduction in the ability to dissipate elastic or dynamic energy. Permanent strains that are due to plastic deformation provide a significant means for energy dissipation, and possibly with little reduction in structural capability.

Unfortunately, nearly all of these factors play a role in the nonlinear behavior of the pile to pile cap connection. Also unfortunate is the appearance that no finite element code can presently address all of these factors. To model the pile-to-pile cap connection, several FEA codes (ANSYS, V81; ABAQUS, v 58; NIKE3D, V33; DYNA3D, V4) were evaluated.

Simple, plain concrete models were created in each code (ANSYS, ABAQUS, NIKE3D, and DYNA3D) and loaded in uniaxial tension and compression. While each codes produced reasonable results for monotonic loading (as verified against experimental results), they generally performed

poorly for cyclic loads. Notably, the codes were unable to adequately accumulate damage over successive cycles of inelastic loading. In particular, they were unable to fully recognize the degradation in stiffness that accompanies compressive damage on successive cycles of inelastic loading.

In light of the problems mentioned above, some effort was applied toward modifying the material models used in NIKE3D and DYNA3D to better reflect the behavior of concrete under damaging cyclic loads. This approach was pursued using the NIKE code. Investigators Sanjay Govindjee & Garrett Hall (at UC Berkley) were contacted regarding work that they have recently (Govindjee and Hall, 1998) engaged in. Work done by Govindjee and Hall looked promising, as their model for inelastic deformation includes components of both damage (cracking) and plastic type responses. Unfortunately, this combination was incorporated only for tensile type load conditions, not compression. Following their work, Lowes (1998) extended the Govindjee & Hall model, but still was not able to successfully include crushing along with plastic deformation under compressive load conditions. Notably, these models are not able to completely represent the accumulation of damage under cyclic load conditions; in particular, they are unable to represent the degradation in stiffness that accompanies compressive damage on successive cycles of inelastic loading. In essence, these investigators were unable to attain "global convergence" or equilibrium from models that included the more significant components.

A fifth finite element code, DIANA (V81) was also reviewed. DIANA was developed by researchers who were specifically interested in solving civil engineering problems. One of the programs primary strengths is the manner in which it deals with concrete and soils. Unfortunately, unfamiliarity with the program and poor documentation resulted in an inconclusive evaluation.

In the end, the FE code used for evaluating the performance of the test models was ANSYS. This selection was due primarily to the second author's familiarity with the program, particularly since models for Phase I had also been constructed using ANSYS.

4.4.2   Model Descriptions

For the finite element (FE) analysis of the steel pipe pile/concrete pile cap system, each experimental case was modeled three dimensionally using the ANSYS finite element program. Brick-like elements were used to discritize the pile's steel jacket and concrete as well as the concrete in the pile-cap. Cylindrical beam elements were used to discritize the interior re-bar and the steel pins used to hold the pile-cap in place during loading. Results of the analyses were then used to identify regions of greatest activity and therefore used as an aid in determining the placement of strain gages in each test. In case primary gages were destroyed during the construction phase, several supplementary gages were typically added to each test model. When supplementary gages were used, the FE model was used to help identify which gages to monitor.

For the first series of load cases, the experimental model (Section 3.2.1) was based on a half-scale representation of a typical pile-to-pile cap connection (originally following the Timber Creek design). The FE models were then built to represent each experimental model. For the final ANSYS (V81) models, concrete was modeled using the SOLID65 elements. Then pile cap re-bar was represented using BEAM188 elements which were connected to the corner nodes of the SOLID65 elements that were used to model the pile cap concrete. The pile jacket was modeled with SOLID45 elements with one element through the thickness of the pile jacket.

For the primary evaluation, the gage measurements from each test model were compared with corresponding values from each FE model (Section 4.4.3).

One problem with the linear elastic models was the lack of an interface between the cap and pile that would allow the cap to "debond" from the exterior of the pile. In the test models, this debonding

was typically the first observable sign of permanent alterations in the connection. It was originally assumed that the tensile cracking material model would account for this debonding behavior via an accumulation of tensile cracks in the elements attached to the tensile face of the pile-to-pile cap connection. Unfortunately, the accumulation of cracks in the connecting elements produced distortions that lead to non-convergent (unstable) solutions.

In an attempt to overcome this problem and to also gather information for strut and tie models (Section 4.3), contact surfaces were included in the model on interfaces between the pile and pile cap. Originally these contact surfaces were only included between the pile jacket and the cap concrete; not unreasonably, this configuration lead to severe distortion in the concrete elements at the embedded end of the pile, as they cracked under the extreme stress concentrations. As a consequence, contact elements were also added at the embedment end of the pile-to-pile cap connection. Evaluations where debonding was considered are presented later (Section 4.4.4).

Model for PC-1

The model for case 1 includes a pile cap reinforcement pattern that is based on the first experimental model (Figure 3.3), with both circumferential and longitudinal bars placed according to the as built configuration.

Also included in the model is a steel load platen to distribute the bearing or axial load at the top of the cap, as in the experimental model. Following the as built design of the first model, the geometric dimensions of the associated elements are listed in Table 4.5. As displayed on the right hand side of Figure 4.10, only half of the geometry is modeled where the lower half is assumed to deform in a fashion that is symmetric to the upper half. As a consequence, the model does not portray any lifting or downward deformation (in the Y-direction) due to unbalanced loads.

Because the first physical test in Phase II also served as the initial test of the load frame, smaller loads were applied to the model several times in order to evaluate the performance of the test frame and the overall test set-up before loading the connection to failure. These load cases were also very useful for evaluating the performance of the linear elastic model. As a consequence, several such evaluations are discussed in the following sections.

Table 4.5: Model 1, Structural Component Key-Dimensions

Structural Component	Element Type	Dimension	
		Parameter	(in)
Pile Jacket	SOLID45	Thickness	0.32
Cap Long. Re-bar	BEAM188	Diameter	3/8
Cap Circ. Re-bar	BEAM188	Diameter	2/8
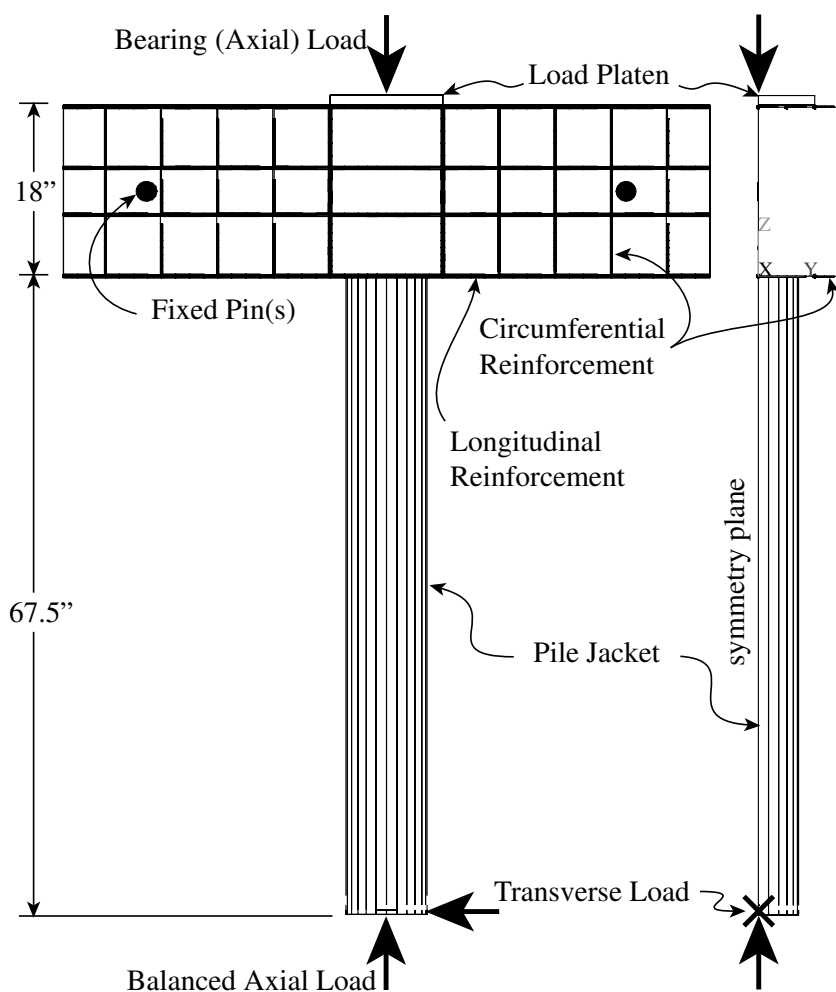
Figure 4.10: Model 1, FE Configuration

Model for PC-2

The model for case 2 (PC-2) includes a pile cap reinforcement pattern that matches that of the first model (Figure 4.10), with both circumferential and longitudinal bars placed according to the as built configuration.

In case 1, the pile jacket was defined to have a thickness of 0.25 inches to match that of the experimental model (PC-1). For case 2, the jacket thickness was defined to be 0.32 inches to match the second experimental model (PC-2). Except for the thickness of the pile jacket, all other components match those of case 1 (Table 4.5).

Model for PC-3

The geometric dimensions of the associated reinforcement elements for the model in case 3 are listed in Table 4.6. This model includes a pile cap reinforcement pattern that is somewhat denser than that of the first experimental model (Figure 4.10), as shown in Figure 4.11. Again, the geometry of the finite element model is based on the as built geometry of the experimental model (Figure 3.9), though some components vary slightly. In particular, the spiral hoop ringing the embedded end of the pile could not be included in the spiral fashion, but was instead modeled as 3 distinct horizontal hoops in the

101

Table 4.6: Model 3, Structural Component Key-Dimensions

Structural Component	Element Type	Dimension Parameter	(in)
Pile Jacket	SOLID45	Thickness	0.25
Cap Longitudinal Re-bar	BEAM188	Diameter	4/8
Cap Circumferential Re-bar	BEAM188	Diameter	3/8
Cap Hoops Surrounding Pile	BEAM188	Diameter	3/8
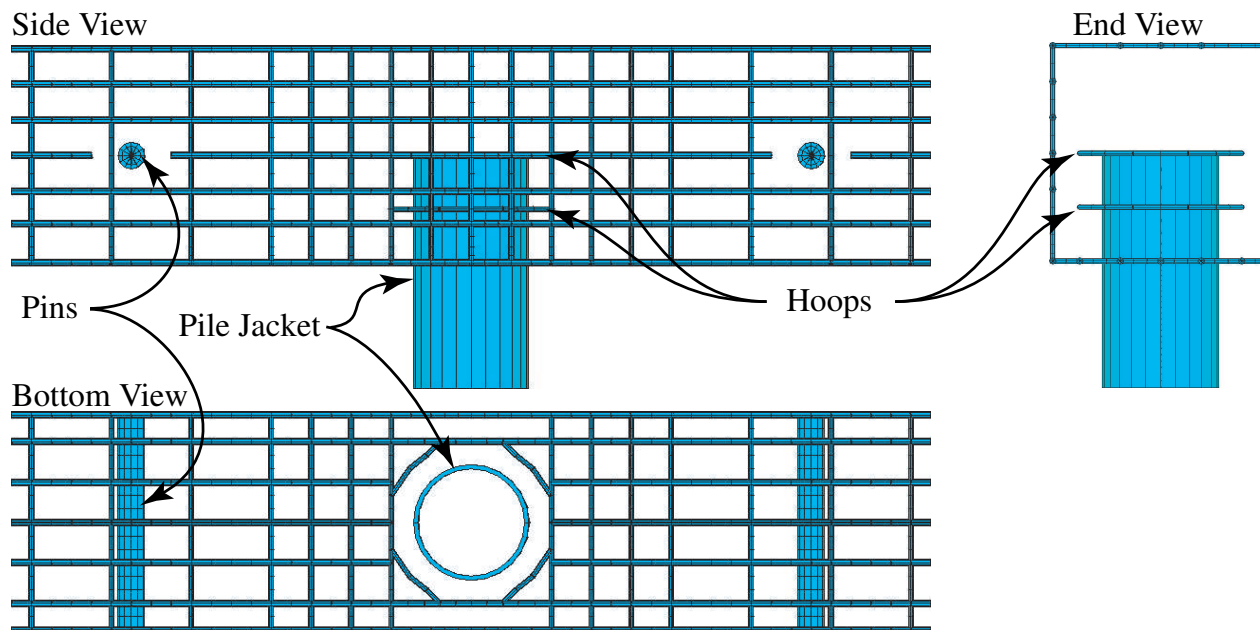
Figure 4.11: Model 3, FE Re-bar Configuration

cap. Because the hoops were included in the experimental model with the intent of maintaining the integrity of the concrete neighboring the pile, in the elastic model, where integrity is not a concern, the three horizontal hoops were considered a sufficiently accurate representation of the spiral hoop in PC-3.

Model for PC-3a

The model for PC-3a includes a pile cap reinforcement pattern that is even denser than that of PC-3 (Figure 4.11). In this case, the circumferential re-bar is spaced approximately on 2 inch centers following Figure 3.11. The geometric dimensions of the associated reinforcement elements are listed in Table 4.7. The reinforcement pattern is then displayed in Figure 4.12. Similar to the model for case 3, the spiral hoop in the experimental model was represented in the FE model using 9 individual horizontal hoops, which are spaced fairly evenly throughout the depth of the pile cap.

Table 4.7: Model 3a, Structural Component Key-Dimensions

Structural Component	Element Type	Dimension	
		Parameter	(in)
Pile Jacket	SOLID45	Thickness	0.25
Cap Longitudinal Re-bar	BEAM188	Diameter	6/8
Cap Circumferential Re-bar	BEAM188	Diameter	3/8
Cap Hoops Surrounding Pile	BEAM188	Diameter	3/8
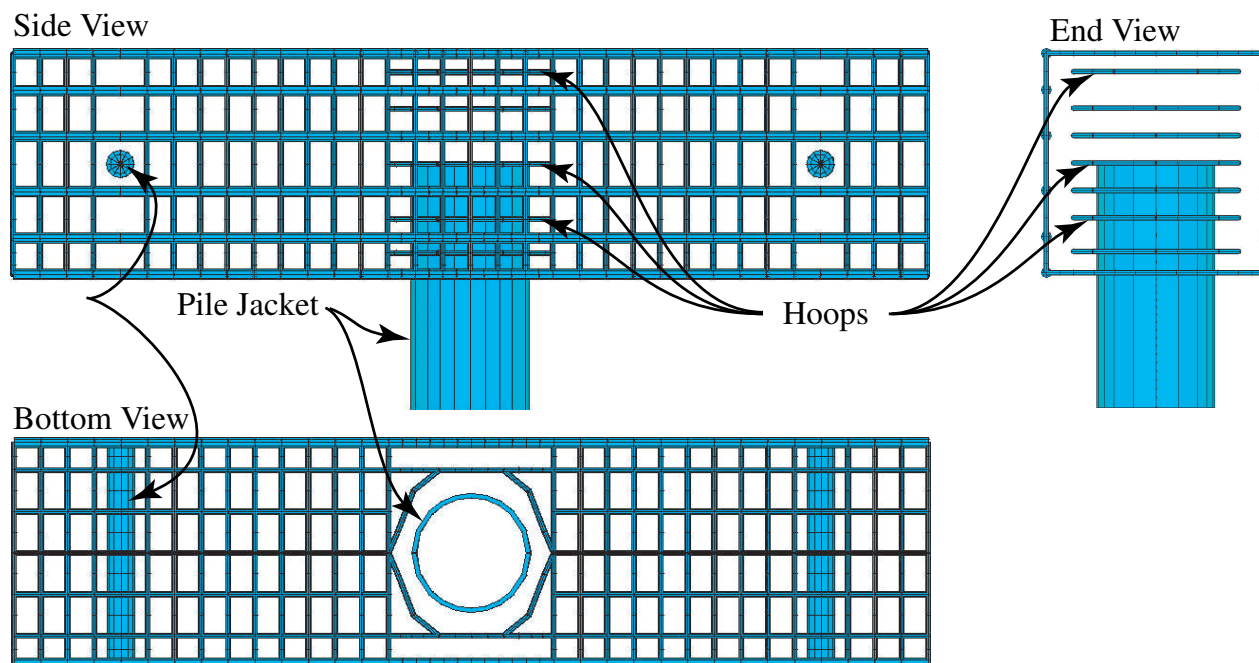
Figure 4.12: Model 3a, FE Reinforcing Details

Model for PC-4

In line with the fourth experimental model (Figure 3.14), the reinforcement pattern is denser than that of all of the earlier models. The geometric dimensions of the associated re-bar elements are listed in Table 4.8. As shown in Figure 4.13, the circumferential re-bar is spaced on ∼1.8 inch centers.

Table 4.8: Model 4, Structural Component Key-Dimensions

Structural Component	Element Type	Dimension	
		Parameter	(in)
Pile Jacket	SOLID45	Thickness	0.25
Cap Longitudinal Re-bar (faces)	BEAM188	Diameter	7/8
Cap Longitudinal Re-bar (top & bot.)	BEAM188	Diameter	4/8
Cap Circumferential Re-bar	BEAM188	Diameter	3/8
Cap Hoops Surrounding Pile	BEAM188	Diameter	3/8
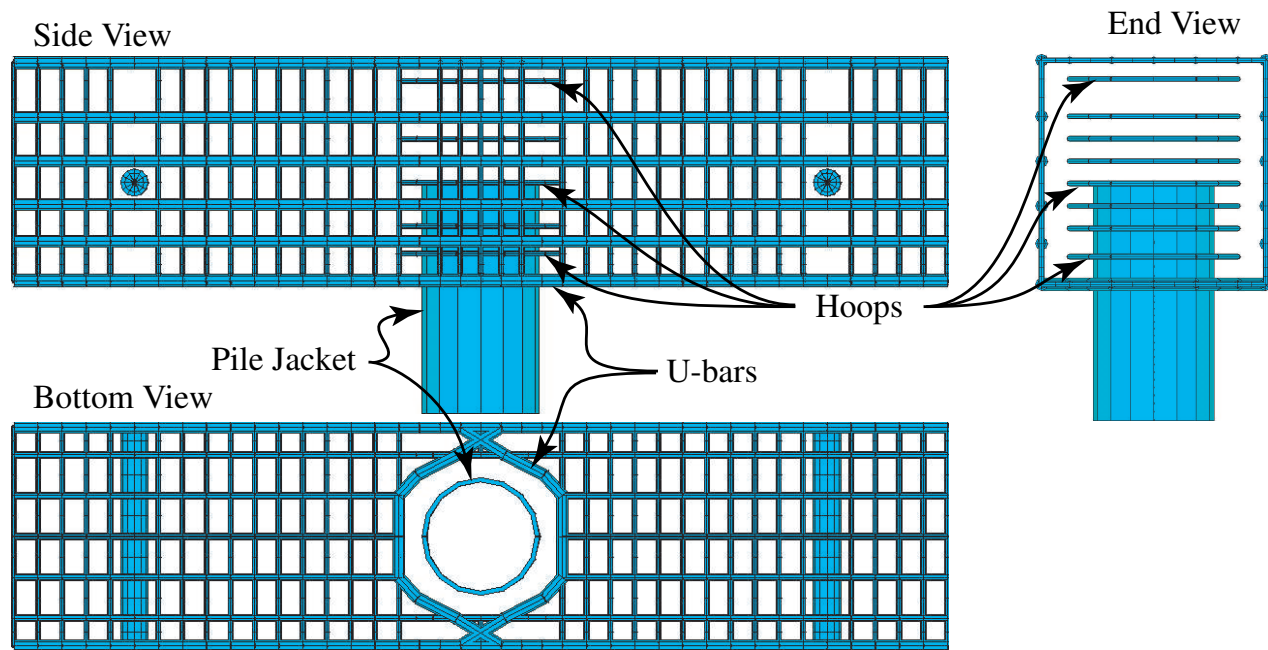
Figure 4.13: Model 4, FE Configuration

Nine horizontal hoops were substituted for the spiral hoop around the embedded end of the pile. Also, notice the addition of the #7 U-bars that loop around the pile at the base of the pile cap overlap each other and extend to each respective end of the pile cap.

4.4.3   Linear Elastic Evaluations

In this section, using linear elastic material models, comparisons are made between the experimental data and the outcomes from the finite element models presented earlier (Section 4.4.2). Though these models become inaccurate relatively early in the load histories that were used, they are useful for investigating the variations that occur between gages and the provide some insight into these behaviors as they diverge from the linear elastic response.

For all of the linear elastic evaluations presented in this section, the elastic parameters were based on the evaluation of data collected from concrete compression cylinders that were cast along with the first pile cap model. Displayed in Table 4.9, are the values for Young's moduli (E) and Poisson's ratios (ν) that were used.

Table 4.9: Linear Elastic Material Parameters

Structural Component	E (MPa)	ν
Pile Jacket	29	0.30
Pile Cap Re-bar	29	0.30
Pile Cap Concrete	2	0.17

Load Case 1.1

As discussed previously (Section 3.5.1), the first experimental test began with the application of the axial load (15 kips) alone. A comparison of measured strains with those generated by the model is displayed in Figure 4.14. In these graphs, lower-case letters are used to distinguish modeled "gage" results from measured results, which are displayed with their upper case designations. The load and instrumentation schematic is displayed in Figure 4.14a. For gages on the external jacket, the modeled

a) Load/Instrumentation Schematic

b) Pile Jacket Strains

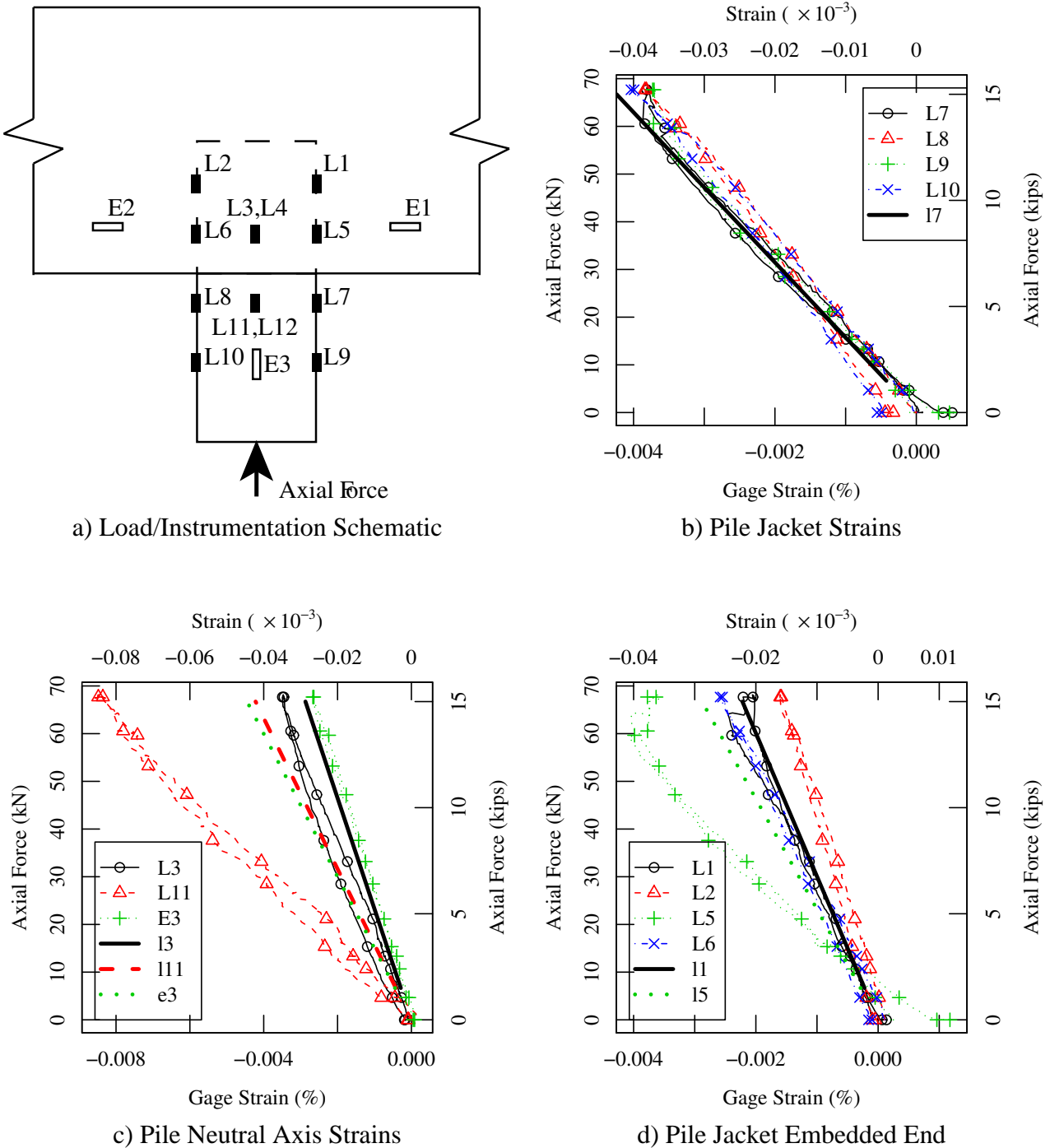c) Pile Neutral Axis Strains

d) Pile Jacket Embedded End

Figure 4.14: Case 1.1: Strain Comparison, Axial Load Only (2000-07-13)

results compare quite favorably with the measured results (Figure 4.14b). From the model, results from gage l7 and l8 match exactly, as do results for gages l9 and l10. At maximum axial load, l7 indicates a strain of -0.00424%, while l9 indicates a strain of -0.00439%. Because the difference is small and barely distinguishable on the graph, only the results for l7 are displayed along with measured results for L7, L8, L9, and L10 in Figure 4.14b.

Considering Figure 4.14c, notice that model and experiment agree quite well for gage L3 (denoted as l3 & L3, respectively). For gage L11, there is a significant difference with the measured results showing approximately twice the strain of the modeled outcome. In this case, the measured results are deemed less reliable, as the axial load was not purely axial during the test and instead was offset toward the side of gage L11.

For gage E3, embedded in the center of the pile, the results are more similar though measured results show strains that are on the order of one-half the modeled outcome. This difference could be due to the embedded gage being offset during construction toward the side opposite the position of gage L11, with the axial load being offset toward gage L11.

For gages L1, L2, L5, & L6, modeled results l1 & l2 matched exactly as did l5 & l6. As a consequence, only l1 & l2 are displayed in Figure 4.14d. Similarly, measured results for L1 & L2 matched l1 reasonably well, particularly L1. Also, gage L6 matched results for l5 remarkably well, though L5 displayed strains nearly twice that indicated by l5 and L6. This variation may be due to local debonding between the pile jacket and the pile cap preventing the loads from being shared of into the cap.

Overall, the results of this comparison indicate that the axial loads and material parameters were represented within expectations.

Load Case 1.2

For case 1.2, the bearing used to transmit axial loads failed during the application of axial and lateral loads. Because of this bearing failure, and hence the increased frictional resistance to lateral loads, the measured responses were not useful for evaluating the performance of the FE model. As a consequence, load case 1.3 is presented next.

Load Case 1.3

For load case 1.3, the axial load was again applied followed by a transverse (lateral) load (Figure 4.15) that was ramped up to 7 kips. Comparing modeled vs. measured outcomes in Figure 4.16b, the modeled outcomes for gages l9 and l10 were indistinguishable from l7 and l8, respectively. Therefore, l9 & l10, were not included. However, notice that measured results for L7 and L9 compare reasonably well with l7, therefore l9 as well. The primary difference is the hysteresis loop demonstrated by the measured data, vs. the straight line given by the linear elastic FE model. Gages L8 and L10 show a similar variation relative to l8 (& therefore l10 as well). For all four gages, the measured strains show a slightly stiffer response than the linear elastic model.

In Figure 4.16c, gages l3, l11, and e3 show the initial response to the axial load, but zero effect from the lateral loads, as expected due to their position on the neutral axis associated with the lateral load. Again, the measured outcomes of L3 and L11 indicate that either the gages were not exactly on the neutral axis or that nonlinear geometric effects were significant. However, because E3 matches the modeled response, the variations in L3 and L11 were more than likely due to slight misalignments with the neutral axis.

Figure 4.15: Model 1: Linear elastic deformed geometry

Given the range of possible sources of difference, the comparison between the measured and modeled outcomes for the embedded gages (Figure 4.16d) show remarkable agreement. Again, as in Figure 4.16b, the primary distinction is the hysteresis effect displayed by the measured outcomes relative to the linear outcome from the linear elastic FE model.

a) Load/Instrumentation Schematic

b) Pile Jacket Strains

c) Pile Neutral Axis Strains

d) Pile Jacket Embedded End

Figure 4.16: Case 1.3: Strain Comparison, Axial and Transverse Loads (2000-07-14)

Load Case 1.4

For load case 1.4, the axial load was again applied followed by a transverse (lateral) load (Figure 4.15) that was ramped up to 6 kips, followed by a reversed transverse load that was ramped up to approximately -5 kips. Comparing modeled vs. measured outcomes in Figure 4.17b, notice that measured results for L7 and L9 compare reasonably well with l7, therefore l9 as well. The primary difference is again the hysteresis loop demonstrated by the measured data, vs. the straight line given by the linear elastic FE model. Gages L8 and L10 show a similar variation relative to l8 (& therefore l10 as well). For all four gages, the measured strains show a slightly stiffer response than the linear elastic model.

In Figure 4.17c, gages l3, l11, and e3 show the initial response to the axial load, but zero effect from the lateral loads as expected due to their position on the neutral axis associated with the lateral load. Again, the measured outcomes of L3 and L11 indicate that either the gages were not exactly on the neutral axis or that nonlinear geometric effects were significant. However, because E3 matches the modeled response, the variations in L3 and L11 were more than likely due to slight misalignments with the neutral axis.
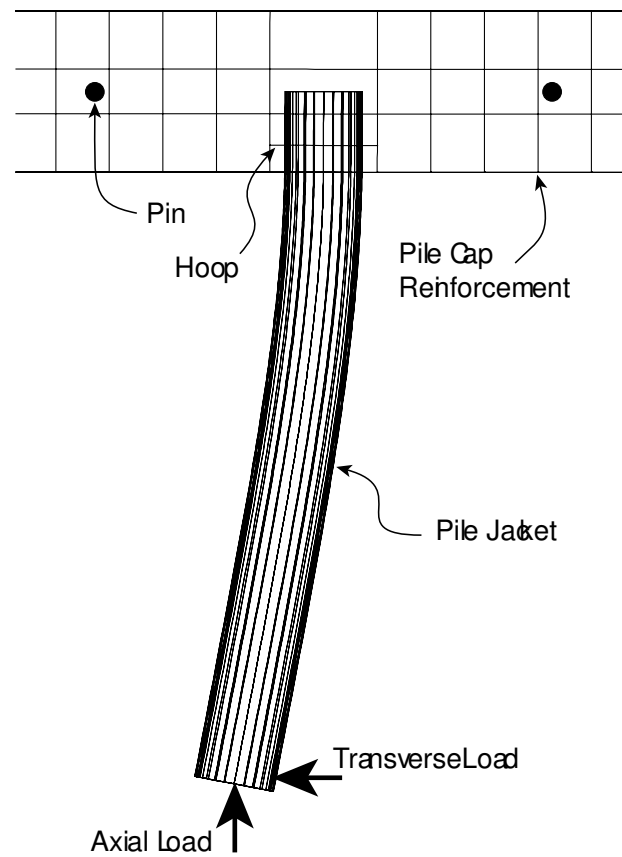
Given the range of possible sources of difference, the comparison between the measured and modeled outcomes for the embedded gages (Figure 4.17d) again show remarkable agreement. As in Figure 4.17b, the primary distinction is the hysteresis effect displayed by the measured outcomes relative to the linear outcome from the linear elastic FE model.
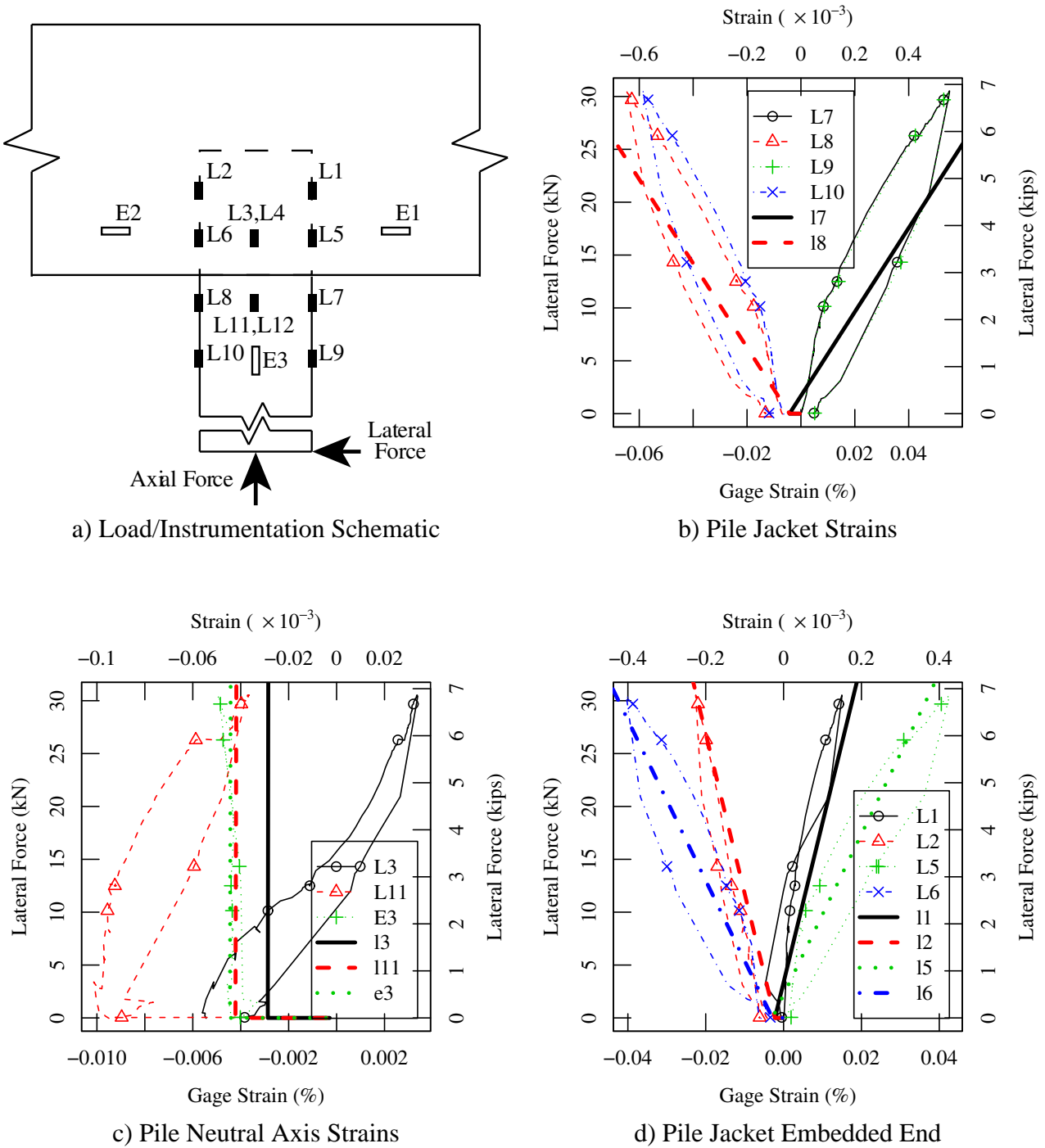
a) Load/Instrumentation Schematic

b) Pile Jacket Strains

c) Pile Neutral Axis Strains

d) Pile Jacket Embedded End

Figure 4.17: Case 1.4: Strain Comparison, Axial and Transverse Loads (2000-07-18)

Load Case 1.5

For load case 1.5, the axial load was again applied followed by a transverse (lateral) load (Figure 4.15) that was ramped up to approximately 13.4 kips at about 5.5 inches (Figure 4.18). From that point on the capacity of the system continued to decrease, as the tip of the pile was displaced as far as 11.4 inches.
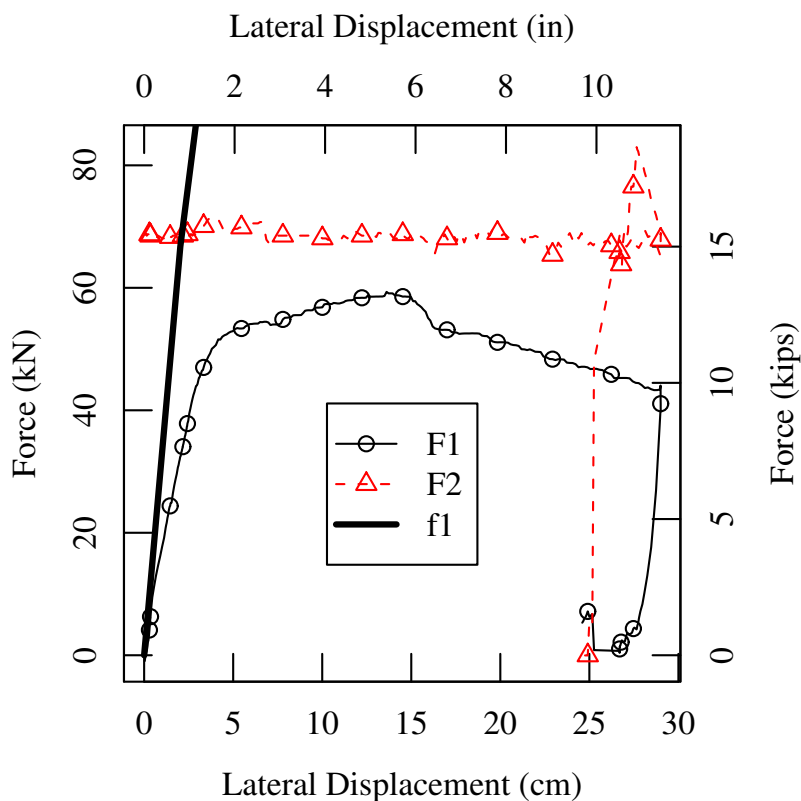
Figure 4.18: Case 1.5: Axial and Transverse Load vs. Lateral Displacement (2000-07-19)

Comparing modeled vs. measured outcomes in Figure 4.19b, notice that measured results for L7 and L9 compare reasonably well with l7, therefore l9 as well. The primary difference is again the hysteresis loop demonstrated by the measured data, vs. the straight line given by the linear elastic FE model. Gages L8 and L10 show a similar variation relative to l8 (& therefore l10 as well). For all four gages, the measured strains show a slightly stiffer response than the linear elastic model.

In Figure 4.19c, gages l3, l11, and e3 show the initial response to the axial load, but zero effect from the lateral loads as expected due to their position on the neutral axis associated with the lateral load. Again, the measured outcomes of L3 and L11 indicate that either the gages were not exactly on the neutral axis or that nonlinear geometric effects were significant. However, because E3 matches the modeled response, the variations in L3 and L11 were more than likely due to slight misalignments with the neutral axis.

Given the range of possible sources of difference, the comparison between the measured and modeled outcomes for the embedded gages (Figure 4.19d) show remarkable agreement. Again, as in Figure 4.19b, the primary distinction is the hysteresis effect displayed by the measured outcomes relative to the linear outcome from the linear elastic FE model.
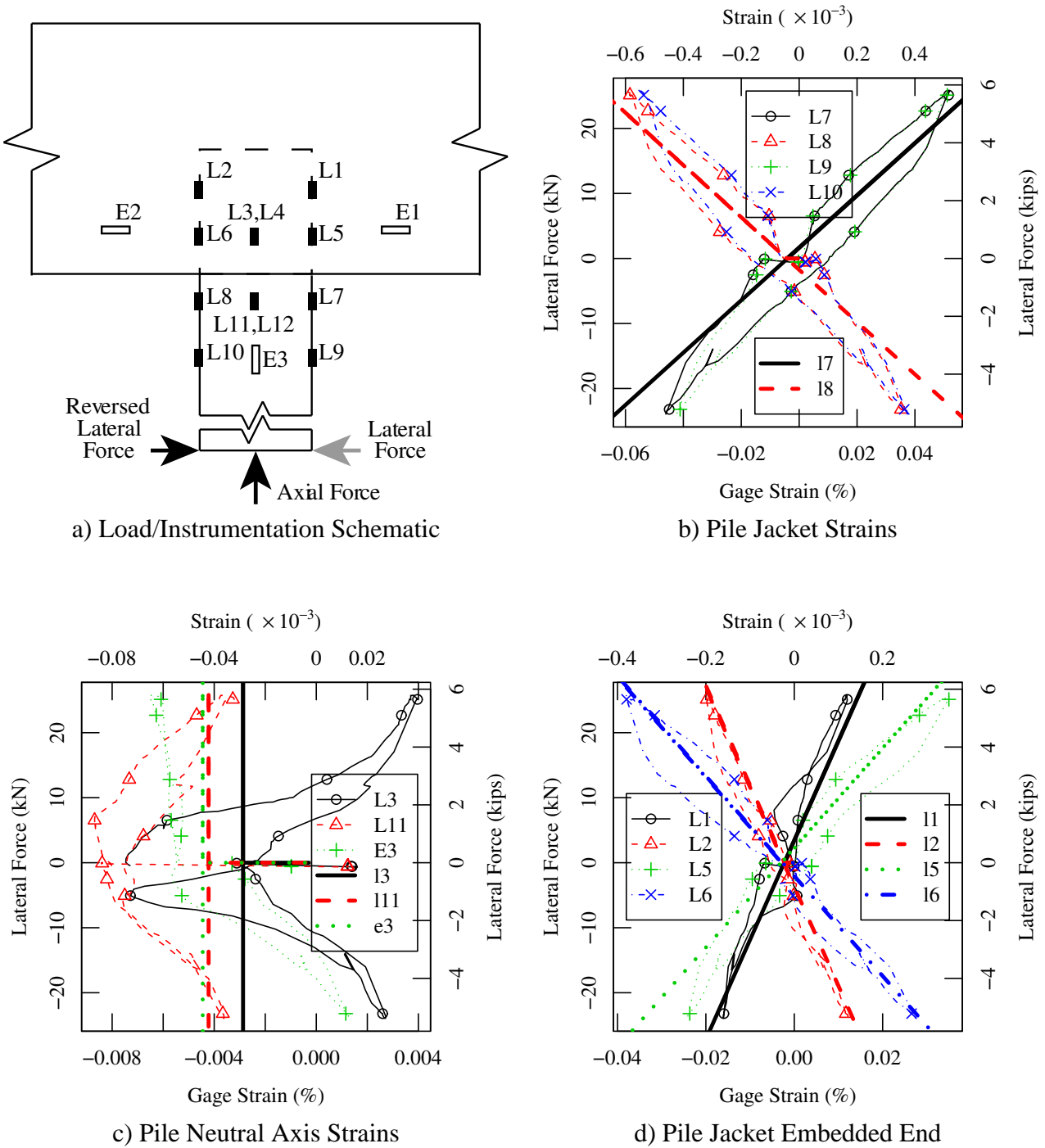
a) Load/Instrumentation Schematic

b) Pile Jacket Strains

c) Pile Neutral Axis Strains

d) Pile Jacket Embedded End
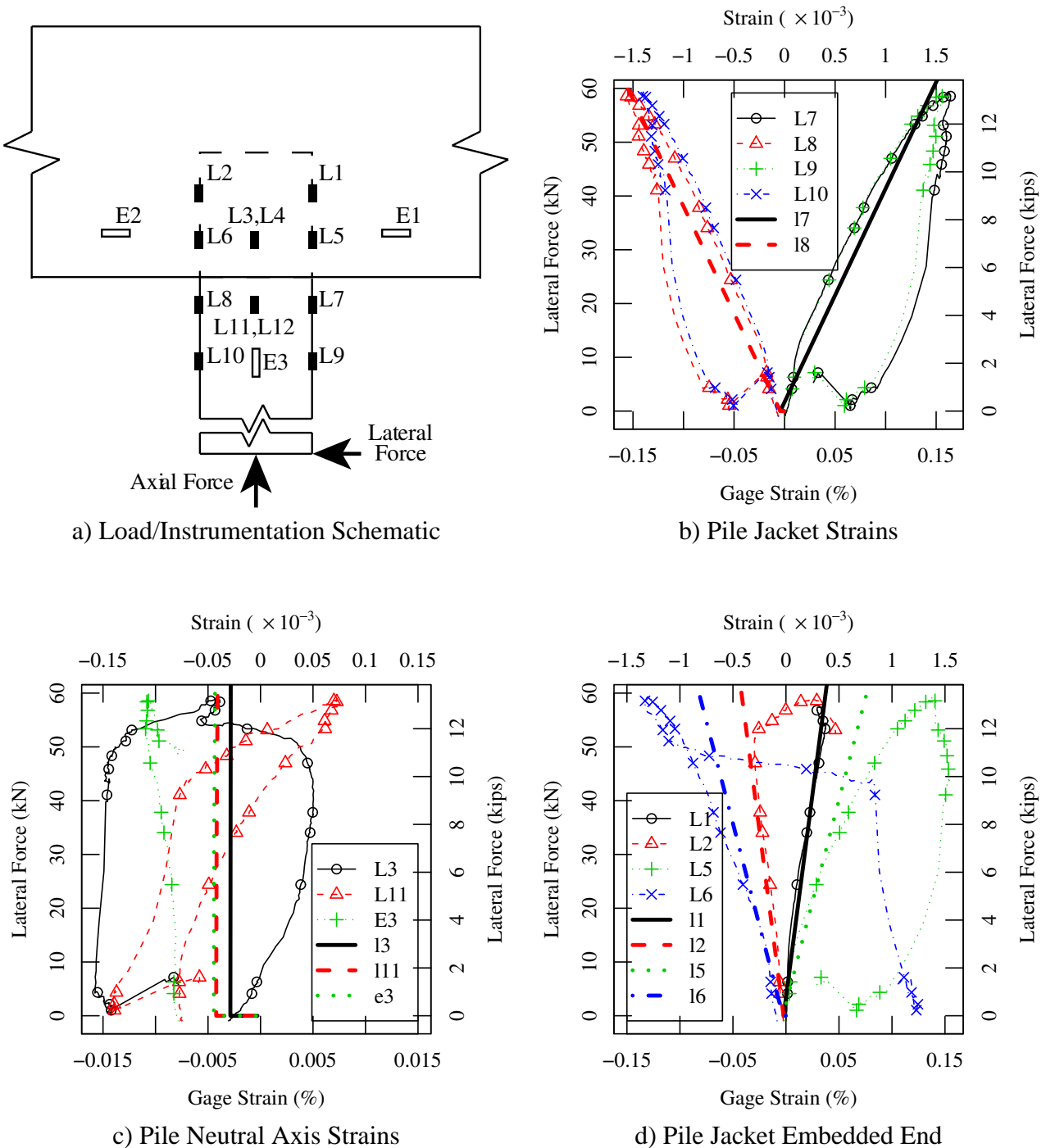
Figure 4.19: Case 1.5: Strain Comparison, Axial and Transverse Loads (2000-07-19)

After reviewing gage data for PC-1, consider the strain distribution illustrated in Figure 4.20. As expected, the strains are concentrated near the interface between the pile and pile cap. In this case, the tensile strains on the right hand interface show magnitudes nearly as high as those of the compressive strains on the left. Unfortunately, this is one of the unrealistic aspects of the linear elastic model. In the experimental test case, the pile jacket debonded to some extent from the pile cap early in the load sequence and was typically the first visible sign of "inelastic" damage.

Figure 4.20: Case 1: Elastic Strains Parallel to Length of Pile Cap for 10 in Tip Displacement

Load Case 2.1

For load case 2.1, recall that the primary distinction from case 1 is the reduction in the thickness of the pile jacket, from 0.32 in to 0.25 in. Figure 4.21 displays the results for the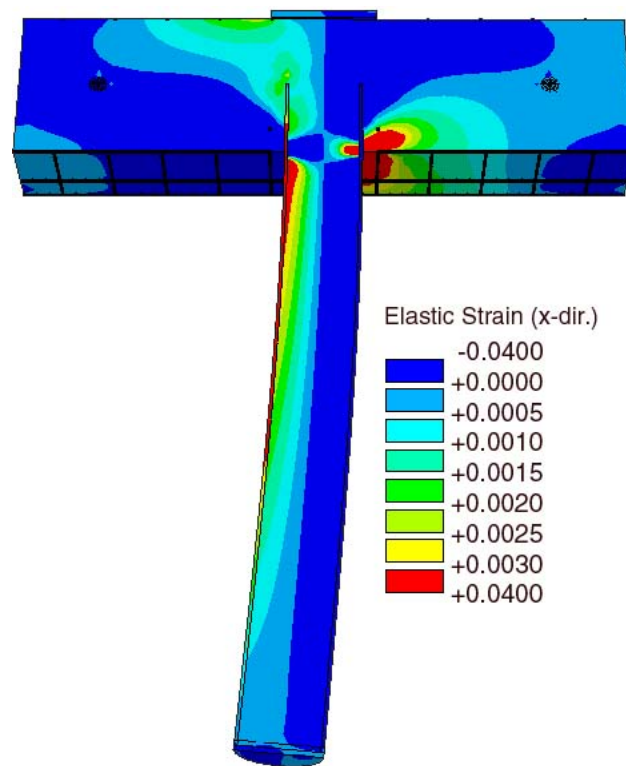 same load as for the case displayed in Figure 4.20. In comparing the two outcomes, it is clear that though the thickness of the pile jacket was reduced, not too surprisingly, the strain distribution for the two is essentially unchanged. Also notice that the contours on the right outline what could be considered a tensile "Tie", and on the left a compressive "strut".

In the physical test of model PC-2, the axial load was applied followed by a transverse (lateral) load that was ramped up to almost 11.7 kips, followed by a reversed transverse load that was ramped up to approximately -8.3 kips (see Figure 4.22). The load was then re-applied in the initial transverse direction to a load of 6.4 kips and reversed again to approximately -5.7 kips. Following this same load cycle with the linear elastic finite element model, the outcome is displayed by the curve denoted by f1. Clearly the experimental model begins to diverge from the FE response as the load rises above ∼6 kips.

However, this initial divergence is small and the experimental response does not truly diverge and become nonlinear until it reaches a load near 10 kips. The initial divergence could be due to several factors and is at least partly due to the tensile separation or partial debonding of the concrete from the pile jacket.

Comparing modeled vs. measured outcomes in Figure 4.23b, notice that measured results for L7 and L9 compare reasonably well with l7 up to loads approaching 10 kips, therefore l9 as well. Beyond 10 kips, as displayed in all figures (Figure 4.22 thru 4.23), the measured responses diverge significantly from the linear elastic response. As a consequence of the non-linear behavior, the responses
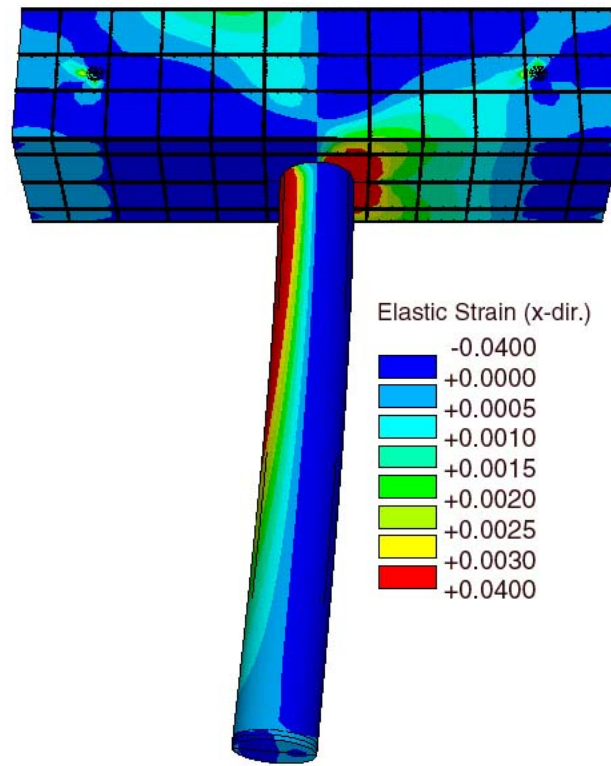
Figure 4.21: Case 2: Elastic Strains Parallel to Length of Pile Cap for 10 in Tip Displacement
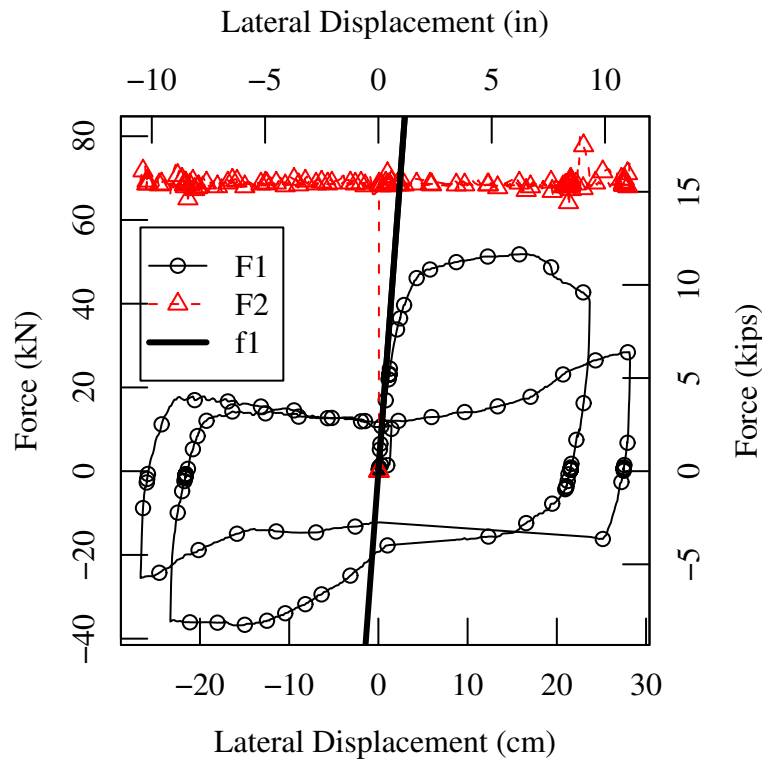
Figure 4.22: Case 2.1: Axial and Transverse Load vs. Lateral Displacement (2001-09-04)

a) Load/Instrumentation Schematic

b) Pile Jacket Strains

c) Pile Neutral Axis Strains

d) Pile Jacket Embedded End
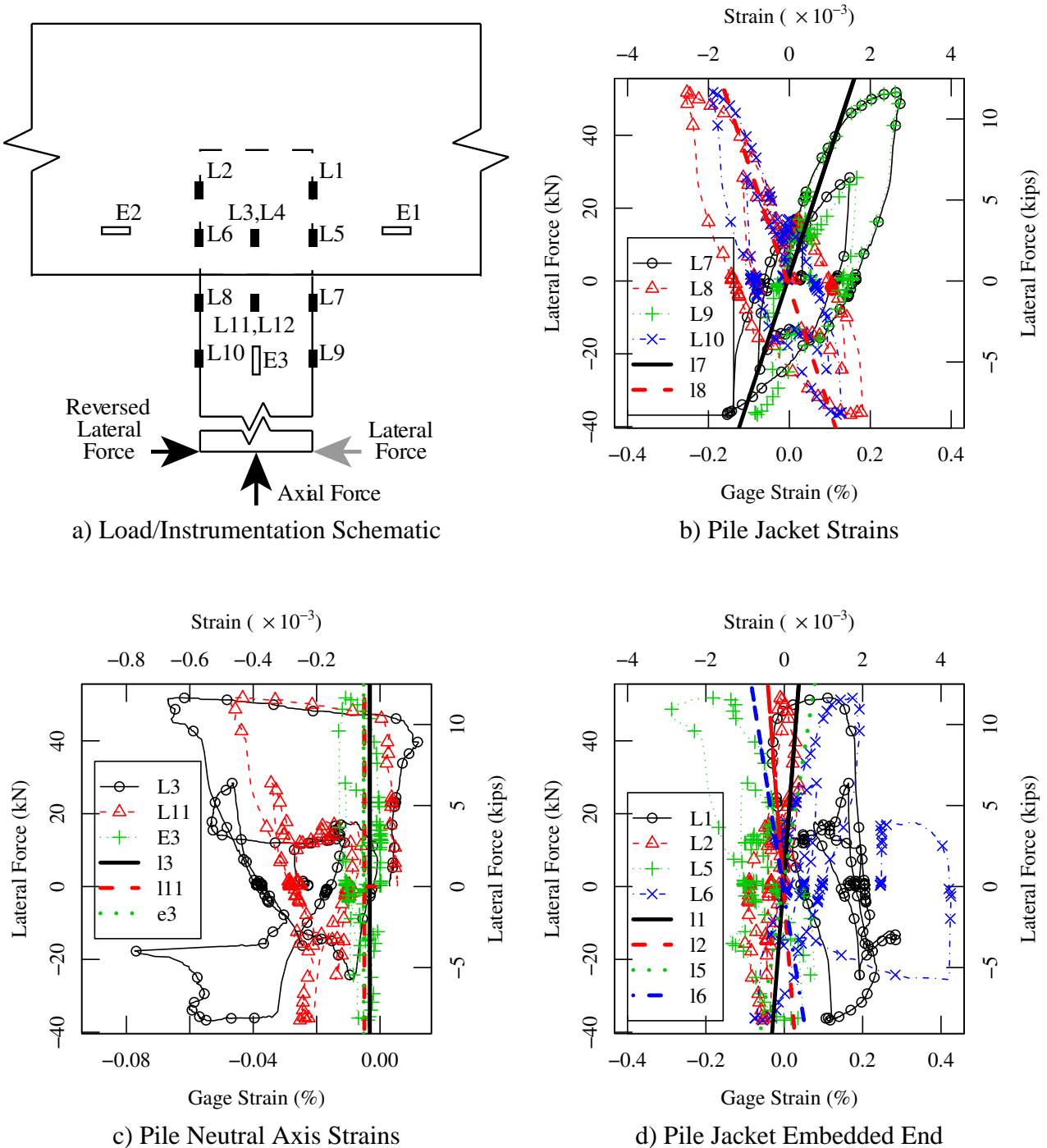
Figure 4.23: Case 2.1: Strain Comparison, Axial and Transverse Loads (2001-09-04)

show significant hysteresis loops that are due to a combination of concrete damage and plastic deformation in the steel reinforcement. The "pinched" form in the center is primarily due to damage in the concrete.

In Figure 4.23c, gages l3, l11, and e3 show the initial response to the axial load, but zero effect from the lateral loads as expected due to their position on the neutral axis associated with the lateral load. Again, the measured outcomes of L3 and L11 indicate that either the gages were not exactly on the neutral axis or that nonlinear geometric effects were significant. However, because E3 matches

the modeled response, the variations in L3 and L11 were more than likely due to slight misalignments with the neutral axis.

Given the range of possible sources of difference, the comparison between the measured and modeled outcomes for the embedded gages (Figure 4.23d) show remarkable agreement. Again, as in Figure 4.23b, the primary distinction is the hysteresis effect displayed by the measured outcomes relative to the linear outcome from the linear elastic FE model.

Load Case 3.3

Prior to load case 3.3, physical model PC-3 was loaded twice to evaluate the performance of the instrumentation. For the first load case on PC-3 (Load Case 3.1), the axial load of 15 kips was applied followed by a lateral load slightly greater that 4 kips. With out relieving the axial load, a reversed lateral load was applied that also reached a maximum near 4 kips. During this load sequence, no visible damage was observed.

Following the first load case (3.1), an axial load (15 kips) was again applied followed by a lateral load that slightly exceeded 9.2 kips.

For load case 3.3, as displayed in Figure 4.24, in the experimental model the axial load was applied followed by a transverse (lateral) load (Figure 4.15) that was ramped up to the maximum structural capacity of the connection with a load slightly in excess of 12.8 kips. In this case, the lateral load was not reversed.

Notice in Figure 4.24 that the experimental load-displacement response diverges from the linear FE response slightly as the load rises above ∼1.5 kip (7 kN), but again does not show truly non-linear behavior until the load exceeds approximately 11 kips (50 kN).
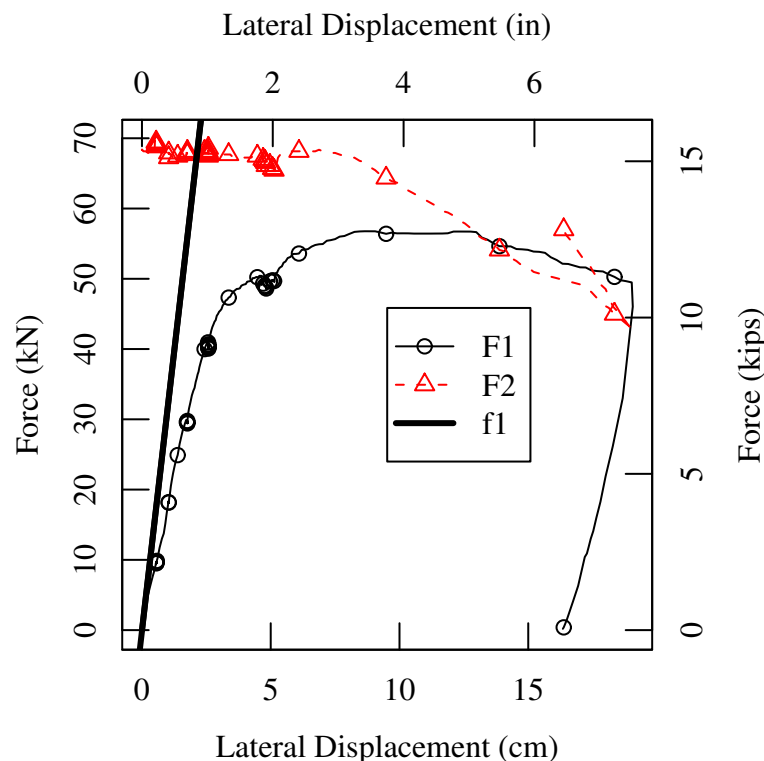
Figure 4.24: Case 3.3: Axial and Transverse Load vs. Lateral Displacement (2002-10-29)

116

Some of the strain responses for this load case (3.3) are shown in Figure 4.25. Comparisons between modeled and measured outcomes in Figure 4.25 are very similar to those displayed for earlier cases. Given the range of possible sources of difference, the comparison between the measured and modeled outcomes for the embedded gages (Figure 4.25d) show remarkable agreement. Again, as in Figure 4.25b, the primary distinction is the hysteresis effect displayed by the measured outcomes relative to the linear outcome from the linear elastic FE model.

a) Load/Instrumentation Schematic

b) Pile Jacket Strains

c) Pile Neutral Axis Strains

d) Pile Jacket Embedded End

Figure 4.25: Case 3.3: Strain Comparison, Axial and Transverse Loads (2002-10-29)

Load Case 3a.1

For load case 3a.1, as displayed in Figure 4.26, in the experimental model the axial load was applied followed by a transverse (lateral) load (Figure 4.15) that was ramped up to the maximum lateral structural capacity of the connection with a load slightly in excess of 17 kips. In this case, the lateral load was not reversed. Notice in Figure 4.26 that the experimental load-displacement response diverges slightly from the linear FE response as the load rises above ∼5 kip (20 kN).

For load case (3a.1) only gages L7 & L8 were used. The corresponding strain responses are shown in Figure 4.27. Again the responses match quite well, in this case up to loads in excess of 10 kips. Beyond that, the pile jacket begins to undergo more significant plastic deformation.

Figure 4.26: Case 3a.1: Axial and Transverse Load vs. Lateral Displacement (2001-09-04)

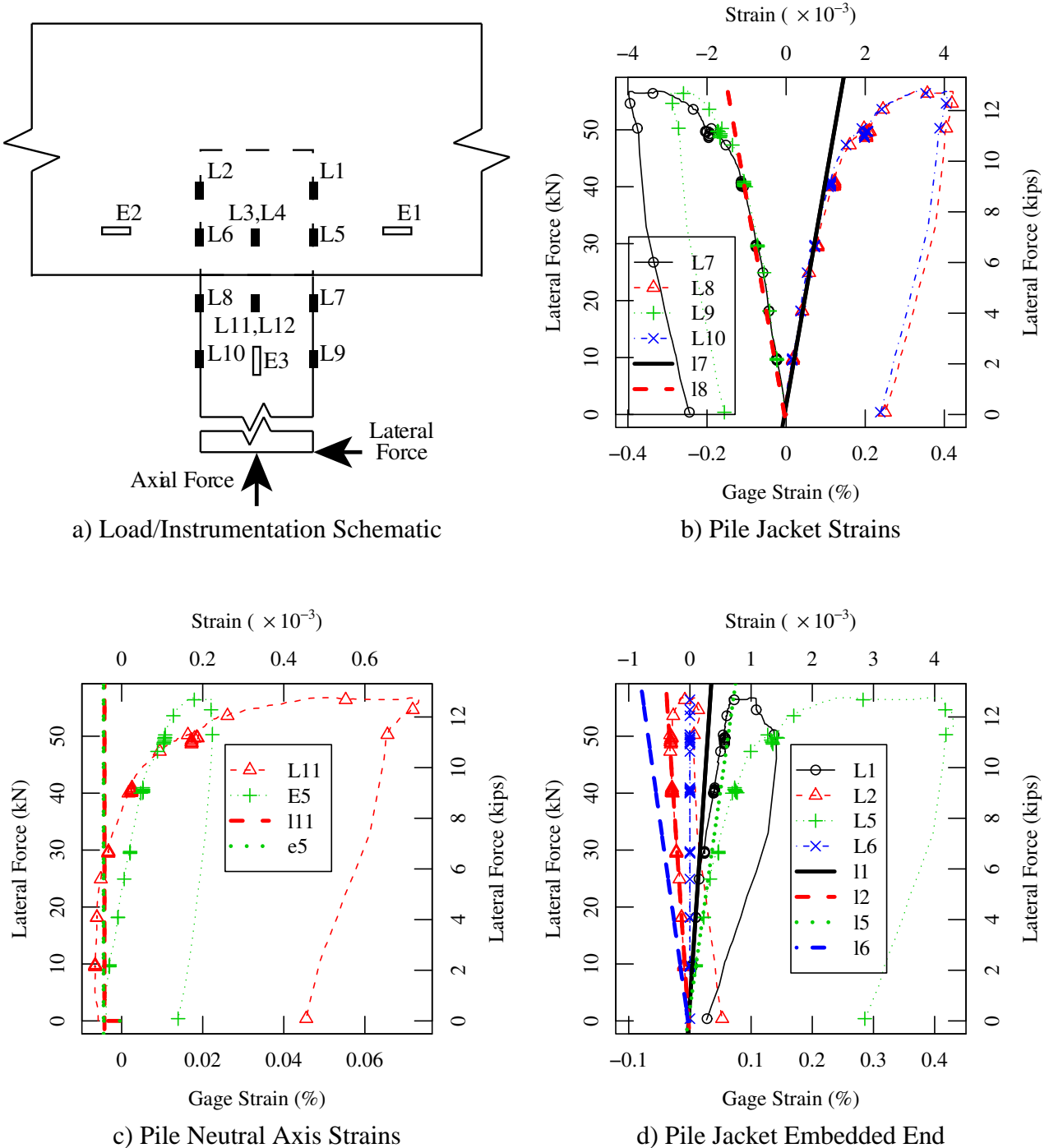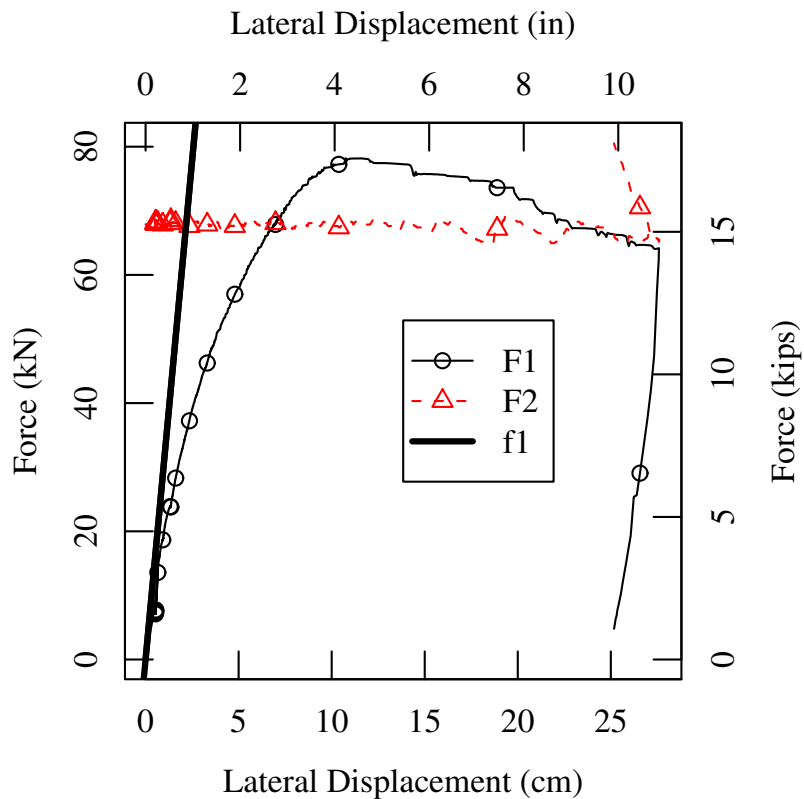a) Load/Instrumentation Schematic   b) Pile Jacket Strains
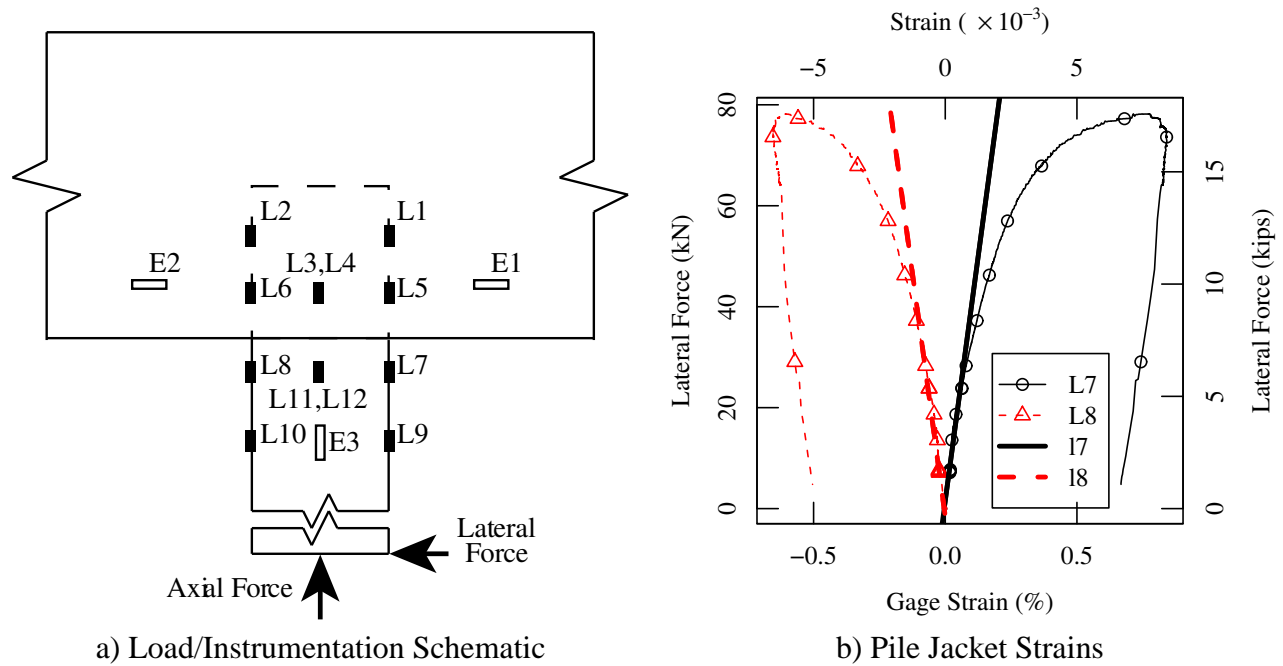
Figure 4.27: Case 3a.1: Strain Comparison, Axial and Transverse Loads (2003-01-30)

Load Case 4

For load case 4, as displayed in Figure 4.28, in the experimental model the axial load was applied followed by a transverse (lateral) load (Figure 4.15) that was ramped up to the maximum structural capacity of the connection with a load slightly in excess of 15.3 kips. In this case, the lateral load was not reversed.

Notice in Figure 4.28 that the experimental load-displacement response diverges from the linear FE response as the load rises above ∼1.5 kip (7 kN), but does not, in this case, appear to go truly non-linear until the lateral load exceeds ∼18 kips.

As with test model PC-3a, only gages L7 & L8 were monitored for test PC-4. Responses for load case 4 are shown in Figure 4.29. For gages L7 & L8 on test 4, it is clear that as the lateral load approaches 20 kips the steel jacket in that area becomes "perfectly-plastic", where the load-strain curve is perfectly horizontal. With both PC-3a and PC4 displaying significant plastic deformation in the pile jacket, in the next section, plastic deformation will be considered in the finite element models.

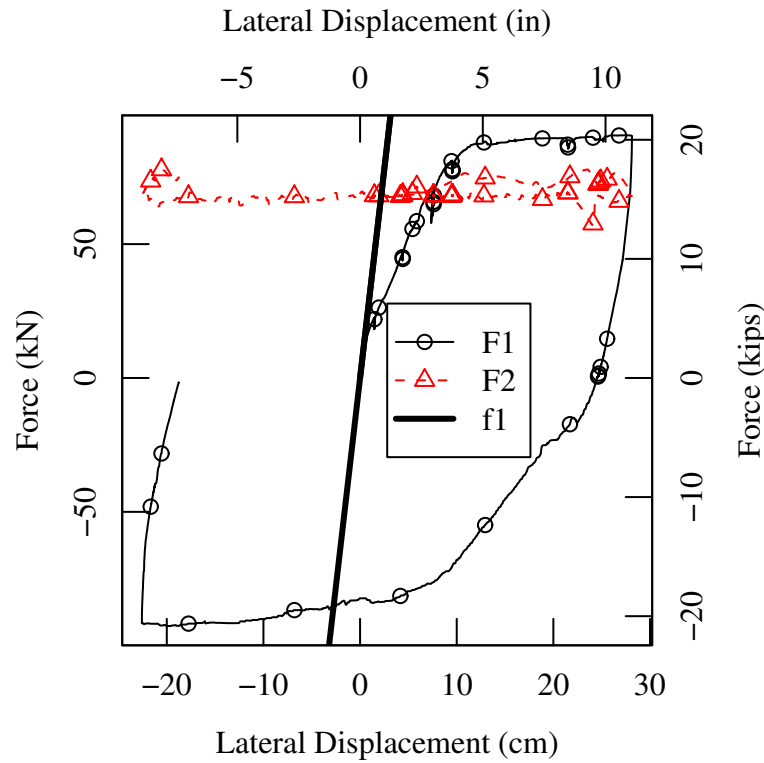Figure 4.28: Case 4: Axial and Transverse Load vs. Lateral Displacement (2003-11-10)
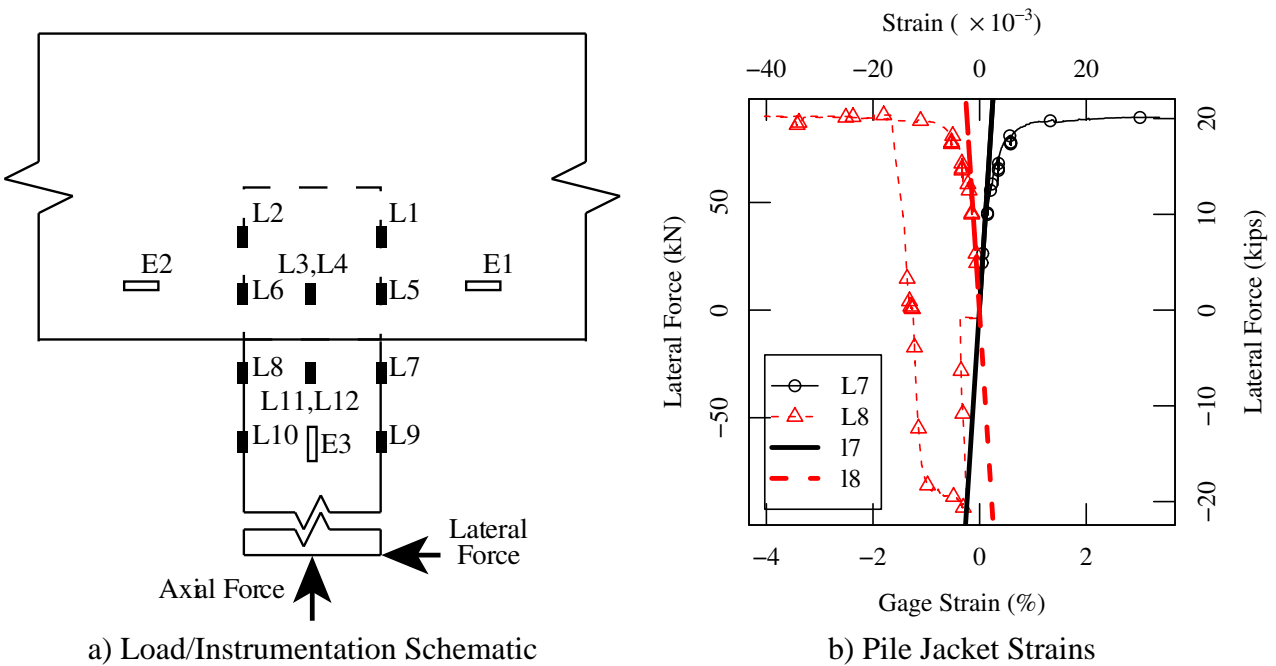

a) Load/Instrumentation Schematic   b) Pile Jacket Strains

Figure 4.29: Case 4: Strain Comparison, Axial and Transverse Loads (2003-11-11)

4.4.4   Non-elastic Evaluations

To accurately model the response of the connection, as was discussed earlier, it is necessary to consider the aspects of concrete damage, the plastic deformation of steel reinforcement along with the steel jacket, and also allow separation between the steel jacket and the pile cap on the tensile side of the pile-to-pile cap joint.

Extensive efforts were made toward modeling the aspect of concrete damage. In the end, the damage modeling project had to be reined in, unfortunately with few results to show. In the following section the remaining two aspects of the joint behavior are considered. Though these models are by definition not entirely accurate, they do show some useful trends and may work as interpretive tools.

For the plasticity model of the steel components (steel jacket and reinforcement), a yield stress of 52 ksi was used with a corresponding tangent modulus of 1 msi. For cases 1 & 2, these plasticity models were applied to the models previously described (Section 4.4.2).

Load Cases 1 & 2

In cases 1 and 2, the steel pile jackets showed no visible plastic strain. In these cases, the deflection of the pile was driven by cracking and deformation of the steel reinforcement in the pile cap. Ignoring the damage to the concrete in the cap, consider the plastic strains of the steel reinforcement in the cap, as shown in Figure 4.30. Notice that in both cases, Figure 4.30a and Figure 4.30b, the maximum plastic strains occur roughly on the 45 degree line from the pile interface toward each of the pins. This matches the 45 degree line where the cracking occurred on the compression side. Recall that the models displayed in Figure 4.30 do not have the ability to debond on the tension face of the jacket. As a consequence, the strains on the tensile side of the model are much higher than those that could be supported by in the experimental test case.

This information is useful and provides a reasonable indication of locations where the cap and re-bar are likely to suffer significant deformation; however, it would be a more useful indicator if "debonding" were allowed to occur between the pile jacket and the pile cap. With this in mind, consider the following models for PC-3a and PC-4.
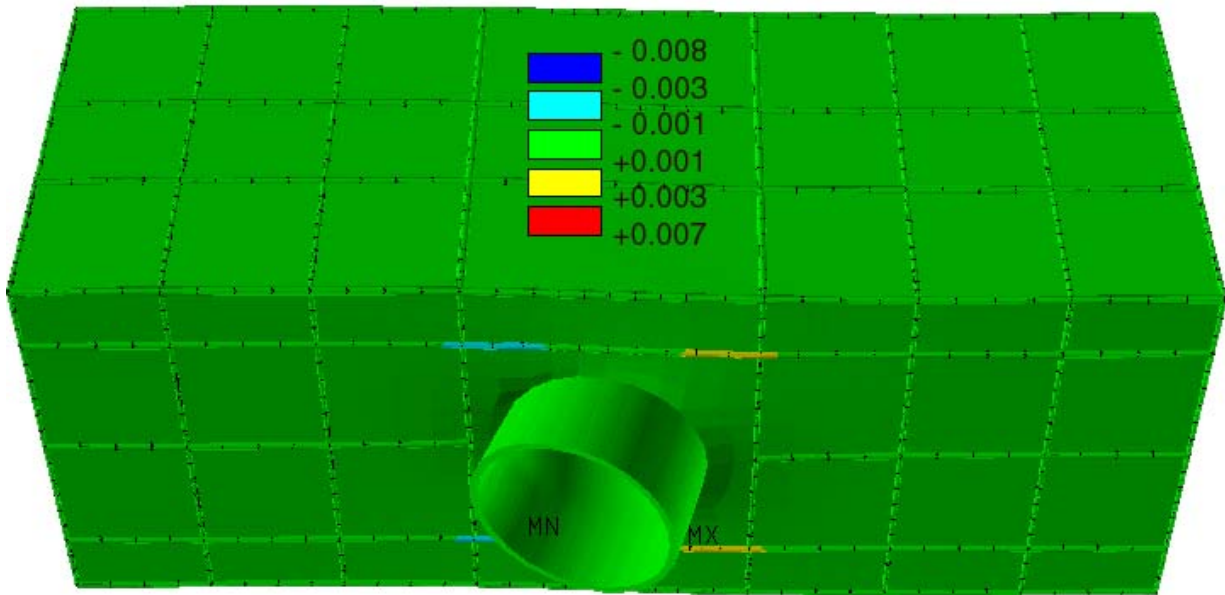
a) PC-1 Plastic Strains
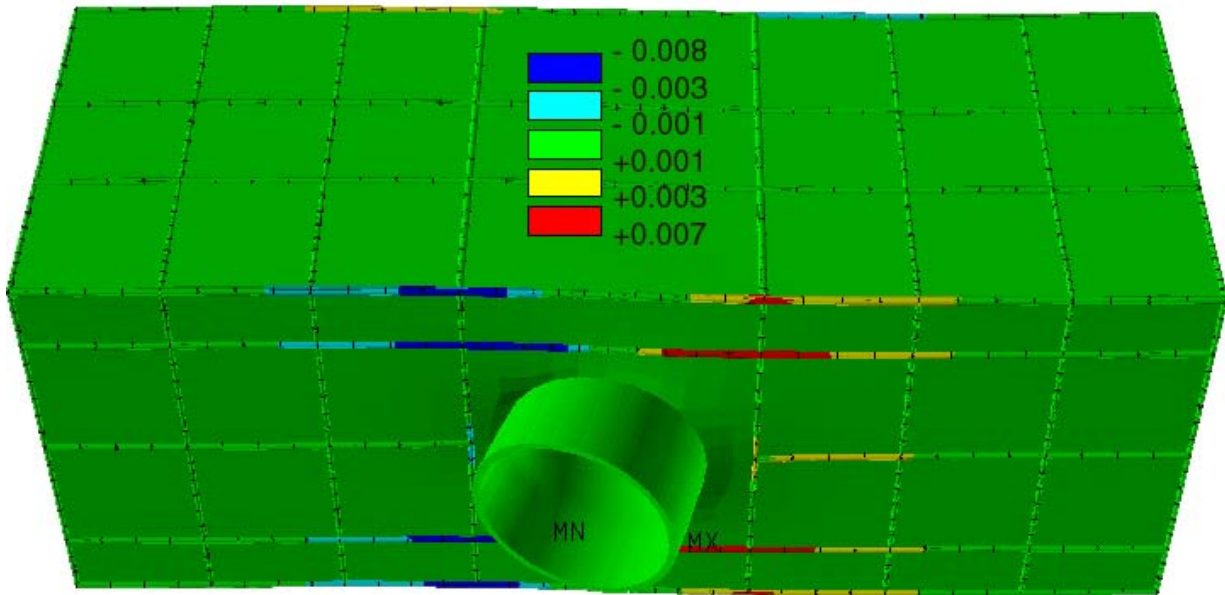
b) PC-2 Plastic Strains

Figure 4.30: Cases 1& 2: Plastic Strains in Pile Cap Re-bar for 10 in displacement

Load Case 3a

In this case, contact surfaces were introduced into the model for the interfaces between the pile jacket and the pile cap. These surfaces were included for all surfaces serving as an interface between the pile and the pile cap, including the embedded end of the pile cap. As an example, consider the geometry shown in Figure 4.31. In this display, notice that the pile is "disconnected" from the pile cap. This is with the pile under a 15 kip axial load. As a consequence, though measures of strain are different, it is clear that the strain distributions in the pile jacket are significantly different than those displayed in Figure 4.20 and 4.21.
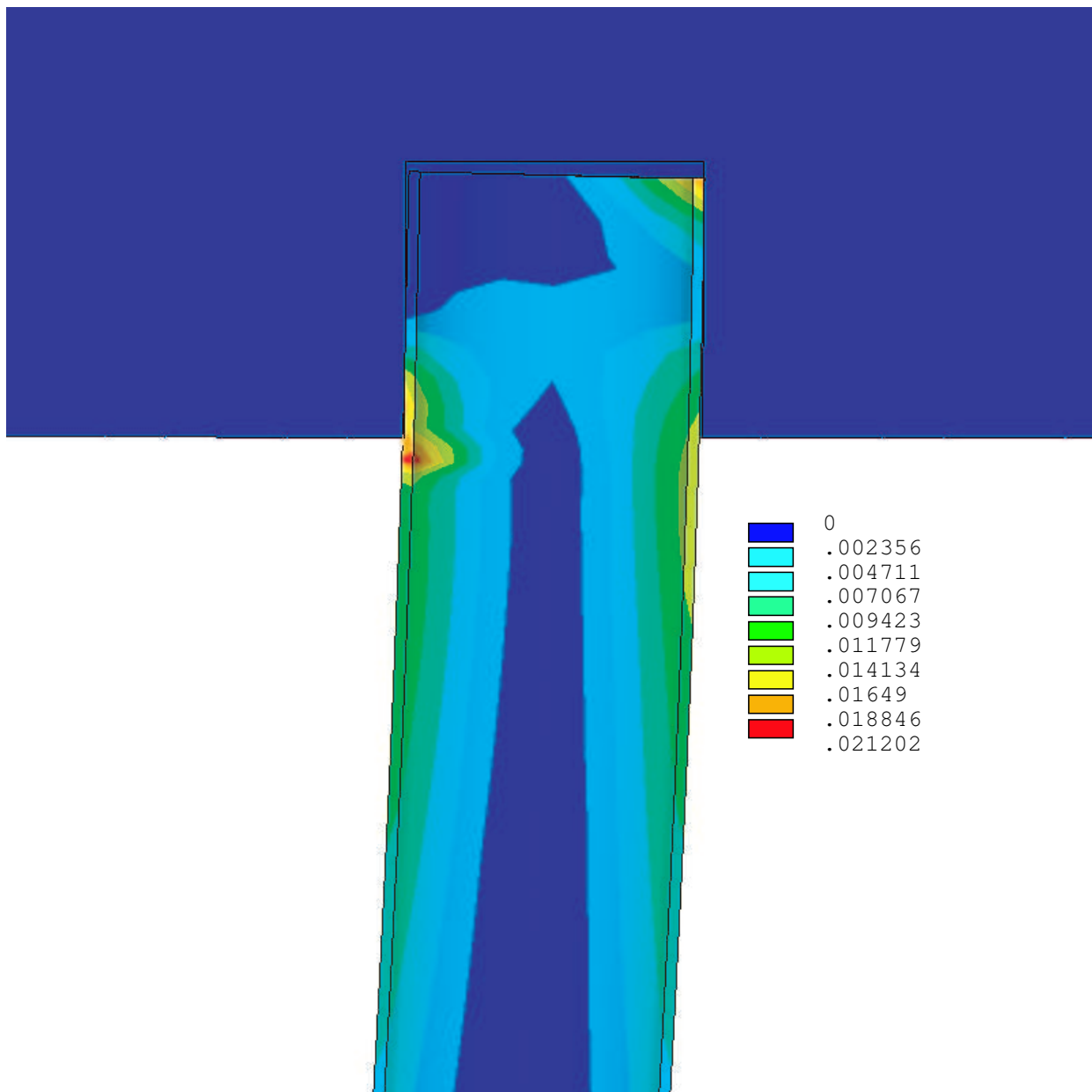
Figure 4.31: Case 3a: Equivalent Plastic Strains in the Pile Jacket

Now allowing both plastic deformation of the steel components and surface separation between the pile cap and the pile, consider the strains displayed in the following figures.

In this case, the modeled response tends to show the first non-linear tendencies as the lateral load approaches 15 kips. Because the concrete has not been degraded through this process, it is not too surprising that the modeled response is much stiffer than the measured response. However, it is interesting that the first knee and the general trends are very similar between the measured and modeled responses.

Following the global response comparison (Figure 4.32), consider the local strain responses shown in Figure 4.33. Notice that the strain responses also indicate that the analytical model is significantly stiffer than the test model. One possible explanation is the difference in the composite action between the concrete interior to the pile and the pile jacket itself.
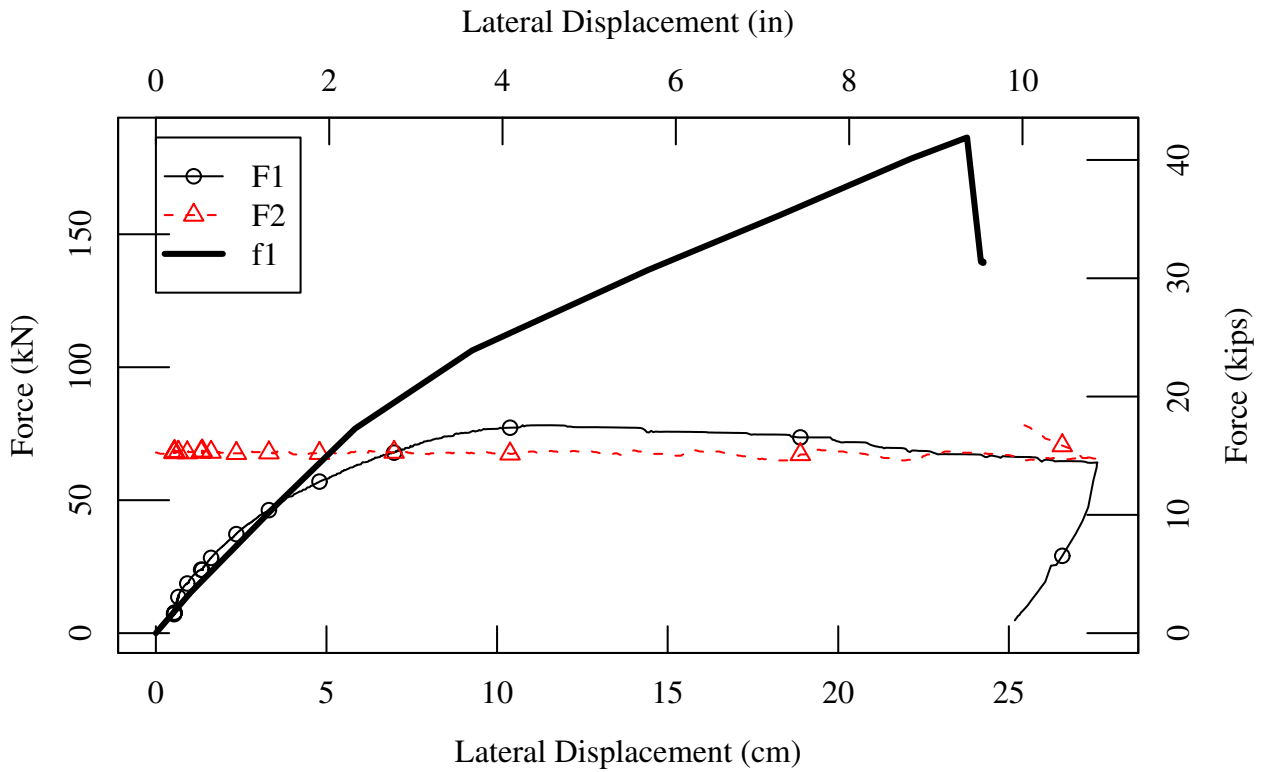
Figure 4.32: Case 3a: Lateral Load vs. Displacement, Non-Linear FE (2003-01-30)

a) Load/Instrumentation Schematic

b) Pile Jacket Strains
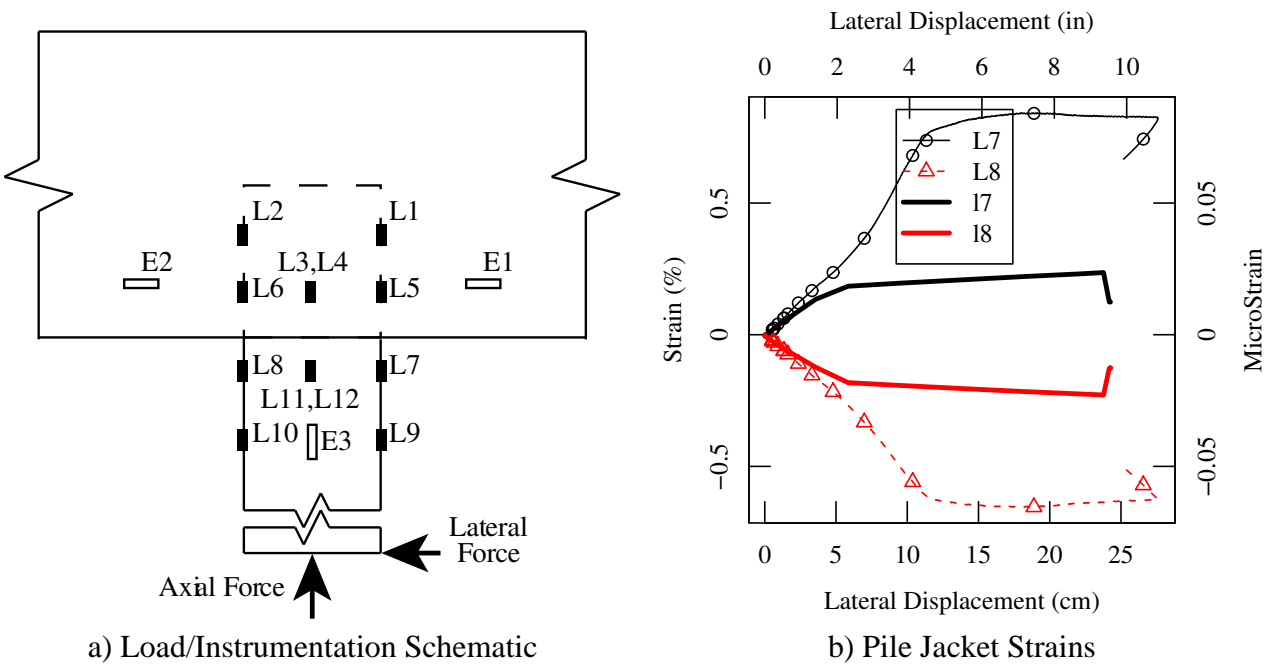
Figure 4.33: Case 3a: Strain Comparison, Non-Linear FE (2003-01-30)

Load Case 4

For load case 4, the nonlinear considerations were built into the model. These considerations included plasticity for the steel components and contact surfaces at the interfaces between the embedded pile and the pile cap. The modeled responses are shown in Figures 4.34 and 4.35.

Showing even better agreement than the previous case, the nonlinear responses start at approximately the same lateral load for both the modeled and measured outcomes. For case 4 in particular, concrete damage was minimized and the primary driver in the nonlinear response was the plastic deformation in the pile jacket. Though the response from the model is in general stiffer than that measured, this difference, due to minor softening of the concrete, can most likely be represented with a plasticity model for the concrete. Unfortunately, such tactics will only work for monotonic load cases.
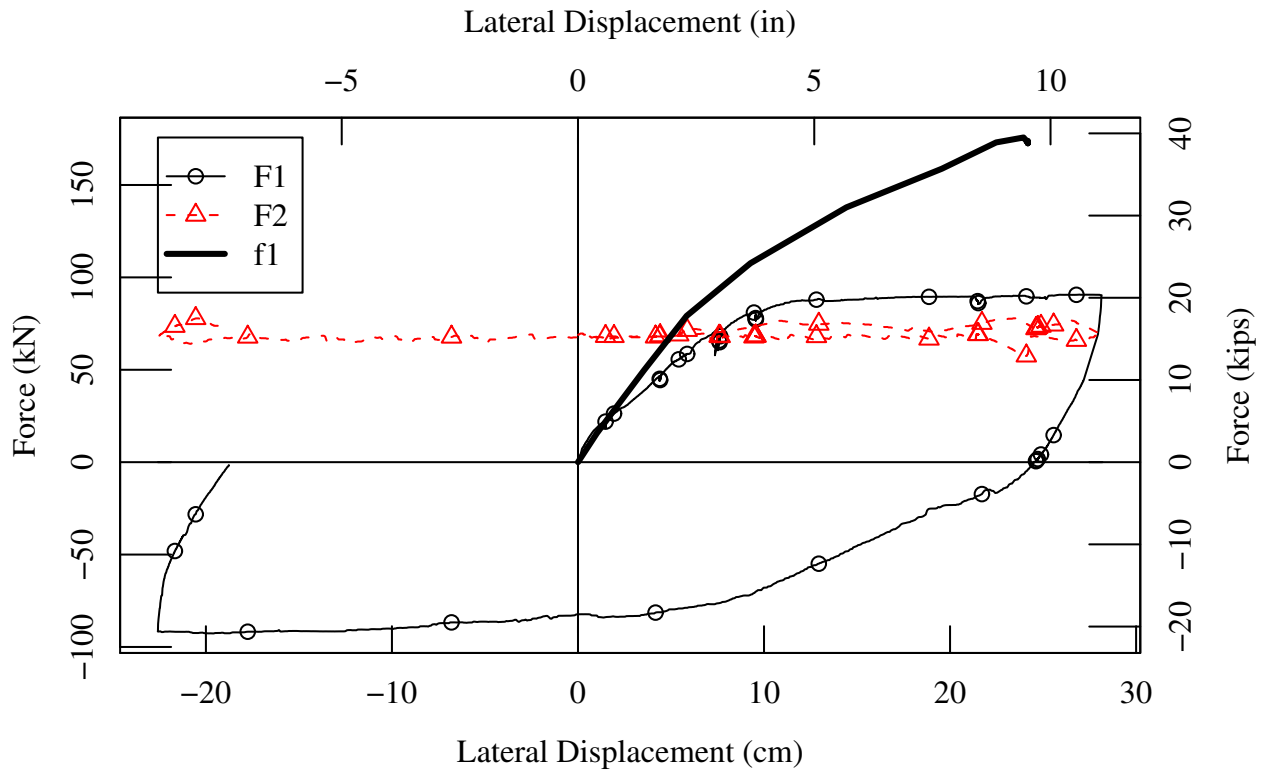
Figure 4.34: Case 4.1: Lateral Load vs. Displacement, Non-Linear FE (2003-11-10)

a) Load/Instrumentation Schematic

b) Pile Jacket Strains

Figure 4.35: Case 4.1: Strain Comparison, Non-Linear FE (2003-11-10)

Chapter 5

Concluding Remarks

5.1 SUMMARY AND CONCLUSIONS

The behavior of a steel pipe pile-to-concrete pile cap connection under extreme lateral loads was characterized in this investigation. Five one-half sized models of the connection were constructed and tested to failure in the structural engineering laboratory at MSU. The geometry of the models was based on a common connection configuration used by MDT in bridge construction. This 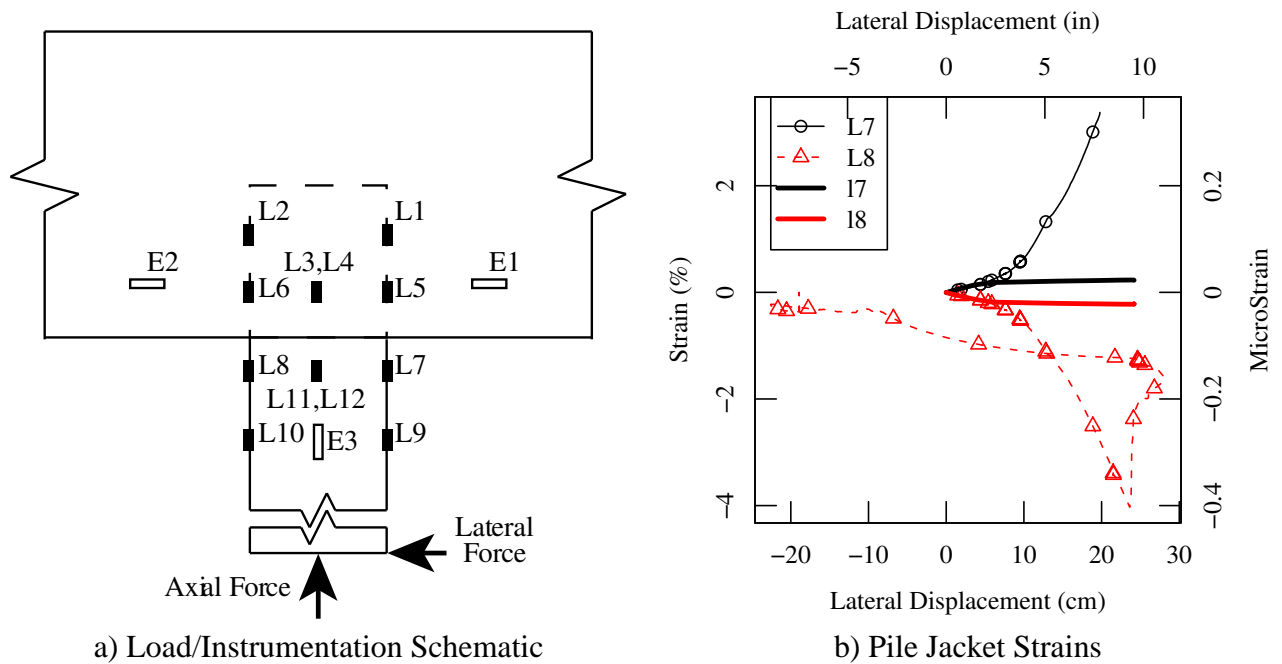connection configuration consisted of a concrete filled, steel pipe pile embedded to the mid-depth of the reinforced concrete cap cross-section. The parameters varied between the connection models were the wall thickness of the pipe pile, and the amount and arrangement of the reinforcing steel used in the cap. The parameters that were held constant between the tests included the dimensions of the cap and pile, and the basic materials used in their construction (although some variation did occur in the strength of the concrete used in each model). The behavior of each model was also analyzed using hand calculations, strut and tie modeling, and finite element modeling, with the objective of assessing how well each approach addressed this particular problem, and if additional insights on the connection behavior could be obtained from these analyses.

In general, as the program progressed, the amount of reinforcing steel in the pile cap models was increased. In the first two tests (PC-1 and PC-2), the longitudinal and transverse reinforcing ratios for the cap were 0.4 and 0.09 percent, respectively, which closely match the reinforcing ratios used by MDT in the full size pile caps. The primary difference between these models was the wall thickness of the steel pipe pile. The D/t ratio of the pile used in model PC-1 was 27, while the D/t ratio of the pile used in model PC-2 was 34.5. The pipe pile used in Model PC-2 was believed to better represent typical practice by MDT in their full size structures. When subjected to a lateral load of increasing magnitude, both models failed through tension cracking of the concrete in the cap. In both cases, the moment carried by the cap at failure was approximately 75 percent of the calculated plastic moment capacity of the concrete filled, steel pipe pile. At the point of maximum resistance, both connections demonstrated ductility ratios of 3.3. Model PC-2 was subjected to a few cycles of reversed load. The resulting load deformation hysteresis curves were "pinched" in shape, with both the maximum resistance as well as the energy dissipated by the connection decreasing on each successive load cycle.

In the third test, PC-3, the longitudinal and transverse steel ratios for the cap were increased by a factor of approximately 2.5 relative to models PC-1 and PC-2, to values of 1.09 and 0.24 percent, respectively. The pipe pile in this (and all subsequent tests) had a D/t ratio of 34.5, the same ratio used in model PC-2. Once again, failure of the connection occurred through tensile cracking of the

concrete. Data from this test confirmed the failure behavior suspected in tests PC-1 and PC-2. That is, once the concrete cracked in tension, the reinforcing steel was unable to carry the tension forces transferred to it without experiencing plastic strains and large deformations. The maximum moment carried by the cap at failure was similar in magnitude to that observed in tests PC-1 and PC-2, leading to the conclusion that little increase in the moment capacity of the cap might be realized until some threshold level of reinforcing steel was surpassed.

The longitudinal and transfer steel ratios used in the cap in model PC-3a were 2.11 and 0.65 percent, respectively, an increase of a factor of five relative to models PC-1 and PC-2. Some details of the reinforcing cage were also changed to more effectively use the longitudinal reinforcing steel in resisting the local tension forces introduced in the cap in the pile embedment zone and in confining the cap concrete immediately adjacent to the pile across the embedment depth. Once again, as the lateral load applied to the connection increased, the connection failed due to tension cracking of the concrete followed by tensile yielding of the reinforcing steel in the cap. In this case, however, a substantial increase in the moment capacity of the cap was observed relative to that seen in earlier tests. In test PC-3a, the maximum moment carried by the cap at failure was 30 percent greater than the moment carried at failure in earlier tests. The ductility at failure, however, was only 2.6, significantly less than that observed in previous tests. One explanation for this loss of ductility is a shift of the cap performance from a ductile under-reinforced condition to a more brittle over-reinforced condition as the amount of steel used in the cap increased.

In test PC-4, the amount of longitudinal and transverse steel in the pile cap was further increased relative to the earlier models. The longitudinal and transverse steel ratios for this model were 2.83 and 0.70 percent, respectively. The reinforcing cage was obviously "congested" when this amount of steel was placed in the cap, and consideration should be given to constructibility issues if additional reinforcing steel is suggested for the cap. Note also that the details of the reinforcing cage were once again altered. In this case, the outside longitudinal bars in the bottom face of the cap (the face through with the pipe pile exits) were U-shaped in nature, looping around the pipe pile to provide optimum resistance to internal tension forces introduced to the cap by the "prying" action of the pile. This model failed through the formation of a plastic hinge in the pipe pile. The maximum moment carried by the pipe pile exceeded its calculated plastic moment capacity by 26 percent. The observed displacement ductility for this connection was 3.9, although the ultimate displacement ductility could be much higher, as the test had to be terminated before the full ductility of the connection was realized, due to limitations of the test fixture. The connection was subjected to one reversed cycle of load. While this load history is short relative to the number cycles involved, the load deformation data that was collected consisted of robust hysteresis curves that exhibited little loss in strength and energy dissipation capacity between the first and fully reversed load cycle.

The response of this steel pipe pile-to-concrete cap connection configuration was also analytically investigated using hand calculations, strut and tie modeling, and finite element modeling. The results from these various analyses were compared with those obtained during the physical tests to determine how well these various techniques replicated the actual performance.

Overall, the simple hand calculations did a good job in predicting the nature of the failure that the connection would experience (i.e., formation of a plastic hinge in the pipe pile, crushing of the concrete in the cap, or cracking and tensile yielding in the cap). The hand calculations were less accurate in predicting the precise load at which failure by these mechanisms would occur. In the hand calculations, the moment capacity of the pipe pile and of the cap were calculated independently. Equations recently developed for use in the seismic design of bridge structures were used to estimate the plastic moment capacity of the pipe piles. In the one test in which a full plastic hinge developed in

the pipe pile (test PC-4), the actual plastic moment capacity of the pipe pile exceeded the calculated value by 26 percent.

The capacity of the cap to carry the moment introduced by the pile in the embedment zone was determined based on two possible failure mechanisms, crushing of the concrete in compression immediately down stream from the pile face in the direction of the applied load, and tensile yielding of the reinforcing steel immediately adjacent to the embedded pile. To investigate crushing of the concrete in the cap, a compression couple was assumed to act on opposite sides of the pile along its embedded length. The accuracy of this approach, however, could not readily be evaluated, as none of the models tested in this program failed through this mechanism. Nonetheless, it could be concluded that in some of the tests, the compression stresses carried by the concrete exceeded the typically assumed limiting value of $0.85 f'_c$ by at least a factor of two.

To investigate yielding of the reinforcing steel in the cap, the compression couple was assumed to be equilibrated internally by a tension couple in the cap. These tension forces were assumed to be carried by the reinforcing steel, alone, after the concrete cracked. Thus, the limiting capacity of the cap for this failure mechanism was calculated based on the area of the longitudinal steel in the cap and the yield stress of this steel. This approach was found to yield good results for moderate to heavily reinforced cross-sections. In a connection longitudinally reinforced with 2.1 percent steel (test PC-3a), the calculated capacity of the cap was within 12 percent of the actual capacity. This approach, however, yielded poor results for lightly reinforced cross-sections. The calculated capacity for a connection with only 0.41 percent longitudinal steel (model PC-2, for example) was 70 percent lower than the actual capacity. This difference was attributed to the importance of the tensile capacity of the concrete in contributing to the resistance of lightly reinforced cross sections.

The behavior of the reinforced concrete cap under the action of the pipe pile was also analytically investigated using a strut and tie approach. A new technique for implementing strut and tie modeling was experimented with, in which the strut and tie model was generated and analyzed using conventional structural engineering analysis software. Attractions of this approach to implementing a strut and tie analysis included that 1) a generic grid of strut elements could be used rather than a network of struts pre-selected by the analyst, as is typically done in traditional strut and tie analysis, and 2) it offered the possibility of obtaining a better solution than available from the hand methods without moving up to the level of sophistication of a non-linear, solid finite element analysis. The hand methods described above only provide information on critical demands in the concrete and the longitudinal reinforcing steel in the cap immediately adjacent to the pipe pile. The strut and tie models provide information on the demands in the transverse ties, along the length of the longitudinal reinforcing steel, and throughout the concrete. One major drawback of this approach was that most structural engineering software programs (including the one that was used in this investigation) perform only linear elastic analyses, so load redistribution within the structure due to cracking and yielding of the materials is not modeled. Similar to the hand models used herein, the strut and tie models were found to yield good results for moderately to heavily reinforced cross-sections ("exactly" predicting when yielding of the reinforcing steel would initiate in model PC-3), while under-predicting the capacity of lightly reinforced cross-sections (low by 50 percent relative to the actual load at which yield initiated in test PC-2). Once again, this problem with lightly reinforced sections was attributed to ignoring the tensile capacity of the concrete in the analysis.

With regard to finite element analysis codes, presently available models do not appear to be capable of accurately modeling concrete damage under cyclic loads. In a related fashion, if the non-linear response of a structure is driven by concrete damage, the response will be difficult to represent accurately. However, for structural connections where the non-linear response is driven by plastic defor-

mation of the steel reinforcement or, as was presented here, components such as the steel pile jacket, then results from this work indicate that the behavior may be representable with reasonable accuracy. In all cases, finite element models are still useful for the evaluation three dimensional variations in the stress-strain responses immediately prior to the onset of permanent deformation. After the onset of permanent deformation, the accuracy of the model is highly dependent on the dominant modes of deformation.

5.2   RECOMMENDED FUTURE WORK

This investigation primarily characterized the behavior of this steel pile-to-concrete pile cap connection relative to one attribute of the connection, that is, the reinforcing steel used in the cap. Further work should address some of the other parameters that are either known or suspected to affect the capacity of the connection. One of the primary parameters of interest is the depth of embedment of the pile in the cap. Other issues of interest include the effects of using dowels threaded transversely through the steel pipe pile in the embedment zone (a practice that has already been employed on some full size structures), the use of a larger spiral around the pile in the embedment zone rather than looping the primary longitudinal bars around the pile, and placing a block out in the concrete filled, steel pipe pile just outside the face of the cap, to force the connection failure to be formation of a plastic hinge in the pipe pile. Relative to this latter idea, an additional connection test was performed outside of this project, in which such a block out was placed in a model that was reinforced similar to model PC-3a. Failure of this connection did indeed occur through controlled plastic hinging of the pipe pile at the block out location. One attraction of the block out approach is the simplicity and predictability of the failure mechanism of the resulting connection. Finally, limited cyclic load tests were conducted during this investigation. In a seismic event, this connection could experience several cycles of reversed load; thus, it is important to understand how this connection will behave under different cycle load histories.

   In all cases, the currently available analytical tools are inadequate to definitively address the various issues enumerated above. Therefore, experimental testing will be a necessary part of any future investigations of connection performance. This project has shown that such tests can reasonably be conducted using the 1/2 size models and test procedures developed in this investigation. These physical results should continue to be compared with the analytical results obtained from hand and computer based calculations, to develop better analysis tools to assist in designing these connections. If consideration is given to designs where concrete damage will be minimal, then finite element analyses may be very useful.

5.3   IMPLEMENTATION OF RESULTS

The results of this investigation provide the designer of a concrete filled, steel pipe pile-to-concrete pile cap connection some indication of the nature of the expected failure of a given connection design, as well as an estimate of its load carrying capacity under lateral force demands. Knowledge of these aspects of a connection's behavior is critical to the designer in determining if his/her design will perform satisfactorily during extreme lateral load events. The main issue relative to the performance of this connection is whether failure will occur in the reinforced concrete cap or in the concrete filled, steel pipe pile. Acceptable designs can be developed for either case. Failure controlled by the pile cap was found to offer only modest ductility (displacement ductility ratio of approximately 3) and energy

dissipation capacity, while, as expected, failure of the pipe pile showed promise of large ductility and energy dissipation capacity.

The controlling failure mechanism can reasonably be predicted by reviewing the relative capacities determined by simple hand calculation for each failure mechanism, namely, compression failure of the concrete in the cap, tensile yielding of the reinforcing steel in the cap, and formation of a plastic hinge in the pipe pile (see Section 4.2). In reviewing the results of these calculations, it is important to consider the following items relative to each failure mechanism:

Compression Failure of the Concrete in the Cap - The critical parameter in this calculation is the assumed compression strength of the concrete adjacent to the pipe pile. Conservatively, this strength can be assumed equal to 85 percent of the unconfined compression strength of the concrete (a value frequently used for concrete in normal stress applications). It is well established that when confined by reinforcing steel, the compression strength of concrete increases. The exact relationship between these parameters, however, is complex, and only a lower bound on the increase in strength realized in the pile cap is available from the results of this investigation, as none of the tested models experienced significant crushing of the concrete in the cap in the pile embedment zone. Based on the test results, a value approximately two times the unconfined compression strength of the concrete can be used in these calculations.

Tensile Yielding of the Reinforcing Steel in the Cap - The hand calculations only address the amount of longitudinal steel in the cap. Both the experimental results and the results from the strut and tie analysis indicate that significant stresses also develop in the transverse steel as the pile is laterally loaded. In the connections modeled in this investigation, the stress levels in the transverse and longitudinal reinforcing bars generally appeared to be of the same order of magnitude when the transverse steel ratio was approximately 25 percent of the longitudinal steel ratio. This proportion was used in all the models tested in this investigation.

The capacities calculated by hand for this failure mechanism (tensile yielding of the reinforcing steel) were significantly less than the actually capacities determined by test for the lightly reinforced caps considered in this study (caps with a longitudinal steel ratio of less than around 2 percent). In such situations, and as previously discussed, the tensile capacity of the uncracked concrete appeared to substantially contribute to the capacity of the cap. In such situations, failure is believed to have initiated through tensile cracking the concrete, followed immediately by yielding of the reinforcing steel. Thus, for lightly reinforced sections that are expected to fail through yielding of the reinforcing steel, the magnitude of the predicted load at which this failure will occur will be conservative.

Formation of a Plastic Hinge in the Pipe Pile - In the one physical model in which connection failure occurred through formation of a plastic hinge in the pipe pile, the measured plastic moment capacity of the pipe pile exceeded its calculated capacity by 26 percent. This value falls between the typical over strength factors of 20 and 50 percent used in capacity design for steel and concrete columns, respectively, and suggests that an over strength factor of at least 30 percent may be appropriate for concrete filled, steel pipe piles.

Relative to the accuracy of the these three calculations, the capacity equation for formation of a plastic hinge in the steel pipe pile appears to have been the most thoroughly researched, and the equation directly addresses many of the parameters known to effect the performance of this type of structural element. Conversely, the cap capacity equations are much simpler in formulation, and

only directly address a few fundamental parameters known to effect capacity. These equations, for example, do not address any issues related to the arrangement of the reinforcing steel, even though this arrangement may be critical to achieving the calculated capacity. In the absence of information in this regard, the capacities predicted by equation can only be assured if the detailing of the reinforcing steel in a new design is similar to that used in the physical models tested in this program. Thus, for example, to insure the formation of a plastic hinge in the pipe pile in a given design, the transverse steel ratio in the cap should be at least 25 percent of the longitudinal steel ratio, "U" shaped bars need to encircle the pile in the bottom face of the cap, a spiral needs to encircle the pile and extend the full depth of the cap, and the longitudinal bars that intersect the pile need to be hooked through the spiral (all of which were done in physical Model PC-4, which failed through the formation of a plastic hinge in the pipe pile). Note that it may be possible in some situations to use professional judgment to alter the details of the reinforcing steel in the cap in a new design without compromising the level of confinement, bar anchorage, resistance to splitting, etc. as was provided by the detailing used in the models tested in this investigation.

In any event, and as may be obvious, many uncertainties remain in performing connection capacity calculations using the methodology described above, particularly relative to the reinforced concrete cap. Certainly, reasonable results are expected when the system being designed is similar in configuration to those evaluated in the experimental program. If new designs deviate substantially from the tested configurations (e.g., shallow or deep depths of embedment, elimination of the spiral encircling the pile in the embedment zone), different failure mechanisms could become important. In light of the complexity of this connection and the absence of any sophisticated and proven design methodologies, the only feasible way to investigate the performance of such designs may be through additional physical testing.

References

AASHTO (2000). *LRFD Bridge Design Specifications*. American Association of State Highway and Transportation Officials, Washington, D.C. 3.2.3

ABAQUS (Rev. 5.8). *The ABAQUS suite of general-purpose, nonlinear finite element analysis (FEA) programs*. Hibbitt, Karlsson & Sorensen, Inc., Pawtucket, Rhode Island, www.abaqus.com. 4.4.1

ACI (2002). *Building Code Requirements for Structural Concrete (ACI 318-02)*. American Concrete Institute, Detroit, MI. 3.2.3

AISC (2001). *Manual of Steel Construction: Laod and Resistance Factor Design*. American Institute of Steel Construction, Chicago, 3rd edition. 3.5.5

ANSYS (V8.1). *Engineering ANalysis SYStem*. Swanson Analysis Systems, Inc., Houston, Pennsylvania, www.ansys.com. 4.4.1, 4.4.2

ATC/MCEER (2001). *Recommended LRFD Guidelines for the Seismic Design of Highway Bridges Part I: Specifications*. ATC/MCEER Joint Venture (a Partnership of the Applied Technology Council and the Multidisciplinary Center for Earthquake Engineering Research). 2.4, 3.2.1, 4.1, 4.2.1

Bruneau, M. and Marson, J. (2004). Seismic design of concrete-filled circular steel bridge piers. *Journal of Bridge Engineering*, 9(1):24–34. 2.4, 4.2.1

Chai, Y. (1996). An analysis of the seismic characteristics of steel-jacketed circular bridge columns. *Earthquake Engineering and Structural Dynamics*, 25(2):149–. 4.4.1

Chai, Y., Priestley, M., and Seible, F. (1994). Analytical model for steel-jacketed rc circular bridge columns. *Journal of Structural Engineering*, 120(8):2358–2376. 4.4.1

Chen, W. (1982). *Plasticity in Reinforced Concrete*. McGraw Hill, New York. 4.4.1

Cheok, G. S. and Stone, W. C. (1990). Behavior of 1/6-scale model bridge columns subjected to inelastic loading. *ACI Structural Journal (American Concrete Institute)*, 87(6):630–638. 2.4

Chung, Y. S., Meyer, C., and Shinozuka, M. (1989). Modeling of concrete damage. *ACI structural journal*, 86(3):259–271. 4.4.1

Collins, M. and Mitchell, D. (1991). *Prestressed Concrete Structures*. Prentice-Hall, Englewood Cliffs. 3.5.3

DIANA (V8.1). *DIsplacement ANAlysis: Finite Element Analysis Solutions*. TNO DIANA, Leicester,UK, www.tnodiana.com. 4.4.1

DYNA3D (V4). *A Nonlinear, Explicit, Three-Dimensional Finite Element Code: For Solid and Structural Mechanics*. Lawrence Livermore National Laboratories. 4.4.1

Govindjee, S. and Hall, G. (1998). A local integration method for coupled damge and plasticity. Structural Engineering Mechanics and Materials UCB/SEMM-98/01, Department of Civil Engineering, University of California, Berkley, California. 4.4.1

Joen, P. H. and Park, R. (1990). Simulated seismic load tests on prestressed concrete piles and pile-pile cap connections. *PCI Journal*, 35(6):42–61. 2.4

Lee, J. and Fenves, G. L. (1998). Plastic-damage model for cyclic loading of concrete structures. *Journal of Engineering Mechanics*, 124(8):892–900. 4.4.1

Lowes, L. N. (1998). *Finite Element Modeling of Reinforced Concrete Beam-Column Bridge Connections*. PhD thesis, Univeristy of California, Berkeley. 4.4.1

Mander, J., Priestley, M., and Park, R. (1984). Seismic design of bridge piers. Research Report 84-2, University of Canterbury, New Zealand. 4.4.1

Mander, J., Priestley, M., and Park, R. (1988a). Observed stress-strain behavior of confined concrete. *Journal of Structural Engineering*, 114(8):1827–1849. 4.4.1

Mander, J., Priestley, M., and Park, R. (1988b). Theoretical stress-strain model for confined concrete. *Journal of Structural Engineering*, 114(8):1804–1826. 4.4.1

Marcakis, K. and Mitchell, D. (1980). Precast concrete connections with embedded steel members. *Prestressed Concrete Institute Journal*, 25(4):88–116. 3.2.1, 4.2.2

Marson, J. and Bruneau, M. (2004). Cyclic testing of concrete-filled circular steel bridge piers having encased fixed-based detail. *Journal of Bridge Engineering*, 9(1):14–23. 2.4

McKittrick, L., Hicks, J., Stephens, J., VanLuchene, D., and Rabern, D. (1998). Performance of steel pipe pile-to-concrete bent cap connections subject to seismic or high transverse loading. MPART Report FHWA/MT-98-005/8117-7, Montana Department of Transportation. 1.1, 4.4.1

MDT (1995). *Standard Specifications for Road and Bridge Construction*. Montana Department of Transportation, Helena, MT. 2.2, 3.2

Mehta, P. and Monteiro, P. (1993). *Concrete: Structure, properties, and materials*. Prentice-Hall, Inc., Englewood Cliffs, NJ, 2nd edition. 4.4.1

NIKE3D (V3.3). *A Nonlinear, Implicit, Three-Dimensional Finite Element Code: For Solid and Structural Mechanics*. Lawrence Livermore National Laboratories. 4.4.1

Park, R. and Paulay, T. (1975). *Reinforced Concrete Structures*. Wiley Interscience, New York. 4.4.1

Priestly, M. and Park, R. (1987). Strength and ductility of concrete bridge columns under seismic loading. *ACI Structural Journal*, 84(1):61–67. 4.4.1

Shama, A., Mander, J., and Aref, A. (2002). Seismic performance of retrofit of steel pile to concrete cap connections. *ACI Structural Journal (American Concrete Institute)*, 99(1):51–61. 2.4, 3.2.3, 4.2.2

Silva, P. F. and Seible, F. (2001). Seismic performance and evaluation of cast-in-steel-shell (ciss) piles. *ACI Structural Journal (American Concrete Institute)*, 98(1):36–49. 2.4

Silva, P. F., Sritharan, S., Seible, F., and Priestley, M. N. (1999). Full-scale test of the alaska cast-in-place steel shell three column bridge bent. Final Report UCSD SSRP-98/13, University of California, San Diego, La Jolla, California. Sponsoring Agency: Federal Highway Administration, Report No. FHWA-AK-RD-99-02. 2.4

Steunenberg, M., Sexsmith, R., and Stiemer, S. (1998). Seismic behavior of steel pile to precast concrete cap beam connections. *Journal of Bridge Engineering*, 3(4):177–185. 2.4